AFOSR 70-2714TR

FIRST PHASE FINAL REPORT

PROPELLANT SPRAY COMBUSTION PROCESSES
DURING STABLE AND UNSTABLE
LIQUID ROCKET COMBUSTION

CONTRACT NO. AF49(638)-1705

Prepared by:

R. D. Sutton
Advanced Programs

Rocketdyne
A Division of North American Rockwell Corporation
Canoga Park, California

October 1970

Air Force Office of Scientific Research
Energy Conversion Division
Arlington, Virginia
Air Force Systems Command
United States Air Force

1.
rel

FOREWORD

This report prepared by the Advanced Programs Department of Rocketdyne, a Division of North American Rockwell Corporation, 6633 Canoga Avenue, Canoga Park, California, summarizes the work performed under Contract No. AF49-(638)-1705, "Propellant Spray Combustion Processes During Stable and Unstable Liquid Rocket Combustion", during the four year period, July 1966 to November 1970. The first phase was formerly titled "Pressure Wave Growth in Monodisperse Spray/Gas Mixtures". The Air Force Project Officer was initially Dr. B. T. Wolfson; for the past two years Lt. Col. R. W. Haffner has served in this capacity. Mr. T. A. Coultas was the Rocketdyne Program Manager.

This report has been assigned the Rocketdyne identification number R-8377.

ABSTRACT

Information resulting from this study will allow formulation of new and very general analytical models and criteria to permit a priori design of reliable and stable liquid rocket motors and supersonic air-breathing engines required for future weapons delivery systems. Specifically the purpose of this program is the acquisition of detailed analytical and experimental information concerning the mechanisms of energy addition from propellant spray combustion to steady flow fields and propagating pressure disturbances. The data will be used to evaluate present or formulate new expressions describing the dynamics that contribute to the coupling processes between the spray and gas flow fields. These expressions form the basis of steady-state and transient propellant combustion models that bear directly on the problem of predicting performance and the onset of high frequency combustion instability in liquid propellant rocket engines.

To overcome past difficulties in comparing analytical and experimental results, an apparatus will be utilized that produces a monodisperse propellant spray uniformly distributed throughout the combustor. The motor, to be operated as a rocket engine combustor

under either stable or transient conditions, provides for optical observation and is extensiv.... instrumented to record pressure wave amplification or decay as a function of parameter variation.

From the test data drop diameters, velocity and pressure wave growth or decay as a function of chamber length and initial conditions will be determined. These data can then be input to appropriate newly developed combustion models and the validity of the coupling term expressions evaluated by directly comparing the resulting predictions to experimental data.

ACKNOWLEDGMENT

CONTENTS

ILLUSTRATIONS

TABLES

INTRODUCTION AND SUMMARY

The long-range purpose of this program is the acquisition of detailed experimental information concerning the mechanisms of energy addition from propellant spray combustion to a steady-state flow field and to a pressure disturbance propagating through an initially steady, burning flow field. The data will be used to evaluate existing expressions or formulate new empirical and analytical expressions describing the droplet processes that contribute to coupling between the spray and gas flow fields.

These coupling term expressions form the basis of steady-state and transient propellant combustion model formulations which bear directly on the problems of predicting performance and the onset of high-frequency combustion instability in liquid propellant rocket engines. However, the presently used coupling term expressions, which are vital to performance and combustion stability predictions, are based on data obtained under inappropriate conditions.

To overcome past difficulties with comparisons between experiment and theory, an experimental apparatus has been developed that is unique in its utilization of a monodisperse propellant spray uniformly distributed throughout the combustor. The motor, to be operated as a rocket combustor under either stable or transient conditions, is quartz-windowed on two sides to permit photographic and optical observation.

Preceding page blank

This experimental device is to be used to determine drop diameters, drop velocity and gas pressure as a function of chamber length. These data are to be input directly into a highly sophisticated one-dimensional steady-state combustion program which will calculate the gas flow field without the need to use all of the spray equations. With the spray and gas flow fields thus defined, the droplet drag coefficient will be directly computed and various drop burning models can be directly evaluated. This information will completely specify the steady-state operation of the motor.

The most suitable quasi-steady droplet dynamic models for steady-state operation can in turn be used with an also newly developed, comprehensive transient analytical model. Comparisons are to be made with transient data from the motor for the same initial conditions used for steady-state measurements. Comparisons include: pressure profiles, drop velocity, and drop diameters as functions of length for various times. In this manner, the validity of the quasi-steady burning and drag models, with regard to their application to transient calculations, can be determined. Further parametric comparisons between the computer program and the motor results will determine the best available models for use in predicting transient processes.

The analytical models developed under this contract were formulated after all of the existing mechanistic theoretical models had been critically reviewed with the intention of selecting one for use in the experimental

2

evaluation of the coupling terms. It was concluded, however, that each
of the existing models (particularly those dealing with transient pheno-
mena) has been overly simplified in one or more areas and were consequently
inadequate for proper evaluation of the coupling terms. Accordingly, new
(and very general) transient and steady-state rocket combustion models have
been developed. These express fully the non-linear dynamics of a multi-
component reacting gas stream with simultaneous mass, momentum and energy
exchange with bipropellant sprays. The models are flexibly formulated so
that the important input parameters, which control the coupling mechanisms,
appear in subroutines of the general spray-gas dynamic computer program.
The computer programs are currently operational.

The primary effort during this investigation has been on the development
of techniques to obtain and evaluate the required data. Consequently, this
final report deals principally with a description of: liquid rocket combus-
tion processes; previously developed steady-state and transient models; the
formulation, development, and checkout of the new overall analytical combus-
tion models; a review of coupling term formulations; and the design, initial
experiments, development and checkout of the monodisperse spray rocket
apparatus. Preliminary analytical and experimental results are presented.

COMBUSTION PROCESSES IN A LIQUID ROCKET ENGINE

OBJECTIVES OF PROGRAM

The intense, rapid combustion of bipropellant liquid sprays in rocket engine combustion chambers presents certain obstacles to the development and application of rocket thrustors. Foremost among these problems are inadequate combustion efficiency and combustion instability. For many years, both experimental and analytical investigations have sought to quantitatively explain and understand the fundamental causes of these problems and to find means of eliminating them.

At present, the development of high-performance stable propulsion systems depends heavily upon testing, which is both expensive and introduces program delays. However, continued improvement of analytical models will ultimately enable reliable performance and stability predictions to be made at design time, significantly reducing system test requirements, development time and expense.

The objective of this investigation has been the development of techniques to allow the acquisition and evaluation of detailed analytical and experimental information, under actual liquid rocket combustion chamber conditions, concerning the mechanisms of energy addition from propellant spray combustion during both stable and unstable (combustion instability) operating conditions.

COMBUSTION CONTROLLING PROCESSES

Analysis of liquid rocket engine combustion requires the formulation of a coupled system of analytical expressions to describe the various physical and chemical processes associated with the conversion of propellants into combustion products.

A number of theoretical models of rocket combustion have been developed and used for a variety of specific purposes. Basically, all of them start with a set of conservation equations describing the behavior of a combustion gas flow field. One or more propellant sprays are presumed to be contained in the gas; additional conservation equations are required for the spray phase. Because the gas stream and sprays coexist and are intermingled, exchange of mass, momentum, and energy occurs between them. This exchange is described by expressions which will be called <u>coupling terms</u>, and which appear in both gas and spray phase conservation equations. The analytical problem is closed by imposing initial and boundary conditions corresponding to the particular problem under study.

The coupling terms are the analytical expressions which describe the mass, momentum and energy transport processes between the spray and the gas. The processes corresponding to these coupling terms are often denoted as the droplet dynamic processes. The coupling terms represent several physical phenomena which occur in a combustion flow field. Among these phenomena are the following:

1. Droplet Burning (vaporization)

    This includes all droplet mass diffusion loss mechanisms; for
    example, subcritical and supercritical pressure droplet burning
    (which may also involve "micro mixing" phenomena), flashing, chemi-
    cal kinetics (if important in the droplet region of influence),
    and effects of convection. This category will be further sub-
    divided and discussed more completely later in this report.

2. Droplet Heating Rate

    This phenomena is coupled with the burning rate. It cannot be
    ignored even at subcritical pressures where "wet bulb" temperatures
    are attained.

3. Droplet Breakup Rate (shattering)

    Under highly convective conditions with high relative gas flow rates
    the droplets may undergo "bag" or "shear" type breakup, the latter
    being more prevalent in a rocket engine. Breakup of the drop
    (usually into smaller than $10\,\mu$ droplets) exposes substantially
    increased droplet surface area to the gas, which increases the
    burning rate. Occurrence of such phenomena has been observed
    during both steady-state and transient operation of a rocket
    engine. It may be one of the mechanisms that sustains combustion
    instability.

4. Droplet Drag Rate

This phenomena determines the relative velocity of the drop
compared with the gas velocity. It interacts with all of the
above phenomena because it determines the amount of relative
convection and also influences residence time of the droplets.

These processes illustrate some of the physical phenomena which will be
denoted simply as the coupling processes; the analytical expressions
corresponding to these will be denoted as coupling terms.

Relevance of Coupling Terms and Processes

At this point the question may be asked, what relevance do the coupling
processes have to the problem at hand? The interest concerns the ability
to detail the information (data) and mechanisms that control the combustion
process. This knowledge has direct influence on the capability to make
reliable performance and stability predictions for proposed designs.

Reliable performance and stability predictions for engine designs can only
be made through use of comprehensive analytical models for steady state and
transient combustion. Reliance on experience and available experimental data
is often not sufficient for adequate new designs.

A part of such models is a generalized set of conservation equations des-
cribing the behavior of the spray and gas flow fields. A crucial part of
these is the coupling terms. These expressions, used to describe the mass

momentum, and energy transport processes between the spray and gas flow field conservation equations, substantially control the formulated model. Thus, all of the steady-state liquid rocket combustion models and the transient liquid rocket combustion models (required for predicting onset, sustenance and even the cause of high-frequency combustion instability) are, if formulated properly, dependent on the validity of the coupling terms for their accuracy.

Thus, the data being sought are needed to determine and evaluate the validity of the expressions used to describe the coupling terms. All of the coupling mechanisms need further investigation and the expressions for them need to be re-evaluated, verified or updated for application to both stable and unstable situations.

Almost none of the many experiments reported in the literature adequately simulate the highly convective, reactive, steep-gradient environment of an unstable rocket motor. Indeed, many are not adequate for even the environment of a stable rocket combustor. Thus, all of the presently used expressions, are, for the most part, based on data obtained under inappropriate conditions.

Hence, a combined analytical and experimental effort was needed to pinpoint the specific coupling mechanisms under stable and oscillatory combustion conditions.

This information will provide a major step toward development of adequate models of performance and instability which will allow confident predictions of new engine designs. This is particularly important at this time when the next generation of chemical propulsive devices are being designed, such as the Space Shuttle Engines. This information could be utilized today if it were available. As a consequence of its unavailability the analysis of the engine design is proceeding with similar coupling terms as those used in the past.

R-8377

INITIAL APPROACH TO THE ACQUISITION AND

EVALUATION OF PERTINENT DATA -

A REVIEW OF PREVIOUS OVERALL COMBUSTION MODELS

INITIAL PROGRAM APPROACH

At the outset of this investigation the assumption was made that some of
the existing theoretical models describing the spray/gas flow field would
be adequate for general steady-state and transient combustion analysis but
that the initial conditions and coupling terms are inadequately known and
described. These inadequacies include the specific characteristics of the
initial spatial distribution of spray mass flows and droplet size distri-
butions, both of which are poorly known; also, steady-state and transient drop-
let evaporation and secondary droplet breakup mechanisms are not fully understood.

The philosophy was adopted that an experiment would be designed in which
the initial and boundary conditions could be controlled to match those for
which the equations of the reacting spray-gas field had been solved. Thus
the ill-defined coupling terms could be isolated. Data obtained therefrom
could be compared with predictions obtained with various expressions for the
coupling terms to evaluate their adequacy. (The experimental conditions however,
must be appropriate to the model being used for evaluation of the coupling
terms. Precise initial conditions must be known and direct experimental
observation of the physical phenomena corresponding to the investigated
coupling term must be obtained under both steady and transient behavior.
An experimental apparatus for acquiring such data has been built and will
be discussed later.)

However, an evaluation of the adequacy of the coupling terms may depend on the overall analytical combustion model being used. Unless the model is accurate and sufficiently general to encompass the various operating conditions, it may not delineate the coupling terms to be investigated.

All of the existing steady-state and transient mechanistic theoretical models were critically reviewed during this investigation with the intention of selecting one or more for use in an experimental evaluation of the coupling terms. It was concluded however, that except for a few existing steady state models, each of the existing models were oversimplified in one or more areas and that they were inadequate for proper evaluation of the coupling terms; this is especially true for the transient models.

To obtain solutions, each model was reduced in complexity by the introduction of simplifying assumptions. In many instances the simplifications permitted reduction of the coupled partial differential equations to a system of ordinary differential or, occasionally, integral equations describing the combustion field. Each investigator decided which simplifications were appropriate for his particular combustion situation. As a result there is great diversity in the simplifying assumption used among the analytical models.

This makes comparisons between the results of various investigators difficult and obscures the basic need for specific improvements appropriate to all of the models. Existing defects in even the formulation of the conservation

equations describing the spray/gas fields (again primarily the transient models) could possibly overshadow effects of coupling terms. This conclusion is evident from the rather lengthy, but nonetheless necessary and quite complete qualitative and quantitative description and review which follows.

The present program utilized, built upon, and extended the work of many previous investigators. A summary of this work will be given, but first a qualitative description of the liquid rocket engine combustion processes is presented.

QUALITATIVE DESCRIPTION OF COMBUSTION PROCESSES - STEADY-STATE OPERATION

After injection of the propellants into the rocket combustion chamber, subsequent steps in their combustion include liquid propellant atomization, spray dispersion and mixing, vaporization, vapor-phase mixing, ignition and chemical reaction. These processes take place in a two-phase flow field of finite length; the limited flow field influences both the process rates and the time available for completing them. A schematic representation of the most important processes is shown in Fig. 1, which also emphasizes their complex interdependence. The process paths to the left side of Fig. 1 should tend to be dominant with injectors designed for efficient liquid-liquid interpropellant contact prior to their atomization. Conversely, paths toward the right side tend to be favored with either gas-liquid propellant injectors or liquid-liquid propellant injections which will accomplish substantial propellant

INJECTION OF FUEL
AND OXIDIZER

CONTACTING OF
LIQUID STREAMS ⟶ ATOMIZATION

MIXING

INTER-SPRAY
MIXING

VAPORIZATION

DROPLET
COLLISIONS

LIQUID-PHASE
MIXTURE

DROPLET
HEATING ABOVE
CRITICAL POINT

PROPELLENTS IN
VAPOR PHASE

VAPORIZATION

LIQUID-PHASE
REACTION

ATOMIZATION

TURBULENT
MIXING

DIFFUSION

VAPORIZATION

RECIRCULATION

GAS-PHASE
REACTIONS

INTERMEDIATE
REACTION PRODUCTS

FINAL REACTION
PRODUCTS

EXPANSION IN
EXHAUST NOZZLE

Figure 1. Schematic Representation of Liquid Propellant
Rocket Combustion Processes

14

atomization and vaporization before much mixing occurs (Ref. 1). Most practical rocket injectors operate between these two extremes so that combustion proceeds simultaneously along many or even most of the process paths.

The combustion processes occur throughout the combustion chamber in a distributed fashion. It is convenient for this qualitative discussion to divide the combustion chamber into a series of discrete zones. Based in part on photographic evidence from transparent model engine firings (Ref. 2), a logical subdivision is shown in Fig. 2 . The transition and distinction between the various zones in the combustion region is certainly gradual and not sharply defined. However, both the position and abruptness of the transitions are influenced by injector and chamber designs, the propellant combination and operating conditions.

Injection/Atomization Zone

Adjacent to the propellant injector is an injection/atomization zone. Because the injection is usually concentrated at discreet sites, with some degree of separation between unlike propellants, within this zone occur large gradients in each direction with respect to propellant mass fluxes and concentrations, liquid atomization and dispersion rates and properties of the gaseous medium. Some of the gaseous constituents come from local propellant combustion, but they are primarily either gaseous injectants or recirculated combustion product gases from the next zone downstream. The principal force for driving recirculating

R-8377

15

LIQUID ROCKET ENGINE STEADY STATE OPERATION
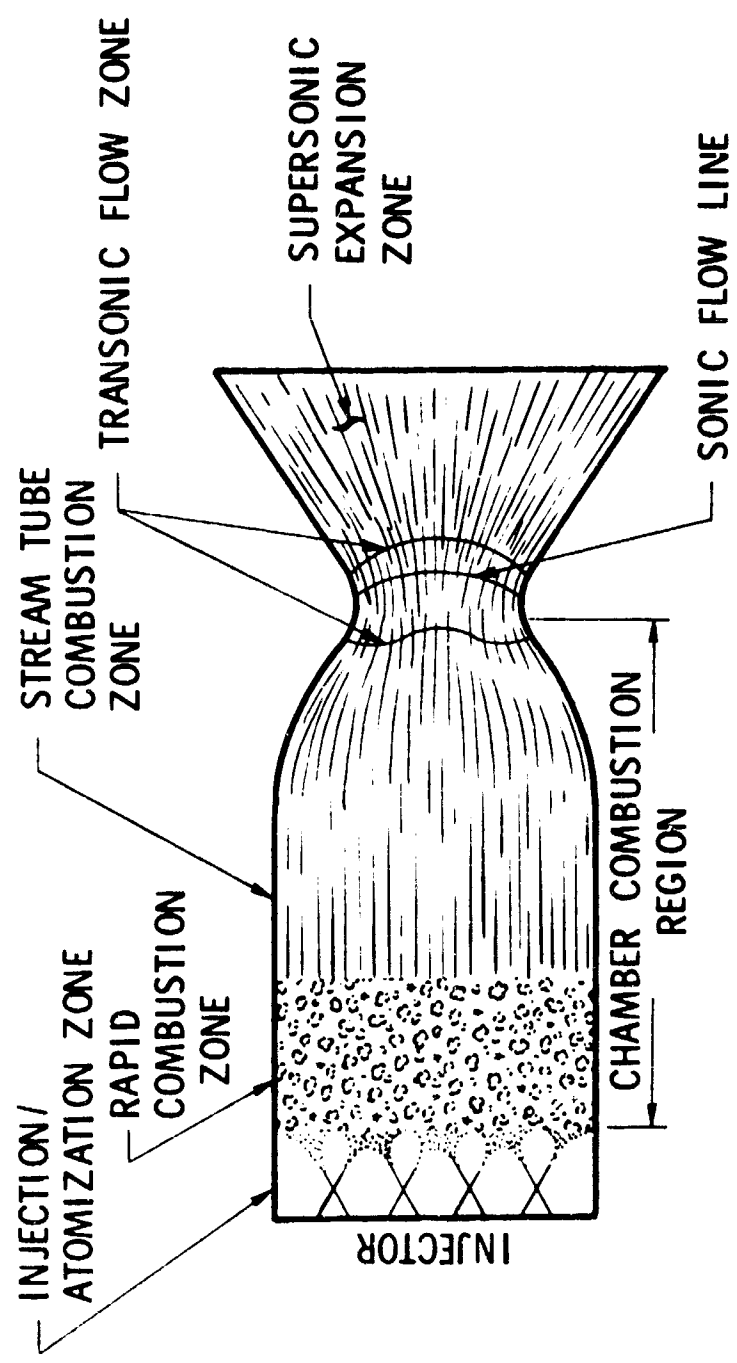
Figure 2. Subdivision of Combustion Chamber into Discrete Zones

gaseous flows is viscous shear between the injected propellants and the surrounding gases. These gases are thereby accelerated in the propellant flow direction and must be continuously supplied by transverse gas flows into the neighborhoods of injection sites. Somewhere in the regions between injection sites, there must be upstream directed flows, as required by continuity of gaseous mass.

The gas-liquid surface shear forces also contribute to distortion and fragmentation of liquid surfaces, i.e., atomization. Some gas/liquid injectors are designed to enhance this shear-breakup mode of atomization, but most liquid rocket injectors provide some kind of liquid-liquid impingement to enhance atomization due to hydraulic forces.

The primary atomization process is gradual to some extent and requires a finite zone length for completion, which is typically on the order of 1/2 to 2 inches. Spray formation and its dispersion from the (approximately point-source) injection sites proceeds simultaneously. Frequently straight line ray dispersion may be a good approximation, although interactions between sprays from neighboring injection sites may turn the sprays.

As liquid propellant sheets, ligaments and droplets are being formed, they are immersed in the surrounding gaseous medium. Generally, the gases are at somewhat or considerably higher temperatures than the liquid spray elements, so that convective heating of the sprays (and cooling of the gases) will occur. Propellant vaporization is usually negligible at first, because the liquid

injection temperatures are far below the propellant saturation tempera-
tures corresponding to the combustion chamber pressure. Continued heat-
ing soon raises droplet temperatures enough that vaporization rates become
appreciable. During the time required to reach that state, the spray
element velocities transport the sprays away from the injector face,
through the injection atomization zone.

For most propellants, liquid-phase reactions are either very fast, essen-
tially preventing mixing between unlike propellants (Ref. 3), or very
slow compared to droplet heating and vaporization. Vapor phase chemical
reactions, therefore, dominate. Since there is little propellant vapori-
zation in the injection/atomization zone, only a small percentage of the
overall combustion occurs in that region. The validity of this argument
obviously depends upon the buildup of reaction rates being slower than the
approach to complete atomization. The relative balance between these
phenomena determines the (approximate) location and the abruptness of the
transition between the injection/atomization zone and the next zone
downstream.

Rapid Combustion Zone

The second zone in the combustion chamber is characterized by essentially
complete primary atomization and comparatively high chemical reaction rates.
Dispersion of the sprays and gaseous recirculation in the first zone have
reduced the magnitude of transverse gradients in this zone but they are
far from being negligible for many rocket engines.

Rapid combustion corresponds to high generation rates of combustion gases. Upon undergoing vaporization and combustion, an element of propellant occupies a volume 100 or more times greater than that which it occupied as a liquid. Expansion of combustion gases from the position where they are formed accelerates the flow axially but also forces transverse flows from high burning rate regions to positions with lower burning rates. These expansion processes simultaneously provide the gases which are recirculated into the injection/atomization zone and close off the recirculation paths by filling them with downstream-flowing gases.

Dense spray droplets accelerate less rapidly than the gases and are only weakly responsive to the combustion gas movements. Acceleration of the combustion gases away from the spray increases the rates of convective heating of droplets and, thus, augments their burning rates. Spray residence times are longer than the gas residence time so that the combustion occurs in a shorter chamber distance than if the spray and gas velocities were equal. The near-injector gradients in spray mass flux persist, however, being degraded primarily by the dispersion and inter-spray mixing established at injection. Lateral flows of combustion gases will be generated whenever there are appreciable spray flux gradients. Eventually the lateral flow velocities become small compared with axial flow velocities and the combustion field approaches stream tube flow which is characteristic of the next downstream zone.

Chemical reactions within the subsonic flow portion of rocket combustion chambers usually occur very rapidly compared with the spray gasification rates (Ref. 4). Further, local mixing rates between a droplet's vapors and gases flowing around it are high in the droplet wake. Reaction rates are high enough that local thermodynamic equilibrium is rapidly attained.

Stream Tube Combustion Zone

As lateral flows of both burning sprays and combustion gases subside, an essentially streamline flow is developed. Vaporization and burning continue with no more than modest transverse gradients in fluxes and properties, but the flow lacks the strong lateral convective components which are a dominant feature of the rapid combustion ne. Continued mixing depends more upon turbulent exchange between neighboring parallel-flowing striations than upon spray dispersion or lateral convection. High flow velocities in this region, however, lead to short residence times so that turbulent mixing is not very effective. Photographs show the flow to be nearly laminar. To a good approximation, large-scale mixing in this zone can be neglected entirely and the two-phase flow treated formally as stream tube flow.

The gradient in combustion rate decays with increasing axial distance due to early consumption of the smallest spray droplets, decreased residence times as axial velocities increase, and eventually depletion of spray mass flux. Chemical reaction rates, on the other hand, remain high well into the exhaust nozzle. The stream tube combustion region may be considered to extend to the vicinity of the nozzle throat.

R-8377

Nozzle Expansion Zones

As the combustion products enter and expand through the nozzle, diminishing pressure and temperature gradually reduce the gas-phase chemical reaction rates until it becomes necessary to consider finite-rate chemistry. With most liquid propellants, this effect becomes important downstream of the nozzle throat. For most high efficiency rockets, performance losses due to incomplete propellant gasification and mixing approach their exit values either upstream of the throat or shortly downstream of it; further changes due to spray combustion effects become small compared with chemical kinetic losses and two-dimensional flow effects, which become important in the transonic and supersonic expansion zones (Ref. 5).

A Definition of "Mixing" Within a Rocket Combustor

Throughout this qualitative description the expressions "gas-phase convective flows" and "gas-phase mixing" have been used extensively. To define what is meant by these phrases, the processes are categorized into three sub-groups: gross gas-phase convective mixing or flows, gas phase turbulent mixing and micro-mixing processes.

Gas Phase Convective Flows. This refers to the strong, lateral gas flows produced in the rapid combustion zone. They are driven by nonuniform gas production and the resultant pressure gradient. They cause mixing on a gross scale, not due to "viscous stress or eddy viscosity effect," but rather to the strong transverse velocities produced. Mixing by these flows is more nearly mechanical and a function of both the direction and velocity of the flow. The effect is readily calculated by a three-dimensional model. As

described, the flows rapidly dissipate and rarely persist over a large portion of the chamber length. Thus, the mixture ratio distribution established by the time the propellants reach the downstream end of the rapid combustion region will normally be carried through most of the thrust chamber and through the nozzle by essentially parallel gas streams. Further alteration in the degree of propellant mixing must rely on gas stream turbulence.

Gas Phase Turbulent Mixing.   Turbulent gas mixing refers to mixing of adjacent-flowing, striated propellants.   As defined here, turbulent mixing would only become important downstream of the decay of the convective flows mentioned above, so its importance (if it is important) would lie only in what has been called the stream tube combustion zone.   The effect of turbulent mixing would be to diminish the performance losses predicted by the spray mixing and 3-D initial combustion analyses applied near the injector.

The frequency of turbulence within a rocket engine is probably on the order of 1000 to 2000 fluctuations per second.   Propellant residence times are on the order of 3 to 5 milliseconds, the primary portion of this time occurring before the start of convergence. Thus, the average number of turbulent fluctuations undergone by the flowing propellant before reaching the nozzle may be about five, which is probably too few to produce significant changes in the composition of the fluid. This order-of-magnitude estimate was confirmed under studies of F-1 engine gas-phase downstream mixing (Ref. 6).   It was determined that very little of the propellants that were not mixed by the near-injector 3-D transverse-flow regions were later mixed and burned because of turbulent gas-phase mixing. Thus, predictions of the mixing loss caused by striations, calculated by a rapid combustion zone analysis followed by a stream tube analysis, appear quite accurate.

R-8377

Many authors attribute the inability of one-dimensional combustion models
to predict performance for injectors with nonuniform propellant flow to the omis-
sion of consideration of high intensity turbulence observed in such engines.
This definition of turbulence is misleading because turbulent mixing as
defined between unlike gases flowing in adjacent stream tubes proceeds
slowly and, within the short gas residence times in this zone, is believed
to contribute far less to overall propellant mixing than the earlier spray
interdispersion and convective lateral gas flows in the rapid combustion
region. The "high intensity turbulence" these authors describe is really the
gas-phase convective flows of the rapid combustion zone. Further, even in
the absence of strong convective flows (i.e., smaller injection nonuniformities)
the mixture ratio distribution across the chamber produced by the injector would
result in a stream tube-like flow that a one-dimensional model cannot describe.
The influence of injection non-uniformities is always exhibited throughout the
chamber; the gas-phase convective flows, if present, tend only to smooth but
never eliminate the nonuniformities.

Micro-Mixing Processes.   This refers to small-scale processes occurring in
the vicinity of the gas-droplet interface. It is only concerned with rates
of droplet vapor/gas mixing in the droplets wake. It also refers to the very
local mixing of droplet vapors and surrounding gas for "droplets" which have
passed through their critical (pressure and temperature) state and whose
burning may be more nearly controlled by diffusive rather than evaporative
processes.

The problem here is how to include these processes in a model. Inclusion in the overall gas-phase conservation equation seems inappropriate because on this "micro scale" one is no more interested in the details of gas mixing than he is in the individual motion of gas molecules when considering continuous single-phase gas flow. For example, the mesh size of the three-dimensional model discussed later in this paper contains between 1 to 5 thousand droplets. Since each mesh size can be assigned only one velocity, density, etc., the flow of vapor from each droplet species within the mesh is lumped with that from every other droplet of the same species. It would be impossible to consider each individual droplet at every mesh point.

Rather this "local" process is within the domain of influence of the drop vapor surrounding gas boundaries and is logically included in the coupling terms concerning the dynamics of droplet burning rates. These coupling terms are functions of the bulk conditions within the mesh point for each drop-group size. If drop vapor/gas mixing rates become the rate controlling process, this can be properly calculated by the inclusion of terms for such a phenomena in the coupling terms.

The same argument also applies to chemical kinetics limitations. Even if bulk gas phase chemical reactions are assumed to be rapid and that equilibrium is obtained, this assumption does not preclude consideration of micro-scale chemical kinetic processes between the drop vapor/surrounding gas. These reactions and those in droplet wakes are also properly treated in the coupling term expressions.

These delineations of "spheres of influences" also have an interesting side effect on the meaning of one-dimensional flow with regard to mixing, etc.

The assumption of one dimensionality does not imply instantaneous gas-phase mixing, but only implies that the vapor flowing from the spray is spread in such a manner that it is distributed uniformly across the flow field at any axial location. Consequently, one dimensionality implies only so far as mixing and related effects are concerned, if at a given axial location one were to divide up the transverse cross section into control volumes, these control volumes would be identical.

QUALITATIVE DESCRIPTION OF COMBUSTION PROCESSES - TRANSIENT OPERATION

During certain periods of a rocket engine's operation, conditions within the combustion chamber are time variant, i.e., the operation is not steady with respect to time. Normally, these transient periods are limited to engine starting and stopping. Additionally some engines have been designed to be continuously throttleable or to operate at two or more discreet thrust levels. The combustion processes during such "normal", or expected, transient operation may differ significantly from the steady-state processes discussed in an earlier section. However, because analysis of these transients is not a subject of this report, no discussion of their differences is undertaken. Interest is focused instead on abnormal transient operation during oscillatory, or unstable, combustion, i.e., pressure oscillations in a combustion device which are sustained by the combustion process. Unfortunately, although a great deal of work has been directed toward this problem, the occurrence of abnormal transient operation is still common in engine development.

The deviations from steady-state combustion which occur during unstable burning depend upon the kind of instability experienced; they are described therefore, in an instability classification context. However, a sharp distinction between classes is not possible, probably because they are closely related and simply represent various oscillatory modes of the complex engine system. Liquid rocket instabilities are classified according to their dominant time-varying processes. They may be divided initially into two categories, depending upon whether the instability oscillation wave length is long or short compared with the chamber dimensions. The characteristics and name of each class are not uniformly defined and used in the literature.

Spatially Uniform (Lumped) Chamber Pressure Oscillations

If the instability wave length is considerably longer than the chamber length and diameter, pressure disturbances propagate rapidly through the combustion space compared with rates of change due to the instability. As a result, wave motion in the chamber may be neglected and chamber pressure can be considered to vary only with time but not to vary spatially (i.e., P_c is a lumped parameter). These instabilities depend upon a fluid mechanical coupling between the propellant feed system(s) dynamics, the propellant combustion rates (delay times) and the combustion gas exhaust rates (pressure relaxation). The driving energy comes from oscillatory combustion but this, in turn, results primarily from oscillatory propellant injection rates. This type of instability is always coupled with feed system, vibration and other effects, and may be further subdivided by the type of feed systems coupling present.

a. Chug (typical frequencies in the range 50 - 250 Hz)

Feed system coupling acts as a pure inertia effect, no wave motion is present in the feed lines.

b. Buzz (Typical frequencies 100 - 900 Hz)

Wave motion is significant in the feed system and may be quite complex. However, wave lengths are still large relative to the chamber dimensions so that wave motion in the chamber may be neglected, i.e., spatially uniform. With moderately high frequency buzz instabilities, it is not unusual to observe wave motion in the chamber, superimposed on the buzz oscillation. If the waves decay spatially, they have little influence on the buzz and analysis can often proceed with the lumped P_c approximation; if they grow, however, the buzz instability may be superceded by initiation of a chamber resonance-type of instability.

The principal differences between steady-state combustion processes and those occurring during chug or buzz instability are that propellant injection rates and chamber pressure are oscillating. If the oscillatory amplitudes are small, their effects on mean propellant atomization, mixing, burning rate, etc., may be insignificant. Even then, however, injection mixture ratio should be expected to oscillate, because of unlike injection velocities and oscillation amplitudes between the propellants, and to have some effect on overall engine efficiency. These moderate deviations from steady-state gradually worsen as instability amplitudes are increased until, at some amplitude, peak pressures are high

enough and last long enough to stop (or even reverse) propellant injection for a portion of each cycle. At this state, the propellant impingement, atomization, mixing, and even vaporization and combustion are very much more chaotic than steady-state and occur in a short, pulse-like fraction (perhaps 1/3 to 2/3) of each cycle of instability. The rest of the cycle is occupied with "blowdown" exhaustion of combustion gases from the chamber and, when the chamber pressure is again low enough, reinitiation of propellant injection.

This type of instability is accessible to analytical treatment and has received considerable theoretical and experimental study. Analysis traditionally follows the automatic control viewpoint of frequency-gain diagrams. Sophisticated treatments of injected propellant flows and accumulation effects (Klystron effect, Ref. 7) and feed system analysis have been added to the basic models. Usually the least well-defined parameter in the models is the combustion delay time, which must often be inferred or obtained from subscale experiments. Nevertheless, "fixes" recommended based on such models (usually in the form of increased injection pressure drop) almost always are able to eliminate the instability.

The breakpoint at which wave motion becomes important in the chamber is not abrupt. In reality wave motion is always there and, in effect, lumped chamber instabilities are really "zero order mode" limits of the following more general wave motion instabilities. In practice, it is found that the chamber gases can be considered to act as a lump until the frequency of

oscillation exceeds roughly one fourth of the frequency of the lowest chamber acoustic resonance mode, above which the wave motion becomes important. For this reason a third class of instability, sometimes referred to as "intermediate frequency," has been neglected. Instability analysis should either consider the chamber gases to act as an inertial lump or to exhibit wave motion.

Chamber Wave Motion Instabilities

This type of combustion instability is characterized by wavelength of the oscillatory motion comparable to the chamber dimensions and, consequently, wave motion in the chamber cannot be neglected. As with chug and buzz instabilities, the driving energy comes from oscillatory spray combustion. With these instabilities, however, in addition to the effects of injection rate fluctuation (if present) there is the combustion response of burning propellant sprays as they are disturbed by passage of a pressure wave through them. Wave motion may increase local burning rates by any of several mechanisms: (1) a pressure effect on the drop vapor, gas phase burning rates, (2) enhanced mixing between gases (such as stripping a vapor-rich wave from behind a droplet), and between sprays and gases (such as displacing a fuel-rich combustion gas into the neighborhood of an oxidizer-rich spray), and (3) increased spray gasification rates. Increased spray gasification may be due to transient increases in convective flow velocities, to increased temperature or concentration gradients, and/or to spray droplet shattering. The instability amplitude depends upon the magnitude of the

response, and vice versa; typically, the interacting processes are driven to a limit represented by abrupt, essentially complete consumption of the propellant sprays. This direct response can be so great that injection rate fluctuations may be of secondary importance. As a result this class of instability can also be further subdivided as to the importance of feed system coupling.

a. Acoustic Instabilities

In this case, feed system coupling effects are negligible. The instability is primarily a function of the driving and damping processes occurring within the combustion chamber. The wave characteristics of the instability are approximated by the modes of the combustion chamber filled with burned gases, hence chamber geometry resonance properties play an important role. Amplitudes of the pressure oscillations are usually very large.

b. Hybrid Instabilities

The most complex of all instabilities, the hybrid class involves a combination of wave motion in the chamber and feed system effects. Resultant frequencies may be (1) close to a resonant frequency for a closed chamber (chamber acoustic mode), (2) may occur nearer to the feed system resonant conditions (with the chamber having the same frequency by matching the boundary conditions at the interface between chamber and feed system), (3) or may occur at intermediate conditions which are near the resonant conditions of the combined chamber and interacting feed system. The feed system effects can

R-8377

be extremely complex. In some cases the amplitude of this instability may not be large, with more nearly sinusoidal shape appearance. However, because the entire engine system (chamber, feed system, etc.) is involved, structural vibration is often present and this can lead to severe engine damage.

Analysis of instabilities with wave motion in the chamber is extremely difficult. For example, no complete analysis of hybrid instability, considering the transient combustion process within the chamber and a highly oscillating feed system, has been accomplished. This type of instability is necessarily associated closely with the particular engine system and, because there are myriads of coupling paths between the chamber and the feed system for any one combination, it is doubtful if a general model describing this type of instability will ever be developed. All too often, even at rather high frequencies, this type of instability does occur in certain engines; and when it does it is only solved by approximate analysis, used at best for guidelines, and by time-consuming trial and error experimental fixes.

As a consequence the remainder of this discussion on non-steady models will be limited to those treating classical high frequency acoustic chamber resonance instability. Feed system effects i.e., wave (or lumped) response in the manifold and its lines are considered negligible; for practical purposes this consideration can be realized. Classical acoustic instabilities are among those most often observed in liquid rocket engines. This type of instability is entirely dependent on the detailed mechanisms of propellant

spray combustion energy addition to the oscillating gas dynamic flow field. Growth or decay of the instability wave then depends on the relative magnitude of the driving processes (those coupling the spray and gas flow fields) and the damping processes (droplet drag, viscosity, oscillating nozzle outflow, wall heat transfer, baffles, acoustic liners, etc.). The droplet dynamic transport processes are generally believed to have relaxation times, under the influence of strong waves, near to the wave residence time in a volume element. Consequently, energy coupling between the passing wave and the spray field is most likely to occur directly near the trailing edge of the passing wave.

Characteristics of "Acoustic Instability Waves". This instability manifests itself in the form of waves having many of the characteristics (frequency, nodal positions, etc.) of classical acoustic chamber resonance, considering the chamber to be closed and filled with only the burned combustion products of the propellants. Wave shape and amplitude are definitely, however, far stronger than those encountered in normal acoustic situations, sometimes approaching detonation-like conditions. It is perhaps surprising that the instability exhibits chamber resonance conditions, especially when one considers that: spray is present, the energy release is distributed axially throughout the chamber; there are accelerating through flow and discharge of products from the chamber, the axial mixture ratio and gas temperature gradient can be large and pressure amplitudes are large enough to make non-linear effects important. Apparently boundary conditions play a stronger role in

determining the modal conditions than these complications. For this reason, arguments of whether the instability is "acoustic" or "detonation-like" are immaterial; these conditions represent only the extremes of the actual spectrum of fluid mechanics which may control instability.

Both transverse (i.e., tangential and radial) and longitudinal modes are observed in cylindrical engines. In most cases the transverse modes are the most important. Instabilities associated with longitudinal acoustic modes rarely exhibit as severe departures from steady-state spray combustion as do the transverse instabilities. The longitudinal modes are, therefore, seldom destructive but may degrade performance, interfere with guidance, etc. Qualitatively, this lack of severe pressure oscillations is possibly due to the interaction of the wave and the nozzle boundary condition, and to the fact that most of the spray is concentrated nearer the injector face. Thus, for an appreciable portion of the non-linear wave's passage, it is propagating through a medium which is removing rather than supplying energy. Most engines utilize small contraction ratios and a great deal of the wave's energy is swept out the nozzle. Amplitudes of longitudinal instabilities have been shown to increase as the contraction ratio is increased; this apparently reduces the energy loss through the nozzle. In the more usual case of low contraction ratios, however, the combustion process during longitudinal instability may be not unlike that during a chug or buzz instability, but with the wave motion superimposed. The similarity may be more than superficial,

because the predominant cause of oscillatory energy release during such conditions is probably injection rate fluctuations.

Often different modes co-exist or they may combined to form a coupled mode. Instability frequencies as high as 18,000 Hz have been recorded although the more normal range is 500 to 5000 Hz. The tangential mode may exhibit both a traveling (spinning of nodal point) or standing nodal pattern. In addition, harmonics of the modes have been observed. The practical limit depends, of course, on the ability of the spray to respond to the frequency of the wave.

Further characteristics have been discussed thoroughly in the literature on liquid rocket combustion instability phenome., most recently in the ICRPG reference text (Ref. 8). Rather than duplicating such treatment here, several more or less self-explanatory charts are reproduced in Fig. 3 through 7 from a variety of sources. . more details, Ref. 8 may be consulted.

Disappearance of Zonal Regions in the Chamber. Under normal acoustic type instabilities, transverse and conceivably severe longitudinal, combustion processes are intermittently established and violently disrupted and there remains no resemblance to the steady-state distribution of spray combustion. What may appear momentarily to be a recognizable injection-atomization zone in the steady-state sense is greatly foreshortened by the instability. In viewing high-speed motion pictures of the injection region, taken during

R-8377

PURELY RADIAL MODES

PURELY TANGENTIAL MODES

COMBINED MODES

SECOND
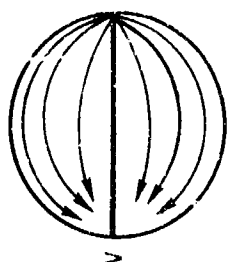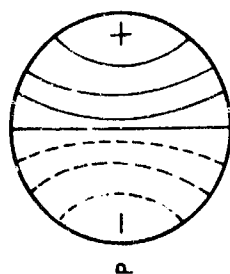
FIRST
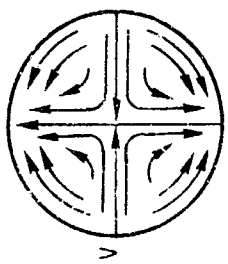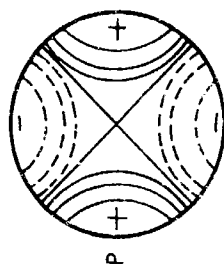
SECOND

FIRST

2ND TANGENTIAL
AND 2ND RADIAL
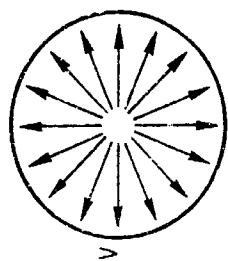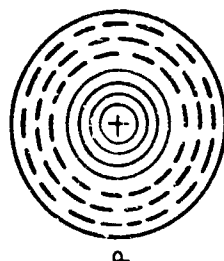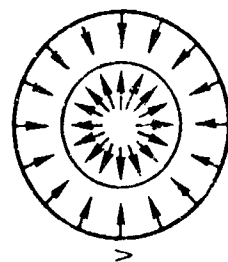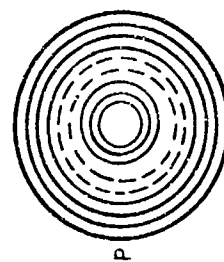
1ST TANGENTIAL
AND 2ND RADIAL
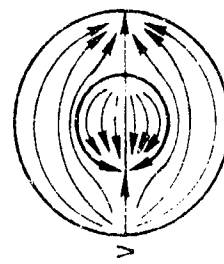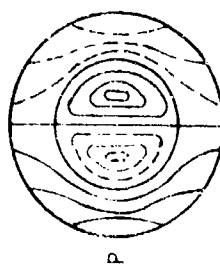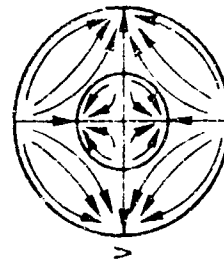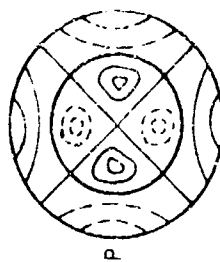
1ST TANGENTIAL
AND 1ST RADIAL

Figure 3. Pressure and velocity Characteristics of Some Typical Acoustic Modes

R-6377
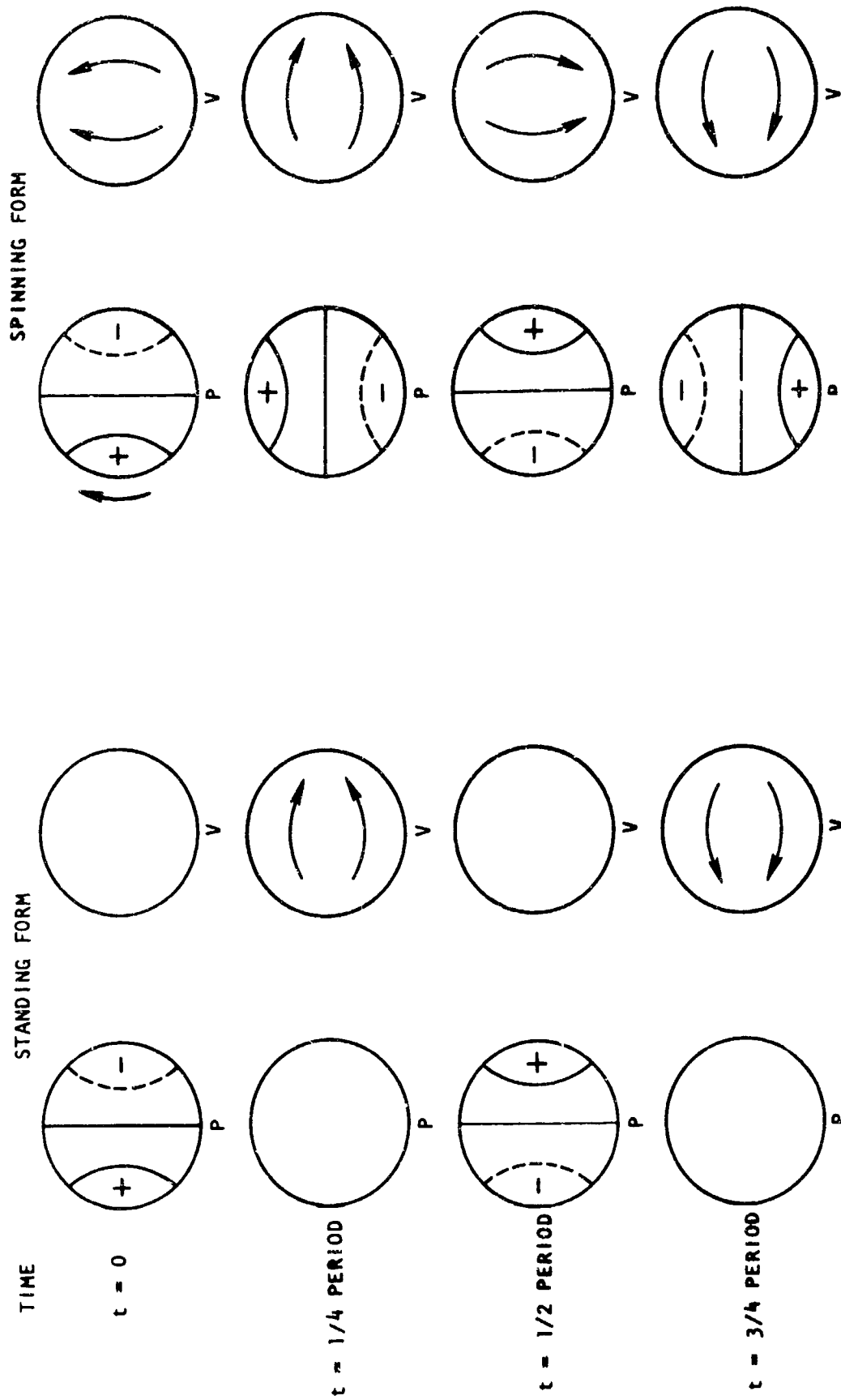
Figure 4. Standing and Spinning Forms of the First Tangential Mode

R-8377

30

STANDING TRANSVERSE WAVE

AMPLITUDE
0.1 TO 2.0
OF P_c

ANGULAR
POSITION

0°

90°

180°

TIME ———→

AMPLITUDE
0° ANGULAR
POSITION

$\dfrac{A_{CHAMBER}}{A_{NOZZLE}} = 10$

$\dfrac{A_{CHAMBER}}{A_{NOZZLE}} = 1.2$

INJECTOR   NOZZLE

CHAMBER
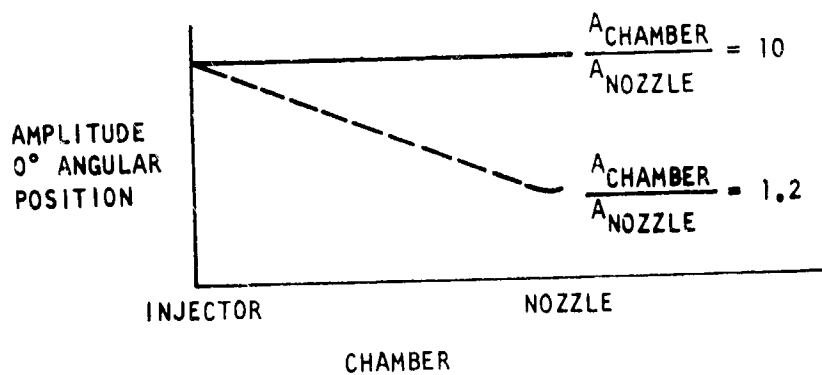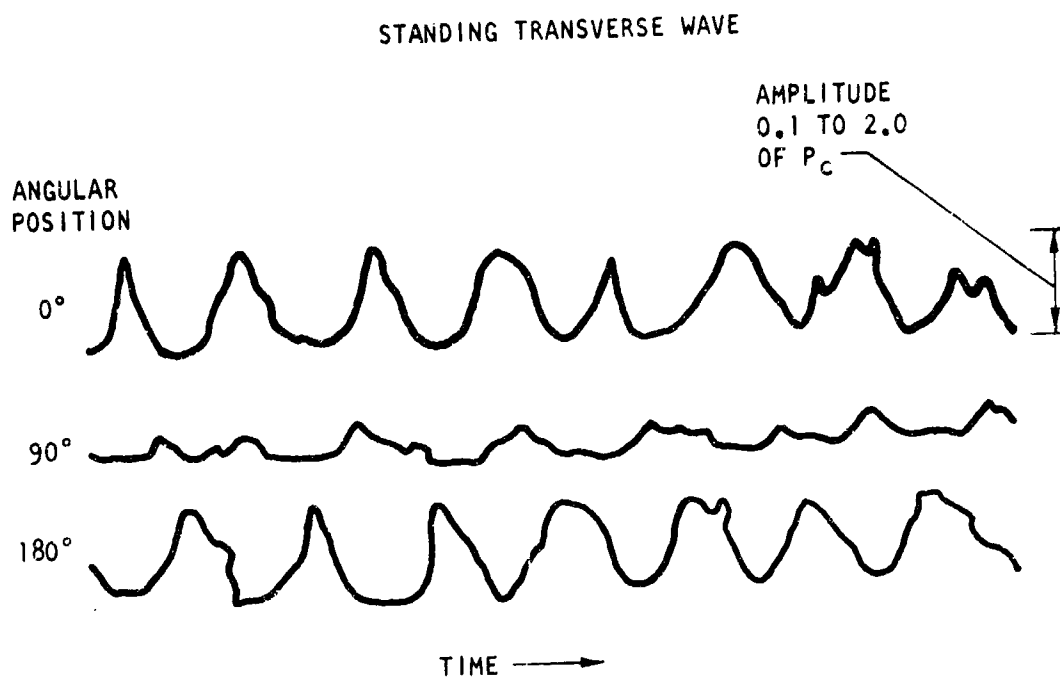
Figure 5 . High Frequency or Screaming Instability

TRAVELING TRANSVERSE WAVE
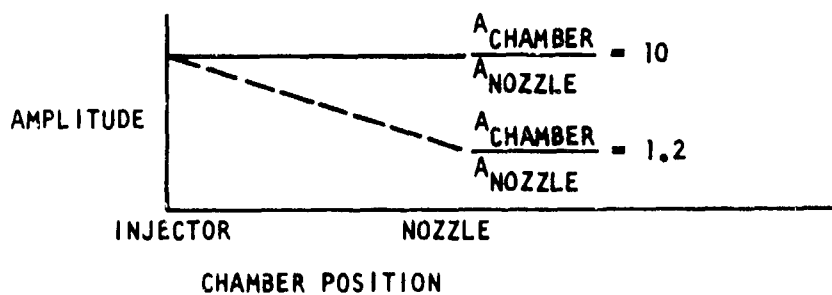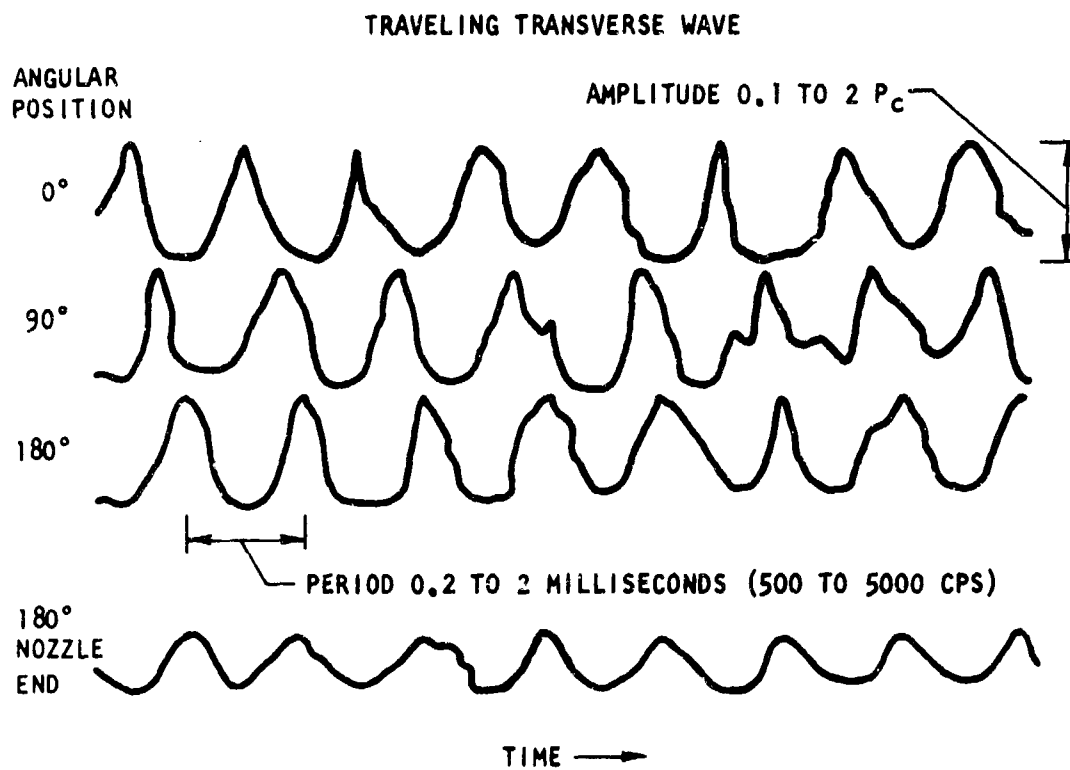
Figure 6 . High Frequency or Screaming Instability

LONGITUDINAL WAVE

INJECTOR AND FEED SYSTEM

AMPLITUDE 0.1 TO 2.0 OF P_c

PERIOD 0.1 TO 2 MSEC (500 CPS TO 10,000 CPS)

CENTER

NOZZLE

TIME ⟶

$$\frac{A_{CHAMBER}}{A_{NOZZLE}} = 10$$

$$\frac{A_{CHAMBER}}{A_{NOZZLE}} = 1.2$$

AMPLITUDE

INJECTOR   NOZZLE

CHAMBER POSITION
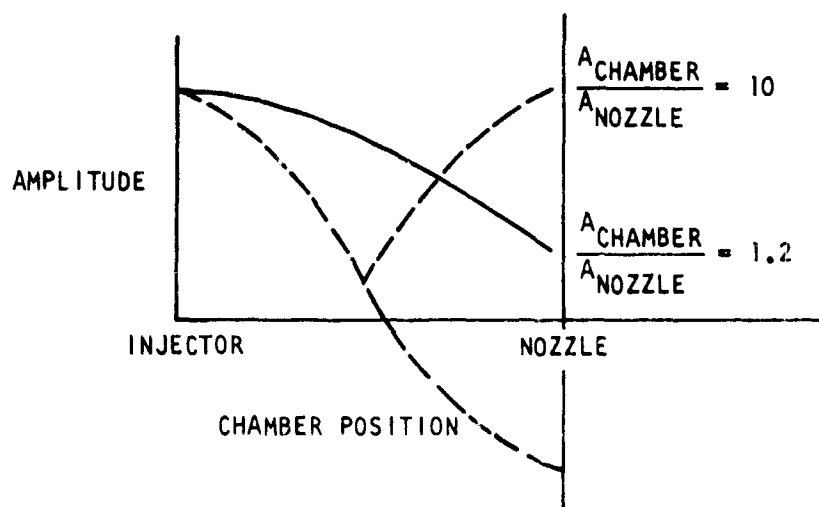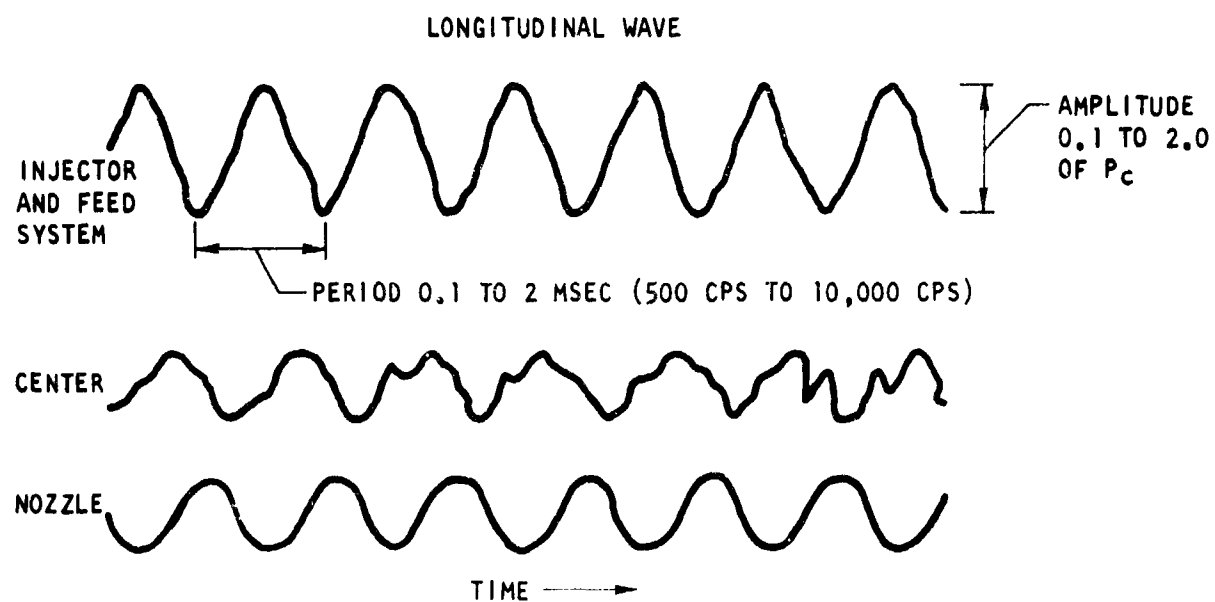
Figure 7. High Frequency or Screaming Instability

such unstable operation in transparent-walled combustors, a powerful impression of chaotic violence is gained that this paragraph but poorly imparts. For analyzing this kind of instability, it is inappropriate, therefore, to attempt to subdivide the combustion chamber into discreet zones, as has been done for steady-state analyses; the entire chamber must be considered as an entity.

A Note on the Relevance of Turbulence During Unstable Operation

Although mixing and turbulence effects were discussed for steady-state operation, little has been said of such phenomena in this section. Indeed, a reader familiar with the field will note that no existing combustion instability computer model contains turbulent equations. This is not due solely to the inordinate number of terms and problems that turbulization of the equations produces. Rather it is due to the more fundamental fact that the frequency of oscillation of the mean flow itself is comparable to or greater than the normally encountered frequency of turbulence. Hence, the definition of time-averaged perturbations becomes meaningless under these conditions. Further, the large convective gas flows due to the often extreme pressure gradients generated during unstable operation renders the consideration of true turbulence to a low priority.

R-8377

REVIEW OF EXISTING COMBUSTION MODELS -
STEADY STATE

There are on the order of 25 reported analytical models for steady-state liquid rocket combustor operation. Despite their differences, almost all prior steady-state analytical combustion models share certain common features. First, most are one-dimensional, which implies that all variables are functions only of distance along the axial flow direction. Transverse gradients in the gas-spray flow and recirculation currents of combustion gases are ignored, i.e., conditions are assumed uniform across the combustion space at any axial location. Secondly, most models deal only with the combustion of completely atomized sprays; additionally, in the one-dimensional models they are presumed to be uniformly intermixed at the upstream boundary of analysis. The injected sprays are most often assumed to be represented by a few discrete droplet size groups, each possessing unique values of average droplet diameter, temperature, velocity, etc. depending upon model complexity. Some models are simplified to the point of dealing with a single droplet size. Thirdly, spray vaporization has been adopted as the combustion-rate-limiting process in most models. This choice was corroborated by the definitive work of Brittker and Brokaw (Ref. 4).

Steady-state combustion models may be categorized and discussed according to the complexity with which the governing gas-spray conservation equations are treated, viz.:

a. One-dimensional, decoupled gas and spray flow fields

b. One-dimensional, coupled spray/gas flow fields, constant physical properties for the gas flow field.

c. One-dimensional, coupled spray/gas flow fields, variable gas flow field physical properties.

d. Quasi-one dimensional models (coupled gas/spray flows, variable properties)

    1. Some detailed injector models

    2. Simplified stream tube models

    3. Coupled stream tube models

e. Multi-dimensional model (coupled gas/spray flows, variable properties).

Within each of these categories varying degrees of sophistication were applied with regard to the "coupling terms" and the initial/boundary conditions. These will be discussed for each model considered in each category.

One-Dimensional, Decoupled Flows

Chronologically, such models were the first to be tried. By neglecting the coupling with the gas however, no true coupling terms are included, i.e., values cannot be calculated for droplet velocities or residence times,

droplet heating or breakup. The mass evaporation rate is calculated to depend only on the first power of the diameter (i.e., droplet diameter regression rate dependent on the reciprocal of the diameter); no convective influence can be considered.

Probert (Ref. 9) was the first to report such an analysis; subsequently his work was extended and refined by others (Ref. 10 through 13). Williams has given an excellent review of this approach (Ref. 14), including effects of various input droplet size distributions. Usually, because of the many parameters involved, results are plotted in terms of dimensionless parametric groups and only very generalized conclusions can be inferred. Even those reached by Williams in his text regarding the effect of droplet size distribution are now known to be substantially altered by droplet drag and convection.

The main advantage of this method was that it was entirely analytical and did not require numerical solution. While the theory was very incomplete and could not give quantitative answers to engine design questions, neverthless, it served as the forerunner for more complete models.

One-Dimensional, Coupled Flows, Constant Gas Properties

During the period when such models were being developed, questions arose concerning the correctness of the assumption that spray vaporization was the controlling process. Miesse (Ref. 15) and Adler (Ref. 16) developed one

dimensional models in the 1950's that were concerned primarily with gas phase reaction rates. Miesse's analysis, using an assumption that propellant vaporization was proportional to a linear regression rate of the droplet surface (a rate which was an order of magnitude too large), led to an inference that chemical kinetics was the combustion rate limiting process. This conflict was essentially resolved by the work of Bittker and Brokaw in 1960 (Ref. 4). They calculated theoretical maximum chemical spatial heating rates in combustion processes and showed that gas phase reaction rates are 10^3 to 10^6 times as fast as typical liquid rocket combustion rates. Thus, spray combustion rates are not significantly influenced by chemical kinetics, but rather are controlled by the physical processes of atomization, vaporization and gross gas phase mixing.

Exceptions to this conclusion might be chemical reactions occurring: (1) within the combustion gas/propellant vapor boundary layer surrounding a droplet (e.g., decomposition of hydrazine), and (2) in low-temperature combustion, which might result from extremely low or high mixture ratios (e.g., gas generator conditions or very poorly designed injectors giving gross nonuniformities in propellant distribution). Consideration of drop vapor kinetics properly belongs in the coupling term expression related to the drop burning rate, which is discussed in a later section. Mixture ratio striations cannot be modeled with a one-dimensional model, but they can be approximated by a multiple stream tube formulation discussed later. (Even if kinetic losses are not accounted for in such a stream tube model, large mixture-ratio variations are likely to so degrade performance that the design

is unacceptable, anyway.) Consequently, the one-dimensional models consider vaporization to be the dominant process in controlling the combustion rate.

One-dimensional models in the coupled flow, constant gas property category correspond to the first attempt to include the combined effects of an interacting spray/gas flow field. The earliest models in this category used an assumption of constant pressure throughout the chamber and considered both propellants (fuel and oxidizer) to be injected as fully-atomized liquid sprays. Relative differences between fuel and oxidizer droplet vaporization rates either were not considered or were assumed to be in a constant ratio equal to the injected mass mixture ratio. These assumptions result in a constant (and often excessive) axial gas temperature, a constant gas molecular weight, and constant gas density throughout the chamber. Under these conditions (having knowledge of the approximate flame temperature for the injected mixture ratio) the only gas conservation equation that is really required is the overall continuity equation.

Mayer (Ref. 17) was one of the first to develop such a model in 1959. His analysis, however, neglected droplet drag and convective processes by equating all drop velocities to the gas velocity. As a consequence this model would grossly under-predict performance for a given engine length.

Spalding (Ref. 18) extended Mayer's analysis to include the interaction of the droplets and gas. To maintain a closed form analytical solution Spalding assumed that all the droplets were of the same size (i.e., a monodisperse

spray) and neglected the difference between oxidizer and fuel droplets. Again, the burning rate was assumed to be inversely proportional to the first power of the diameter; this is a reasonable assumption if droplet temperature and gas composition and temperature are considered to be constants. (Most burning rate models, such as those of Godsave (Ref. 19) or Williams (Ref. 14) etc., reduce to this form under the above conditions.) The analysis at first neglected convection, but was later extended (Ref. 20) to include simplified corrections for the convective conditions. This was one of the first steady-state models that could account for some of the observed trends with liquid rocket engines. Williams has also given an excellent condensation of this Spalding model in Ref. 14.

Other similar models were reported during the late 1950's but the application of this approach to analyzing liquid rocket engines largely reached its culmination in 1960 with Priem and Heidmann's work (Ref. 21) on propellant vaporization as a design criteria for rocket combustors. They extended the analysis of previous authors to a realistic droplet size distribution and, for the first time within an overall model, considered droplet heating and its effects on vaporization. The formulation of Ref. 22, based on spherical heat and mass transfer between a high temperature gas and a contained droplet, was used. The analysis required computer solution. Although the assumptions of constant pressure and constant gas properties were retained, this was the first model in which a moderate degree of sophistication was applied simultaneously to both the gas phase and spray equations, to the coupling term expressions (burning and heating rates, drag coefficients), and to the initial

conditions. These developments were so important to useful applications of combustion analysis that Ref. 21 is sometimes the only work cited in reference to steady-state combustion models.

Priem and Heidmann also applied their model to correlation of experimental data from a range of research scale combustors with several different propellants and varied operating conditions. An empirical equation was developed for correlating changes in design parameters and operating conditions to evaporation efficiency or performance. This correlation has since been used by many investigators for rapid estimation of the effects of design change on performance. An interesting recent application was to multiple stream tubes (Ref. 23).

One-Dimensional, Coupled Flows, Variable Gas Properties

Programs in this category represent the most detailed and complicated of the modern, purely one-dimensional combustion models. They employ computerized numerical solutions and remove the restrictions of constant gas physical properties. All of them consider the spray to be input with known or specified drop size distributions. The first such model in this category was that of Burstein, Hammer and Agosta (Ref. 24) in 1962. While retaining the ratio restriction that rates of fuel and oxidizer spray vaporization occur at a constant ratio, this particular model included an integrated gas phase momentum equation and thus accounted for pressure variation along the length of the chamber.

In that same year, work at Rocketdyne culminated in the public .ion of Lambiris and Comb's state-of-the-art summary regarding stable combustion in liquid propellant rocket engines (Ref. 25), which presented the first complete non-restrictive one-dimensional combustion model. A complete set of conservation equations for both the spray and gas phases were included. In addition, appropriate expressions for the coupling terms were included. Godsave's formulation (Ref. 19) for droplet burning rate, modified for convective conditions, was applied independently to both the fuel and oxidizer sprays thus allowing inclusion of an axial mixture ratio variation. This, together with axial pressure variation, and tabulated combustion gas properties, yielded axially varying gas temperatures and densities. In addition, as in Burstein's work (Ref. 24), simplified expressions for droplet breakup were included. The initial sprays were input with specified distributions of droplet sizes. The use of empirical drag coefficient correlations which account for droplet flattening at high Reynolds numbers (Ref. 26) were also introduced in this computer program model.

Basically, this same model has been modified and enlarged by a number of investigators to include droplet heating (and its effect on mass vaporization rates), supercritical burning of droplets, gas phase injection of one propellant, and the decomposition double-flame front models typically applied to hydrazine-type fuels. The version developed at Dynamic Science (Ref. 27) has been disseminated rather widely. Improved numerical methods and extensive functional tables of physical properties were employed in the most recent version (Ref. 28).

In practice the gas phase energy equation has been simplified by employing the assumption that the composition and stagnation temperature of the gas are equal to the thermodynamic equilibrium values at the local gas-phase mixture ratio and stagnation chamber pressure. Other gas properties (static temperature, density, etc.) are evaluated from the respective stagnation values by applying local isentropic Mach number corrections under the assumption of frozen composition expansion.

This process, although not strictly valid for a reacting gas, consequently neglects heat and drag energy transfer from the gas to the drops. These terms are, however, properly included in the spray equations and the effect upon total burnout of the droplet is properly calculated (energy is conserved). Sutton (Ref. 29) investigated this assumption thoroughly by comparing the approximate results with results from an "exact" one-dimensional formulation which retains the complete energy equation and includes extensive tables of gas phase properties as functions of enthalpy, pressure and mixture ratio. He concluded that the simplified energy equation produced gas temperature errors on the order of 3 to 5% at low subsonic flow Mach numbers and influenced the droplet burnout location even less. Because the simplified energy equation permits use of simplified tables of combustion gas properties, based on standard thermochemical equilibrium calculations (e.g., Ref. 30), computerized models employing this approximation have been used extensively at Rocketdyne and other locations to aid in the design of new engines and to correlate performance data from existing engines.

More recently, only two significant additional versions of true one-dimensional models have been formulated. The first was by Hammer, Agosta and Peschke (Ref. 31) in 1966; this model incorporates the major provisions previously discussed and includes the complete formulation for the energy equation including the equilibrium solution. The second is the previously mentioned due to Sutton and Combs (Ref. 29); it incorporates a full energy equation similar to Hammer's et al., but uses tabular data from prior equilibrium analyses. In addition, axial direction effects of gas phase conduction, diffusion and viscosity are also included. The models of Ref. 31 and 29 represent the most nearly "exact" formulations to date for steady one-dimensional propellant spray combustion.

One-dimensional models have been extensively used. Their utility stems largely from the basic assumption of one-dimensionality. The analysis is nearly independent of the detailed features of the particular injector used (except for spray droplet sizes and velocities) so that a single model formulation can be applied easily and quickly to a wide range of injectors, propellants, combustors, etc. Hence, when applied to the downstream regions of engines which fall within the approximate domain of one-dimensionality, their performance predictions depend entirely upon the accuracy of input initial conditions and the expressions used for the coupling terms describing the interaction between the gas and spray phases. It is, in fact, the accuracy of the input conditions (especially the mean drop size and drop size distribution) that relate the one-dimensional model to the particular injector design and make it useful from a design standpoint. As a consequence, a great deal of auxiliary work has sought systematic determination of how spray

dropsize distributions and mean droplet sizes depend on injection element
design parameters, e.g., orifice diameters and injection velocities. This
has usually been done experimentally by using molten wax to simulate imping-
ing liquid propellants (Ref. 32). More recently the technique has been
extended to gas/liquid propellants where dropsize measurements are per-
formed in a pressurized rig, thus simulating the proper gas density,
velocity, and flowrate, Ref. 39. Minimization of recirculation for single
element tests, through use of a base bleed is taken into consideration.
Results, of course, are applicable to both one- and multi-dimensional programs.

The one-dimensional character of such models is also their major limitation.
When applied to engines that have even moderately nonuniform mixture ratio
distributions (e.g., wall film cooling), the models fail to predict perform-
ance adequately. They are similarly unable to provide information on local
multi-dimensional problems such as those which arise in studies of injector/
chamber compatibility. Adaptations of one-dimensional models such as those
described next have offered some approximate, but not complete, solutions to
these problems.

Quasi-One-Dimensional Models
The simple one-dimensional approximation is inadequate to describe the axial
flows and distributions existing near the injector of a liquid rocket engine.
As indicated above, it is important to avoid use of one-dimensional models in
this region. However, before adoption of the current approach of developing
empirical spray mass and dropsize distributions through cold flow and molten
wax studies, some quasi-one-dimensional combustion models were developed in an
attempt to calculate the progress of the propellant combustion within this

injection/atomization zone. Typically, multiple coupled one-dimensional
flows were assumed to represent the real flow associated with a single
injection element. Primary interest was in the degree of partial combus-
tion accomplished and in locating a reasonable starting point for the
downstream zone at which the one-dimensional approximation was applicable.

Some Detailed Injector Models. The first of these models (Ref.25)
related to self-impinging doublet injection. The model described the
region from the center of a fuel spray fan, through a forced mixing region,
to the center of a neighboring aligned oxidizer spray fan. A one-dimen-
sional flow zone was established for each of those regions and a fourth
zone was used for a gas flow (without spray) surrounding the other three
zones. Spray and/or gas transfer among zones was analyzed as combustion
proceeded. A number of poorly understood phenomena were lumped into
empirical "incomplete atomization" factors for each spray-bearing zone.

This was a highly physical model involving geometrical zone prescription
which drew heavily from high speed photographic records of transparent model
motor firings with aligned-element like-doublet injectors. Thus the compu-
ter program model was very specific for that type of injector and had limited
versatility. It was not possible, for example, to analyze injectors with
elements aligned only on one side, etc. As a result it received only limited
use and principal reliance was placed on the one-dimensional model for com-
bustion analysis of all impinging-type elements.

R-8377

A second model, however. because it dealt with the more readily generalized analysis of coaxial gas-liquid injection, has found extensive use. The need for such a model was soon recognized after attempting to correlate performance from such an injector with the basic one-dimensional model. Unlike the impinging type injector, which atomizes the entering jets near the injector face. the gas-liquid coaxial injector may have a liquid jet penetrating 3 to 4 inches from the injector, with simultaneous atomization and burning strongly coupled and distributed throughout that length. Since cold-flow correlations cannot possibly include effects of superimposing combustion on the atomization rates and drop sizes, their principal value for coaxial elements lies in mixing studies rather than in providing combustion model dropsize initialization. As a result, a model for this widely used injector type must include both the atomization and vaporization processes in the formulation.

The first generalized coaxial model (Ref. 33) was formulated for axisymmetric, cylindrical single element combustion, assumed to be representative of the overall engine combustion. In its original form it applied strictly to injectors having "flush posts," i.e., both an inner cylindrical tube through which the liquid propellant was delivered, and a surrounding annular space for passage of the gaseous propellant were terminated at the injector face. Upon injection, large velocity differences immediately initiate "shear-stripping" of liquid spray from the jet surface. Appropriate equations were contained within the model for calculating both jet stripping rates and local mean drop sizes produced.

Initially, there were two discrete parts to the model. The first, adjacent to the injector, was characterized by an onion-skin type layered structure of spray. This region was assumed to be axisymmetric and non-combusting. When input conditions regarding flammability limits of concentration and flame velocity were satisfied, flame spreading was assumed to be rapid enough that the non-burning region was terminated by a plane flame front standing in the spray laden gases.

The second part of this model was like that of the usual one-dimensional model except that it (1) added a residual liquid oxidizer jet that penetrated into the combustion zone and retained equations for the subsequent atomization of that jet, and (2) allowed for a second zone of axially flowing, fully-burned or non-burning gases surrounding the combusting one-dimensional spray-gas mixture. Mixing between zones was approximated by specifying (input) a linear rate of ingestion of the outer gas flow into the spray-gas flow. In addition, the outer zone was completely coupled to the inner zone through the assumption of no radial pressure gradient. Both zones obeyed their respective conservation equations and their areas were mutually adjusted to match the axial pressure gradient profile and still maintain a full-flowing chamber. This portion of the model is the forerunner of current multiple stream tube models discussed later.

Recently Sutton and Schuman (Ref. 34) have redeveloped the model to bring the one-dimensional zone up to the injector face, and in addition, developed equations to describe the process occurring within the recessed "cup". Excellent results have been achieved with this model when predicted performance

has been compared with measured values from engines such as Rocketdyne's J-2, J-2S and Aerospike. These particular engines are built to deliver relatively uniform flow fields for highest performance.

Simplified Stream Tube Models

In contrast to the foregoing, highly physical models for single element combustion, a quite different quasi-one-dimensional approach considers the entire combustion field to be composed of a large number of stream tubes, with non-uniform striated flows created by the injector persisting throughout the chamber length. Introduced by Wrubel (Ref. 35), analyses neglecting mixing between neighboring stream tubes have been applied to both injector/chamber compatibility (Ref. 36 and 37) and combustion inefficiency (Ref. 23 and 32) problems. The utility of a stream tube approach depends upon how realistic it is to neglect turbulent mixing and, further, upon accurate description of the injector-imposed striations (i.e., whether or not the convective cross flows of the rapid combustion zone appreciably changes the cold flow measured injector striations).

Turbulent mixing between unlike gases flowing in adjacent stream tubes has been shown to proceed slowly (Ref. 6) and, within the short gas residence times typical of rocket combustors, is believed to contribute far less to overall propellant mixing than the spray interdispersion associated with injection and atomization, although this has not been unequivocally proven. Injector-imposed striations in the flow are usually characterized experimentally; cold-flow techniques are well-established for bipropellant liquid injection (Ref. 38, 32). Immiscible propellant simulants are flowed through an actual rocket injector and a collection apparatus is used to sample the flow at a large number of points in some downstream plane. Both mass flux and mixture ratio distributions are derived from the liquid collection data. Again, this technique has recently been extended to gas/liquid propellant

systems and mass measurements are often made in a pressurized rig through use of a special two-phase gas probe, Ref. 39. Minimization of recirculation through use of a base bleed is again considered and the probe has gas sampling capability to determine the amount of extraneous gas injected. Naturally, all valid cold flow results are applicable as initialization parameters for streamtubes or full three-dimensional programs. Their direct use in the streamtube case is of course limited to more uniformly injected spray patterns. In fact, for most of the injector elements and patterns using liquid/liquid propellants an analytical spray initialization program is now available that replaces the need for cold flow measurements, Ref. 37. Such programs are not yet available for a general description of gas/liquid or gas/gas injection. As an application example, the mean $c*$-efficiency among n stream tubes, each having flowrate $\dot{w}_n$ and mixture ratio C_n may be approximated as:

$$\overline{\eta_{c*}} = \frac{\sum\limits_{n} c*(C_n)\dot{w}_n}{c*(\overline{C}_i)\sum\limits_{n} \dot{w}_n}$$

where $c*(C_n)$ is a function of mixture ratio and $\overline{C}_i$ is the mean injection mixture ratio.

In addition to the incomplete mixing accounted for by the foregoing, there also may be appreciable degradation of performance due to incomplete spray gasification. While these two sources of performance loss may be coupled, with the presence of one making the other worse, the simplest approach is to treat each separately and assume that their combined effect is the product of the two. Thus, a wide range of experimental $c*$ efficiency data has been correlated successfully (Ref. 39 & 40) by:

$$\eta_{c*,\text{pred}} = (\eta_{c*,\text{mix}})(\eta_{c*,\text{evap}})$$

where $\eta_{c*,mix} = (\overline{\eta_{c*}})$ is the mass-weighted mean c* efficiency among the stream tubes, assuming complete evaporation within each stream tube and that there is no mixing between them, and $\eta_{c*_{evap}}$ is a mean spray evaporation efficiency, calculated by one-dimensional combustion model analysis for mean initial-plane conditions obtained by mass-weighted averaging over all stream tubes, i.e., assuming complete mixing. Neglecting the coupling between mixing and evaporation losses appears to be justified, to a certain extent, by the degree of correlation attained; in the cited references, the predicted efficiencies were consistently within about ±1% of the experimental hot-firing values, which ranged from about 85 to 99%.

A somewhat different, uncoupled stream tube approach was taken in Ref. 23, where the stream tubes were initialized near the injector and a separate one-dimensional spray combustion analysis was performed for each stream tube utilizing Priem's empirical correlation equation referred to earlier (p.47). Imperfect mixing was accounted for by mixture ratio variation from stream tube-to-stream tube and the combustion analysis accounted for in-complete evaporation. Regarding interactions between mixing and evaporation within a given stream tube, then, this formed a coupled model. Uncoupling took the form of absolutely no interactions between stream tubes. Initial-ized with a given percentage of the chamber cross-sectional area, each stream tube was thereafter assigned that percentage of local flow area. As a re-sult, neighboring stream tubes with unequal mass fluxes or unequal specific burning rates could be said to be flowing side-by-side with quite unlike pressures. Starting with a uniform injection-end pressure could not,

therefore, result in calculation of sonic flow at the geometric throat positions for all stream tubes simultaneously. Such physical unrealities made little difference to the Ref.23 application of the results; only an integrated, overall approximation of energy release inefficiency was required for subsequent use in analyzing the nozzle expansion efficiency. As with the preceding application to c*, the predicted values of specific impulse were shown to be in agreement with some experimental values.

Coupled Stream Tube Models

The lack of physical reality associated with the foregoing simplified stream tube models makes them inapplicable to situations in which local details of the combustion flow field are of interest. For example, analysis of combustion chamber wall heat transfer, ablation and erosion requires detailed local combustion gas temperatures, velocities and compositions as well as information about spray splashage on walls. Two related stream tube combustion models have been developed which provide improved approximations to reality in coupling together a multiplicity of one-dimensional combustion models, one for each stream tube, and solving them simultaneously. One model, developed in conjunction with an injector/chamber compatibility analyses (Ref.37), was designed for use downstream of a three-dimensional model of the rapid combustion zone (see the next section). It was extended (Ref. 41) to axisymmetric flow in the second version, includes the earlier stream tube initialization directly from injected flows, and utilizes a spatial distribution of pressure in the nozzle to make the transonic flow portion of the

solution more nearly realistic. By using a one-dimensional, coupled spray/ gas flow formulation, these models were made fully-coupled. They are still based on the assumption of no mixing (i.e., no mass, momentum or energy exchange) among stream tubes.

The model formulations differ from the one-dimensional formulation in several important ways, which arise from the fact that that a given tube is not physically confined by walls but is permitted to be squeezed to a smaller size by higher flowrate, faster burning neighboring stream tubes (and vice versa). That is, in the previous one-dimensional models, the cross-sectional flow area is a known, independent parameter, while in the multiple stream tube formulation, it appears as a dependent variable for which solutions must be found. Cross-sectional areas of individual stream tubes can vary, however, only under the constraint that the sum of all stream tube areas must equal the local chamber cross-sectional area. This constraint, in the form of an area conservation equation, is what couples one stream tube's combustion model to the others.

If there are S stream tubes, there are S sets of one-dimensional model equations. Only one equation (area conservation) has been added in the multiple stream tube formulation, while S dependent variables (areas) have been added. To close the problem, therefore, either $S - 1$ equations must be added or $S - 1$ dependent variables removed. The approach taken in Ref. 37 was removal of dependent variables by assuming that static pressure is constant across any given plane normal to the mean flow, rather than varying from stream tube to stream tube. The computer program solved for the

pressure level at each plane, beginning at an initial plane near the injector and marching to the throat.

Programmed for computer solution, the first version stream tube combustion model was one in a series of related computer programs for overall injector/chamber compatibility analyses. While it was possible to assemble input data manually from full injector cold-flow data (as with the preceding simplified stream tube models) or from a Liquid Injector Spray Pattern computer program output, it was structured to receive punched-card input data generated by its immediate predecessor in the series, a three-dimensional combustion model described in the next section. Similarly, it generated punched-card output for subsequent Boundary Layer Heat Transfer program analysis (Ref. 37).

This stream tube model of Ref. 37 was "formless" in the sense that not very specific knowledge was needed concerning a tube's position or cross-sectional shape. As a result, the downstream boundary condition was assumed to be one-dimensional sonic flow through the nozzle throat plane. The model in its second version was given a specific spatial form in Ref. 41 by specifying axisymmetric annular stream tube flow. Adopted to conform to the JANNAF (ICRPG) reference Two-Dimensional Kinetic computer program (Ref. 42) analysis for the supersonic nozzle expansion, this configuration gave stream tube positional data which permitted much more satisfactory nozzle analysis, by means of two model extensions. First, the longer path lengths taken by stream tubes nearer the wall than those near the chamber axis could be accounted for analytically by using each tube's actual path as the independent variable, rather than chamber axial length. Second,

the stream tubes' pressures in the nozzle could be made to conform to those for transonic flow. (In practice, these were simplified to local conical convergence - or divergence - and to the pressure distribution for a homogeneous, constant flowrate transonic flow.)

The axisymmetric stream tube combustion computer program was combined, in the work of Ref. 41, with other distinct computer programs to form an overall engine performance analysis computer program which begins with analytical computation of bi-propellant spray distributions produced by a prescribed injector design and ends with calculation of specific impulse and thrust coefficient for vacuum exhaust of combustion products from the nozzle. The three-dimensional combustion model, because its results currently need to be examined for consistency before proceeding with further analysis, was omitted from this combined model. Thus the axisymmetric stream tube model was initialized directly from the calculated injected spray distributions, unlike its predecessor. Similarly, it provided partial initialization of flow data along a supersonic start-line for analyzing the flow in the divergent section of a nozzle.

Multi-Dimensional Model

As a part of the injector/chamber compatibility analysis of Ref. 37, a three-dimensional steady-state spray combustion model has been developed for analyzing the "rapid combustion zone" of Fig. 2. The model formulation is based on three major simplifying assumptions concerning the combustion field. First,

it is assumed that immediately downstream of the injection/atomization (pre-reaction) zone there are strong enough transverse gradients in spray mass flow (and, therefore, in burning rate) to produce transverse convective flow forces which are large compared to gas-phase viscous forces. The viscous terms in the gaseous momentum equations are, therefore, neglected. The second assumption, that accounting for turbulent motion is not required, follows directly from the first. The third simplifying assumption concerns the transverse pressure gradients; before stating it, the model formulation will be describe

The mathematical formulation for the 3-D combustion model utilizes the cylindrical coordinate system (r, Θ, z). Because there are three independent spatial variables, the mass, momentum, and energy conservation equations (for both the combustion gas and propellant spray phases) are partial differential equations. These sets of governing equations are coupled through mass, momentum, and energy exchange between phases; several additional equations provide values for the coupling terms. The gas phase energy equation has been replaced by tables of combustion gas stagnation properties as functions of mixture ratio (for a given chamber pressure) and the adiabatic expansion equation. Specification of appropriate initial plane and boundary conditions completes the model.

The system of equations is solved by means of a digital computer program. "Marching" in the axial (z) direction is used, with simultaneous solutions at discrete nodal points in the r, Θ plane found sequentially in predictor-corrector cycles. The gas-phase conservation equations are partially elliptic

and, because elliptic partial differential equations are not well-posed as initial-value problems, the third simplification was introduced to avoid the numerical instability certain to result from that fact: the pressure gradients in the r,Θ directions are prescribed, rather than calculated as dependent variables.

Unless the pressure gradients are prescribed properly, the transverse gas velocities will differ from reality approximately as the square root of the errors in pressure gradient. Because of this, the 3-D model is properly viewed as a transition model which acts to distribute the propellant sprays more realistically before starting a stream tube analysis than if the stream tube structure had been begun immediately after the pre-reaction zone.

As reported in Ref. 37, transverse pressure gradients were effectively forced to vanish by making axial gas velocity a function of z only. Improving upon this simplification is one of the goals of current research on improving the injector/chamber compatibility analysis method.

Summary of the Steady-State Review

This review includes current as well as previous steady-state programs. The coupled stream tubes and three-dimensional formulations are actually digital computer programs corresponding to the generalized formulations developed under this contract. In this respect they are believed to be the best and most complete multidimensional models presently available.

As is shown later, evaluation of the coupling terms under steady-state conditions requires use only of a one-dimensional model. There are several existing ones that could have been used, Lambiris and Combs (Ref. 25), Sutton and Schuman (Ref. 34), or Hammer, et al (Ref. 31). However this model is also required to supply the initial conditions for the transient model and a new transient model was required. Hence, to insure that the one-dimensional steady-state model was sufficiently general to allow evaluation of coupling terms and also to provide compatible inputs to the new transient model, a new generalized steady-state model was developed. This model is the one mentioned in the review, i.e., Sutton and Combs (Ref. 29) and also represents an outgrowth of the generalized formulation developed under this contract.

REVIEW OF EXISTING COMBUSTION MODELS -
TRANSIENT

The addition of time as an independent variable, in a combustion model formulation for rocket combustion, complicates the analysis far beyond that of the steady-state problem. For this reason, and because detailed experimental combustion distribution data for evaluating model predictions are much more difficult to obtain than steady-state data, instability analyses have not been developed as far toward accounting for spatial combustion details as have steady-state analyses. Until quite recently, instability analyses could be distinguished and subdivided instead according to whether feed system coupling (lumped P_c) or chamber wave motion were considered dominant and whether combustion was treated in an approximate integrated manner or in a more physically-based, differential way.

The full range of liquid rocket combustion instability analysis has recently been fully systematized and detailed in the forthcoming ICRPG reference book (Ref. 8). Within the scope of this report, only those involving combustion chamber resonance, and further, those lacking feed system coupling, are of interest, i.e., acoustic instabilities. Little work has been done on modeling of more complicated instabilities.

The central problem in analyzing chamber resonance instabilities is obtaining solutions in one or more spatial dimensions and time, either numerically or with analytical approximations, for a coupled system of nonlinear transient conservation equations with appropriate boundary conditions. Constant injection rates are assumed for the injection-end boundary condition, with no coupling to the feed system. The instabilities treated are acoustic resonances of the combustion space, with complications introduced, as noted earlier, by two-phase flow and combustion. Formulations in one-dimension and time represent longitudinal modes of instability. The transverse (tangential and radial) modes require transient formulation in two spatial dimensions, at least.

Non-steady models, whether one or multi-dimensional, consider the liquid propellants to be injected as sprays containing (at best) a range of discrete droplet size groups. Assumptions with regard to the spray behavior are the same as those developed for the steady-state models. Non-steady models are always started downstream of the injection process, after atomization, etc., has been completed. To date, none has attempted to describe the transient

behavior of the entire mixing-atomization region near the injector in the presence of high amplitude oscillatory conditions. To couple this region with the spray region downstream, the analysis would be required to describe the details of the transient spray flow from each element in the injector and couple this information with a full three-dimensional transient combustion model extending to the supersonic portion of the chamber. It is not surprising that this task has not been accomplished and that all existing models, regardless of their complexity, neglect the detailed behavior of the injection region. Consequently, most analyses that include droplet dynamics employ the assumption that droplets enter directly into the chamber through the injector face and that the transient distribution of spray mass at the injector face remains as it was during the steady-state condition. Gas phase conditions depend on whether gaseous propellants were injected; if not then the axial component of the gas velocity at the face is assumed to be zero.

The effect of neglecting the near injection region on the accuracy of stability predictions is not entirely clear. It appears that, for liquid-liquid or gas-liquid impinging type injectors with strong hydraulic momenta, jet breakup and mixing would occur rapidly even under steady-state conditions and the effect of the wave on the jets themselves could be neglected. The more important phenomena probably involves the effect of the wave (break-up, inter-element mixing, etc.) on the dense spray field. This may not, however, be the case for shower-head or co-axial-type injectors. Here, the atomization processes control much

of the combustion rate and coherent jets may exist as far as 3-4 inches into the chamber. The effects of strong waves on primary atomization may be important for these types of injectors.

Time Lag - Perturbation Models

The earliest instability models used a nonphysical global treatment of combustion, i.e., the time lag concept introduced by von Karman in 1941. This approach was well developed for feed-system coupled and longitudinal instabilities (Ref. 43) before the more nearly physical, local spray combustion models were applied to instability analysis. These two distinct approaches have since been developed concurrently.

In 1951, Summerfield published the first theory (Ref. 44) dealing with unstable combustion in liquid propellant rocket motors. Both he and Tsien (Ref. 45) used the concept of time lag in its original form as a characteristic constant for each rocket motor. Crocco (Ref. 46) first introduced the idea of a time varying combustion time lag, $\mathcal{T}$, in his analysis of high frequency longitudinal instability modes. With this concept a total time lag was used to approximate the effect of the combustion process, i.e., products of combustion from a given element of injected propellant were considered to appear instantaneously after a discreet, well-defined time interval after injection. This artifice allowed the specific details of the combustion process to be ignored. The magnitude of the time lag may be considered to vary with local conditions in the chamber as well as with time.

The rates of the various processes occurring during the time lag were assumed to depend on (correlated with) the values of the local pressure. (All other factors were not implied to exert negligible influence on the rates; rather, their variation, and therefore, their effects, are described by pressure effects.) The correlating parameter, n, is known as the interaction index. In its simplest form, the time variation of $\mathcal{T}$ was assumed to be related to n, mean pressure, the pressure perturbation amplitude and $\bar{\mathcal{T}}$, (the space/time average of $\mathcal{T}$). In the model formulations the coupling term for the perturbed spray mass addition rate to the gas was replaced directly by the parameters n, $\bar{\mathcal{T}}$ and the pressure perturbation amplitude.

A downstream boundary condition was defined at the beginning of nozzle convergence in this and all subsequent time lag models. Proper representation of this boundary conditions became extremely important and consequently the models include lengthy analyses of the behavior of supercritical nozzle flow under oscillatory conditions. Indeed, in some of the models, attention to satisfying the downstream boundary condition was more elaborate than the treatment of chamber combustion phenomena.

Crocco and Cheng (Ref. 43) first treated linear longitudinal oscillations via the time lag concept. Later Scala (Ref. 47) and then Reardon (Ref. 48) extended the linear analysis to include transverse (three dimensional) oscillations. Reardon developed a more complicated dependency of the perturbed burning rate on interaction indices corresponding to radial and tangential velocity

perturbation effects as well as local pressure. In addition, his burning
rate expression approximately related the distribution of combustion to pro-
pellant injection density distribution. The only droplet coupling term
specifically retained in these analyses was droplet drag which appeared in
a simplified form. Droplet heating and other effects were neglected.

For stability predictions, the time lag models employed the classical approach
of linear acoustics (small perturbation) referenced to the one-dimensional,
steady state operation conditions. Neutral stability conditions, wherein
amplitudes neither increase nor decrease with time were established. The
locus of operating points of the system which satisfy the conditions for
neutral oscillation formed stability limits, dividing unstable and stable
regions of operation. These stability limits were presented in terms of
dependency upon n and $\bar{\tau}$.

The linear time lag models are based upon first order perturbation of transient
equations of motion. Appropriately transformed and with the downstream boundary
condition applied, the models provide two equations relating three dependent
parameters: n , $\bar{\tau}$ and the eigenvalue or resonant angular frequency of the
chamber, ω . Specification of any one of these allows calculation of the
other two. The most convenient procedure is to prescribe the value of ω ,
and solve for n and $\bar{\tau}$.

Recently a monograph by Crocco and Sirignano (Ref. 49) has been published which gives a complete description of the analysis of the oscillatory flow behavior of supercritical nozzles.

The time lag models have serious defficiencies. The linearization restricts their applicability to the growth of instability from infinitesimally small disturbances, they cannot be used to analyze the commonly observed, abrupt initiation of instability by sudden finite amplitude disturbances. The sinusoidal wave forms predicted by the models are quite different from the non-linear shapes frequently observed in pressure measurements on actual engines. Finally, the linear studies cannot predict anything about the ultimate, limiting value of oscillation amplitudes.

To overcome these difficulties, partial non-linear extensions to the linear theory have been developed. Sirignano (Ref. 50) and Zinn (Ref. 51) studied, respectively, longitudinal and transverse mode combustion instability for pressure waves of finite amplitude. Both authors, however, assumed that mass and energy addition occurred only in an arbitrarily thin region next to the injector face. Sirignano employed the short nozzle assumption (Mach number at the nozzle entrance remains constant) while much of Zinn's work was devoted to the oscillatory nozzle flow. Zinn's work represents the most complex treatment of the nozzle to date; he used a third-order perturbation approximation and required that the nonlinear waves be continuous. With both models periodic finite wave amplitudes were proportional to the square

root of the normal displacement from the linear stability limit. (Inter-pretation of portions of these waves indicated that triggering of finite amplitude oscillation is possible. However, the waveforms exhibited none of the sharp peaks observed in experiments, which is not unexpected with a perturbation approximation.)

Oscillation frequency was assumed to depend on the magnitude of the power series expansion factor used in perturbing the equations. Frequency devia-tions from the linear solutions, due to finite amplitude waves, were indeed found to depend on the order of the expansion factor required. The results were strongly dependent on the form of the imposed boundary conditions, one of which was concentrated combustion at the injector face. This condition is difficult to relate to actual processes. Major difficulties with these two models are their great algebraic complexity and their inability to predict waveforms and nonlinear behavior for values of n and $\bar{\tau}$ that are not close to the linear stability limit. The characteristics of instabilities triggered by finite disturbances cannot be found.

Mitchell (Ref. 52) extended the longitudinal case to include the effects of distributed combustion, discontinuous waves, and nonlinearities with n and $\bar{\tau}$ values reasonably far removed from the linear stability limit. Mitchell's approximation is valid only to second order in shock strength, i.e., to the order of the steady state Mach number at the nozzle entrance. Hence, although it extends the nonlinearity of previous analysis, the consideration of most nonlinear coupling terms is still limited. No consideration was given to droplet drag or heating.

Recently Zinn and co-workers have employed an approximate numerical scheme
which is a modification of the Galerkin method. The method facilitates
approximate solution of the nonlinear partial differential equations com-
prising instability models. Preliminary results indicate the approach is
promising, Ref. 53.

Thus, several problems with the time lag approach are evident. First, the
concept itself eliminates consideration of the actual physico-chemical com-
bustion processes that occur in the liquid propellant rocket engine. Further,
stability limits are presented in terms of n and $\bar{\tau}$; therefore, the assump-
tion must be made that each engine (i.e., injector type, flow distribution,
contraction ratio) has particular values of n and $\bar{\tau}$. Knowing these, one can
then determine stability of the engine. However, it is very difficult to
determine these parameters for a particular engine configuration. Although
experimental effort has been and is being pursued (Ref. 54) to determine
reasonable approximations of n and $\bar{\tau}$ for actual engines, the results are far
from being complete enough and general enough for application to wide ranges
of propellants, engine, and injector designs. Application of the sensitive
time lag theory is the subject of a computer program user's guide (Ref. 55)

Use of perturbation techniques in the model formulations introduces unavoid-
able problems to any attempt to obtain nonlinear solutions. Most of the models
consider only first order (linear) effects; at best second or third order
effects are considered. As the order or the approximation increases the

algebraic manipulations become prohibitively complicated. As Mitchell

has pointed out in his paper, the successful analysis of even slightly

nonlinear problems depends critically on the selection of the proper

expansion parameter in the perturbation analysis, and the basis for

selection is not always evident.

Finally, in all of the aforementioned models, a major fault lies in the

basic development of the conservation equations. Although the gas pnase

continuity and momentum equations are developed correctly, the lack of a

locally time varying mixture ratio equation renders the energy equation

and the equation of state inaccurate. In particular, the equation of

state is written as

$$P = \rho RT$$

Where R = constant, i.e., no consideration is given to axial variations of

the molecular weight. Also no consideration is given to dissociation effects

in the energy equation; specific heats are taken to be constant. The steady

state initial conditions $(\bar{p}, \bar{T}, \bar{\rho})$ are taken to be constant throughout the

chamber. These assumptions limit the models, regardless of their other assump-

tions or perturbation techniques, to consideration only of liquid bi-propellants

whose fuel and oxidizer sprays always vaporize in a constant ratio of rates

equal to the injected mixture ratio. Further, the form of the conservation

equations, regardless of the perturbation order, requires the pressure wave

amplitude to be small so that it does not disturb the local mixture ratio.

These considerations make the time lag models inapplicable to hydrogen/oxygen propellants, as one example. Axial molecular weight variations with these propellants may range between 2 to 12. Even low amplitude waves in H_2/O_2 engines can drastically alter local mixture ratios due to the high gasification response rate of liquid oxygen spray. Consequently, with temperature overpredicted by an energy equation (neglecting dissociation) and pressure determined from an equation of state that neglects mixture ratio variations, the resultant pressure may be overpredicted or under predicted by factors of 2 to 4 or more. Even though the assumptions regarding the equation of state are allowable to the order of the perturbation analysis, it cannot properly be applied to a real engine system triggered by a finite disturbance. This serves further to indicate the limitations of perturbation analysis to highly nonlinear systems.

In this vein, it is interesting at this point to consider some results from Culick's 1961 Ph.D. thesis on gas and liquid rocket combustion instability (Ref. 56). Culick did not assume a time lag concept, but did employ a first order (linearized) perturbation analysis. In this respect the model is similar to those of Scala and Reardon, although Culick used different techniques to obtain the downstream nozzle boundary conditions. The equations used in Culick's model differ from Reardon's and Scala's only in that he neglected droplet drag, the momentum source term due to mass addition and the droplet velocity (items often neglected by many other authors and usually believed to contribute little to the problem). Upon first order perturbation

R-8377

and assuming that $\bar{p}$, $\bar{T}$ and $\bar{\rho}$ are constants throughout the chamber at steady state conditions (consistent with the perturbation order and equivalent to Scala's and Reardon's work), Culick was able to show that the perturbed continuity equation (which is solved for ρ') became independent of the rest of the equations. As a consequence, the oscillating pressure and velocity could be determined without considering the mass release (source) contained in the continuity equation. However, more complete nonlinear models, such as Priem's (discussed in the next section), indicate that the continuity equation and its mass release source overwhelmingly determine the nonlinearity of instability.

The fact that first order perturbation analysis removes completely the physical coupling of the equations is disturbing and casts doubts on the applicability of any perturbation scheme unless carried to very high order where, unfortunately, the algebra becomes prohibitive.

Computerized Nonlinear Models

During the same time that many authors were pursuing the time-lag perturbation approach, others were concerned with the detailed physical processes involved within the oscillating and reacting spray-gas flow field. Models that have considered physical coupling processes have traditionally retained more complete nonlinear conservation equations.

These computerized models begin by utilizing some form of initial conditions as supplied by a steady-state computer model (although the degree of sophistication used in the steady-state analysis varies) and then disturb this initial condition. The result is the predicted growth or decay of the pressure disturbance amplitude as a function of its initial magnitude, the steady-state conditions and the engine configuration.

Most analyses of this type have been limited to one-dimensional longitudinal or quasi-one-dimensional transverse wave motion. Only very recently has a nonlinear transient two-dimensional model been developed.

The first attempt at formulating such a model developed from the work of Torda in the middle 1950's. In 1958, Torda and Burstein (Ref. 57) published a forerunner of a longitudinal model. The equations as presented did not consider droplets and represented the coupling terms through fictitious mass and energy sources. A method-of-characteristics solution to this limited set of equations was discussed, but not implemented. Later Torda and Schmidt (Ref. 58) extended this concept and refined the equations. The coupling terms, however, were left in unspecified form. The numerical calculations presented in the paper concentrated upon motions of the gas phase. No droplet dynamics were included. Coupling terms were introduced in the gas-phase equations by means of arbitrary forcing and feedback functions. Although the numerical scheme used was apparently not stable enough to handle strong waves in the chamber, the paper gave interesting results about the nature of the coupling terms necessary to cause instability. With a linear feedback function specified

for the coupling terms, no instability could be triggered in the chamber. However, with a quadratic feedback term the chamber pressure oscillation amplitudes increased rapidly. Unfortunately, these feedback functions, though interesting, cannot be related to physical phenomena.

The first nonsteady longitudinal model to include physical terms was written by Burstein and Agosta (Ref. 59) in 1962. Except for the absence of an energy source term (due to mass addition) in the energy equation, the conservation equations were quite complete. Coupling terms included expressions for droplet heating and droplet vaporization (the El Wakil equations, Ref. 22) and droplet drag. Initial conditions were based on a steady-state model (Ref. 24) that assumed a constant ratio of vaporization between the injected liquid fuel and oxidizer sprays. As a result, no axial gradients of mixture ratio or gas temperature appeared. As noted before, this corresponds to constant molecular weight in the equation of state. Neither that equation nor the energy equation allowed for dissociation. Lack of a time varying droplet number concentration equation also required that the droplet number density be the same under nonsteady and steady-state conditions, which is quite unrealistic. This nonsteady model, however, was one of the first to allow an input range of initial droplet diameters.

The model was programmed for solution through use of the method of characteristics. The accuracy of the numerical scheme was such that the instability could be analyzed only up to the point of formation of steep-fronted shock-like

waves. Solutions were not obtained during the subsequent unstable opera-
tion. However, interesting correlations with experimental data were
presented.

Use of the El Wakil equation, for quasi-steady droplet evaporation, in a
nonsteady combustion model can be questioned (Ref. 60). Perhaps of equal
or more importance as discussed for the time-lag models, is the lack of an
equation allowing molecular weight shifts due to mixture ratio gradients and
dissociation. The conservation equations as applied are thus limited to
consideration of weak waves which do not disturb the gas phase mixture
ratio. Application to strong waves can cause significant errors in the
calculated pressure amplitudes. In practice the models were applied to
strong waves. This, combined with possible inadequacy of steady-state
coupling terms, probably can account for departures from experimentally
observed behavior.

In 1962, Priem published the first physical non-linear model directed toward
tangential resonant instabilities of a liquid rocket combustor (Ref. 61).
Recognizing this to be a three-dimensional problem, Priem began with a
fairly rigorous derivation of the full equations of motion for a two-
phase reacting gas. In the first application of Priem's theory, droplet
drag and droplet heating were ignored. Further, it clearly was not feasible
to perform the incredible number of computations involved in considering three-
dimensional nonlinear flow. Hence, Priem considered only an annular element

of a cylindrical combustor. Located at the outer wall of the engine, the element had only an incremental thickness Δr. Although Priem originally considered it to extend over the whole chamber length, it is usually applied to only a short ΔZ (axial) increment. To obtain the equations for this annulus Priem assumed that a number of variables and gradients vanish, viz.: $V_r = V_{\ell_r} = V_{\ell_\Theta} = 0$

$$\frac{\partial}{\partial r} = 0 \qquad\qquad \frac{\partial V_Z}{\partial \Theta} = 0$$

$$\frac{\partial^2}{\partial^2 z} = 0 \qquad\qquad \frac{\partial V_\Theta}{\partial Z} = 0$$

(The restriction $V_{\ell_\Theta} = 0$ has been subsequently removed by other authors, Ref. 62 and 63. This has left, as the set of governing equations: continuity, tangential momentum, Z momentum, energy and equation of state. Further, the time variations of the axial velocity were assumed to be equal to zero throughout the combustor, i.e., V_Z is a prescribed constant value with time. Upon nondimensionalization and assuming that the molecular weight is constant and equal to the steady-state value (no dissociation, no mixture ratio shift), nondimensional equations were derived in which certain parameters were found to play important roles. These are $\mathcal{L}$, the burning rate parameter at steady-state conditions, and $\Delta V = V_n - V_{\ell_Z}$ the velocity difference between gas and spray in the annulus. However, the nonsteady equations still contain a burning rate at the nonsteady condition and the

variables $\dfrac{\partial V_z}{\partial z}$, $\dfrac{\partial P}{\partial z}$, and $\dfrac{\partial T}{\partial z}$ (which are functions of time) for which relations must be found. The steady-state expression was used for the nonsteady burning rate term. Nondimensionalization of the burning rate equation revealed a strong dependence on ΔV and further led to the introduction of a rather nebulous term called Mvap, the reduced mass of unvaporized propellant. (This term could have been eliminated if an equation for droplet spray continuity had been added).

Note again, that the use of this quasi-steady vaporization rate is question-able. Of equal, if not greater importance, however, are the assumptions used to obtain equations for the remaining axial gradients. Priem assumed that none of the terms vary in the axial or radial direction and that the axial derivative terms do not vary with angular position (being average values and functions of time only). It was then further assumed that the total mass, mome. cum, and energy in the annulus do not vary with time so that the conservation equations had only to be integrated in the Θ direction and all time varying terms in the integrated equations were set equal to zero. These integrated total annulus equations supplied the additional equations needed to solve for the axial gradient terms. Combined with the integrated local conservation equations and the burning rate expression, the entire system was solved numerically with a digital computer.

However, the consequence of assuming that the total mass, momentum and energy in the annulus do not vary with time is most serious. It provides for no relief flows in or out in the axial direction. A simple physical consequence

of this is that, when a strong finite disturbance is input on one side of the annulus, the program is forced to predict low (or even negative) density on the other side to maintain constant mass within the annulus. Clearly this is not an acceptable assumption. It thus appears that the integration scheme itself may cause oscillating conditions and be one reason (along with the fact that the waves are constrained in an annulus) that the Priem model predicts low values for stability levels. Burstein (Ref. 64) investigated this effect mathematically (since it was the controlling factor in his r, Θ, t, "pancake" model, discussed later) and came to the conclusion that this assumption violates the rule of forbidden signals for hyperbolic equations.

Like all previous models, Priem's also suffers from the facts that no mixture ratio variations in time are allowed and that the forms of the equation of state and the energy equation physically limit the model to consideration of small disturbances. When applied to LOX-CH$_2$ combustion, for example, the model has serious deficiencies. These are less important for liquid-liquid bipropellant systems and the model has been successfully applied in explaining trends, or correlating, experimental stability data and in predicting relative stabilities of various candidate engine designs.

Stability predictions are made by interpreting the results of digital computer program numerical solutions of the set of equations. The solution proceeds in time from a given input set of initial conditions and boundary conditions representing the particular engine design and operating point being analyzed.

Growth or decay of pressure oscillation amplitude from an initial disturbance of preselected magnitude is determined. Successive computer runs are made with various magnitudes of initial disturbance to determine a "neutral stability" level. Priem plotted a large number of such neutral stability predictions as families of $\Delta V'$ curves on burning rate parameter, $\mathcal{l}$, versus reduced initial disturbance magnitude, P_c/P_c, graphs. $\Delta V' = \Delta V/$speed of sound.

Relative stability predictions are often made, without running the computer program, by comparing disturbance levels obtained for candidate designs from these more or less generalized charts. Such comparisons are usually made at each design's minimum value of $\Delta V'$, i.e., for that region in the combustor which is most sensitive to disturbance. The data needed to enter the charts are most often obtained from steady-state combustion analysis using one of the one-dimensional combustion models.

The basic Priem instability model has been modified and extended by several investigators. Beltran and Breen (Ref. 63) studied spatial sensitivity of the combustion field by using annular elements at varied radial and axial positions. Coultas and Kesselring (Ref. 64) formulated a rectangular one-dimensional version and studied stabilization by combustion space baffles. Campbell and Chadwick (Ref. 28) made a number of improvements in the model while extending its capabilities to high (supercritical) chamber pressures.

Recognizing the importance of the full nonlinear approach, Burstein and co-workers (Ref. 64) have recently been working on a full two dimensional transient

model. Their first attempt at developing this model dealt with a pancake-type motor using an r, θ, t coordinate system. Gas phase conservation equations were set up quite rigorously, although momentum source terms from spray evaporation were neglected, as was gas viscosity. Conservation equations for the spray were neglected though coupling terms were provided for the spray mass and energy addition. Apparently this was accomplished by using a modified Godsave droplet evaporation model with constant diameter for the drop. The vaporization rate again was taken to be quasi-steady. Since drag and droplet heating were neglected, convective effects on the drop depended only on the gas phase. Information was not given on how the number density of droplets was calculated; it apparently was assumed to be constant since no time varying droplet number concentration equation was included. The equation of state again assumed constant molecular weight and, like models in the past, neglected dissociation and mixture ratio shifts with the attendant limitations on wave analysis.

Only limited results were obtained from the pancake model when combusting droplets interacted with the strong spinning wave. Energy accumulation in the plane z = constant led to pressure amplitudes that became unrealistically large. It was clear from the analysis that the axial influence must be properly included for the combustion model to be coupled to the gas flow field. This ill-posed problem is similar to the situation required in the Priem analysis. The addition of the extra dimension apparently increased the sensitivity to assumptions governing the axial direction. Application of Priem's

condition (constant mass, momentum and energy in the plane) was not suffi-
cient to allow good prediction of the pressure wave for the reasons stated
earlier.

Of more importance, however, is their second model, a toroidal, θ, z, t
analysis. This is the first fully nonlinear model to investigate both
tangential and longitudinal motion. The boundary condition at the exit
was satisfied by specifying a large enough nozzle expansion ratio to
provide supersonic outflow, and at this point, setting all gradients with
respect to z equal to zero. Again appropriate gas phase equations were
derived, although source terms for momentum due to mass addition and droplet
drag effects in the gas phase were neglected. Conservation equation for
the droplets (mass continuity drag and energy) were included but no coupling
term for the heat addition to the droplet was utilized. Also, cross gradient
terms, i.e., $U_{j_\theta} \dfrac{\partial U_{j_z}}{\partial \theta}$ in the droplet momentum (drag) equations were
omitted. Further, no droplet number concentration equation was provided.
Lack of this equation and a physically-based steady-state model for initial
conditions prevent rigorous application of physical coupling terms. That is,
the source terms of mass and energy from the droplets to the gas phase depend
not only on the drop models but on the number of droplets per unit volume.
Since no droplet number concentration equation was provided and no value was
present from a steady-state model, in practice the source term for mass addi-
tion was prescribed as a nondimensional perturbed parameter of pressure. In
addition, no mixture ratio or molecular weight variations were allowed. The
equation of state and energy equation are like those for the pancake model.

Predicted overpressures are greater than are observed experimentally in cylindrical engines. However, the model is annular and allows no expansion and decay of the waves in the radial direction so that comparisons to annular engines operating unstably would be more appropriate. Whatever the limitations of the model as formulated, it has the potential of being one of the most important and informative ever written.

Recently Agosta and co-workers (Ref. 65) have developed a refinement of their longitudinal model. The equation for this model appears to be quite rigorous; conservation equations for both spray and gas flow fields are included. Programming is done by a finite difference method, changed from the original which used the method of characteristics. Ref. 66, given as the source of the equations, lists no time varying mixture ratio or droplet concentration number equations. However, in Ref.65 Agosta states that mixture ratio and droplet concentration effects are included. It is not clear how this is accomplished. The model does use as initial conditions the sophisticated steady-state model of Hammer's, et al, which includes mixture ratio. It is possible that the droplet concentration from the nonsteady model is taken to be the same as that in the steady-state. Then, allowing for time variation in droplet mass allows provision for a quasi-steady mixture ratio equation, from which the energy equation and tables provide approximate variable, dissociated gas properties. Agosta uses physical coupling terms for dropleg drag, heating, and mass addition. In particular the droplet heating equation provides for radial temperature gradients within the drop. Although he references the use of evaporation kinetics for nonequilibrium conditions (Ref. 67) that work was

concerned with low pressure ignition conditions and it is not clear if or how he applies this to high pressure instability conditions. It appears as though quasi-steady terms are still used for the mass evaporation.

This represents one of the first transient models that considers mixture ratio and molecular weight variation. Further extension of the droplet model to include temperature gradients appears to give good correlation of experimental and predicted results. However, an artificial heat rate increase to the droplets due to wave passage was used to obtain at least a portion of the noted analytical and experimental agreement. This model and more inclusive versions of Bursteins toroidal model do, however, show great promise in their ability to analyze the combustion stability problem. With more modern computers the extension to three-dimensions and time, with consideration of mixture ratio and molecular weight variation, should be both possible and practical within the near future.

Summary of Transient Review

Before leaving this discussion of nonsteady models, three factors should be emphasized. First, none of the models (except for Culicks approximations) have included gas phase chemical kinetics in the gas conservation equations. This is consistent with our approach that chemical kinetics delays within the mixed gas phase are negligible, even in the presence of wave motion. This, as discussed briefly in the steady-state section, does not rule out all kinetics or even local micro-mixing processes. Coupling could indeed be controlled by drop vapor mixing and chemical kinetic considerations (gas phase flames) but terms accounting for such phenomena should be

contained within the coupling expressions since these local processes are within the domain of influence of the drop and its surrounding vapor/gas mixture.

Second, no multi-dimensional transient model considers turbulence. This is consistent with prior description.

Third, and this is where most of the models are deficient (e.g., neglect of varying mixture ratio and molecular weight) even though combustion and droplets are present in some of the models, they all predict wave frequencies close to calculated chamber acoustic resonant modes considering the gas phase to be uniformly at the burned gas temperature. In particular, Culicks linearized model presents corrections to the pure chamber model due to the presence of combustion, mean flow and real boundary conditions, etc. All of these corrections are quite small. More rigorous models such as the physical nonlinear ones, Bursteins longitudinal and toroidal model and Priem's model, also predict the wave frequency to be close to that of the basic chamber resonant mode for the region modeled.

It is not surprising that the models predict such results. None of them (except for Agosta's recent model) are capable of considering mixture ratio or molecular weight variations. As a consequence the models are consistent only when used with initial conditions that consider the mixture ratio and hence the temperature to be nearly uniform through the chamber. Since the mixture ratio is considered to be the same as that which was injected, it

is not surprising that the predicted waves travel through the chamber at speeds corresponding to the speed of sound of the burned gas at the injected mixture ratio. Although this is also an experimentally observed fact for engines having large mixture ratio and temperature gradients, the models give no information about the processes that cause this to occur for such striated conditions. The complete explanation for the observed correspondence of the wave frequency in engines having large mixture ratio gradients to the predicted fully burned chamber resonant mode is still not understood. It is, as has been previously stated, apparently more controlled by the geometry and boundary conditions than any other factors.

Almost all of the existing models contain deficiencies. In particular, the conservation equations are not entirely complete and omission of terms could bias the evaluation of coupling expressions during unstable operation. To eliminate this possibility and insure that the accuracy of the models depended solely on the expressions for the coupling terms, it was decided that a new formulation was required.

DEVELOPMENT OF A COMPREHENSIVE
FLOW FIELD FORMULATION

As a result of the review it was concluded that few steady-state and no transient models were adequate for rigorous description of the processes occurring within the engine. Further, to identify and appreciate the nature and implications of any simplifying assumptions used in model formulation it was desirable to start with a general formulation.

Consideration of general steady-state performance predictions required the model to be three-dimensional. Meaningful analytical simulation of convective cross flows requires a three-dimensional model. The model should be capable of calculating the local mass flux and composition anywhere in the chamber cross section. Treatment of transverse gradients should readily predict formation of, and intermixing between, areas with striated flows.

Further, local wall compatibility problems could only be analyzed with a model which considered transverse wall-directed flows.

Multidimensional considerations were obviously required for general non-steady analysis. Further, if the model were to be applicable to all propellant combinations and actual finite amplitude disturbances, local time varying mixture ratio and droplet number concentration effects must be considered. Introduction of these equations and addition of proper tables of physical properties would remove the restrictions present in all the non-steady models discussed previously.

Although not originally intended as part of this AFOSR program, the need for a more comprehensive analytical formulation to unify the results of analytical and experimental research in the fields of liquid propellant injection and combustion was so evident that a generalized model was developed.

The model formulation, written in vector-tensor notation expresses the dynamics of a multi-component reacting gas stream which undergoes simultaneous exchange of mass, momentum, and energy with contained propellant liquid sprays. Both gas and liquid spray phases are described in terms of continuum mechanics, with sprays represented by a discreet number of droplet size groups, each of which is treated as a separate phase. These formulas are presented below with emphasis on those aspects which have been neglected before. Attention is given to the species and energy equations and proper treatment of their terms. The formulation is structured to incorporate particular laws and/or correlations for the coupling terms as they are developed. The model is applicable to either liquid-liquid or gas-liquid injection. The formulation is stated without showing the derivation.

FLOW FIELD FORMULATION

Assumptions used in the derivation are: (1) ideal gas law is a valid state equation, (2) effects of turbulence can be neglected*, (3) dilute sprays

---

*Time averaged perturbations become meaningless during acoustic instabilities, when mean-flow oscillations due to wave motion have frequencies comparable with turbulent fluctuation frequencies. Further, propellant residence times in rocket combustors are typically only 3 to 10 times the mean turbulent fluctuation periods, therefore, an element of propellant is effected only slightly by turbulence, even during steady-state operation. In addition, gas-phase cross convective flows overwhelm the effects of turbulence. These effects have all been discussed previously.

occupy a negligible fraction of chamber volume*, (3) each drop size group represents a separate liquid phase and exchange terms between liquid phase are not included*, (5) drag contributes only kinetic energy to the spray energy equation, and (6) secondary "shear" breakup of droplets initially formed during primary atomization produces resultant droplets so small that they evaporate immediately upon formation.

The formulation is structured to incorporate analytical correlations for the interphase coupling terms, which appear on the right hand sides of certain equations (they can be identified readily by their appearance in both the gas and spray equations, but with opposite signs). Coupling term expressions and initial and boundary conditions are needed to complete the formulation.

Spray Phase Conservation Equations - Parent Droplets

a) Droplet Number Concentration

$$\frac{\partial N_j^n}{\partial t} + \text{div} \left(\vec{u}_j^n N_j^n \right) = 0 \tag{1}$$

b) Droplet Spray Mass Density

$$\frac{\partial \rho_j^n}{\partial t} + \text{div} \left(\vec{u}_j^n \rho_j^n \right) = - N_j^n \dot{m}_{j_{vap}}^n$$

$$- N_j^n \dot{m}_{j_{BU}}^n + \text{any other mass-} \tag{2}$$
$$\text{loss mechanism}$$

---

*The assumption of dilute sprays for purposes of this investigation was valid. However, this may not be true for some engines in the region very near the injector face. Means have been found to include collision effects in the 3-D computer model describing the rapid combustion zone, Ref. 37.

The individual droplet mass may be related to the droplet diameter by complex relationships involving radial temperature and density gradients in the droplet or as simply as,

$$m_j^n = \frac{\pi}{6} (D_j^n)^3 \rho_{\ell,j}^n \qquad (3)$$

if the drop temperature is uniform.

Note: $\rho_j^n = N_j^n m_j^n$ always.

c) Droplet Momentum

$$\frac{\partial}{\partial t} (\rho_j^n \vec{u}_j^n) + \text{div} (\rho_j^n \vec{u}_j^n ; \vec{u}_j^n) = N_j^n \vec{F}_j^n$$

$$- N_j^n (\dot{m}_{j_{vap}}^n + \dot{m}_{j_{BU}}^n + \cdots) \vec{u}_j^n \qquad (4)$$

The drag vector is given by

$$\vec{F}_j^n = \frac{\pi}{8} \left\{ \rho(D_j^n)^2 |\vec{u} - \vec{u}_j^n| (\vec{u} - \vec{u}_j^n) C_{D_j}^n \right\}$$

$$- 24 \pi (D_j^n)^3 \text{ grad } p$$

The drag force includes both frictional drag and the drag due to volume forces across the drop arising from a pressure gradient. Use of a drag coefficient $C_{D_j}^n$ determined for drops in a steady nearly-constant-pressure flow field is correct for accelerating drops. For decelerating drops, the total transfer of drop momentum to gas pressure may not be realized, but this condition is not important in a rocket engine.

d) Droplet Thermal Energy

$$\frac{\partial}{\partial t}\left(\rho_j^{\,n} H_j^{\,n}\right) + \text{div}\left(\vec{u}_j^{\,n} \rho_j^{\,n} H_j^{\,n}\right) = N_j^{\,n} Q_j^{\,n}$$

$$- N_j^{\,n}\left(\dot{m}_{j_{vap}}^{\,n} + \dot{m}_{j_{BU}}^{\,n} + \cdots\right)H_{j_s}^{\,n} \qquad (5)$$

This formulation utilizes the JANNAF thermo-chemical data. Thus the naturally occurring "dead state elements", such as H_2, O_2, etc., are assigned zero heat of formation. The chemical energy for many systems is thus contained primarily in the heats of formation of the combustion products. This is reflected in the combustion property tables described later that are used with the gas phase mixture ratio equation. It is always necessary regardless of the propellants utilized to ensure that both the enthalpies of the spray and the gas phases are based on the same standard datum and are compatible. Specific examples for $H_2 - O_2$ combustion are presented later in the report for the one-dimensional programs. In general, for any system, the relation between $H_j^{\,n}$s and $T_j^{\,n}$s is

$$H_{j_s}^{\,n} = H_{j_i}^{\,n} + \int_{T_{j_i}^{\,n}}^{T_{j_s}^{\,n}} C_{p_j}^{\,n}\, dT$$

where $H_{j_i}^{\,n}$ is a reference enthalpy which is a slight function of pressure at $T_{j_i}^{\,n}$ and includes the effects of the heats of vaporization and also formation of the species, if any.

If temperature is not uniform within a drop, $\rho_j{}^n$ $H_j{}^n$ cannot be separated and complicated integral relationships must be used for this term. Because the heating rate, $Q_j{}^n$, affects only the sensible enthalpy of the drop (in the absence of decomposition), this equation (assuming $c_{p_j}{}^n$ to be constant during the increment of heating) can often be simplified with little loss of accuracy to

$$\frac{\partial}{\partial t}(\rho_j{}^n T_j{}^n) + \text{div}(\vec{u}_j{}^n \rho_j{}^n T_j{}^n) = \frac{N_j{}^n Q_j{}^n}{c_{p_j}{}^n}$$

$$- N_j{}^n (\dot{m}_{j_{vap}}{}^n + \dot{m}_{j_{BU}}{}^n + ---)T_{j_s}{}^n \qquad (6)$$

Again, however, unless $T_j{}^n$ is assumed uniform throughout the drop, $\rho_j{}^n T_j{}^n$ cannot be separated. The energy that is transferred to the gas phase is the surface enthalpy so it is still necessary to calculate $H_{j_s}{}^n$.

e) Droplet Shear Wave Build-up for Predicting Onset of Droplet Breakup

    Treating the shear buildup on the surface of the droplets as a
    property the following equation can be derived.

$$\frac{\partial(N_j{}^n \psi_j{}^n)}{\partial t} + \text{div}(\vec{u}_j{}^n N_j{}^n \psi_j{}^n) = N_j{}^n \frac{1}{\tau_{B.U._j}{}^n}$$

where $\psi_j{}^n$ = nondimensional state of shear (breakup) buildup, zero at all points except where a critical value of $\dfrac{W_e}{\sqrt{R_e}}$ is exceeded.

When the critical value of $\dfrac{W_e}{\sqrt{R_e}}$ is exceeded the drop is assigned a breakup state. Should the drop fail to meet the critical value during the buildup to the breakup point $\psi_j{}^n$ is set back to zero until the process begins (if it does) again. The calculation of $\psi_j{}^n$ progresses only so long as the critical value of $\dfrac{W_c}{\sqrt{R_e}}$ is exceeded.

The term

$\tau_{B.U._j}{}^n$ = induction time required for breakup state (shear wave buildup on droplet surface) to be maintained for actual shear breakup to occur. It has a nonzero value only when $\dfrac{W_e}{\sqrt{R_e}}$ exceeds a critical value (c.v.).

that is

$$\frac{1}{\tau_{B.U._j}{}^n} = \psi_j{}^n = 0 \;\; \text{if} \;\; \frac{W_e}{\sqrt{R_e}} < \text{c.v.}; \;\; \dot{m}_j{}^n{}_{B.U.} = 0$$

$$\frac{1}{\tau_{B.U._j}{}^n} \;; \;\; \psi_j{}^n \geq 0 \;\; \text{if} \;\; \frac{W_e}{\sqrt{R_e}} \geq \text{c.v.} \;; \;\; \dot{m}_j{}^n{}_{B.U.} = 0$$

when $\psi_j{}^n \geq 1$; $\dot{m}_j{}^n{}_{B.U.}$ = finite value as long as $\dfrac{W_e}{\sqrt{R_e}} \geq$ c.v.

f) Droplet Residence Time

The following equation may be used to calculate the time for a parent droplet to flow from the injector to the point in question under conditions existing at the specified time.

$$\frac{\partial}{\partial t} \left(N_j^{\,n} \, \tau_{res_j}^{\,n} \right) + \text{div} \left(\vec{u}_j^{\,n} \, N_j^{\,n} \, \tau_{res_j}^{\,n} \right) = N_j^{\,n}$$

at $Z = Z_0$ (initial plane) $\tau_{res} = 0$

Only at steady state does the equation, because of the Eulerian derivative, actually "track" the drops.

The equations as presented neglect collisions between the droplets of different drop group sizes. Because of the Eulerian form of the equations, however, properties of the drops of the same initial group size from different elements meeting at the same increment will be averaged. This could be avoided, for consistency, by the inclusion of an additional subscript delineating separate elements. Or, more rigorously, a collision term should be included in the droplet momentum equation accounting for interaction of all initial drop group sizes. Work on describing such phenomena is presently underway, Ref. 37 .

Spray Phase Conservation Equations - Microdroplets

These equations would describe the microdroplets that result from breakup of the parent droplets. These droplets do not break up further, but are heated and vaporize. Equations for them are considerably more complex than those shown

above because breakup is occurring simultaneously throughout the chamber. It would be an enormous task to distinguish microdrops of, say, the rth initial drop group size found at Z_1, r_1, θ_1 from drops of that same initial drop group size formed at some previous increment and now flowing into Z_1, r_1, θ_1. Hence, characteristics (diameters, temperatures, momentums, etc.) must be averaged for all the drops of the same initial drop group size flowing into the same increment.

These equations are of secondary importance and, therefore, are not presented here. Work by Nicholls, Ref. 68 has shown that under the influence of waves or high convective gas flows the resultant breakup (micro) droplets are exceedingly small, near one micron diameter, on the average. Hence, $\dot{m}_{j}^{n}{}_{B.U.}$ of the parent droplet is nearly equivalent to direct delivery of the droplet mass to the gas phase and can be easily modified to include such an effect. It will be treated then as such in the conservation equations.

Gas Phase Conservation Equations

a) Reduction of Species Conservation to Mixture Ratio Conservation

1) Species Conservation Equation

$$\frac{\partial(\rho\omega_i)}{\partial t} + \text{div } (\rho\omega_i\vec{u}) + \text{div } (\rho\omega_i\vec{U}^i) = r_i$$

$$+ \sum_{n}\sum_{j} (\Omega_{i,j} \, N_j^{\,n} \, (\dot{m}_{j_{vap}}^{\,n} + \dot{m}_{j_{BU}}^{\,n} + \cdots))$$

$$(7)$$

Under the assumptions that: (1) the usual binary diffusion approximation holds

$$\rho \omega_i \vec{U}^i = \rho \mathscr{D}_i \text{ grad}_i \tag{8}$$

where $\mathscr{D}_i$, the gas phase diffusion coefficients, are considered to be nearly equal for all species, and (2) gas phase reaction rates are large compared to the delivery rate of vaporized species from spray droplets to the gas stream, the species conservation equation rigorously reduces to the following relation for the local time varying mixture ratio. Note that statement (2) is consistent with the approach that chemical kinetics delay within the gas phase, after mixing has occurred, is negligible even in the presence of wave motion. Again, this does not rule out all kinetics or even local micro-mixing processes. Coupling could indeed be controlled by drop vapor mixing and chemical reaction rates (gas phase flames) but terms to describe these phenomena belong in the coupling term expressions. These local processes are within the domain of influence of the drop vapor - surrounding gas boundary conditions.

2) Mixture Ratio Equation

$$\frac{\partial(\rho c)}{\partial t} + \text{div } (\rho \vec{u} c)$$

$$- \rho \bar{\mathscr{D}} \left\{ \text{div (grad } c) - 2 \frac{|\text{grad } c|^2}{c + 1} \right\}$$

$$- \left\{ \text{grad } c \cdot \text{grad } \rho \bar{\mathscr{D}} \right\}$$

$$= (2c - 1) \left\{ \sum_n \sum_j N_j^n (\dot{m}_{j_{vap}}^n + \dot{m}_{j_{BU}}^n + \cdots) \right\}^{oxid}$$

$$- c^2 \left\{ \sum_n \sum_j N_j^n (\dot{m}_{j_{vap}}^n + \dot{m}_{j_{BU}}^n + \cdots) \right\}^{fuel} \tag{9}$$

The mixture ratio equation is used in conjunction with tables that provide all gas phase equilibrium properties as functions of c, H, and p for state calculations.

98   R-8377

In practice, it has been found that effects due to diffusion are masked by gas phase convective velocities and hence $\overline{\overline{D}}$ may be set equal to zero.

b) **Global Continuity**

$$\frac{\partial(\rho)}{\partial t} + \mathrm{div}(\rho\vec{u}) = \sum_n \sum_j \left(N_j^{\,n} (\dot{m}_{j_{vap}}^{\,n} + \dot{m}_{j_{BU}}^{\,n} +\cdots) \right)$$

(10)

c) **Gas Momentum**

$$\frac{\partial(\rho\vec{u})}{\partial t} + \mathrm{div}\,(\rho\vec{u};\vec{u}) = -\,\mathrm{grad}\,p + \mathrm{div}\,\underline{\underline{\tau}}$$

$$-\sum_n \sum_j N_j^{\,n}\,\vec{F}_j^{\,n}$$

$$+\sum_n \sum_j N_j^{\,n}\,(\dot{m}_{j_{vap}}^{\,n} + \dot{m}_{j_{BU}}^{\,n})\vec{u}_j^{\,n}$$

(11)

d) **Gas Energy**

$$\frac{\partial\left\{\rho\left(H + \frac{u^2}{2}\right)\right\}}{\partial t} + \mathrm{div}\left\{\rho\vec{u}\left(H + \frac{u^2}{2}\right)\right\} = -\,\mathrm{div}\,\vec{q}$$

$$+\,\mathrm{div}\,\vec{u}\,\underline{\underline{\tau}} - \sum_n \sum_j N_j^{\,n}\,Q_j^{\,n} - \sum_n \sum_j N_j^{\,n}\,\vec{u}_j^{\,n}\cdot\vec{F}_j^{\,n}$$

$$+\sum_n \sum_j N_j^{\,n}\left\{\left(\dot{m}_{j_{vap}}^{\,n} + \dot{m}_{j_{BU}}^{\,n} +\cdots\right)\left(H_{j_s}^{\,n} + \frac{(u_j^{\,n})^2}{2}\right)\right\}$$

$$+\frac{\partial p}{\partial t}$$

(12)

the enthalpy is given as

$$H = \sum_i \omega_i H_i = \int_{T^\circ}^{T} \sum_i \omega_i C_{P_i} \, dT + \sum_i \omega_i H^\circ_{f_i}$$

where $H^\circ_{f_i}$ is the heat of formation of the species i at standard conditions, T°.

T is the gas temperature.

Also the gas phase heat transfer term

$$q = -k \text{ grad } T - \sum_i \rho \mathcal{D}_i H_i \text{ grad } \omega_i$$

The combustion property tables contain all of the required information to compute these variables as functions of C and p. The enthalpy H in the tables contains both sensible and chemical energies; further the tables contain all the species present at the state point.

e) Equation of State

$$P/\rho = RT \left[\sum_i \frac{\omega_i}{M_i} \right]^{-1} \qquad (13)$$

where R is the universal gas constant

M_i is the molecular weight of the individual species.

and all required species data is obtained from the state points contained in the combustion property tables.

Reduction to One-Dimension Application

Application of the comprehensive model requires reduction from vector notation to a coordinate system, imposition of initial and boundary conditions and expressions for coupling terms. In reducing the general equations to one spatial dimensions, it is necessary to replace

$$\rho, \; \rho_j^{\,n} \; \text{and} \; N_j^{\,n} \; \text{by} \; A\rho, \; A\rho_j^{\,n} \; \text{and} \; AN_j^{\,n},$$

respectively, when these appear in the left hand sides of the mass, momentum and energy conservation equations. In addition, the entire right hand sides of these equations must be multiplied by A.

FURTHER RELEVANCE OF FLOW FIELD FORMULATION

Even though the development and subsequent programming of reductions of the generalized formulation caused curtailment of some listed items of work of this investigation, application of the model to other problems is straight-forward. The analytical accomplishments include:

1. The only currently available complete multi-dimensional steady-state formulation.

2. The only steady-state or transient model available which is believed adequate to permit delineation of the important coupling terms and enable evaluation of expressions describing them.

3. The analysis formed the basis of an operational Air Force combustion model computer program (Injector/Chamber Compatibility Program, Contract No. FO4(611)-68-C-0043) that includes a full three-dimensional model of the Rapid Combustion Zone and a program reduction of the complete formulation to encompass a stream tube combustion analysis of the downstream region. This is the first mathematical analysis of coupled spray combustion and compatibility (heat transfer) effects. This computer model is being used for design purposes.

4. The analysis formed the basis of an operational NASA steady-state performance oriented combustion model similar to, but somewhat more inclusive regarding performance, the ICC program. At present this model is being proposed as the liquid rocket performance standard for the United States.

5. As a result of item 4, the model is being used for an Air Force sponsored program to develop a performance model for pulse mode operation.

For further information regarding the use of the model, refer to Ref. 37 .

REVIEW OF EXISTING COUPLING TERM EXPRESSIONS USED FOR
DESCRIBING THE COUPLING PROCESSES

Fairly lengthy reviews have been presented pertaining to existing steady-state and transient overall combustion models. These were necessary because

such comprehensive reviews were not available, and they were needed to determine the necessity of developing new combustion models for use with the experimental data in evaluating the coupling term expression. Though the goal is to evaluate the validity of such expressions, the program emphasis to date has been the development of the techniques required to achieve this accomplishment.

A review of the coupling terms is also in order but the emphasis here will be on brevity. Further, unlike the overall combustion models, recent comprehensive reviews have been published for most of the coupling terms and there is no need then to repeat the entire reviews here. The coupling processes within an engine (or any combustion spray field) i.e., droplet heating and burning, drag, break-up, etc., have traditionally been treated as if resulting from the summation of such processes occurring to individual, isolated droplets. As such, it represents an interesting, academic problem easily simulated in a laboratory and has attracted many investigators. This of course accounts for the wealth of information existing for at least simple versions of the coupling processes and the existence of many reviews in the literature. Recent investigators and some reviewers however have been emphasizing the complex interactions between droplets that may exist in a dense burning spray field. This aspect will be emphasized below where definitive data of such interaction is available. To date, the effects of such interactions are believed to strongly influence droplet drag and breakup. The exact effect on droplet heating and burning processes is not at present known.

Droplet Heating and Burning (Vaporization)
Very recently Rosner, in Chapter 2, of Ref. 8, has published a comprehensive review of droplet heating and burning processes. This section will attempt to summarize his conclusions and relate them to the processes occurring within a rocket.

Consider the experimentally observed behavior of an isolated fuel droplet when suddenly placed into a near stagnant, subcritical pressure, hot, oxidizer containing gas. Such experiments typically involve photographically following the rate of diameter decrease of a fuel droplet suspended on a thermocouple junction. The reverse situation is just as valid, i.e., oxidizer drops in fuel vapors. These observations, as reflected in diameter and temperature changes, are shown in Figs. 8 and 9, taken from Ref. 8. The diameter initially expands, until the droplet approaches an evaporative "wet bulb", and then decreases with time (at the rate d^2 linear with time). After some period of time the mole fraction of droplet vapors around the drop reaches a critical limit and ignition occurs. The droplet temperature rapidly readjusts to a higher combustible wet bulb condition and the burning rate is substantially more rapid.

In actuality these experimental observations are for porous spheres playing the role of droplets and conditions are such that quasi-steady (QS) assumptions are at least partially valid. The QS assumption involves neglect of the $\frac{\partial}{\partial t}$ terms of the conservation equations applied to the heat transfer and diffusion field surrounding a droplet. It is not surprising that the QS assumptions have been invoked in the past; resulting expressions for the coupling terms are often utilized in more general models such as the steady-state and transient rocket spray field combustion programs described earlier. These programs require iterative solution of the complete gas and spray conservation equations at many increments in space (and time). Further, the computations are often performed for a range of droplet sizes. Thus during a typical steady-state computer run over 4000 separate droplet "state" computations may be performed for each spray.
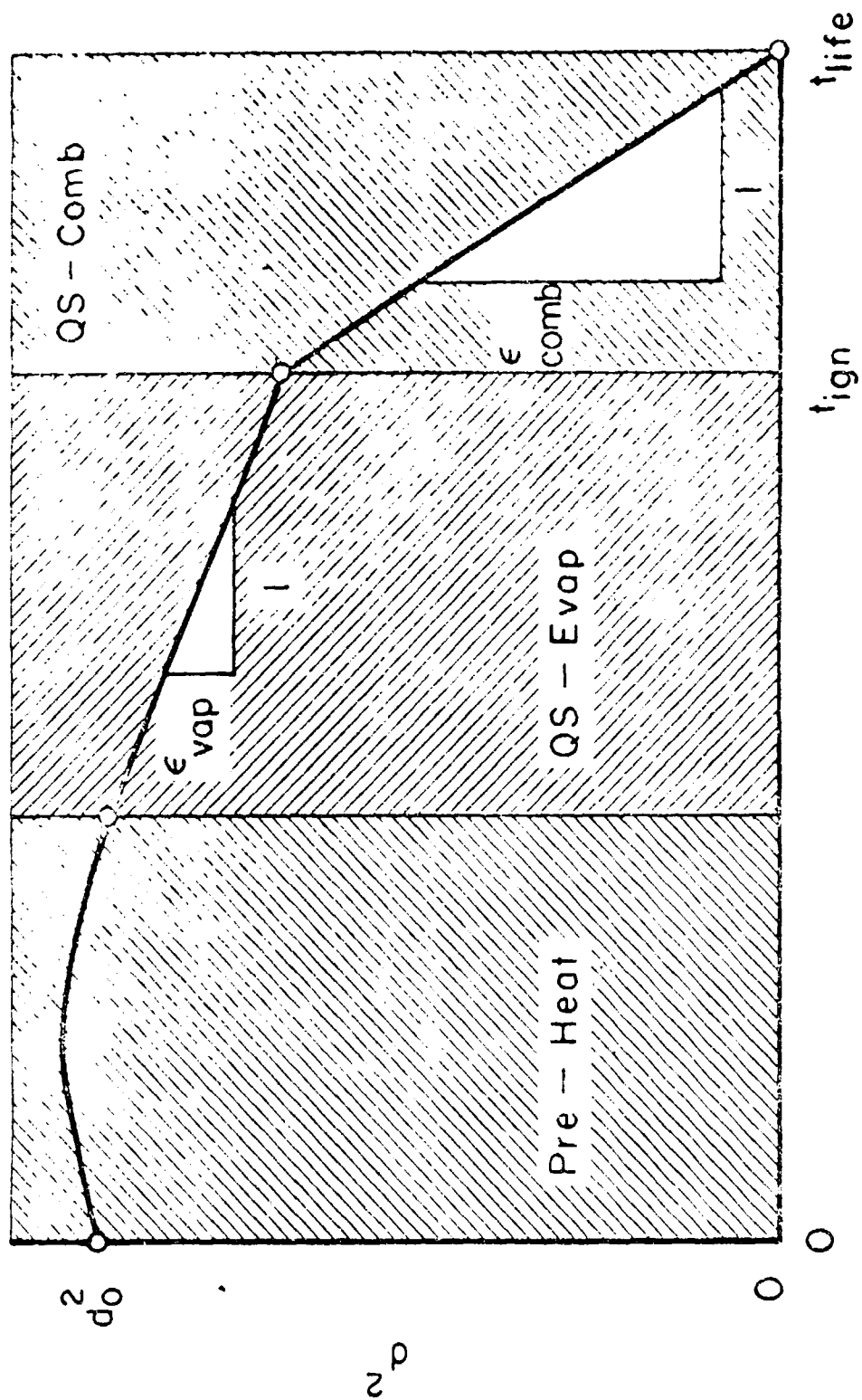
Figure 8. Drop Diameter Decrease as a Function of Time
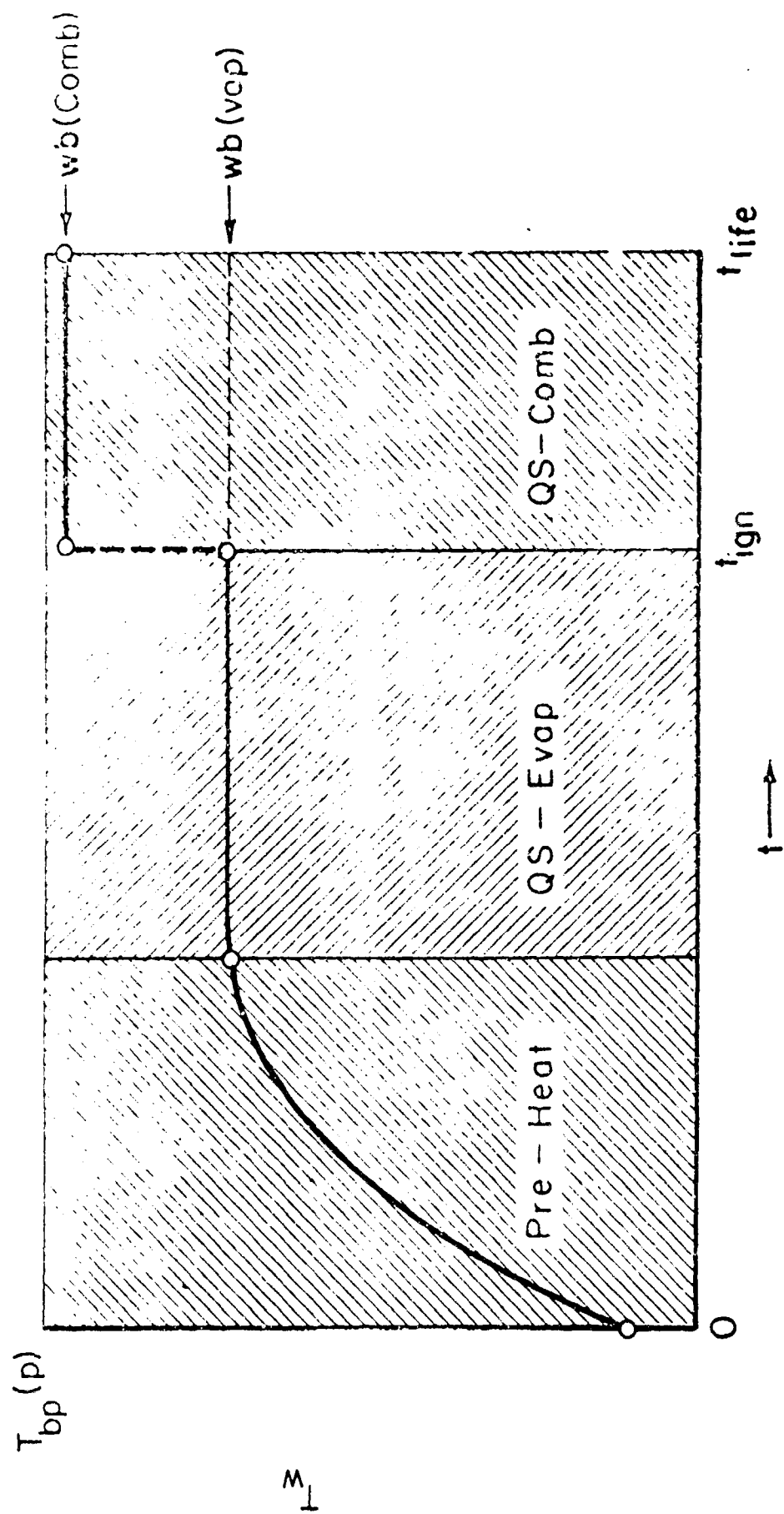
Figure 9. Drop Temperature Increase as a Function of Time

R-8377

phase equation. Should any of the coupling terms be highly complex (require a large computer program for itself) computations times can become astronomical. Only recently have some transient models been developed; Strahle, Ref. 69, analyzed the forward stagnation point of a droplet in a convective flow, Manrique, Ref. 70, analyzed a uniformly heating droplet in a stagnant atmosphere, and Ledwell, Ref. 71, recently developed a theory for burning droplets in which he accounted for moving boundaries and apparently some small convection. However, none of these models has proven feasible for incorporation into an overall rocket combustion program. Recent work by Ledwell, Ref. 72, indicates some work is being done toward this end.

It should be specifically stated at this point that the consideration of droplet heating, whether it is uniform or non-uniform, does not remove the QS assumptions. A fully transient model must consider transient effects in the gas around the drop.

In any event it is not surprising that the vast majority of analytical work regarding droplet heating and burning has invoked the QS assumptions. Considering the regimes of droplet vaporization and burning presented in Fig. 8 and 9, it is also evident why the problem has traditionally been attacked from two viewpoints.

Droplet Heating and Evaporation. The first of these viewpoints is based on the work of El Wakil, Ref. 22, and others at the University of Wisconsin. This viewpoint concentrates upon the preheat and evaporation regimes of figures 8 and 9.

The calculation of single droplet evaporation is based on a spherically symmetric model of simultaneous heat transfer and mass transfer across a gas-side boundary or film separating a liquid droplet from the surrounding hot combustion gas . The liquid droplet temperature is assumed uniform through the drop. Forced convection and resultant nonspherical transfer processes are accounted for through empirical Nusselt number correlations for both heat and mass transfer. The Nusselt number correlation used in the mass transport equation was obtained by Ranz and Marshall (Ref. 73) from analogy with heat transfer:

$$Nu_M = 2(1 + 0.3 \ Sc_f^{1/3} \ Re_f^{1/2})$$

They verified this equation by data from vaporization of water droplets in heated air. The equations derived thus account for both droplet heating and evaporation. Reference to Fig. 8 and 9 indicate that droplet heating certainly cannot be entirely neglected as it can occupy an appreciable portion of the droplets lifetime. Recent work by Savery (Ref. 74) gives good correlation with experimental data under such conditions, even up to high pressure convective evaporation, providing proper relations concerning the presence of other gases on the vapor pressure and "heat of vaporization" are taken into account.

Thin Flame Droplet Burning Model. In contrast to the previous model, which is truly a vaporization model, a thin-flame droplet combustion model envisions the droplet as being surrounded by an actual flame envelope (Fig. 10).* The

---

*In the thin-flame approximation, the actual combustion zone thickness approaches zero (for mathematical simplicity). If the droplet of interest is fuel, for example, fuel vapors are transported outward to the flame zone where they react at a stoichiometric mixture ratio with oxidizer arriving from the surrounding free stream gas. No oxidizer vapor penetrates beyond the flame. Reaction products generated at the flame sheet may diffuse in both directions.
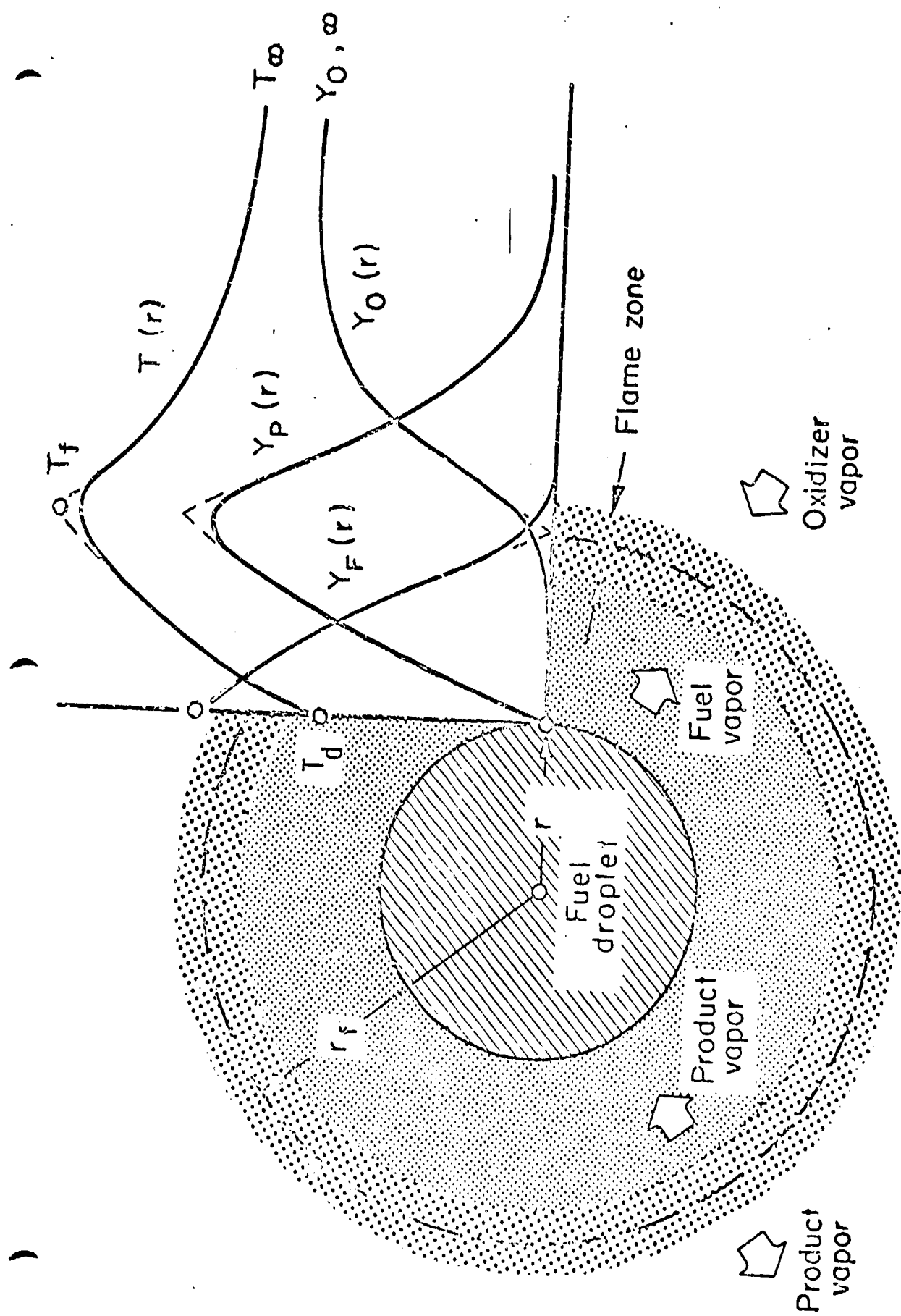
Figure 10. Thin Flame Zone Droplet Burning Model

theoretical development of such a model is described by Penner (Ref. 75). A
key assumption of his derivation is that the droplet remains at a constant
wet bulb temperature so that the thermal energy arriving at the liquid surface
is just sufficient to provide the heat of vaporization. As a result of this
assumption, such a model cannot describe the initial droplet heatup from its
injection temperature. For chamber pressures substantially below the pro-
pellant's critical pressure, however, this is sometimes acceptable, because
wet bulb temperatures can be rapidly attained and the predominant portion of
propellant droplet life times are spent vaporizing at the wet bulb temperature.

Generalized equations for the flame zone radius and temperature of the flame
zone are included in this model. Williams, Ref. 14, removed the thin flame
zone limitation by setting the Lewis number equal to one and assumed a one
step reaction mechanisms to occur in the drop boundary region.

In practice, the flame radius equations are little utilized since again con-
vective conditions are correlated by the Ranz-Marshall equation. Spalding
(Ref. 76) found this equation to provide a reasonably accurate account of the
experimental effect of mild convection on burning spheres.

There is nothing inherent in either Williams or Penners formulations that
precludes droplet heating. Recently, in fact, Dickerson, Ref. 77, added the
diffusion equation to Penner's formulation and developed a comprehensive model
that includes the surrounding flame and uniform droplet heating. However, a
problem arises here in that simple application of such a model requires that the
droplet immediately ignite with heatup occurring under burning conditions. In

that case the physical-ignition-delay time would be zero. Calculation of the actual ignition delay time, for given surrounding conditions, is still in the premature stage. As discussed later, however, in a rocket engine such considerations may be purely academic.

Comparison of Model Extremes. At first glance Williams' model would appear to yield much faster burning rates than Penner's, which in turn predicts faster burning than the El Wakil types. The comparisons are best made at the wet bulb conditions of each model. This can easily be obtained for the evaporative type models by setting the heating rate for the droplet equal to zero and solving for the "wet bulb" evaporation rate. The results are as follows:

Evap: $\quad \dfrac{\dot{m}}{N_{u_H}} \approx D_d \, Ln \left[1 + \dfrac{\overline{C}_p \, (T_\infty - T_d)}{\Delta H_V} \right]$

Penner: $\quad \dfrac{\dot{m}}{N_{u_H}} \approx D_d \, Ln \left[1 + \dfrac{\overline{C}_p \, (T_c - T_d)}{\Delta H_V} \right]$

Where T_c is at or near the stoichiometric flame temperature of the thin flame region.

Williams: $\quad \dfrac{\dot{m}}{N_{u_H}} \approx D_d \, Ln \left[1 + \dfrac{\overline{C}_p \, (T_\infty - T_d) + \omega_{o,\infty} \, Q}{\Delta H_V} \right]$

Where $\omega_{o,\infty}$ is the oxidizer mass fraction at ∞ (if one is burning a fuel droplet)

and Q = the heat released per unit mass of oxidizer consumed.

But note that in comparing Penner's and Williams model

$$\bar{c}_p T_c \approx \bar{c}_p T + \omega_{o,\infty} Q$$

so that Penner's model just represents the extreme of Williams, in that all chemical reaction is considered confined to a flame sheet of negligible radial thickness. In practice, the two models predict very nearly the same burning rate. Both however predict even faster burning rates than the evaporative model for equivalent T_∞ temperatures.

Extension of Model Extremes to Droplet Heating. The evaporative model in its traditional formulation includes uniform droplet heating. Further, as Ref. 77 has shown, Penner's (or Williams) model may also be extended to include uniform droplet heating by the addition of drop vapor diffusion equations. One must of course, in the latter case, assume the flame is anchored around the drop from the inception of heating and burning. Obviously the latter models would heat the entire droplet to wet bulb conditions faster than the evaporative models. And since the burning rate can be shown to be greatest at the wet bulb condition (the droplet vapor pressure, or mole fraction, at the surface is greatest at this condition and the concentrating gradient is the driving force for mass diffusion) the flame sheet models would produce still greater overall burning rates than the evaporative model, even when droplet heating is considered.

Furthermore, there is actually no need to limit usage of the models to uniform heating. Both model extremes predict under QS assumptions the heat flux to the droplet surface, Q_d. Normally one assumes

$$\frac{\pi}{6} \rho_\ell c_{p_\ell} (D_d)^3 \frac{dT}{dt}$$

so that uniform heating results. However there is nothing to prevent the use of the transient heating equations within the drop, and equating heat flux gradients at the surface as the boundary condition. This in fact, is precisely what Agosta's non-uniform droplet heating model does, Ref. 65. This appears to be a more valid method of calculating non-uniform droplet heating than either Parks, et al, Ref. 78, or the Grossman model, Ref. 79. In the former work no coupling of the burning rate and droplet heating was allowed; while in the latter work the difference between T_c-T_d was held constant, an assumed exponential internal droplet temperature was utilized, and the mass flux was then calculated as the solution to the equations. The results of Ref. 79 predict slower burning rates than a uniform droplet heating model while Ref. 65 predicts just the opposite. From a physical standpoint it would appear that a non-uniform droplet heating model should yield faster evaporation (burning) rates since the surface would more rapidly approach the wet bulb condition. Thus the absolute "realistic" extremes one can imagine in describing droplet burning rates would range from a uniform droplet heating, evaporative type (El Wakil) model to a non-uniform heating, flame sheet model in which the flame is anchored from the inception of heating and burning.

Under even mild convective conditions, experimental data and analytical analysis indicate that non-uniform heating may not be possible due to the development of internal circulation (caused by shear) within the droplet, Ref. 80. In any event, again because the axial gas temperature in a rocket rapidly reaches its maximum value and most propellants in droplet form heat rapidly, the difference in the absolute range of extremes is not as large as would be expected, Though it certainly would be analytically and experimentally observable.

<u>Validity of Model Extremes at Stagnant Wet Bulb Conditions</u>. All of these

aforementioned models avoid mathematical treatment of reaction kinetics within

the boundary layer. For the stagnant environment wet bulb case, recent analytical

solutions using the method of matched asymptotic expansions (Ref. 81) have shown

that vaporization and thin-flame models actually represent limiting cases of the

more general treatment which considers finite rate chemistry. Further, the

combustion enhanced gasification rate can be expressed compactly in terms of

these two limiting solutions and an appropriate Damköhler number (ratio of

characteristic diffusion time to chemical reaction time). This Damköhler

number, D_1, may be calculated from

$$D_1 = (\text{const.}) \ \frac{k'(T_{f,ad}) \ e^{n \ D_d^2}}{\mathcal{D} \rho} \ \sim \ p^{(n/2)} \ D_d$$

where a single chemical reaction step or order "n" has been assumed. The rate

constant, k', is evaluated at the adiabatic flame temperature.

For most practical cases, a multivalued solution of the burning rate as a function of

D_1 is found, with an unstable branch as illustrated in Fig. 11. As a result, gas-

ification should closely approximate either of the two limiting cases until an

auto-ignition or auto-extinction region is reached, whereupon a rapid transition

is to be expected. In these calculations one step reaction kinetics were utilized

and for each value of, $p^{n/2} \ D_d$, such parameters as ambient oxidizer concentration,

temperature level, etc. were held constant. The resultant curve is for droplet

vapors having reasonably large activation energies. What this implies is that

there are certain values of $p^{n/2} \ D_d$ where only vaporization (or burning) would

be possible, but that there is a large region in which either gasification rates
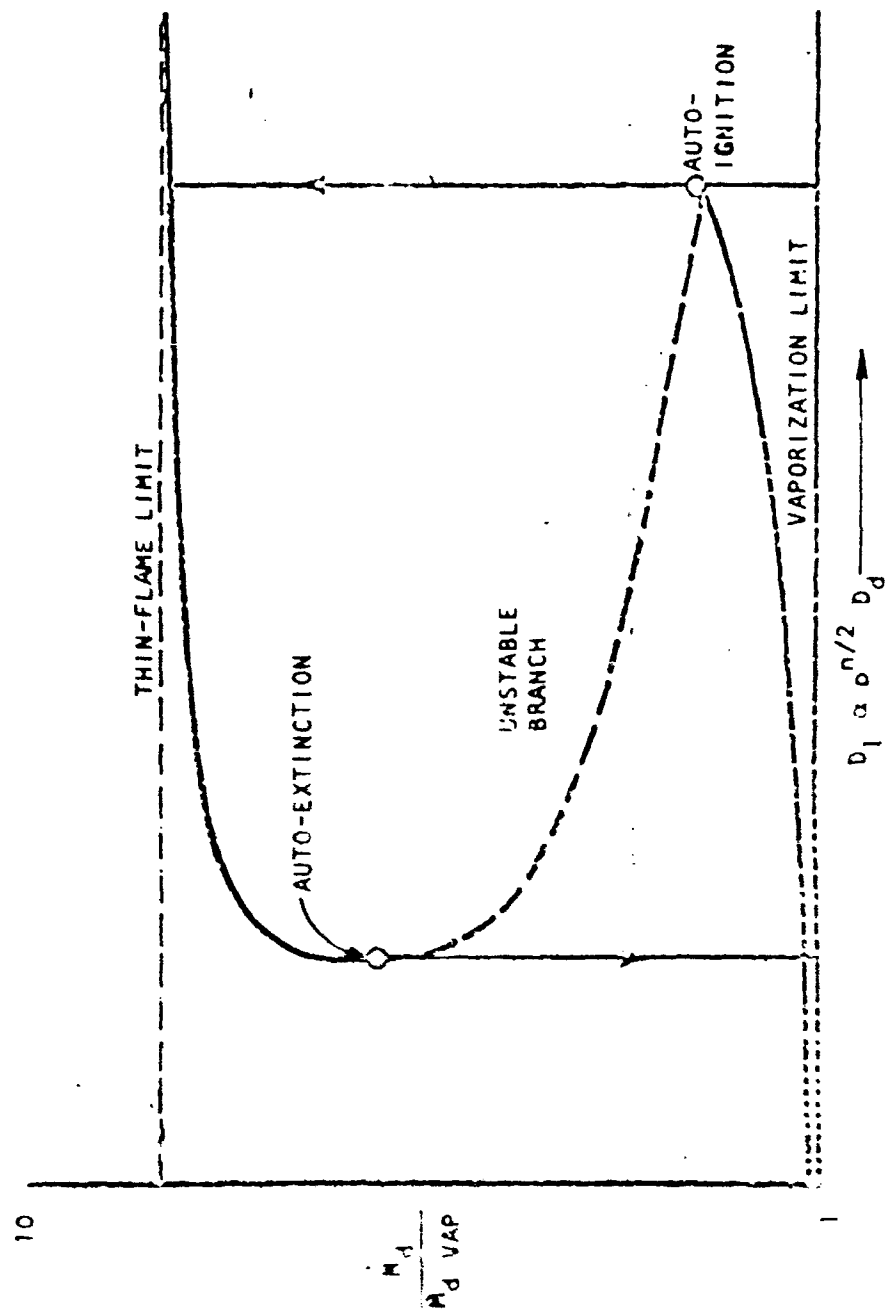
Figure 11. Vaporization and Burning Rates as Functions of Damköhler Number

much like pure vaporizations or flame sheet burning are both possible. Note the curve of Fig. 11 says nothing about the rates of ignition or extinction or when they occur (in the droplets history). Quasi-steady, wet bulb conditions were assumed for the calculations, that is, the profiles of concentration, etc., are determined for each point in the curve. The theory predicts only whether or not ignition, etc., can occur. Further, the actual limits of the curves depend in particular on the assumptions involved, oxidizer concentration in outer gas, etc. Extensive computation would be required to map out similar curves for various conditions. What is important from the standpoint of the models discussed, however, is the indication that for almost all values of D_1, the El Wakil type model well represents the lower curve, while the thin flame model is close to the upper curve. By the time oxidizer levels are decreased in the combustion gas of a rocket engine, the gas temperature would be close to the flame sheet model so it appears that such effects would tend to cancel each other if parametric studies were performed at various bulk gas conditions.

Effects of Convection. The choice of which model extreme is most appropriate is still not clear. It should be recalled that the analysis represented in Fig. 11 is for stagnant conditions. In a rocket engine the flows can be huge, relative velocities between the drops and gas of a few hundred to 2000 ft a second, and relative Re up to 1000 in value ($Nu \approx 30$). In reality the droplet flow field conservation equations should be solved for r, Θ coordinate dependents, but so far this has only been developed for creeping flow solutions, $Re \ll 1$ (Ref. 62). In place of this it is necessary to use Nu number corrections to account for convective effects (distortion, etc.).

Further, convection introduces flame extinction problems. Spalding, Ref. 83, has developed a semi-quantitative treatment according to which there is a finite upper limit (set by homogeneous chemical kinetics) to the flux of fuel vapor that can be consumed by a diffusion flame zone. The effect of increased relative velocity is to continuously increase the fuel flux "imposed" on the flame; this results in an increased flame zone thickness, decreased concentration and temperatures and ultimate local extinction of the flame. The theory predicts that U_{ext} should depend linearly on D_d, although this has not been adequately, experimentally confirmed. In any event

$$\frac{U_{ext}}{D_d} \sim fcn \ (T, \ concentration, \ P, \ etc.)$$

and indications are that U_{ext} is quite small in most cases, Fig. 12, Ref. 83a, as an example. In a rocket engine it is possible that in many cases the more appropriate model to use might be the vaporization extreme. Spaldings treatment assumes the flowing external gas to be of near ambient condition. In a rocket the external flowing gas may be high temperature. In such a case extinction may still occur but the following agreement seems more plausible. Schuman and Sutton, Ref. 114, have investigated such cases with a new droplet burning model developed from original ideas due to Schuman. They conclude that what is important is the path taken by a packet of vapor leaving the surface of the droplet. Under such conditions, considering the temperature, concentration gradient around the drop, and the short residence time in the boundary layer due to the large convective flow, the important criteria is the ratio of time the packet of vapor spends in the regions where temperature and concentration effects would allow ignition compared to the ignition delay time. Results of the calculation to date indicate that, at least, for LOX-hydrogen combustion, that ignition of the LOX vapor does not, in high convective flows, occur until the packet is in the droplet wake where residence times are large, and "micro-mixing" processes are rapid.

R-8377

117

Figure 12. Effects of Cor‎‎‎ction on Droplet Gasification

R-8377

<u>Summary of Burning Rate Models.</u> Moderate convection has been found experimentally
to force the flame into the droplet wake. In any case, the flame enhancement of
gasification is removed, resulting in a vaporization process. It is known, also,
that flame-holding capability of the droplets is quite sensitive to the free-stream
gas temperature. Insufficient data are available as yet to define the relationship
between these effects well enough to predict with confidence the extent of flame
enhancement on droplet gasification under any prescribed environment. It must be
emphasized that both the theoretical treatments and droplet burning experiments
(from which the foregoing concepts derive) pertain, with few exceptions, to the
nonconvective situation. Application of models based on this information to the
highly convective environment prevalent in a rocket thrust chamber must be made
with caution and with maximum reliance on empirical verification.

In cases with highly convective environment, the El Wakil equations often give a
correlation between predicted and observed behavior. In any event heating and gasi-
fication rates are enhanced by forced convection; the empirical Nusselt number cor-
relation of Ranz and Marshall is invariably employed. There are potential problems
with this correlation at very high convective conditions. It is not known how well
it accounts for drop distortion, high mass transfer rates on the film thickness, and
whether it is entirely applicable to burning droplets. However, there is no better
correlation to date. Further, in comparing models which use these film based cor-
relations it is necessary to be consistent in the definition of film property evalua-
tion for all the models to obtain valid comparisons.

The discussion has been primarily concerned with subcritical droplet burning of bi-
propellant type sprays. There are of course other contributions of mass addition to
the gas phase. These may include micro-mixing phenomena such as the burning of super-
critical drops (Ref. 8, Chapter 2), for which no adequate model considering the effects
of convection exists. Figure 13 presents a plot of $\dfrac{\dot{m}}{D_o N_u}$ versus Pc utilizing both

R-8377   119
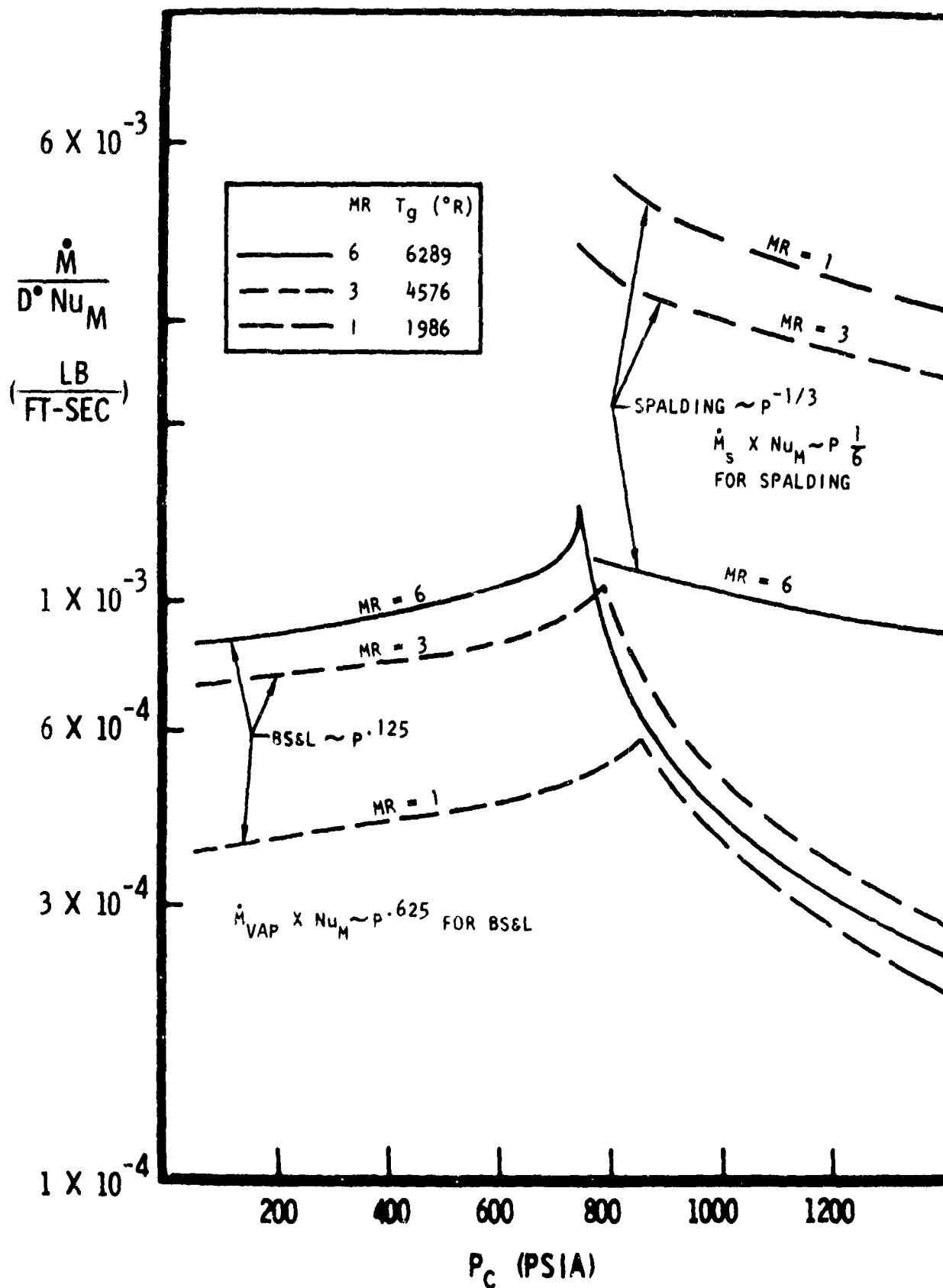
Figure 13. Mass Evaporation Rate as a Function
of Pressure

the original El Wakil equations at wet bulb (-ailed BS & L cn the plot) and Spalding's
supercritical model. Near the critical point the discontinuity, except ac a mixture
ratio of 6, between the two models is so great that under convective conditions the
model does not predict the gradual increase of rocket engine efficiency with pressure
as found experimentally. Note that the decreasing right hand side of the BJ &L quations
is not real but is due to the neglect of real gas properties on the vapor pressure
and the "heat of vaporization". Further, the use of Spalding's model or Rosner's in a
rocket combustor is not really correct, since their original derivations were for non-
changing boundary conditions and a supercritical packet or "droplet" flowing downstream
in a rocket combustor experiences a continuously changing boundary condition. Adaptation
of the models to such conditions is not straightforward as discussed in Ref. 28.

Preliminary results from Schuman's model, Ref. 114, indicate that it may be the best
diffusion model available for use within a rocket engine. It is applicable to both
subcritical and supercritical operation and at very low pressures collapses to the
original El Wakil equations.

As previously stated the El Wakil droplet heating and vaporization model ceases to be
accurate as the pressure exceeds the critical pressure of the droplet fluid. In its
application in most spray combustion models, it has been used to calculate droplet heat-
ing to the critical temperature. However, when doing so the droplet vapor pressure has
been assumed to vary only with liquid temperature; if the effect of ambient pressure
on vapor pressure is accounted for, even with the old model, all droplets are always
calculated to reach a "wet bulb" temperature below the critical temperature. However,
this temperature becomes infinitesimally close to the critical temperature and the
vaporization rate is predicted to be extraordinarily high.

The El Wakil model has been extended and improved to overcome this phys'cally unreal-
istic result. The new model will be referred to as the droplet diffusion model. The

main difference between it and the old model is that the radial mass flux of combustion gas in the film surrounding the droplet is no longer assumed to be equal to zero. Instead, the molar flux of combustion gas is defined at the droplet surface through a moving control volume formulation such that changes in the droplet radius, due to droplet density changes and diffusion, cause it to be greater than or less than zero. That is

$$M_{cg} \, N_{cg} = \rho_{m_d} \, \frac{dr_d}{dt} \tag{1}$$

Thus, as the droplet "burns" the external diffusing combustion gas is allowed to enter the control volume and occupy that fraction of the volume vacated by the receding droplet surface.

The diffusion rate, or burning rate, is defined by the diffusion equation and is

$$\dot{m}_j^n = \frac{2 \pi D_j^n}{B} \left(\frac{p M_{v_{jf}}}{\mathcal{R} T_f} \right) \mathcal{D}_{v_{jf}} \left(\frac{Nu_m}{2} \right) \ln \left[\frac{1 - x_{v_{cg}} B}{1 - x_{v_j}^n B} \right] \tag{2}$$

where

$$B \equiv 1 - A \, \frac{M_{v_{jf}}}{M_{c_{gf}}} \tag{3}$$

NOTE: Here f refers to "film" conditions.

$$A = \frac{M_{cg} N_{cg}}{M_{v_j} N_{v_j}}$$

The droplet heatup rate is defined to be

$$Q_j^n = \frac{k_f z N_H D_j^n}{(C_{p_{v_{jf}}} - A C_{p_{cgf}})} \left\{ \frac{(C_{pv_{jf}} - A C_{p_{cgf}})}{(e^z - 1)} (T_{cg} - T_j)^n - \Delta H_{v_j}^n \right\} \tag{5}$$

where

$$z \equiv \frac{(C_{p_{v_{jf}}} - A C_{p_{cgf}})}{k_f B} \left(\frac{Nu_m}{Nu_H} \right) \left(\frac{p M_{v_{jf}}}{T_f} \right) \mathcal{D}_{v_{jf}} \ln \left(\frac{1 - x_{v_{cg}} B}{1 - x_{v_j}^n B} \right) \tag{6}$$

The "droplet" diameter is defined such that

$$\overset{.}{m}{}_{j}^{n} = -\frac{d}{dt}\left(\pi \frac{D_{j}^{n3}}{6}\rho_{j}^{n}\right)$$

(7)

It should be noted that the model does not include the solubility of the combustion gas in the propellan', either as a·liquid droplet or as a gas pocket. Upon being heated through the critical temperature, a liquid droplet may be thought of as a "virtual droplet" with a discrete semi-permeable surface which permits outflow of propellant vapor but blocks inflow of combustion gases.

Comparison of the foregoing droplet diffusion model equations with the old model equations, e.g., as given by El Wakil, shows them to be very similar. The major differences are the appearance of the parameters A and B in Eq. (2), (5), and (6). Examination of Eq. (1), (3) and (4) shows, however, that A and B depend upon the heating and vaporization rates so that the droplet diffusion model must be solved implicitly by iterative methods.

On the other hand, if the heating and vaporization rates are low enough that dr_d/dt vanishes, the droplet diffusion model reduces rigorously to the El Wakil model. This is consistent with all the assumptions in their derivations being identical except for that expressed by Eq. (1). The major assumptions are (1) spherical symmetry, (2) quasi steady-state behavior, (3) diffusion is a two-species process, (4) the temperature within each drop is uniform, and (5) the outer boundary condition may be expressed in terms of the droplet Nusselt number and the free-stream gas properties. Chemical reactions are not taken into account directly in the droplet heating and diffusion models but combustion is calculated by specifying a bulk gas equilibrium flame temperature and zero droplet vapor mass fraction in the local free stream. Also taken into account are the non-ideal effects of total pressure on both the propellant vapor pressure and heat of vaporization.

R-8377

Other mass loss mechanisms may also include effects such as "flashing" (where the drop or portions of it reach a sufficiently high temperature so that drop vapor pressure becomes higher than chamber pressure and hence "flashes" into a vapor) which may occur during periods of transient burning. Or other processes may include drop vapor accumulation effects in the drop wake or a variety of other phenomena that have received little or no analytical attention. There is also an entire field of monopropellant droplet combustion; the reader is referred to Chapter 2 of Ref. 8, for a complete discussion of this subject.

Additionally, no model yet available appears entirely suitable for use in describing highly oscillatory combustion (instability), (Ref. 60).

In any event all of the models suffer the same limitations: extensions of their formulations, usually developed for and checked experimentally under near-stagnant flow conditions, to the highly convective, high temperature and pressure gradient conditions of a rocket engine. Additionally the models represent the effects of a single droplet, yet dense sprays are present in the rocket; the effects of interaction are not known. All of these phenomena require further investigation.

Drag Force

Calculation of the drag force coupling terms, which appear in the gas and spray phase momentum equations, is usually accomplished through specification of individual droplet drag coefficients, computation of individual droplet drag and summation over all droplets that constitute the spray(s) being analyzed. The drag coefficients most often used are expressed as empirical correlations of appropriate experimental data. Sometimes the expressions are given the form of a theoretically derived drag coefficient (Stokes' Law) with "corrections" to account for effects neglected in the theory. For lack of definitive liquid droplet drag data, correlations for solid spherical particles are frequently applied to calculations of spray dynamics. The following discussion,

therefore, deals mainly with solid particle drag coefficients, with only some quali-
tative concluding remarks concerning deviations caused by spray droplet distortion,
circulation, vaporization and vapor combustion.

The classical, theoretical solution for the drag force on a single spherical body
in an infinite, low-velocity fluid is known as Stokes' Law:

$$F_D = 6 \pi \mu u r$$

As derived and discussed in many standard texts (e.g., Ref. 84, 85, 86, and 87) this
results from an exact solution of the Navier-Stokes equation, neglecting the non-linear
convective, or inertial, terms. It agrees with experimental data in the "creeping-flow"
regime corresponding to $R_e \leq 1$, but under predicts drag for higher Reynolds numbers.
Defining the drag coefficient by

$$F_D = \frac{1}{2} \rho u^2 C_D A_{cs}, \text{ where } A_{cs} = \pi r^2$$

the Stokes Law drag coefficient is

$$C_D = \frac{12 \mu}{\rho u r} = \frac{24}{R_e}$$

Stokes' derivation does not fully satisfy the boundary condition at infinity (Ref. 85),
a difficulty attacked by Oseen who retained the convective terms in that far field. The
Oseen equations were still linear and an exact, infinite-series solution was obtained.
One result may be written as a first order correction of Stokes' Law:

$$C_D = \frac{24}{R_e} \left[1 + \frac{3}{16} R_e + 0 (R_e^2) \right]$$

which is but a slight improvement, overpredicting the drag for $R_e \geq 1$ about as much as
Stokes' Law under predicts it.

Improved accuracy presumably could be achieved by retaining more terms, but it has
been shown that terms like $R_e^2 (Ln R_e)$ are missing because of Oseen's initial simplifi-
cations of the governing equations. By a method of matched inner and outer expansions,
Proudman and Pearson in 1957 (discussed in Ref. 85 and 87) derived the more accurate
1st order solution:

$$C_D = \frac{24}{R_e} \left[1 + \frac{3}{16} R_e + \frac{9}{160} R_e^2 (\mathrm{Ln}\, R_e) + O(R_e^2) \right]$$

whose range of validity has apparently not been determined. (It may be noted, however, that a second order solution with subtractive terms would apparently be needed to prevent overpredicting C_D for $R_e \geq 1$ even more than does Oseen's solution.)

The "standard" drag coefficient for a sphere in a steady fluid flow has been determined experimentally; data plots appear, e.g., in Ref. 84, 85 and 86. For the range $R_e < 200$, it is well-approximated by:

$$C_D = \frac{24}{R_e} \left[1 + \frac{(R_e)^{2/3}}{6} \right]$$

as well as other formulae which have been used.

Deviations from the "standard" drag coefficient for a single sphere are observed if there are complexities in the fluid flow (e.g., ordered or turbulent fluctuations, vorticity, axial acceleration, rarefaction, compressibility), if the particle is complex (distorted shape, rough surface, porous, fluid) or if there are several or many particles which may interact with each other. Some of these phenomena have been studied analytically for low Reynolds number flow, but most of them are so complex that empirical correlations are required.

A number of complexities, such as axisymmetric asphericity, arbitrary shapes, slip flow at the particle surface and multiple particle interactions, are treated analytically for creeping flow ($R_e < 1$) in Ref. 87. One of the most interesting analytical developments, to be found there, is the solution for interactions between particles. A numerically complicated "method of reflections" is used to account for particles that are close enough together to interact; typically, interparticle spacings on the order of 10 or fewer particle radii lead to appreciable effects. An interaction factor λ is defined such that

$$F_D = 6\pi\mu \; \mathrm{ur}\,\lambda$$

Values of λ calculated by the method of reflections applied to two particles agreed very well with experimental data. Solutions are also given for three and four interacting particles, but beyond two particles available experimental data are very sparse.

As indicated in Figs. 14 and 15, the interaction between particles reduces the drag force experienced by an individual particle in creeping flow. Thus, sedimentation speeds of dust or liquid suspensions are higher at high particle concentrations than at low concentrations. Soo (Ref. 86, Chap. 5) plotted the opposite effect (i.e., increasing drag coefficients with increasing particle concentrations) as applying uniformly over the range $Re > 10^{-2}$. His graph, however, was based on correlations derived from fluidized bed and packed bed pressure drop data and it is not indicated whether the correlations were valid in the creeping flow regime or were simply extrapolated from higher Reynolds numbers. Certainly, drag coefficients are found to be increased by multiple particle interactions when Reynolds numbers are high enough that the convective terms should not be neglected. Additional definitive experimental data were reported by Rowe (Ref. 88) for 1/2-inch diameter polyethylene spheres in water at Reynolds numbers of 32-96. Drag on one sphere in a fixed array of spheres was measured as a function of particle spacing and expressed as a ratio of the drag at a given spacing to that for one in isolation at the same superficial fluid velocity; results are reproduced in Fig. 16. A best-fit curve through the data is given by:

$$\frac{F}{F_\infty} = \frac{0.68d}{x} + 1$$
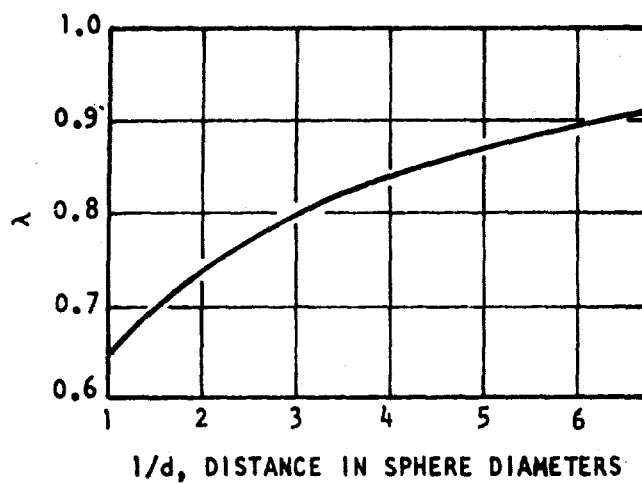
Figure 14. λ vs l/d for Two Spheres Falling Parallel to
Their Line of Centers. (Ref.87)
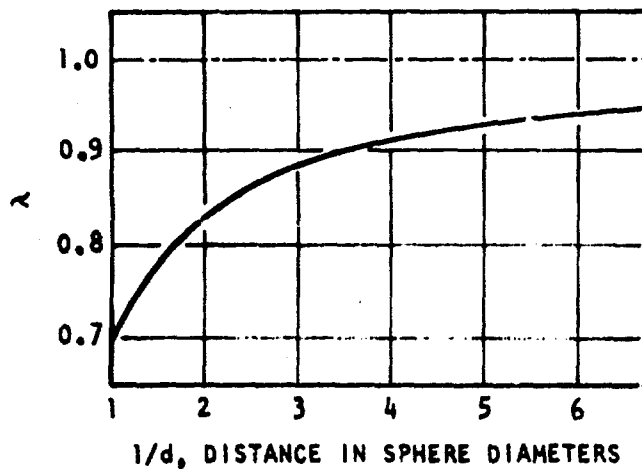
Figure 15. λ vs l/d for Two Spheres Falling Perpendicular to
Their Line of Centers. (Ref.87)
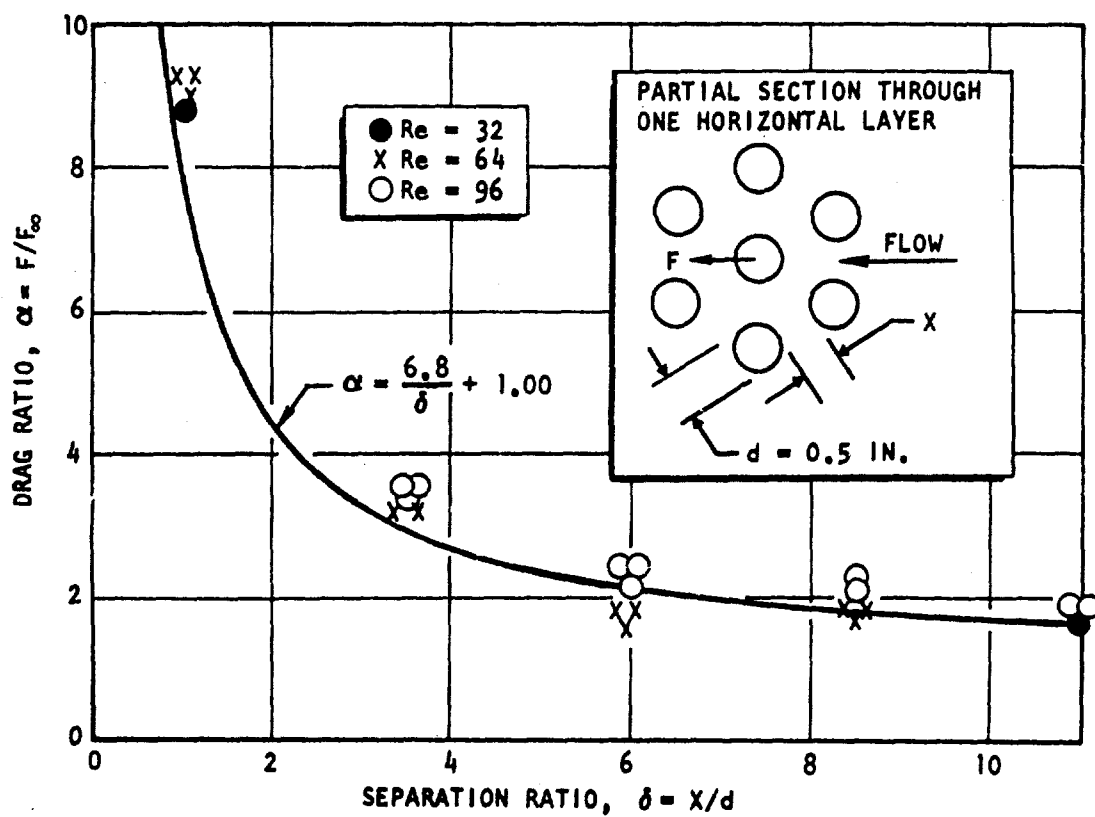
Figure 16. Variation of Drag Ratio with Separation (Ref. 88).

with d = sphere diameter and x = space between adjacent spheres. This formula gives a value of 69 for x/d = 0.01 which, Rowe stated, agreed well with an experimental value for packed spheres. Note that there is no apparent systematic variation with Reynolds number here, which is unlike the fluidization, packed bed correlations quoted by Soo. Part of the explanation for these results may lie in the semantics of the problem. If F_{∞} is based on the same upstream velocity as when the particle interaction is present part of the apparent increase in drag force may be due to the increased interstitial velocity and closely spaced particles.

In another recent experimental study, Rudinger inferred drag coefficients from shock tube measurements on the acceleration of small (62 micron) airborne glass beads (Ref. 89). Particle loading ratios of 0.05 to 0.36 lb particles/lb gas correspond to values of Roew's x/d of about 17 to 35, from which drag coefficients about 1.2 to 1.4 times the isolated particle values might be inferred. As Reynolds numbers were reduced from about 200, however, Rudinger observed values that diverged rapidly from that factor, reaching ratios as large as about 25 at Reynolds number of 10 (Fig. 17). He gave a mean correlating line as

$$C_D = \frac{6000}{R_e^{1.7}}$$

and observed that points move essentially along the correlation with changes in shock strength but are translated to the left if smaller particles were used by an amount that is less than the direct effect of particle size on Reynolds number. After examining several potential causes of the high drag coefficients, such as impulsively accelerated flow, delayed mixing of wakes into the gas stream, electrostatic effects, non-constancy of particle sizes and densities and particle collisions*, Rudinger developed a simplified flow model whose solutions reproduce,

_____
*An explanation, proposed by Soo (Ref. 86), of earlier Rudinger high C_D data in terms of gas viscosity increases due to temperature rises across shock waves appears not to be supported by changes with shock strength moving along the correlation, since the largest differences from "standard" sphere drag occur at low R_e numbers, i.e., at low shock strengths.
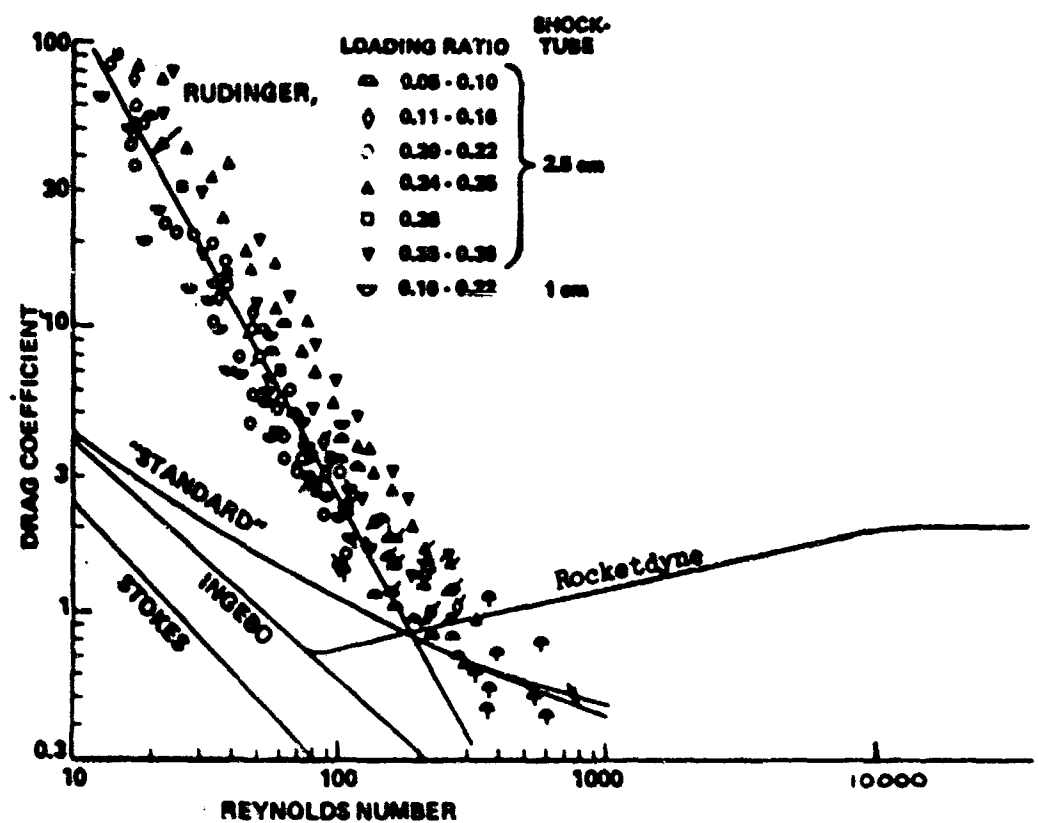
Figure 17. CORRELATIONS OF DRAG COEFFICIENT AND REYNOLDS NUMBER
AND EXPERIMENTAL RESULTS. SHAPE OF SYMBOLS INDICATES
RANGE OF THE LOADING RATIO. PARTICLE DIAMETERS ARE
29 μm (OPEN SYMBOLS) AND 62 μm (FILLED-IN) SYMBOLS. THE
"FLAGGED" SYMBOLS REFER TO POINTS IMMEDIATELY BEHIND
THE SHOCK FRONT.

at least qualitatively, the major features of his experimental findings. The fundamental bases for the model are that transverse motions of a particle inter-mittently carry it through other particles' wakes so that velocity is perturbed and that these perturbations are not self-cancelling but, through the non-linear convective terms is the momentum equation, accumulate as substantially deviations from the steady-flow, single particle drag. This re-emphasizes the importance of the convective terms in development of theoretical models. However, though his qualitative arguments may be correct, at this point the quantitative data appears to yield suspiciously large values of C_d.

Such transverse displacements and particle interactions can be readily imagined to have accentuated importance in a turbulent gas-particle flow. If a single particle is large compared to the scale of fluid stream turbulence, its drag coefficient will be lower than in laminar flow with the same mean velocity (due to delayed boundary layer separation). However, in flows of suspensions, the particles are usually small compared to the turbulence scale and the particle interaction effects should be similar to those discussed for laminar flow. Ex-perimental studies of drag coefficient variations with turbulence intensity have been reported by Clamen and Gauvin (Ref. 95).

In addition to the convective effects, Carlson and Hoglund (Ref. 90) have dis-cussed and correlated effects on particle drag coefficients due to slip flow around the particles (rarefaction) and high relative velocities between par-ticles and a carrier gas (compressibility). Their empirical correlation was expressed as a set of multiplicative factors applied to Stokes' Law:

$$C_D = \frac{24}{R_e} \frac{F_{convection} \, F_{compressible}}{F_{rarefaction}}$$

Drag coefficients are lowered by both the compressible and rarefaction factors, which may deviate appreciably from unity in the nozzle portions of rocket combustors. A more recent algebraic expression derived by Crowe (Ref.91) apparently represents some experimental data better than does Carlson's, particularly as free-molecular flow is approached.

Although Rudinger found little influence of flow acceleration on his spherical particle drag coefficients, other investigators (e.g., Ref.92) have observed appreciable reductions due to acceleration. The magnitude of reduction has been expressed analytically (Ref.93) as a function of an acceleration modulus, Ac,

$$\frac{C_D - C_{DO}}{C_{D_o}} \geq - \frac{\pi}{9} \ Ac$$

where $C_{Do} = C_D \ (Ac = o)$ and $Ac = \frac{2a}{u^2} \frac{\partial u_d}{\partial t}$ with a = sphere radius, u = local gas velocity and u_d = local particle velocity. For drag coefficients of the order of unity, the magnitude of ΔC_D is of the order of Ac so that the effect of acceleration can be neglected for $Ac \leq 0.1$ or so.

Liquid droplet drag coefficients have been found to differ substantially from those for solid spheres under certain conditions. Droplet evaporation may cause some reduction in C_D but large effects are seen when the droplet vapors burn. Related analytically to reduced surface skin friction (Ref.93), this effect may also be enhanced by lowered profile or form drag resulting from vapor burning in the droplet wake.

Droplet distortion also influences C_D. Rabin et al (Ref. 94) observed that small individual propellant droplets exposed to weak shocks follow Ingebo's correlation (Ref. 92) for accelerating spheres at Reynolds numbers below about 80, but experience increased drag at higher Reynolds numbers, eventually approaching the observed behavior of flat discs normal to the flow. Some, but little effect of fuel droplet burning (in O_2) was seen in the C_D data, apparently distortion being the more important effect. As a result, a combination of Ingebo's and Rabin's empirical correlations has been used for droplet drag calculations in many analytical spray combustion models. In these applications, no modifications have been introduced to account for the other complexities discussed earlier (particle interactions, turbulence, compressibility, rarefaction, etc.). It is apparent that improved capability for rocket combustion analysis will require that these phenomena be investigated and correlated.

Droplet Breakup

A liquid droplet in a flowing gaseous medium will, in general, travel at a different velocity than the surrounding fluid and thus will experience pressure and viscous drag forces. Depending upon the size of the droplet, the relative velocities, the flow duration and several gas and liquid physical properties, the droplet may be deformed by these forces, even to the point of disintegration, or breakup. Consideration of these phenomena is important to analysis of propellant spray combustion: droplet breakup acts to increase propellant gasification rates and to reduce propellant residence times in a combustor.

There are two distinct modes of droplet breakup: bag and shear. Bag breakup is moderately slow, being characterized by gradual pressure-force distortion of a spherical drop to a planetary ellipsoid, a flattened disc, a rim with a bag extending to the leeward side, continued stretching of the bag until it ruptures and, finally, separation of the rim into a number of medium size droplets under surface tension forces. Shear breakup occurs faster and more continuously than does bag breakup. In this mode, as droplet distortion due to pressure forces proceeds, viscous shear forces on the droplet surface simultaneously set up a circulating boundary layer flow within the droplet and a complex capillary wave pattern on its surface. Breakup apparently involves both stripping of wave crests and liquid boundary layer separation from the droplet at its perimeter.

An excellent, carefully documented review of experimental and analytical studies of drop shattering was given in 1966 by Dabora and others (Ref.96) working under Prof. J. A. Nicholls at the University of Michigan. Subsequently, most

of the published work on drop breakup has been conducted by that same group.
The approach taken in this report section is to give a brief precis of the
1966 review, including the most pertinent references and summarizations of
results from more recent studies.

Experimental studies in the 1950's by Lane (Ref. 97), Hanson (Ref. 98) and Hines
(Ref. 99) delineated the different modes of breakup. Results were correlated
in terms of critical Weber numbers (We $= \rho\, u_d\, D/\sigma$). Bag breakup occurred for
Weber numbers exceeding 3.6 to 8.4 and was superceded by shear breakup for Weber
numbers much in excess of 10. Rabin, et al (Ref. 100) found that a more reproducible
demarcation between bag and shear breakup was We $\tilde{=}$ Re$^{1/2}$. Because of the rather
restricted range of occurrence of bag breakup, most effort has been devoted to
shear breakup. A majority of experimental studies has been conducted in shock
tubes with quite weak (Ref. 97, 98, and 100) to moderately strong (Ref. 102 and 96)
shockwaves. There is general agreement that breakup results from the convective
flow behind the shock, rather than from any action of the shock front itself.

Droplet breakup transients are important; particular emphasis has been placed
on the total breakup time (from first exposure to completion of disintegration)
and on the breakup delay time (from first exposure to beginning of disintegra-
tion). Because total breakup times are difficult to measure accurately, Wolfe
and Anderson (Ref. 101) dealt primarily with breakup delay times. Most
other investigators, however, have maintained interest in the total time;
to some extent, discrepancies in their results may be attributed to rather
subjective determination of the "completion" of breakup. There is substan-
tial general agreement, from analytical studies as well as empirical correlations

that total breakup times are of the form

$$t_b = C \ \frac{D}{u - u_d} \sqrt{\frac{\rho_\ell}{\rho}}$$

were C is a constant. The exponents on the diameter, velocity difference and density ratio parameters have varied somewhat, in some studies, from those given here.

The liquid stripped from a droplet normally is very finely divided and is commonly referred to as micro-spray or micro-mist. Mean product droplet sizes have not been measured, although there are indications that they may lie in the sub-micron to a few microns range. As shear breakup proceeds, the parent droplet mass is depleted faster than its drag force diminishes, it accelerates with respect to the gas and the velocity gradient is thereby reduced. Eventually, the surface stripping may cease, leaving a residual droplet in the 30 to 50 micron range and traveling nearly at local gas velocity. Accounting for such residual spray may be important to rocket performance analysis.

Droplet deformation under shear breakup conditions as denoted by D/D_{sphere}, has been found to proceed linearly in time for about $1/3$ of the total breakup time (Ref. 103)to a maximum value on the order of 3 to $3\frac{1}{2}$. As this deformation progresses, the gas velocity across the perimeter grows rapidly, as shown by an analysis of potential flow around a planetary ellipsoid (Ref.104) enhancing stripping. For a minor to major diameter ratio of 0.3, the perimetric velocity is nearly double that at the perimeter of a sphere. This shows that it is important to account for droplet distortion in analyzing shear breakup.

All of the cited investigations were concerned with the breakup of isolated, individual droplets. Use of the derived breakup rate expressions in spray combustion analysis has usually resulted in overprediction of spray combustion rates and performance as compared with experimental firing observations. One presumed explanation for such discrepancies is that interparticle interactions (sheltering) must reduce substantially the breakup rates. This effect has not been investigated systematically at all; the only observations that have been made are some unreported two-drop experiments by Rojec at Rocketdyne. With two equal diameter 1500μ, RP-1 drops spaced about 1/2 drop diameter apart with one directly behind the other, the front drop's breakup proceeded normally while the second drop appeared to be essentially undisturbed for about half of the first drop's total breakup time, Fig. 18. These drops were subjected to a fairly mild shock in ambient air. Shock overpressures were approximately 20 psi; no ignition of the droplets was observed. These drops were free of any suspension. It thus appears that droplet breakup in a dense spray may be half, or less, as fast as isolated drop breakup. This effect needs to be investigated quantitatively and thoroughly.
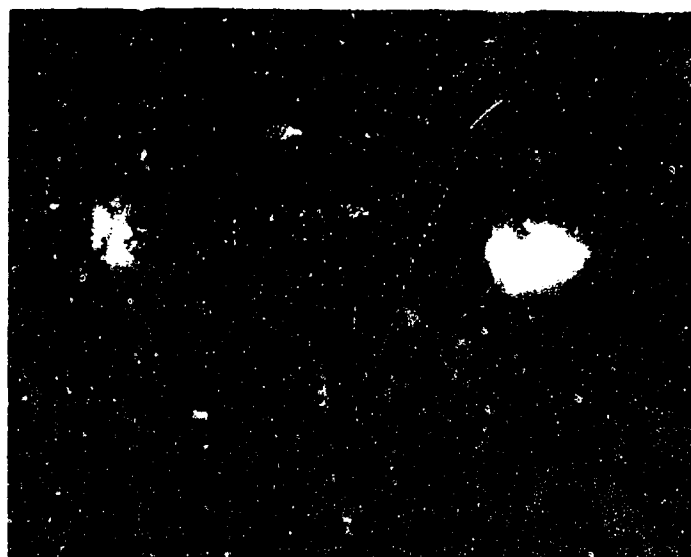
t_o = Onset of Breakup of
Right Hand Drop
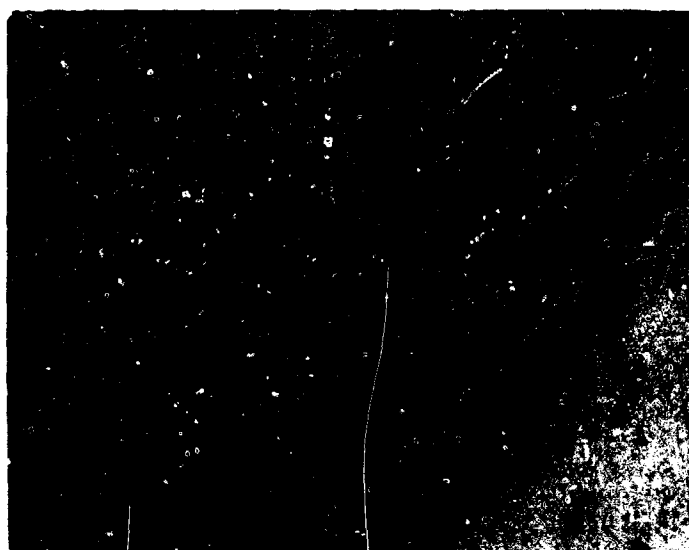
$t = t_o + 50 \mu \sec$

Figure 18. The Effect of Droplet Sheltering on Drop Breakup

METHOD OF ANALYSIS

REQUIREMENTS FOR OBTAINING DATA

As discussed previously, data are required to determine the processes
controlling spray combustion, which will permit evaluation of the
expressions used to describe the coupling terms. The coupling terms
of importance have been delineated. The purpose of this section is to
describe the methods used to obtain quantitative information about these
controlling transport processes.

It is clear from the preceding discussions of the coupling terms, that
experimental data used to gain information regarding the transport
processes must be obtained under conditions which simulate liquid rocket
operation.

Because of the highly convective, reactive, steep-gradient environment
of the rocket motor, the transport mechanisms of interest have proven
difficult to isolate and characterize. It is not surprising then that
most of the present expressions used to describe the transport coupling
processes (whether analytically or experimentally derived) were obtained
from conditions far removed from rocket spray combustion.

EXPERIMENTAL DATA REQUIRED

To overcome past deficiencies, definitive experimental results are required. In particular, the experimental conditions should simulate a liquid rocket engine. In addition, the initial conditions must be accurately defined, particularly the spray mass (dropsize) and spatial distribution. This has been a major deficiency in the past; experimental firing conditions have not been fully characterized. The experimental effort should produce results which can be realistically compared to the prediction of analytical models. This is particularly true if one is attempting to characterize the transport processes. Knowledge of the initial conditions in this case is of overwhelming importance because such items as droplet diameter and velocity are contained in the expressions for the transport processes.

In the past, information regarding precise initial conditions (i.e., initial spray mass and dropsize spatial distributions) were not known, but had to be assumed. Similarly, the downstream distribution and degree of uniformity of the spray flow field were unknown. For instability studies, perturbation sources were ill-defined and little information existed on the growth and decay rates of perturbation waves.

In addition to overcoming these problems, the experimental effort should also provide some means of directly or indirectly observing the physical phenomena (transport coupling process) being investigated. Further, quantitative data regarding this phenomena must be obtainable during both steady-state and transient operation. It is evident from all of the requirements of the experimental program that a very special device in which to perform the experiments and obtain the data, is required.

ANALYSIS REQUIRED

No less demanding is the analytical program that must accompany the experimental effort. The coupling processes (i.e., the fluid dynamics controlling the transport process) obviously depend not only on the droplet spray parameters, such as diameter, drop velocity and liquid density, but also on the gas-phase composition and conditions as well. The experimental program, as will be shown, can readily provide only the drop diameter and velocity as a function of geometry and operating conditions. Of the gas-phase parameters, however, the only one easily measured is the gas pressure. Other parameters such as the gas density, velocity, temperature and species composition must be calculated from overall steady-state and transient combustion models.

It is possible that with highly sophisticated techniques, such as laser doppler techniques, or cross turbulent correlations and zone ranging radiometry the gas-phase parameters could be measured. However, at present, these techniques are still undergoing development and, in addition, are extremely complex and costly to use. Further, it is doubtful that they could provide a more usable measurement of the needed gas parameters than an accurate combustion model.

However, it must be emphasized that the combustion model, if it is to be used to calculate the gas-phase parameters and evaluate the coupling mechanisms, must be accurately formulated. No omissions or simplifying assumption can be permitted in the conservation equations for the spray/gas flowfield that would affect the evaluation of the coupling terms. Indeed, only the coupling terms themselves should be treated as unspecified. In this manner, if the experimental work can provide sufficient information

to eliminate the need for a priori specification of the major coupling

terms, then the combustion model can be used to calculate the gas flow

field.   This, in combination with the experimental datu, allows the form

of the coupling terms to be calculated in an inverse fashion. A specific

method for this inverse calculation is described in the next section.

OVERALL METHOD OF APPROACH

The physical phenomena represented by the coupling terms should be
isotropic, i.e., equally sensitive to velocity gradients or pressure
gradients imposed from any direction. The coupling terms should,
therefore, be independent of direction and of the instability mode
experienced. Thus, for evaluation of the terms, it is reasonable
to use one-dimensional (steady and transient) models. Once evaluated,
the appropriate coupling terms may be utilized for performance or
stability predictions in any of the models, whether one-dimensional
or multi-dimensional.

Consequently, an experimental device was designed and constructed to
produce results compatible with the one dimensional models and which
may be realistically compared with the model predictions.

EXPERIMENTAL PROGRAM

Summary of Development

An experimental system has been designed, built and cold-flow tested, but
not yet successfully hot fired to produce the desired results. The experimental

apparatus is unique in that it utilizes a monodisperse propellant spray uniformly distributed throughout the combustor. Conditions in the spray combustion field are designed for precise control and definition. These characteristics of the flow are those (the initial conditions) that one is often forced to assume in order to obtain tractable mathematical models, but have rarely been approached in experiments to test the validity of analytical predictions.

The motor, operated as a rocket combustor under either stable or transient conditions, is quartz-windowed on two-sides to permit photographic and optical observations. Because the design conditions are uniform and well-defined, accurate determination of droplet behavior (particularly axial variation of drop diameter and velocity) should be facilitated. In addition, a special perturbation device has been designed that should introduce a planar, variable-amplitude initial pressure wave, which travels upstream from the nozzle throat.

The propellants utilized in this program are gaseous hydrogen (GH_2) and liquid oxygen (LOX). A photograph of the combustion system installed in a special test stand at Rocketdyne's Combustion and Heat Transfer Laboratory is shown in Fig. 19. Some modifications have been made to the system that do not appear in the photograph. The engine fires vertically downward into a small flame bucket shown in the foreground. Propellants are delivered through feed systems which are dynamically decoupled by high-pressure drop devices from chamber pressure oscillations. Thus, when the engine is operated in an unstable-combustion condition only acoustic instability effects associated with the chamber alone are observed because the injection flowrates remain
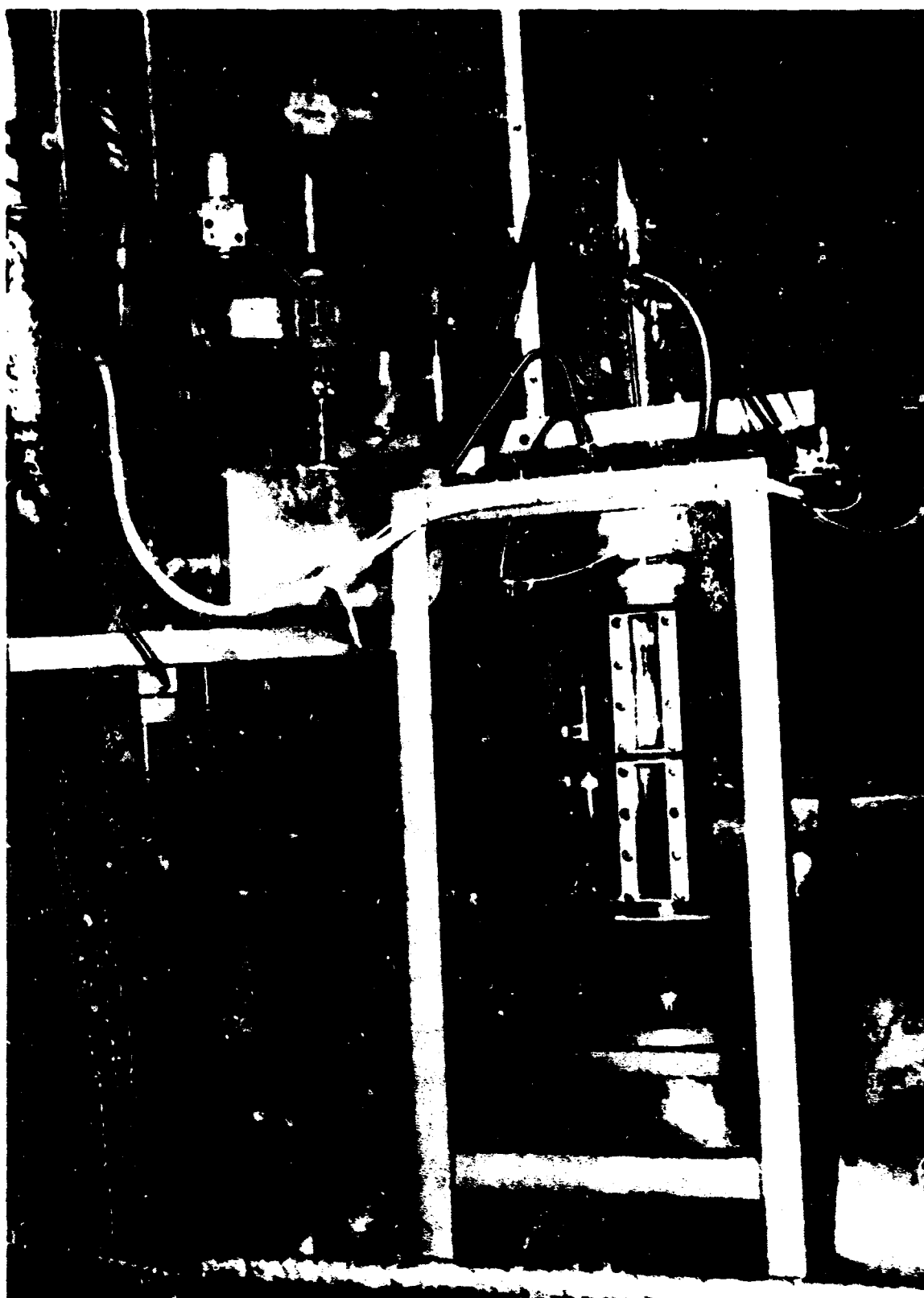
SAA54-5/27/68-S1B

Figure 19. View of Installed Combustion System
at Research Lab

essentially constant. The amplification or attenuation of the instability

waves are to be monitored and conditions which lead to wave attenuation or

growth can be determined by variation of experimental parameters.

The experiment can thus provide known initial conditions and direct experi-

mental observation (obtained under both steady and transient behavior) of

physical phenomena corresponding to the coupling terms to be investigated.

This unique device was designed, developed and brought to operational status

during this contract. An extensive investigation of the methods of producing

spatially uniform single drop-size (monodisperse) sprays was conducted to

aid the design. An oscillating piezo-electric crystal was used in the LOX

manifold to obtain the only known experimental hardware capable of producing

monodisperse sprays of a cryogenic fluid and the only known device capable

of producing (in principle) monodisperse sprays of any fluid when operated

under liquid rocket engine conditions.

Liquid oxygen spray is introduced through an injector consisting of 480,

.015-inch-diameter drilled holes.   The spray is burned with a concurrent

hydrogen gas stream injected through porous metal (Rigimesh) strips on the

injector face. The resultant flow is believed to be as near one-dimensional

as is practical to achieve. Further, the monodisperse qualities of the

generated spray have been thoroughly verified by extensive cold flows (full

flow and row-by-row). The monodisperse characteristics of the spray were

found to be good. The addition of a high-velocity gas simulating the

hydrogen had no disrupting effect on the spray formation.

Although the selection of a cryogenic propellant (LOX) produced some difficulties in achieving monodisperse spray production, these difficulties were considered acceptable because of the advantages of the propellant combination. First the LOX/GH_2 propellant combination is the primary one in use today. Almost all of the large space vehicles, such as the Space Shuttle, will utilize LOX-hydrogen propellants. Another advantage is the photographic properties of this propellant combination which are excellent. Both GH_2 and the resultant combustion product (H_2O) are transparent in the spectral range of visible light. In fact, GH_2 neither emits nor absorbs light and H_2O has bands only in the ultraviolet and infra-red regions. No vapors exist that could physically occlude the field of view, such as those encountered when trying to photograph combustion of N_2O_4- N_2H_4 or many hydrocarbon-oxygen propellants. No special window purges were required that could destroy the one dimensionality of the flow field.

Therefore, LOX-GH_2 combustion is amenable to direct photographic observation of the axial variation of droplet burning rates (i.e. diameter change) and droplet velocities. Photographic methods to achieve such measurements were investigated and found to be entirely feasible.

These data, in combination with the combustion models described later, will permit determination of the physicochemical droplet dynamic processes responsible for controlling steady-state combustion and regulating rapid combustion energy additions to pressure waves.

The data will be obtained under a variety of chamber operating conditions: mixture ratio variations from 0-6, chamber pressure up to 300 psia (steady-state), various initial drop sizes (500 to 1000μ). Data will be obtained during both stable and transient combustion. In this manner a considerable variation of experimental conditions, and corresponding data, can be input to the steady-state or transient models.

Comparisons of the experimental data with the predictions from the models will allow definition of appropriate expressions for the coupling terms.

Detailed Description of the Combustion System Development

The initial intent was to build an electro-mechanically vibrated injection device with a large number (400 to 500) of liquid oxygen streams disintegrating to form a spray of uniformly-sized droplets (in the 500 to 1000μ diameter range) falling at 30 to 40 ft/sec down a cylindrical steel tube. Annular injection of hydrogen some distance below the injector would provide a combustible mixture which would be ignited and brought to steady through-flow combustion conditions. It was roughly estimated that the evaporating droplets could fall 4-to-6-feet through the combustion gases without undergoing large changes in droplet diameter or, by inference, large changes in their ability to respond to a pressure disturbance.

This original approach has been subjected to analytical and experimental investigation and modification. The modifications are summarized in the following paragraph and are discussed in detail in succeeding subsections.

The fundamental modification involved the injection scheme for achieving monodisperse atomization. Rather than electromechanical vibration, the investigation centered around piezo-electric-crystal driven oscillations of liquid manifold pressure, a technique offering higher frequency capability with reduced sealing and liquid heating problems. The higher frequency capability permitted consideration of smaller diameter droplets; an extensive preliminary evaluation of cryogenic atomization indicated that more precise control of droplet size might be expected with smaller sizes. Capillary jet breakup into uniformly sized droplets, however, was found to require quite low injection velocities (regardless of the driving method used) -- so low, in fact, that the droplet residence times were calculated to be high enough for complete evaporation to occur in a moderately short travel distance. A steady-state combustion model was used to calculate acceptable combustion tube operating conditions. The model predictions resulted in further modifications: re rsion to large diameter droplets ($\sim 750 \mu$), concurrent injection of hydrogen from the LOX injector, shortening of the combustion tube, and provisions for photography of the spray during steady-state combustion.

Monodisperse Spray Injection Concepts. Means of achieving a continuous stream of constant diameter liquid oxygen droplets were investigated in the first few months of the program. This investigation culminated in the selection of an injection method for the combustion tube. The investigation considered atomization of one to five liquid streams; the final injector (discussed later) has 480 individual stream injection points uniformly spaced over a 2.00-inch square surface.

Despite limitations, which will be discussed, the most promising approach for producing a monodisperse liquid spray was based on Rayleigh's analysis of the instability of laminar capillary jets (Ref. 105). In a recent review of this subject (Ref. 106), Nicholls, et al., reached essentially the same conclusions as those expressed by Rayleigh's analysis:

1. Capillary instability induced disintegration of a cylindrical liquid jet into droplets of a uniform size can be enforced by imposing an oscillation of the correct frequency on the jet.

2. The oscillation frequency for maximum instability has the following relationship to the jet diameter and jet velocity:

$$f_{opt} = \frac{u_j}{4.508 \, d_j}$$

3. The frequency can be varied over a range from about $0.85 \, f_{opt}$ to $2.0 \, f_{opt}$ while maintaining uniform droplet diameter. Outside that range, the atomization no longer results in a monodisperse spray.

4. The product droplet size is related to the jet velocity, diameter, and oscillation frequency by:

$$D_d = \left(\frac{3 \, u_j \, d_j^2}{2 f_j} \right)^{1/3}$$

and, at the frequency of maximum instability,

$$D_{d,opt} = 1.89 \, d_j$$

R-8377

5. The jet velocity must lie between a minimum given by

$$(u_j)_{min} = \left(\frac{8\sigma}{d_j \, \rho_j}\right)^{1/2}$$

and the transition to turbulent flow at a Reynold's number on the order of 2300.

Substitution of the frequency equation into that for the product droplet size indicates that, as shown, the resultant droplet size is independent of the jet velocity. This result is due to the fact that Rayleigh's analysis assumes an inviscid jet. Wickemeyer, Ref. 107, has extended the analysis of capillary instability to include the effects of aerodynamic forces, jet velocity and viscosity. Although his analytical results did indicate some effect of the jet velocity, experimentation at R_e above 600 failed to confirm the analysis. His experimental findings at $R_e \geq 600$ indicate that

$$f_{opt} = \frac{u_j}{4.26 \, d_j}$$

and hence

$$D_{d_{opt}} \approx 1.8 \, d_j$$

This drop size was also the minimum he was able to produce experimentally.

Further, he experienced some difficulty in producing monodisperse sprays with L/D ratios below 33. In this L/D range his jet did not produce a parallel flow.

The latter result is contrary to results obtained during this program in that no problems were evident at L/D's as low as 3-10. Also the measured optimum droplet diameters from this program were more nearly described by Rayleigh's criteria than Wickenmeyer's. The difference may be due to the short L/D ratios and large jets used in our experiments. Possibly such geometries do not allow laminar flow to fully develop. This possibility is suggested by the fact that the actual injector of this program has been flowed at $R_e \geq 10,000$ and still produces fairly uniform, monodisperse droplet flow.

The experimental investigation was made with an electrically driven piezo-electric crystal to provide the imposed oscillation. This device has the potential advantage of very high frequency capabilities and of minimal sealing and coupling problems at elevated pressures.

The first experiments were made with a 2.0-inch diameter barium titanate crystal coupled to an injection manifold through an aluminum resonance rod. Liquid water streams were formed by flow through short pieces of capillary tubing soldered into an injection face plate. Cold flow characterization of this device with water discharged into ambient air, various capillary tube diameters and a range of frequencies showed that its behavior conformed to the foregoing classical conclusions. An example of five streams of water droplets discharged from 0.012-inch diameter capillaries is shown in Fig. 20.
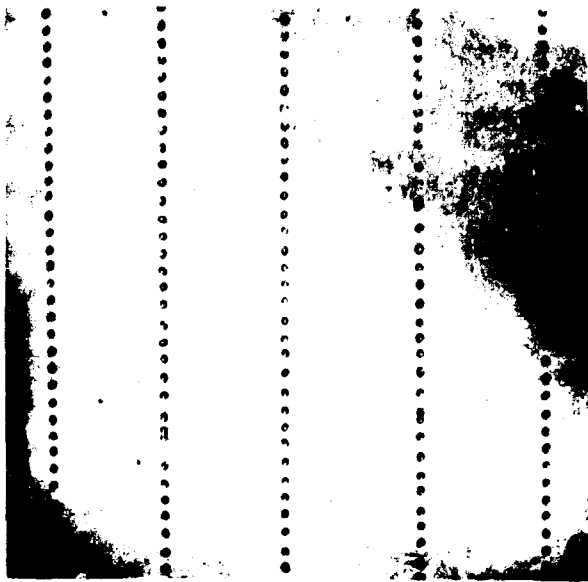
Figure 20. Array of 500-Micron Diameter Water Droplets Produced by Modulating 0.012-in. Diameter Streams at 2,340 cps
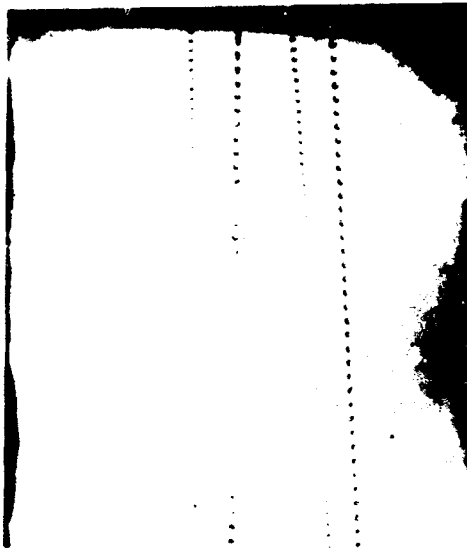
Figure 21. Four Monodisperse Water Droplet Streams from Four Different Diameter Holes Drilled Through a Piezoelectric Crystal

Another series of experiments was made with the piezoelectric crystal itself as the injector plate. An ultrasonic drilling method was used to drill 0.005-, 0.007-, 0.010-, and 0.015-inch diameter holes through a 1.0-inch diameter by 0.10-inch thick crystal. Figure 21 shows excellent monodisperse atomization of all four water streams at an oscillation frequency of 1950 cps. Interestingly, since each of the liquid streams has its own optimum frequency for maximum instability, this photograph shows satisfactory monodisperse atomization for frequencies of about 0.5 f_{opt} for the 0.005-inch jet to about 2.6 f_{opt} for the 0.015-inch jet.

The drilled crystal injector was evaluated in two extensive series of experiments with cryogenic liquids. The apparatus employed is shown schematically in Fig. 22. Tests were first conducted with liquid nitrogen (LN_2) as a simulant for liquid oxygen (LO_2) in order to avoid the oxidation hazards while developing the equipment and test techniques. In none of the experiments with LN_2, however, did the injector actually produce truly monodisperse sprays. It was suspected at the time that the LN_2 might be near a state of incipient boiling, so that slight gasification could result from slight pressure changes. This would act to absorb or decouple the oscillatory energy from the injector or even disrupt the liquid jets. Some support for this interpretation resulted from the second series of experiments, in which successful monodisperse atomization was achieved with LO_2 subcooled a few degrees below its boiling point by passage through an LN_2 bath. Results are shown in one frame of a 16 mm Fastax motion picture of a liquid oxygen spray reproduced in Fig. 23 .

R-8377

FIGURE 22. APPARATUS FOR STUDYING PIEZOELECTRIC CRYSTAL
ATOMIZATION OF CRYOGENIC LIQUIDS

R-8377

155
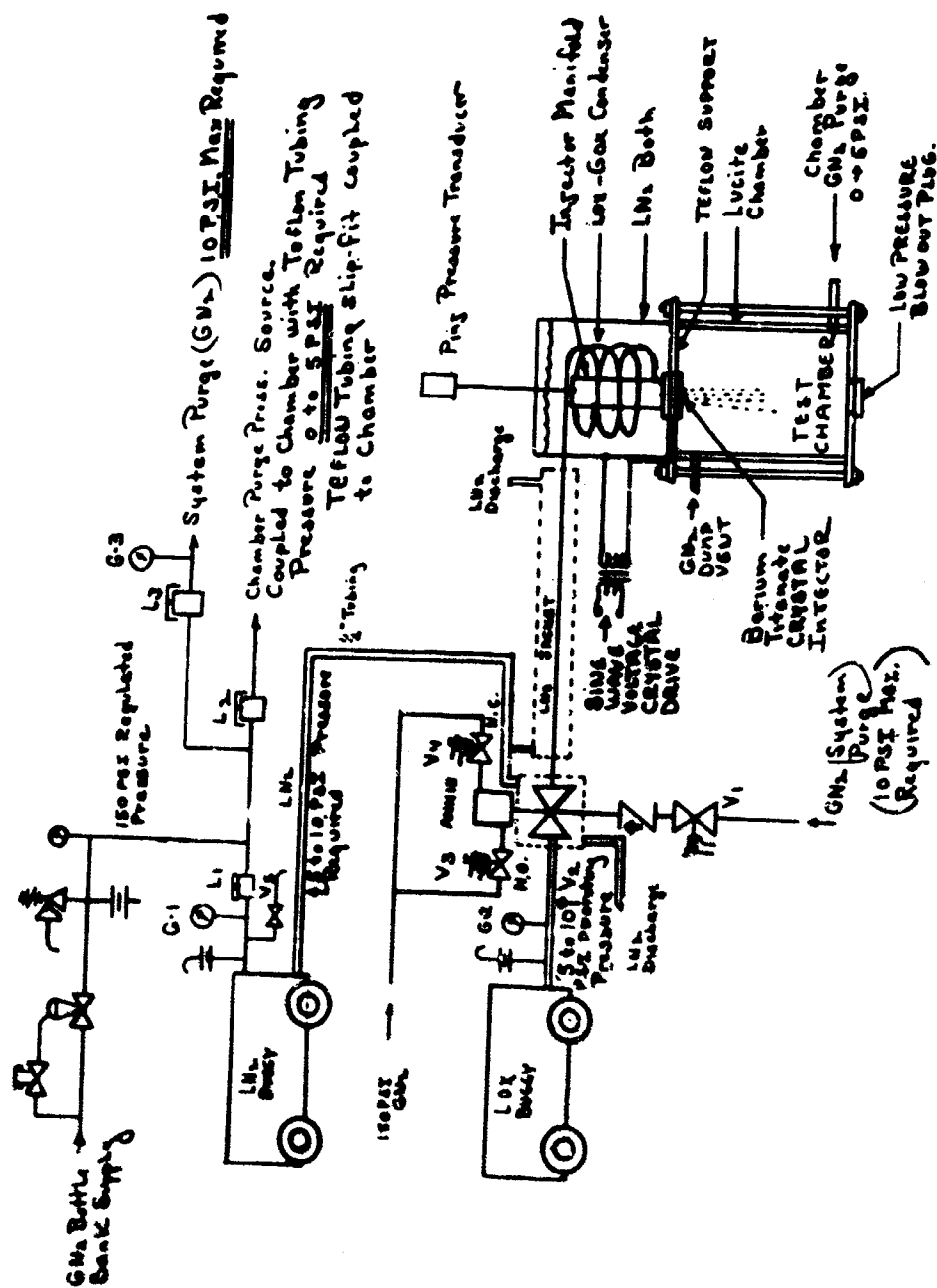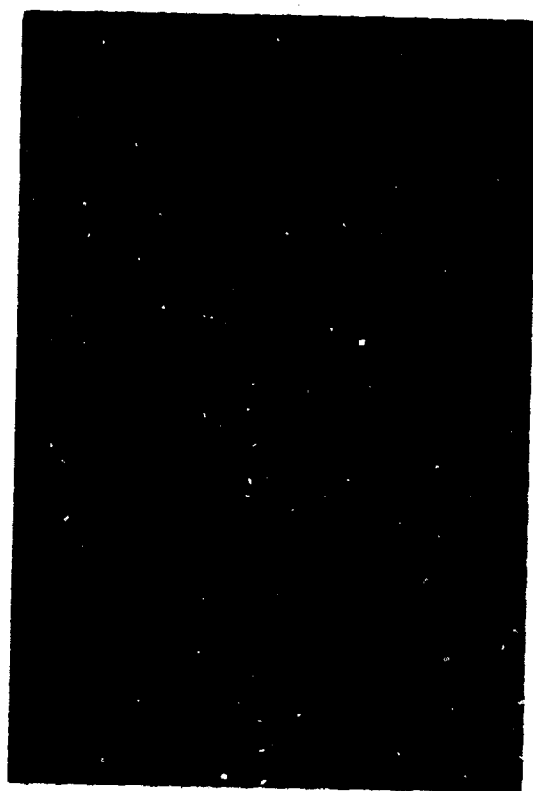
Figure 23. Four Monodisperse Liquid Oxygen
Droplet Streams from the Four Holes
Drilled Through a Piezoelectric Crystal

156

This drilled crystal injector configuration was subsequently found to be impractical for a full injector. A representative of the crystal manufacturer expressed serious doubts that the crystal would retain its response properties and structural strength if it were perforated with several hundred holes. It was regretfully decided not to use this concept, which had otherwise looked very attractive for the hot firing injector.

As a result, the earlier, capillary tube technique was adopted for LO_2 spray production. Rather than relying on mechanical transmission of oscillatory crystal energy through the injector structure, however, the crystal was installed integrally in the injector's LO_2 supply manifold. By forcing the liquid to flow through a few, moderately high ΔP holes drilled in the crystal, which spanned the manifold, the injection manifold was effectively decoupled from the hydraulic and acoustic characteristics of the upstream supply system.

A sizeable number of experiments was made in determining that good droplet formation could be achieved with this technique. Three streams, formed from ⁻.0035, 0.006, and 0.008-inch diameter capillary tubes, were examined. A typical example, with drop diameters ranging upward from 170 μ is shown in Fig. 24. The results of these tests strongly emphasized some potential problem areas: (1) monodisperse atomization was not achieved for injection velocities much above 5 ft/sec, presumably as a result of turbulent flow through the capillaries (L/D ratios for these experiments were larger than for the final design of the injector), (2) injection pressure drops are extremely low-- flowrate control by some auxiliary upstream device is mandatory, (3) vorticity in the transparent chamber, induced by low velocity tangential injection

Fig. 24 . Liquid Oxygen Droplets formed from Three
Different Diameter Capillary Tubes. Crystal
in Supply Manifold Driven at 2140 cps

158

R-8377

of "de-froster" nitrogen, disrupted monodisperse atomization, and of course, (4) prevention of capillary plugging demands scrupulous cleanliness.

At this point, the injection concepts were discussed with Professor A. K. Oppenheim and his associates at the University of California, Berkeley. In view of their successful experience in simultaneously injecting liquid through a capillary and gas through a surrounding annulus, and considering the potential disruption by uncontrolled recirculation, it was concluded that both propellants should be introduced into the chamber together, i.e., through a single injector. This decision considerably complicated the design of an injector, with an attendant increase in fabrication difficulty and expense. Minimization of the number of injection sites became very attractive, so an analysis of the combustion tube's steady-state operating conditions was undertaken to help optimize the design.

Analysis of Steady-state Experimental Conditions. Knowledge of the LO_2 spray droplet's behavior during steady-state combustion tube operation is essential to successful analysis and correlation of pressure wave growth. It is also essential for proper design of the experimental apparatus and selection of operating conditions. An existing digital computer model was used for aiding in the design of experimental apparatus. The model employs a typical evaporation-rate controlled formulation. It was obtained by modifying the formulation presented in Ref.33 for appropriate combustion tube conditions.

Initial analysis, carried out for 225 minimum diameter injection tubes
(a 15 by 15 square array with 1/8-inch between tubes) revealed immediate
conceptual difficulties in that: (1) the LO_2 injection rate was severely
limited by the combination of tube size, number of tubes, and most import-
antly, injection velocity, so that (2) only relatively low injection mixture
ratios were possible, and (3) the droplet velocities were so low that they
were completely consumed on passing only a short distance downstream of the
injector face.

The combustion region is of the primary importance and must be long
enough to install sufficient instrumentation to obtain definitive data.

As originally envisioned, there would be a region of sufficient length
where the relative velocity would be quite low and droplet size change
would be negligible. The attainment of this configuration requires (for
a fixed number of delivery tubes) both higher jet velocity and higher H_2
mass flowrate (i.e., higher combustion product velocities and, hence,
greater drag) than that previously calculated. These would result in
drop velocities sufficiently fast for the drop to travel an appreciable
distance during the first portions of burning, yet not undergo breakup.
However, raising the H_2 mass flowrate when it was not known if one could
raise the jet velocity (i.e., the mass of oxidizer delivered) could lower
the mixture ratio to an unacceptable level as well as promote breakup.

Although it was not possible to completely achieve the initially desired
concept, it was desirable to simulate it as closely as possible. There
are two requirements that allow achievement of this desired result; both

have been mentioned, high jet velocity (a factor of 3 or 4 would lengthen the combustion region by a significant amount) and high combustion gas velocity (increased propellant flow rate).

The first of these is particularly desirable and automatically allows the second while still maintaining small relative velocities. It appears possible that the laminar jet region (Hagen-Poiseuille flow) may be maintained at Reynolds numbers greater than 2300 (up to say 15,000) if the entrances to the delivery tubes are well-rounded and if the delivery tubes are short (L/D's of 3 - 10). The final injector design was able to achieve drop production at about $R_e \approx 10,000$.

However, even if higher jet Reynold's numbers were not attainable the combustion region could be lengthened by one or both of the following methods: (1) increasing the propellant flow rate through the addition of gaseous O_2 to the H_2 stream or (2) by utilizing the same number but larger diameter delivery tubes, thus producing larger drops. (The cost of machining a given number of tubes goes down as the size of the tube increases).

Part of the injector characterization study included these methods and they are reviewed in detail below.

Gaseous O_2 may be added to the H_2 flow in amounts just below that required for flammability and, furthermore, improves the overall mixture ratio. However, if this method were used without being able to raise the jet velocity (it is

desirable to do both), the desired requirement that the combustion region be one of low relative velocity cannot be entirely met. Because the low relative velocity requirement stems from single droplet breakup criteria, and because the spray droplets will actually experience a fair amount of sheltering provided by neighboring droplets, probably this requirement can be relaxed. The limiting aspect for this approach is likely to be too rapid consumption of the spray in the burning region, in which case larger initial droplet sizes would be ultimately required.

The other method, production of larger drops, directly increases the oxidizer flow rate. This allows (for the same mixture ratio) higher hydrogen mass flow rate and, thus, an increase in combustion gas velocity. Disadvantages here are the initial size of the drop, which is quite far removed from actual rocket engine conditions, and of course the same breakup questions that apply for the first method.

After a detailed comparative study of these competing methods, the latter was chosen. Premixing gaseous O_2 and H_2 prior to injection appeared to involve too high risk of hardware destruction to warrant its use unless the objectives could not otherwise be met.

Modified Tube, Injector Designs. The modified tube and injector designs appear in Figures 25 and 26. The gas phase is now introduced through the injector face with separate manifolding for the liquid phase oxidizer and

ANG -31 ; 8 REQ'D

PIEZO ELECTRIC
CERAMIC - 2" DIA. x
.30 THICK;
*G 1400 M , FULL ELEC-
TRODES - ELECTRA-
SCIENTIFIC CO.;
ELECTRA WAY,
FULLERTON, CALIF.

R3C1698;
2 REQ'D

R3C1690

R3C1691

ROCKETDYNE
A DIVISION OF NORTH AMERICAN AVIATION, INC.
CANOGA PARK, CALIFORNIA · McGREGOR, TEXAS

MONO-DISPERSED
SPRAY ENGINE

SIZE	CODE IDENT NO.	
D	02602	R3D1699

SCALE Full   SHEET

Fig. 25 Combustion Tube Design

R3D169T

ANG-31; 8 REQ'D

R3C1696

R3C1694 ; 4 REQ'D
MS29513-261 ; 4 REQ'D

PIEZO ELECTRIC
CERAMIC - 3" DIA &
.30 THICK;
SG 1400 M, FULL ELEC-
TRODES - ELECTRA-
SCIENTIFIC CO. ;
ELECTRA WAY,
FULLERTON, CALIF.

R3C169B,
2 REQ'D

R3C1690

R3C1691

PARKER "V" SEAL -8814-2003-0431
2 REQ'D
PARKER SEAL COMPANY
CULVER CITY, CALIF.

R3C168A

RD261-2001-0039

ANG-LENGTH
WILL DEP
(MINIMUM
TO BO

NOTE: UNLESS OTHERWISE SPECIFIED

R-0377

13

RSE 1693

RSC1695 ; 2 REQ'D

ANG - LENGTH TO SUIT , 32 REQ'D
WINDOW THICKNESS
(MINIMUM THREAD ENGAGEMENT
TO BE .43")

RD261-2001-0049

MONO-DISPERSED
SPRAY ENGINE

ROCKETDYNE
A DIVISION OF NORTH AMERICAN AVIATION, INC.
CANOGA PARK, CALIFORNIA · NEOSHO, TEXAS

| D | 02602 | R3D 1699 |

Fig. 25. Combustion Tube Design

R-8377

Fig. 26. Injector Design

165/166

gaseous fuel. The Rigimesh acts to diffuse the flow, promote good mixing and hold gas-jet interference to a minimum. This scheme is felt to give a more nearly uniform gas-spray flow than bringing the gaseous propellants in further downstream where recirculation could create problems. Furthermore, a number of propellant combinations may be utilized. The design is not limited to hydrogen and oxygen.
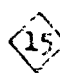
The final design specified 750μ drops (with a possible monodisperse operating range of 500μ to 1000μ) formed by capillary jet atomization of streams from 480, 0.015-inch diameter delivery tubes. Normal machining practices could be used to drill these holes, whereas smaller holes would require advanced (beyond state-of-the-art) techniques, such as laser or ultrasonic drilling, etc. The increased number of holes was necessary to achieve pressures above 100 psia at reasonable contraction ratios.

The tube is 20-inches long and has transparent quartz windows on two sides for photographic purposes. A constricting section (other than the nozzle) to obtain complete combustion, initially proposed, is no longer necessary. The modifications have brought the system much closer to the ideal engine it attempts to model. Fabrication of the system has been completed.

Description of Fabricated Combustion System

LOX Dome and Crystal Mechanism. Attached to the top of the combustion tube, as shown in Fig. 25 are the injector, the crystal holder (with the crystal inside),

and the LOX dome (manifold) which attaches to the LOX supply lines. The
LOX dome and crystal mechanisms are shown in Fig. 27 . Originally the LOX
entered through the capillary tube shown in the LOX dome. This tube pro-
vided a high pressure drop between the LOX tank and the engine, thus assuring
nearly constant flow rate to the engine even when large chamber pressure
excursions occurred. After the photograph of Fig. 27 was made, the capil-
lary tube was replaced by a drilled orifice, providing the equivalent Δ P.
The change was made to prevent plugging in the small capillary tube and to
facilitate orifice changes during runs with different flow rates. In addi-
tion, the flow distribution was improved by providing four LOX flow ports
into the dome, rather than one. Two of the LOX ports (located on opposite
sides of the dome) are connected to the drilled orifices providing high ΔP
between the tank and engine, while the other two LOX posts connect directly
to check valves, thus, providing an alternative low ΔP path to the LOX tank.
Selection of flow through either or both sides (simultaneously) is possible
through manipulation of flow valves $\langle 14 \rangle$ and $\langle 15 \rangle$ shown in the propellant
system schematic, Fig. 36 . Provision for the low pressure flow path allows
safe inspection at low tank pressures of the spray during cold flows and
chilldown prior to a hot firing. Safety limitations require that personnel
leave the test stand area when tank pressures exceed 300 psia. Prior to hot
firing, the low pressure valve $\langle 14 \rangle$ is remotely closed and the LOX tank pres-
sure increased to provide a high Δ P path for the LOX flow.

Figure 27. LOX Dome and Crystal Mechanisms

LXW73-3/18/68-S1E

R-8377

159

After filling the dome, the LOX flows through a low pressure (50 psi) drop, high porosity Rigimesh filter which serves to distribute the flow over the crystal. The crystal is loosely constrained on all sides within a Teflon seat, shown fitted around the crystal in Fig. 27. The crystal and its Teflon holder, in turn, fit loosely within the aluminum crystal holder (also Fig. 27) which is bolted between the injector and dome. The crystal holder includes seals for the electrical leads to the crystal. The bottom of the Teflon seat rests directly upon the back of the injector providing approximately 1/4-inch of space between the injector and crystal.

LOX flows uniformly across the top of the crystal and around the sides of the crystal in the space between the crystal and the holder. The LOX then flows radially inward toward the center of the crystal face filling the volume between the injector and crystal created by the 1/4-inch vertical space produced by tabs on the Teflon seat. Effectively, the crystal is immersed in the liquid oxygen. This method thus eliminated any need to "clamp" the crystal and drill holes through it to allow LOX passage.

Injector. LOX enters the 20 milled slots in the back of the injector as shown in Fig. 28. At the bottom of each slot, and located uniformly along it, are 24 drilled, 0.0145-inch diameter well-rounded orifices. LOX enters these 480 holes and is discharged into the chamber tube as showerhead jets. Operation of the crystal synchronizes the instability of these jets into Rayleigh-like capillary breakup. These discharge orifices are more clearly apparent in Fig. 29 and 30.

1XW73-3/18/68-S1F

Figure 28.   Back View of Injector

R-8377

171
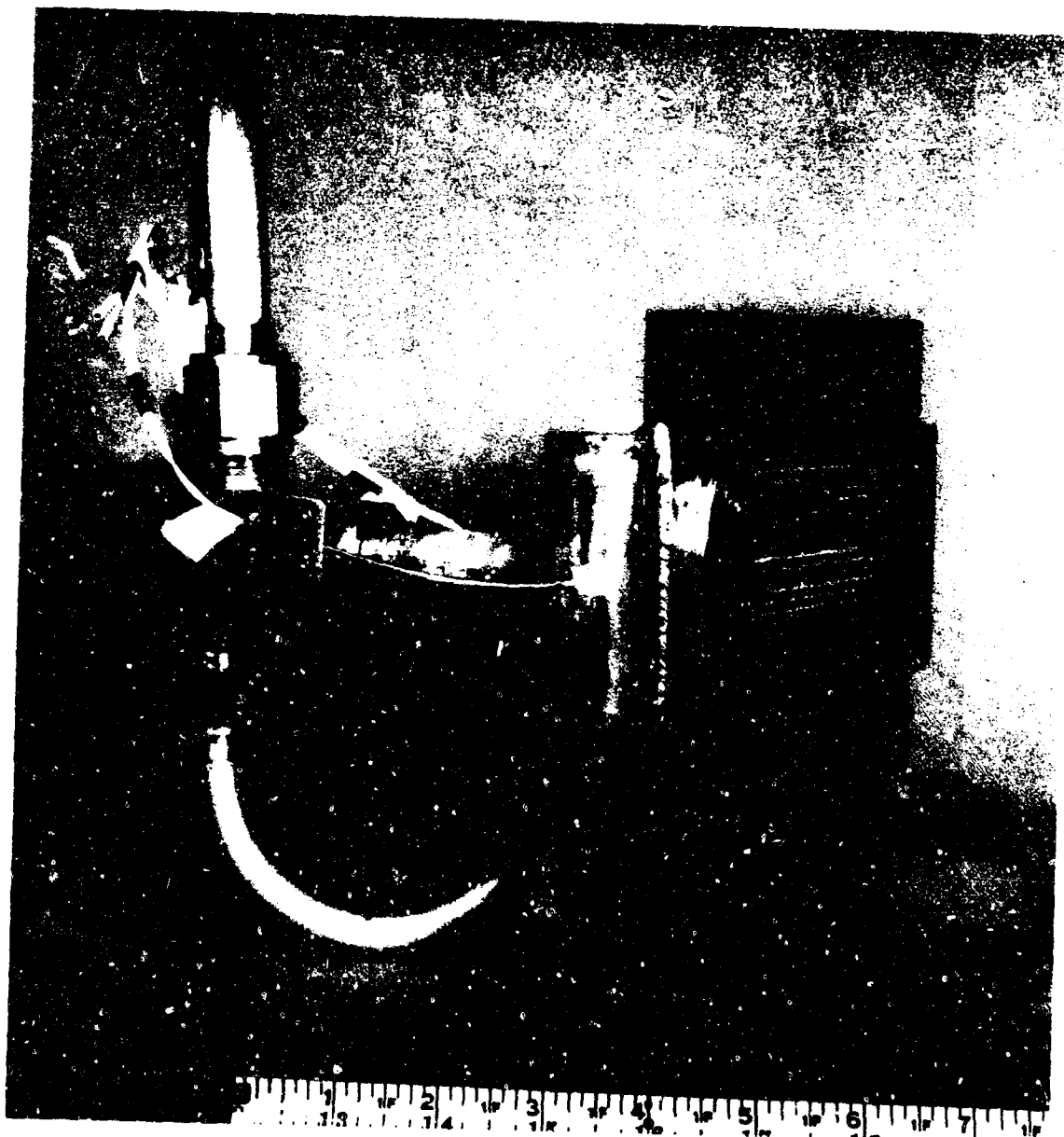
1XW73-3/18/68-S1G

Figure 29.   Side (Frontal) View of Injector

R-8377
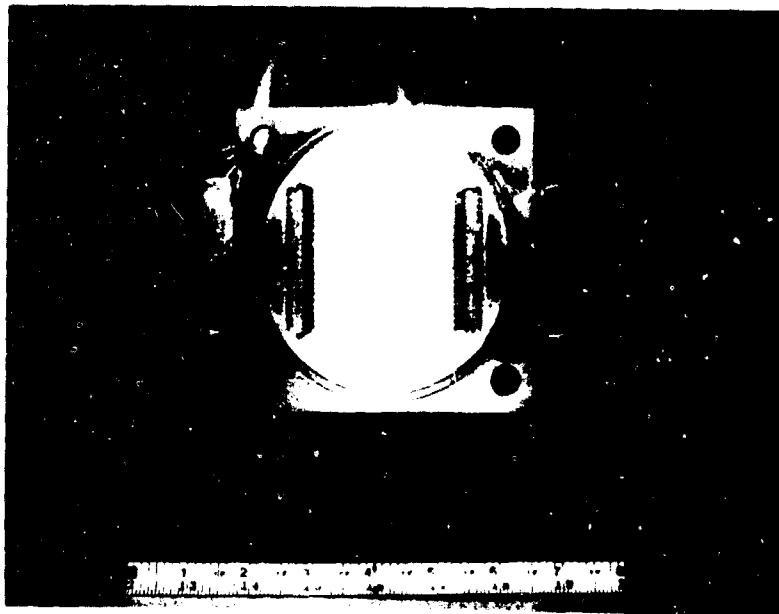
1XW73-3/18/68-S1D

Figure 30. Front View of Injector

The injector also introduces the fuel (hydrogen) into the chamber. Between the rows of LOX discharge orifices are strips of Rigimesh behind each of which is a separate hydrogen manifold passages. These passages, shown in Fig. 29, are fed by manifolds located on each end of the strips. These manifolds (shown open on Figs. 29 and 30) connect, in turn, to large entrance manifolds located on two sides of the injector. The larger manifolds are fed by supply lines which connect to the main hydrogen supply, Fig. 38.

Combustion Chamber - LN$_2$ Bath - Windows

The combustion chamber is shown in Fig. 31. It is made from stainless steel and is windowed on two sides. After the photograph of Fig. 19 was taken, a number of minor modifications were made. Additional Kistler transducer locations have been provided (13 in all), particularly for pressure wave measurements near the thrust and injector face.

In addition, the stainless steel LN$_2$ bath atop the chamber has been replaced by a Teflon bucket. The function of the LN$_2$ bath is to subcool the LOX and prevent flashing during the droplet formation. Some heat input from the lines and valves located between the tank and the injector occurs, of course. Similarly, the crystal operation produces some (but very little) heat. The LN$_2$ bath thus, assures LOX temperatures below the saturation temperature. The Teflon material on the bucket acts as an insulator to prevent rapid LN$_2$ boiloff and to block heat transfer between the bath and the combustion chamber.
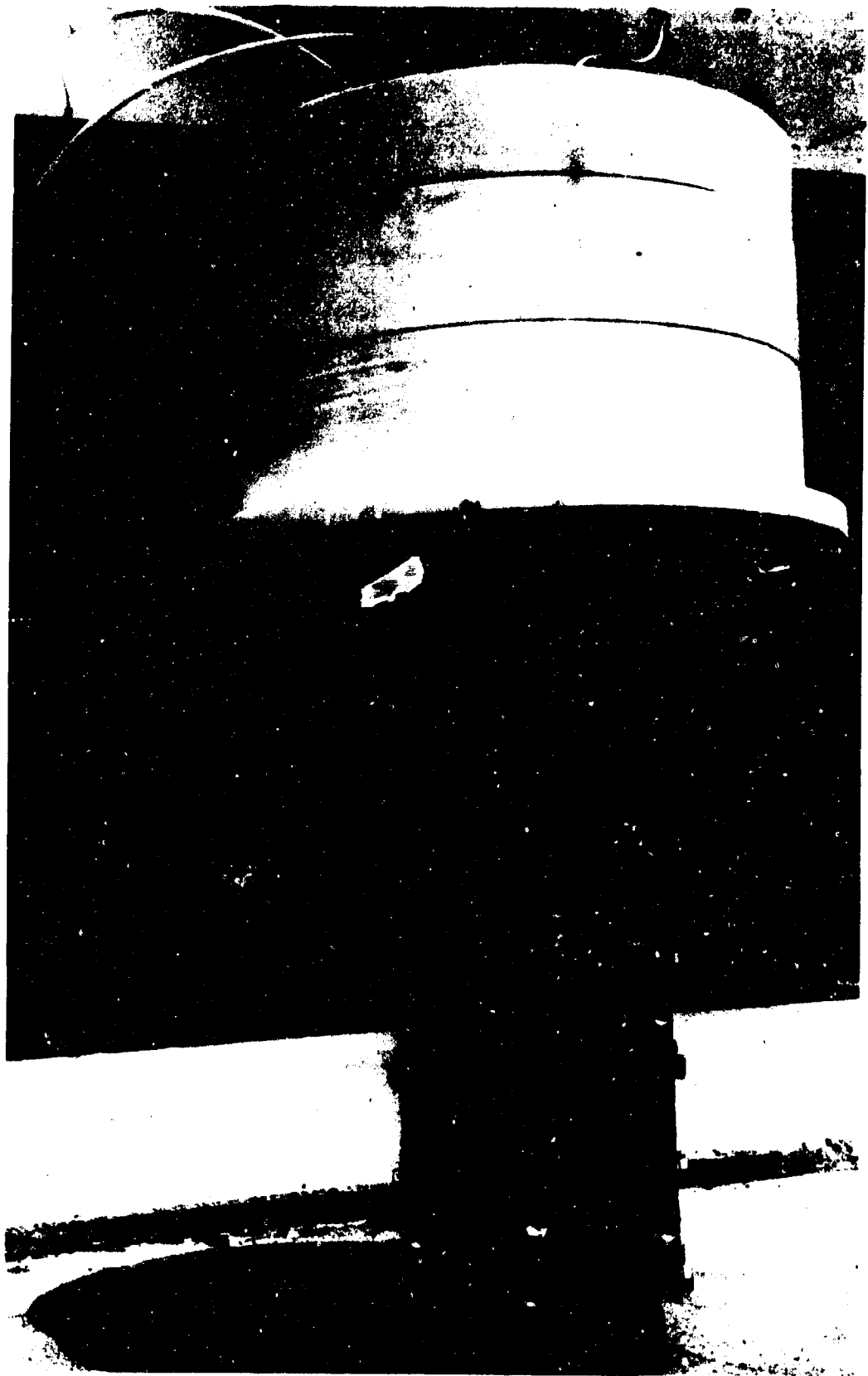
R-8377

5AD34-4/11/69-S1B

R-8377

175

Figure 31. Photograph of Modified Combustion Chamber
and LN$_2$ Bath

Heat transfer between the bath and the combustion chamber is quite serious. Not only does it chill the quartz windows, which may crack them, but also it causes condensation and ice formation on the windows which occludes them. The 3/4-inch-thick Teflon base on the bucket substantially alleviated this problem. In addition, a 1/4-inch-thick Teflon seat was added between the combustion tube and the injector. All bolts which connect the dome, etc., to the chamber (and provide a heat transfer path) have been sleeved with Teflon. This procedure eliminated much of the remaining heat transfer problem. A view (into the bucket) of the completed installation, with injector, crystal holder and dome system, is shown in Fig. 32. Most of the fittings are for two 18-foot heat-transfer coils to chill the LOX. One coil is required for the low pressure line and another for the high pressure LOX line.

Although the heat transfer problem is effectively diminished by the above modification it is not entirely eliminated, nor is the LN_2 boil-off with attendant vapors that tend to sweep over the windows and cause ice formation. Over long periods of operation (i.e., 2 to 3 hours of LN_2 in the bath) ice formation on the windows again becomes a problem. This was unfortunately accentuated by the method used to install the windows. As shown in Fig. 33 the 3/4-inch-thick quartz windows are held in place by aluminum window frames. The frames are constructed in such a manner that a fairly deep well is produced between the outside of the window frames and the outer edge of the windows. Collection of moisture, and subsequent ice formation, became a serious problem even with the greatly reduced heat transfer rates.

R-8377

Figure 32. View Into the LN$_2$ Bath Atop The Combustion Tube

1XW73-3/18/68-S1I

Figure 33. Combustion Tube Windows
and Window Frames

178

R-8377

This problem was finally solved by installing thin 1/8-inch-thick quartz windows over the entire length of the well area and directing heated GN_2 into the well area between the inner 3/4-inch pressure windows and the outer windows. Tapped holes for the fittings are shown in Fig. 31 . The completed installation is shown in Fig. 34 and 35. Note particularly in Fig. 34 the four small drilled holes at the inner top of the window frame. These holes are drilled in the top end of each frame and provide the exit path for the GN_2. In addition, to prevent ice formation on the outer cover windows it was necessary to install a window purge of heated GN_2 entirely around the perimeter of the windows (Fig. 34 and 35). This combination completely solved the ice-formation/water-condensation problem.

Initial hot-fire operation of the system resulted in cracking of the pressure windows. Quartz is sensitive to thermal shock or rapid pressure loadings, particularly if such effects result in tensile stress within the windows. Failures were traced to the rigidity of the installation technique. This was alleviated by reducing the size of the windows and floating them in silicone rubber (RTV-102). This allows some movement along the length and width of the windows. The windows are separated from metal contact by gasket material in the inside and heavy O-rings on the outside, against the bevelled inner edge of the window frames.

The convergent nozzle section and throat insert (made from OFHC copper) is contained in a steel throat plate section (Fig. 36). The contraction ratio is easily varied by changing copper throat inserts. The steel throat-plate

Figure 34. Close-Up View of Installed
Window-Frame Purge System.

R-8377

Figure 35. Assembled Combustion Tube
with Window Purges.
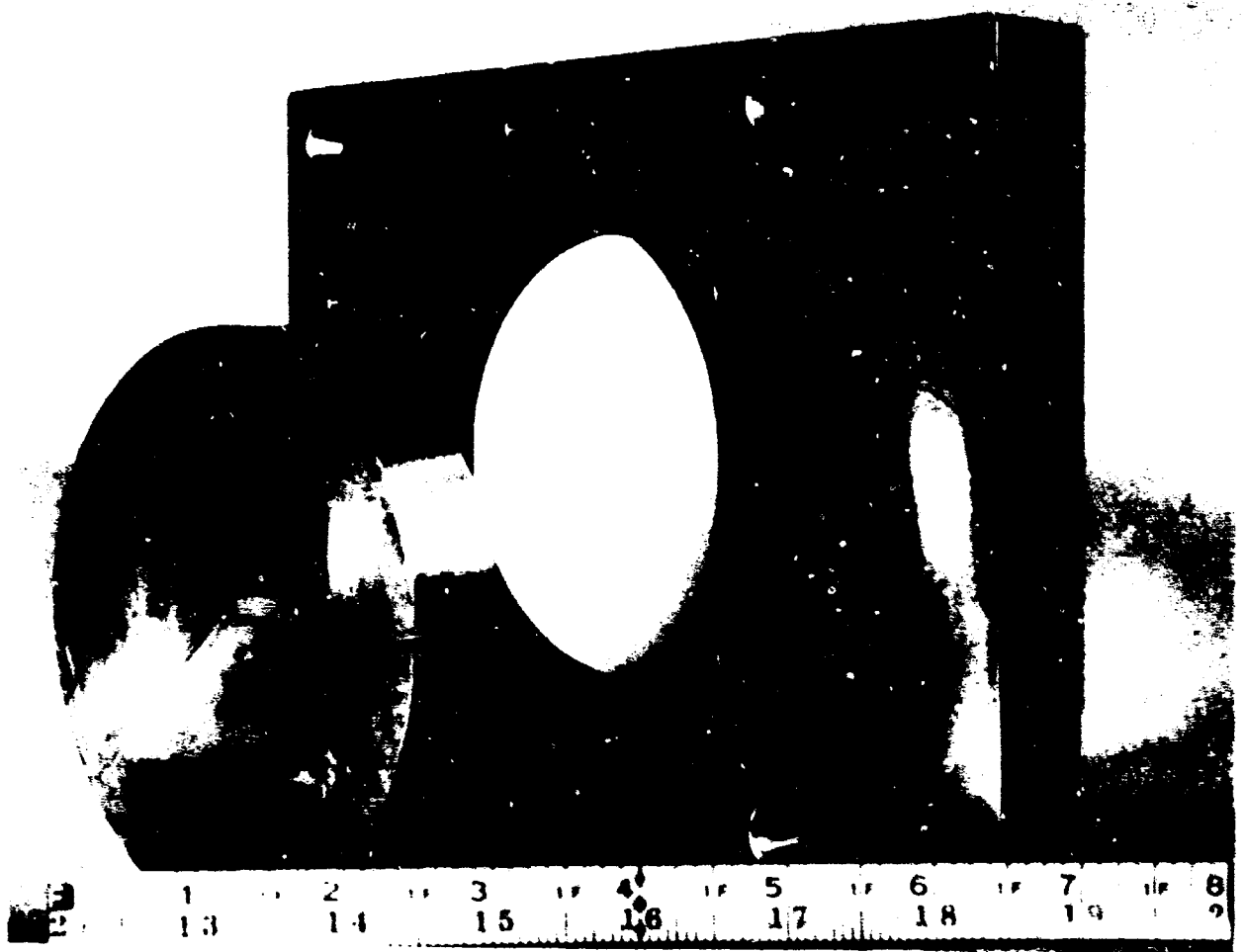
LXW73-3/18/68-S1C

Figure 36. Convergent Nozzle Section (Throat Insert)

section also serves as the bearing surface for the perturbation device. This device is a small plate (contained in a rail and covering the width of the chamber) explosively moved across the small dimension of the throat. The throat is effectively closed for approximately 20 - 50 microseconds, thus providing a well-defined pulse that is essentially planar in nature and small in duration compared to the period of the fundamental natural frequency (1500 cps) of the chamber.

Rigidity and alignment of the chamber in the test stand is controlled by adjusting bolts attached to the steel throat plate. These are shown in Fig. 19.

Injector Cold Flow Results

Following fabrication of the injector the device was cold flowed with TRIC (trichloroethylene) water, and liquid oxygen. Both full injector flow and row-by-row flow tests were performed. The full injector flow tests were also performed with and without GN_2 (gaseous nitrogen) gas flows simulating the gaseous hydrogen. Row-by-row tests were performed to determine if misalignment (in any direction) of the jets was present. These flows were achieved by blocking off 19 of the 20 milled slots on the reverse side of the injector. Some problems in distribution were observed using this method but they were not detrimental. A typical example of the row-by-row tests is shown in Fig. 37 . The particular fluid used in these tests was water at Re = 2300. Alignment was checked not only by the frontal view shown in this photograph but also
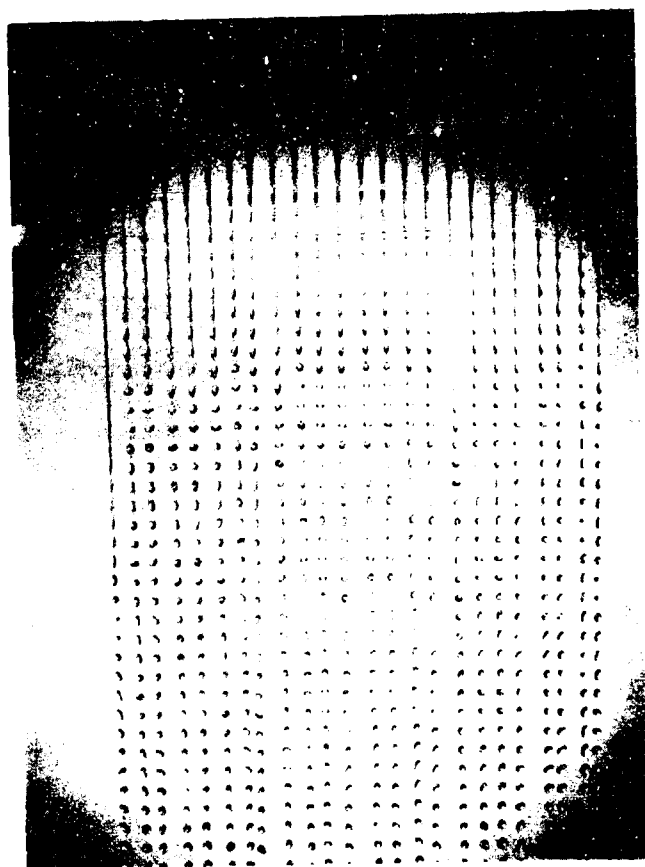
Row #6   #14
ΔP = 3.9 psi,   Re = 2300
f = 3763 H_2O

Figure 37.   Row-By-Row Injector Cold
              Flow Tests

along the row itself, i.e., in the plane normal to the photograph. Results of these tests indicated that eight of the 480 holes were hopelessly misaligned and they were subsequently blocked. Figure 37 also shows the excellent planar qualities of the flow field. This was typical of all rows and indicates the flow field is essentially one-dimensional in nature.

These row by row tests were performed in the absence of co-flowing gas. Clearly evident on the photograph is the oscillatory nature of the droplets which is retained long after formation. Approximately every seventh row the cycle is complete. Damping of this oscillation is dependent on surface tension and convective forces. Interestingly, the addition of a gas flow simulating the hydrogen in the full injector tests damped these oscillations rapidly and resulted in quite uniform and spherical droplets. Unfortunately, those results are on 16 mm film and difficult to observe unless projected. Further, no disruption of the flow field occurred with the gas tests; in fact, the gas flow appeared to stop tendencies toward collision and agglomeration.

Figure 37 also indicates the presence of small satellite droplets. These droplets, for the most part, rapidly disappear through agglomeration with the next droplet in line. They can, however, be eliminated entirely by timing of the frequency. Further, full cold flow injector tests produced better distribution and relatively few of these satellite droplets.

In all respects the drop production capabilities of the injector was deemed
satisfactory. Row-by-row tests were performed at Reynold's numbers up
to 10,000 and although the quality of the spray slightly but gradually
deteriorated above Re $\approx$ 2300, sufficiently near monodisperse spray was
still produced at the high flowrates.

Operation of the Combustion System As a Rocket Engine

Following assembly of the combustion system, it was installed in the test
stand in the manner shown in Fig. 19. The test stand is supplied by a
number of propellant, purge, water, and LN_2 systems.

Propellant System. The schematic of the main propellant systems is shown
in Fig. 38 . Primary emphasis is placed on the LOX and hydrogen systems
supplying the test stand. Some other systems, because they interact with
the main propellant lines, are also shown. However, no source supply
(except for LOX) systems are presented. These source supplies are common
to all the test stands at the laboratory and are quite elaborate in detail.

Gaseous hydrogen flow, delivered from the bottle banks, may be split, if
desired, with one portion passing through a large LN_2 heat exchanger. Flows
are subsequently joined in a spiral mixer located downstream of the heat
exchanger. Control of the proportion of the flow that is cooled allows
delivered injection temperatures to be predetermined at any desired level

PROPELLANT SYSTEM SCHEMATIC
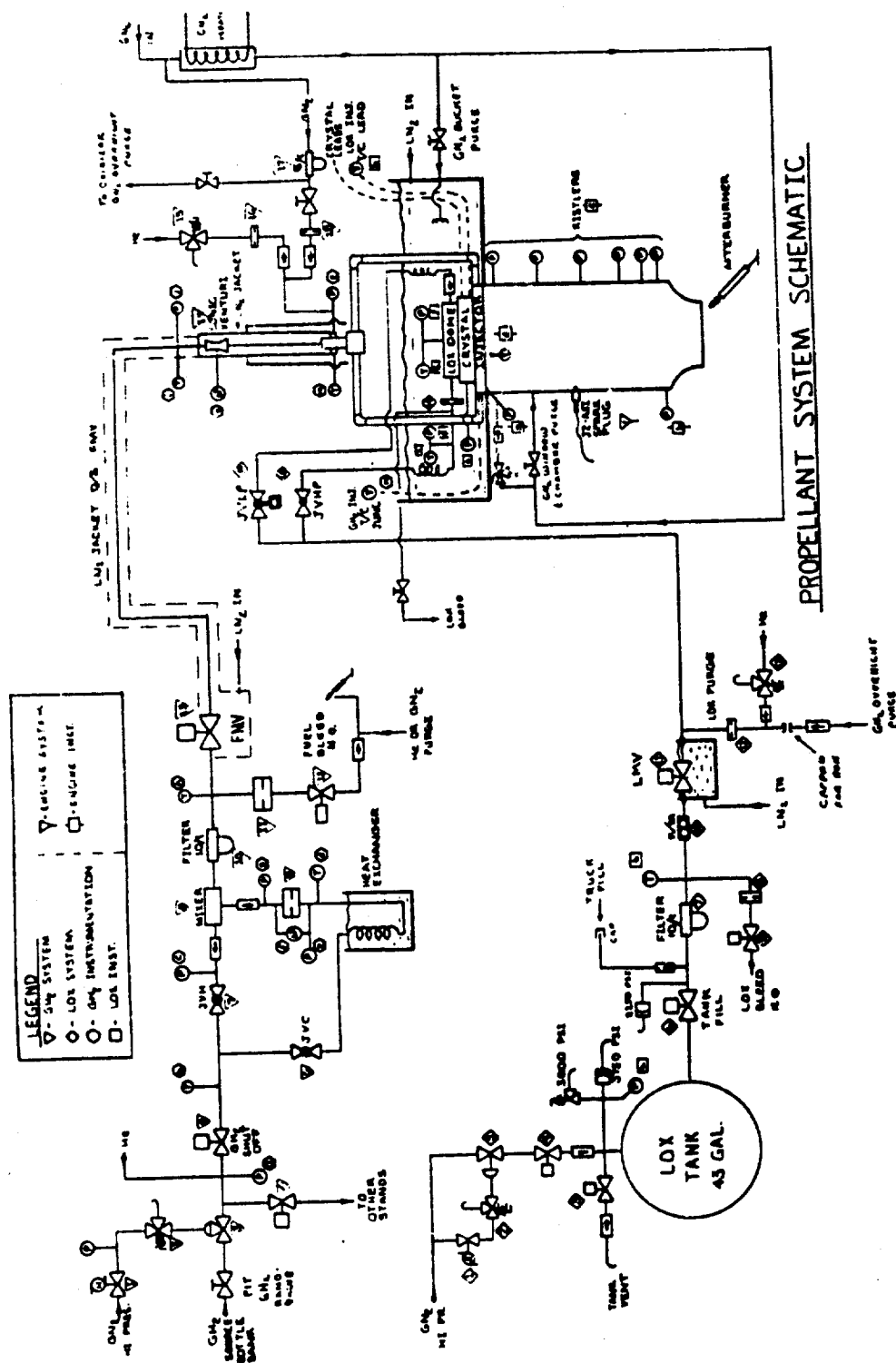
Figure 38. Propellant System Schematic

between ambient and LN_2 temperature. Liquid nitrogen jacketing around, and downstream of the fuel main valve aids in this temperature control. Total flow control is maintained and measured by a calibrated sonic venturi close coupled to the engine hydrogen supply inlet. Appropriate GH_e and GN_2 purge systems are used.

Liquid oxygen is supplied from a GN_2 pressurized tank. Supply lines are vacuum (or LN_2) jacketed from the tank to the coil inlets in the bath. The liquid oxygen main valve is cooled by a LN_2 bath. LOX flow may enter the engine through either the low ΔP or high ΔP system lines. Both supply valves $\langle 14 \rangle$ and $\langle 15 \rangle$ remain open during chilldown until liquid oxygen spray is produced within the chamber at ambient pressure.

The liquid nitrogen flow around the main propellant supply lines and valves is continuous, either dumping into the engine bath or overboard. Engine bath LN_2 level is maintained through actuation of an automatic valve, balancing boil-off and overboard runoff.

Heated GN_2 to the chamber window wells and window purge system is provided through use of a counter-flow electrical heater capable of providing GN_2 temperatures of 200°F.

<u>Hot Fire Operation</u>. Unlike most LOX-GH$_2$ engines the combustion system utilizes a LOX-rich start sequence. This is done to insure proper crystal operation and liquid oxygen spray production at the chamber prior to hot firing. A schematic of the crystal circuit is presented in Fig. 39. Upon verification of chilldown, the valve to the low pressure coil is closed and the pressure in the tank increased to maintain proper flowrate. Flowrate is continuously monitored by reading the digital output of the flowmeter located in the LOX supply lines. Upon reaching proper flowrate utilizing the high Δ P side, an additional increment of pressure equal to the expected chamber pressure for the run is added to the tank pressure. This insures rated LOX flowrate at full chamber pressure.

During this operation the GH$_2$ supply pressure is regulated to provide the desired flow. The fuel bleed is manually opened and the entire GH$_2$ system upstream of the main valve is chilled to operating temperature. The fuel bleed restrictor orifice ∇11∇ is sized to pass the same flow as the venturi.

The actual start and shutdown sequence of the engine is automatically controlled through a digital sequencer. Spark ignition occurs simultaneously with opening of the fuel main valve. This valve incorporates special controls to produce a slow ramp opening rate. Mainstage rated hydrogen flow is gradually approached with minimum disturbances of the co-flowing LOX jets and spray. The ignition source is sequenced off at completion of FMV opening (some 400 ms) and complete mainstage testing is approximately one second

R-8377
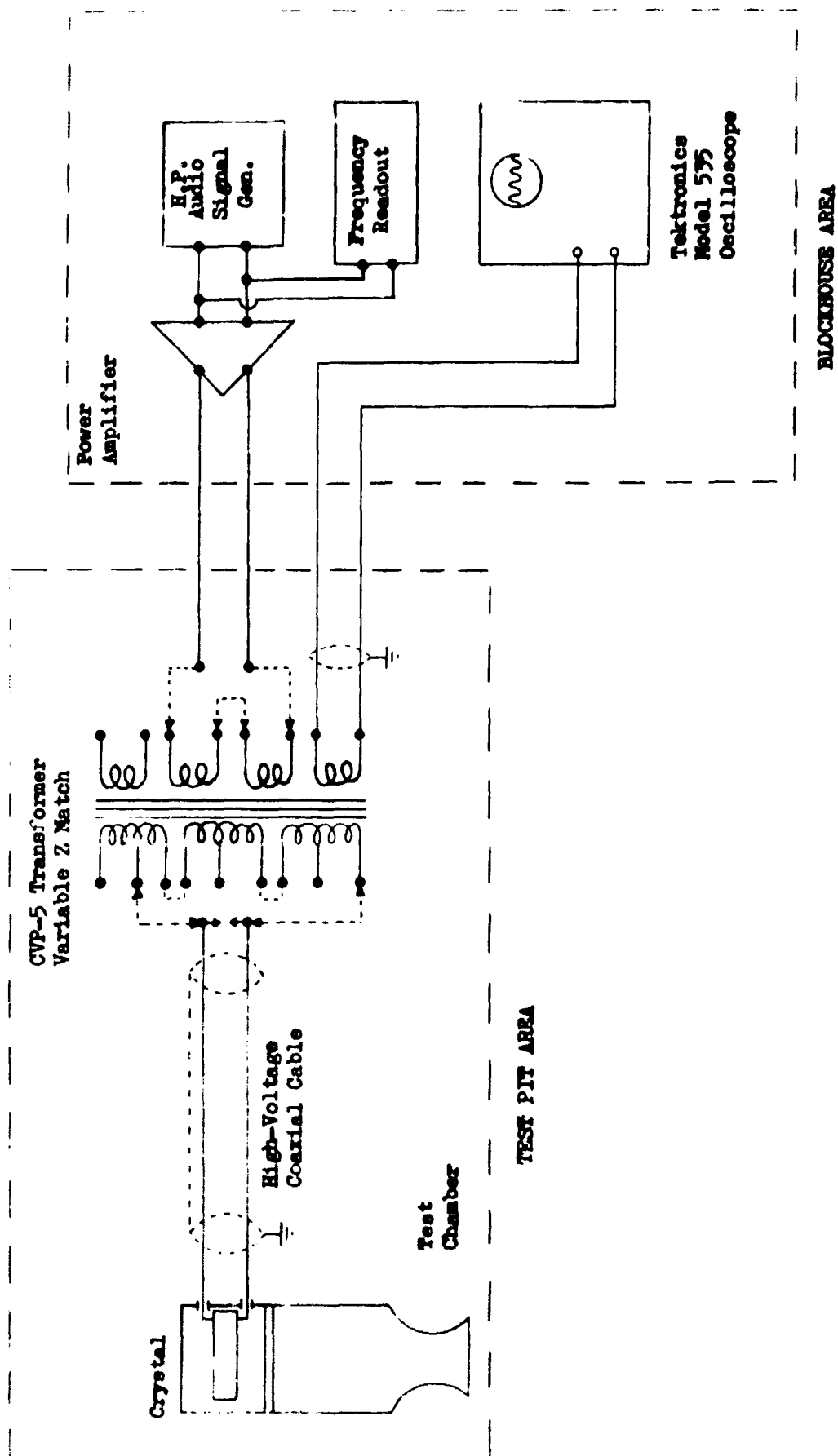
Figure 39. CRYSTAL SCHEMATIC

in duration. A special shut-down sequence is then activated which closes
the LOX tank fill valve, Fig.38 and opens the LOX bleed valve. This
allows the LOX accumulated in the 18-foot coil to reverse flow and exit
through the bleed valve. Rated hydrogen flow is maintained during this
entire time. The hydrogen serves to burn that portion of the oxidizer
which continues into the chamber. Fortunately the high pressure drop
orifice acts as a reverse flow restrictor to the LOX compared to the
bleed valve path and, as a consequence, the mixture ratio and, hence,
temperature in the chamber during this shutdown sequence produces no
damaging effects to the windows or steel walls. In the absence of the
long hydrogen shutdown, direct burning of the windows with that small
oxygen flow coming into the chamber had been experienced.

The entire propellant system and combustion device are extensively
instrumented. Reference to Fig.38 reveals a large number of strategically
placed thermocouples and pressure transducers. These are recorded both
on an oscillograph and a digital recorder (Beckman). Cutoff frequency
for the FM tape system is 20,000 Hz.

A list of all instrumentation and valves, etc., appear in Table I.
Further, a complete description of recording capabilities is presented in
Appendix I.

TABLE I

TEST HARDWARE DESCRIPTION

GH_2 SYSTEM

HARDWARE

1. GH_2 PRESSURIZING MOTORIZED LOADER

2. GH_2 PRESSURIZING CONTROL MAROTTA

3. GH_2 PRESSURIZING REGULATOR 1" - 0-2000 psia

4. AUX PAD ANNIN

5. GH_2 SHUTOFF ANNIN - 1"

6. JAMESBURY VALVE - COLD SIDE

7. JAMESBURY VALVE - HOT SIDE

8. GH_2 MIXER

9. SHARP EDGE ORIFICE = .200" DIAM.

10. 10μ FILTER

11. BLEED RESTRICTOR ORIFICE - .116" - SAME FLOW AS VENTURI

12. GH_2 BLEED ANNIN - $\frac{1}{2}$" N.O.

13. GH_2 MAIN ANNIN - $\frac{1}{2}$"

14. SONIC VENTURI - .104" DIAM.

15. GHe FUEL PURGE MAROTTA

16. GHe FUEL PURGE RESTRICTOR ORIFICE - 50 psi - .032"

17. 5μ GN_2 FILTER   GIVES $V_0 = 1$'/sec

18. GN_2 FUEL PURGE RESTRICTOR ORIFICE - 140 psi - .032"

LOX SYSTEM

HARDWARE

1. LOX TANK PRESSURIZING MOTORIZED LOADER

2. LOX TANK PRESSURIZING MAROTTA

3. LOX TANK PRESSURIZING REGULATOR

4. LOX TANK PRESSURE ANNIN

5. LOX TANK VENT ANNIN

6. LOX TANK FILL ANNIN - $\frac{1}{2}$"

7. LOX FILTER 10 μ

8. LOX BLEED RESTRICTOR ORIFICE - .173" - 50 psi in tank (.8 lbs/sec)

9. LOX BLEED ANNIN - $\frac{1}{2}$" N.O.

10. LOX FLOWMETER

11. LOX MAIN ANNIN - $\frac{1}{2}$"

12. GHe OXIDIZER PURGE RESTRICTOR ORIFICE - Removed (Gives about same flow as fuel purge)

13. GHe OXIDIZER PURGE MAROTTA

14. JAMESBURY VALVE - LOW PRESSURE SIDE

15. JAMESBURY VALVE - HIGH PRESSURE SIDE

16. LOX HIGH PRESSURE RESTRICTOR ORIFICE (2) - Variable per test request

INSTRUMENTATION

0-3K	a.	PLOXTK - LOX TANK PRESSURE
LOX	b.	TLOX U/SFM - TEMP LOX UPSTREAM FLOWMETER
LN_2	c.	TLOX U/SO - TEMP LOX UPSTREAM ORIFICE
0-2.5K	d.	PLOX U/SO - PRESS. LOX UPSTREAM ORIFICE
LN_2	e.	TLOX DOME - TEMP LOX DOME
0-400	f.	PLOX DOME - PRESS LOX DOME
0-400	g.	PLOX CRYS - PRESS LOX CRYSTAL
LN_2-Cu Con	h.	TLOX INJ - TEMP LOX INJECTION - LN_2 ref.

R-8377

ENGINE SYSTEM

HARDWARE

1. J2-ASI SPARK PLUG FOR CHAMBER IGNITION

INSTRUMENTATION

0-350   a. PCINJF - PRESSURE CHAMBER INJECTOR FACE

0-350   b. PCSTCONV - PRESSURE CHAMBER START OF CONVERGENCE

0-700   c. KISTLERS 1 → 6 - HIGH FREQ. FLUCTUATING PRESSURE MEASUREMENT

AMB   d. T/C CHAMBER

R-8377

INSTRUMENTATION

0-2K	a.	PGH_2 SUP - PRESSURE GH_2 SUPPLY
AMB	b.	TGH_2 SUP - TEMP. GH_2 SUPPLY
0-2K	c.	$PAGH_2$ U/SM - PRESSURE AMBIENT GH_2 UPSTREAM MIXER
-300°+	d.	$TCGH_2$ U/SO - TEMP. COLD GH_2 UPSTREAM ORIFICE
0-2K	e.	$PCGH_2$ U/SO - PRESSURE COLD GH_2 UPSTREAM ORIFICE
0-100	f.	$PCGH_2$ Δ PO - PRESSURE DROP ACROSS COLD GH_2 ORIFICE
0-2K	g.	$PCGH_2$ U/SM - PRESSURE COLD GH_2 UPSTREAM MIXER
-300°+	h.	TGH_2 D/SM - TEMP GH_2 DOWNSTREAM MIXER
0-2K	i.	PGH_2 U/SV - PRESSURE GH_2 UPSTREAM VENTURI
-300°+	j.	TGH_2 U/SV - TEMP GH_2 UPSTREAM VENTURI
0-500	k.	PGH_2 TV - PRESSURE GH_2 THROAT VENTURI
0-400	l.	PGH_2 MAN - PRESSURE GH_2 MANIFOLD
-300°+	m.	TGH_2 MAN - TEMP GH_2 MANIFOLD
-300°+	n.	TGH_2 INJ - TEMP GH_2 INJECTION - LN_2 ref

Methods to Achieve the Desired Information
from the Experimental Tests

Experimental data is to be obtained under a variety of chamber operating
conditions. Both steady-state and transient operation is to be monitored.
During either mode of operation, initial injection mixture ratio can be
varied from 0 - 6, chamber pressure from 50 - 300 psi, and initial drop
size from 500 to 1000 $\mu\mu$. Hydrogen injection temperature can be varied
from LN_2 conditions to near ambient.

During nonsteady operation the motor can be pressure pulsed with a perturbation
source. This perturbation source consists of a small plate shot across the
nozzle throat plane at varying speeds. The throat is closed to flow for a
few microseconds and a ram pressure develops at this point. The phenomena
is much like that compared to the sudden closing of a gate valve in a pipe-
line. Duration of the pressure pulse, i.e., closure of the throat can be
controlled either through size of the perturbation plate or through its
velocity across the nozzle. Amplitude can be controlled by the presence
of holes in the plate allowing only partial closure of the throat. There
is, of course, a maximum amplitude of the wave ram and it can be approxi-
mately calculated to be close to three times the throat pressure, Ref.108.
Higher amplitudes can be achieved through use of explosive devices located
at the throat, although these do present some difficulties in analytical
modeling. Following passage of the closure (perturbation) device, the
nozzle again is fully opened. Part of the pressure perturbation relaxes
due to convective flow out of the nozzle. Amplitude is also affected by

the expansion of the throat to the chamber, a contraction ratio varying between 3 - 12 depending on the throat insert.

The perturbation source is located at the throat to insure planarity of the wave by the time it contacts the major portion of the spray. Additionally the wave has the entire chamber length to travel before it interrupts (if it does) the production of monodisperse spray at the injector. If it does not consume all the spray on the first pass, reflection from the face will result in wave propagation down the chamber, back through spray which initially resulted from monodisperse production. Another important reason for locating the perturbation source at the throat, and the manner of perturbation production, (throat closure) is that such a disturbance can be accurately modelled analytically. By specifying only wave ram-type perturbations ($u = o$ at throat for some Δt) the computer model can accurately calculate the pressure produced. Other methods such as blasting charges produce both overpressures and reverse velocities which are extremely difficult to specify and model.

In any event, a considerable variation of experimental conditions and corresponding data can be input to the analytical models. The data itself will be composed of: fully characterized initial conditions (uniform, monodisperse spray), well defined perturbation source, pressure variation as a function of time and space, and direct measurement of droplet diameters and velocity also as a function of time and length. With these data, such items as burning and breakup rates (from droplet diameters) and drag coefficients (from drop diameter and velocity) can be deduced. Further, pressure monitoring of the

amplification or attenuation of the perturbation wave can determine the range of conditions which lead to the onset of instability.

Photographic Requirements. It is evident that what makes the experiments valuable is full knowledge of the initial conditions of the rocket and subsequent experimental determination of the droplet behavior in the chamber. The fact that conditions are uniform (monodisperse, etc.) throughout the chamber (one-dimensional flow) and initially well-defined facilitates the observation of the droplets. But this observation must result in quantitative data for use in the models. Thus, photographic techniques for measuring droplet diameters and velocities must be used.

Photography within transparent rocket engines is not new; photographs within such devices were taken as early as the 1950's. Rarely, however, has the photography been used for other than general observation or for streak films useful for instability correlations. The distribution of drop sizes and nonuniformity of the injection pattern has precluded the axial measurement of drop diameters and velocity which are representative of the spray field as a whole. Little quantitative data in actual drop diameter and velocity variation in a combustion spray flow field has been obtained. In many cases photography was only possible when massive window purges were used to remove propellant vapors that were occluding the windows. These purges, in turn, destroyed any chance for one-dimensionality of the flow field. Data from such photography, if obtained, could not be used with a combustion model to ascertain burning rates, etc.

These were the major factors that led to the selection of the monodisperse spray flow field and of LOX and GH_2 as the propellants. Photographic properties of this propellant combination are excellent. Both GH_2 and the resultant combustion product H_2O are transparent in the visible light portion of the spectrum. Figure 40 presents the spectrum resulting from combustion of LOX and GH_2. No vapors exist that could physically occlude the field of view such as occurs with $NTO-N_2H_4$ propellant combinations. Thus, no window purges are required and the one-dimensionality of the flow field is retained.

Photographic Techniques. Photographic methods to achieve the required measurements were investigated and found to be feasible. A tabular summary of possible methods and their use is presented in Fig. 41 .

Without doubt the results of Wruker and Matthews, Ref.109 have shown the great potential of holographic techniques. This is particularly so in that with one hologram all of the rows of spray may be studied. However, their work does indicate problems with high spray density. This can be overcome by utilizing a two-beam system, but this is fairly expensive to build. Further, if the spray field is monodisperse and uniform then depth of field problems are not as serious.

For this reason, to date, the experiments have utilized the Fastax camera and strobe, spark shadowgraphy and the ballistic camera with a continuous

OXIDIZERS CONTAINING O,F & FUELS CONTAINING H,C,O & N

OH NH CH CH   HF   HF   VERY WEAK H₂O

.2   .3   .4   .5   .6   .7   .8   .9   1.0

1000
100
10
1
.1

SCALE

NITROGEN TETROXIDE & 50% UDMH + 50% HYDRAZINE

OH NH CH   NO₂   VERY WEAK H₂O

.2   .3   .4   .5   .6   .7   .8   .9   1.0

1000
100
10
1
.1

SPECTRAL WAVELENGTH ~ MICRONS

ULTRAVIOLET | BLUE | GREEN | YEL-LOW | OR-ANGE | RED | INFRARED

INTENSITY

LOX / RP-1

OH   CH   C₂   CARBON CONTINUUM

.2   .3   .4   .5   .6   .7   .8   .9   1.0

1000
100
10
1
.1

RELATIVE

HYDROGEN & OXYGEN

OH   H₂O   H₂O   H₂O   H₂O

.2   .3   .4   .5   .6   .7   .8   .9   1.0

1000
100
10
1
.1

FIGURE 40. TYPICAL PROPELLANT COMBINATIONS - OPTICAL SPECTRUM

R-8377

FIGURE 41

PHOTOGRAPHIC TECHNIQUES INVESTIGATED

TECHNIQUES CONSIDERED	LIMITING DROPLET PARAMETERS		ADVANTAGES	DISADVANTAGES
	MIN. SIZE-μ	MAX. VEL.		
FASTAX CAMERA & STROBE (1 μSEC)	50 100	50'/SEC 100'/SEC	PROVEN IN PRACTICE RELATIVELY INEXPENSIVE	1) LIMITED DEPTH OF FIELD 2) LOW MAXIMUM DROPLET VEL. 3) VELOCITY MEASUREMENTS LIMITED TO FAIRLY LARGE DROPS, LOW VEL.
BECKMAN-WHITLEY CAMERA & LASER (20-30 NANO SEC PULSE)	10	200'/SEC	MEASURE SMALL DROPS AT HIGH VELOCITY	LIMITED DEPTH OF FIELD (BUT THIS IS PROBABLY NOT IMPORTANT FOR UNIFORM SPRAY?)
BALLISTIC CAMERA & CONTINUOUS LASER SOURCE	100	200'/SEC.	PRODUCES VELOCITY DISTRIBUTION IN ONE DATA RUN	1) LIMITED DEPTH OF FIELD 2) SENSITIVE TO TRANSVERSE MOTION 3) RELATIVELY LARGE DROPS
FLUORESCENT PHOTOGRAPHY	10	200'/SEC.	1) MEASURE SMALL DROPS AT HIGH VELOCITY 2) ALL DROPLETS IN FOCUS	1) LIMITED DEPTH OF FIELD 2) DOUBTFUL IF DYES COMPATIBLE WITH LOX
HOLOGRAPHY	10	200'/SEC.	DEPTH OF FIELD PROBLEM DOES NOT EXIST	1) SINGLE BEAM TECHNIQUES REQUIRE LOW DROPLET DENSITY 2) TWO BEAM SYSTEM FAIRLY EXPENSIVE TO BUILD

light source to quantitatively determine the axial drop-diameter (due
to burning and/or breakup) and velocity variation of burning liquid oxygen
sprays under actual rocket conditions.

Spark shadowgraphy is similar to use of the strobe and Fastax except some-
what shorter duration times may be obtained with the spark and still pictures
may be taken. In practice, a drop of 100μ represents only $\sim \frac{1}{350}$ of the
initial mass of the injected drop (720μ). Thus, even if the minimum view-
able drop is 100μ, this represents over 95% of the lifetime of the droplet
and is more than sufficient to obtain the desired data. Further, some initial
analytical predictions presented in the Results Section indicate that for a
typical test, C.R. = 12.3, over 14 inches of travel is required for the drop
to obtain a velocity of 100 feet/sec and some 17 inches to reduce to 100μ,
in size. This represents the entire windowed section of the engine.

Some concern has been expressed over the ability to backlight a burning LOX
drop and accurately determine its diameter. Factors such as the steep gradients
in density between the LOX surface and combustion gas flow could distort the
light path and appear to enlarge the droplet over its actual size. If the
boundary layer around the drop were large (say equal to or greater than the
drop radius) this might indeed be a problem, particularly if a flame of high
temperature were also anchored around the droplet. Under convective conditions
however, as discussed in the review of the coupling terms, the flame is believed
to be swept into the wake and the boundary layer to be of negligible thickness
($<$ 1/4 of the drop radius). It is doubtful if this would interfere with the

accuracy of drop diameter determination. However, this can be checked to some degree by comparing the initial diameters under burning conditions to those obtained under cold flow.

Appendix II presents the equations utilized for setting film speeds, camera locations, and magnification ratios, etc. The photographic setup varies with subject (diameters or velocities) and the axial location of interest. Normal accuracy is taken to allow image movement on the film of no more than 10% of the diameter of the droplet.

ANALYTICAL PROGRAM

Summary of Development

Comparison of the experimental data obtained and the prediction of the models is to be used for evaluation of the adequacy of expressions for the coupling terms. The purpose of this section is to describe how the experimental and analytical programs will be used to make this evaluation. For this purpose the generalized model was reduced to one-dimensional steady-state and transient forms and programmed for a digital computer. These reduced models were programmed in a flexible form so that the important input parameters, which control the coupling mechanisms, appear in subroutines. The only unknowns that appear in the programs are expressions for the coupling terms because the models match the initial and boundary conditions of the experiment.

Steady-State Model. The steady-state combustion model formulation is unique
in that it allows either complete calculation specifying coupling terms a
priori, or direct input of the experimental data (drop diameter and velocity
as a function of axial length). For this purpose the model uses the experi-
mental data to bypass the droplet continuity equation (mass addition rate
coupling term) and the droplet momentum equation (drag force coupling term).

Evaluation of the coupling terms is straightforward when the model is
combined with experimental data. First the experimentally determined drop
diameter (or radius, r) and velocity u_d as a function of axial distance,
x, allows the gas flow field to be accurately obtained through use of the
gas phase equations and the droplet energy equation. The only coupling
term that is required at this point is the droplet heating rate, and it is
of lesser importance than the other coupling terms for mass rate addition
and drag. This is because, as will be shown, under steady-state conditions
LOX droplets rapidly heat to the "wet bulb" condition and thereafter remain
at near constant temperature (and density) until consumed. Thus, even if
the initial term used to describe the droplet heating rate is not entirely
accurate, it has only a minimal effect on evaluation of the other coupling
terms.

The need to consider expressions for these other terms has been eliminated
through use of the experimental data(to replace 2 of the 3 spray differential
conservation equations). When the gas flow field has been determined, the
spray momentum equation (which was not initially utilized) and the experimental

velocity data may be used for direct calculation of the drag force, and hence, the drag coefficient. In turn, use of the spray continuity equation (also not initially needed) and the experimental drop diameter variation may be used for comparative evaluation of burning rate expressions.

Through repeated evaluations with various droplet heating rate expressions, the data will allow determination of the most appropriate heating rate expression.

If droplet breakup occurs, it can be observed photographically and the droplet axial variation still determined. Delineation of vaporization and breakup coupling expressions is still possible because breakup will either occur at some point downstream (allowing upstream correlation with vaporization models) or can be eliminated by going to large contraction ratios (lower gas velocities).

Transient Model. The transient model, to be used to evaluate coupling-term expressions for describing the onset and sustenance of combustion instability, differs from previous models in that it allows for variations in droplet number density, gas phase mixture ratio and/or molecular weight. Just as for the steady-state evaluations, the model can be used with experimental data directly input. However, the experimental data is time-varying and, therefore, this approach is more difficult for this case. A better approach appears to be the use of the best coupling terms determined from the steady-state evaluation or other experiments and subsequently evaluating these terms by comparing model

predictions with the observed results for pressure wave growth or decay, droplet velocities, diameters as a function of length for selected times, and the observance (if it occurs) of the onset of breakup, etc.

In this manner the best expressions for the coupling terms can be determined.

Philosophy of the Model Formulations. The general equations of the vector-tensor formulation presented earlier appear in what is known as the "divergence free" form. That is, the equations are written with no coefficients preceding all differential operations as they appear on the left hand side. This is a result of deriving the equations from a "stationary control volume" viewpoint. Removal of the continuity equation from the momentum and energy equations, etc. results in the perhaps more familiar "following the fluid" form. Both forms are Eulerian as the independent variables are taken as the field coordinates and time. As far as the analytical derivation is concerned the forms are identical; however, it can be shown, Ref.110 and 111, that the divergence free form,at least for the gas phase equations, is to be favored for use in computing jump conditions across discontinuities in the absence of viscosity. Further, although the gas phase equations were written for convenience with the coupling terms appearing on the right hand side, it is more computationally appropriate to replace them with the spray differential operations. The coupling terms then appear only in the spray phase equations. The latter equations may be reduced to the "following the fluid" form with no loss of computational accuracy, i.e., droplet velocity,

etc., does not undergo a finite jump in calculating through a shock wave.
An example using the momentum equation is presented below.

From Equations (4) and (11) in the Flow Field Formulation Section it is clear
that the gas phase momentum equation could be written as

$$\frac{\partial}{\partial t}\left(\varrho\,\vec{u} + \varrho_j^n\,\vec{u}_j^n \right) + \text{div}\left(\varrho\,\vec{u}_j\,\vec{u} + \varrho_j^n\,\vec{u}_j^n\,;\vec{u}_j^n \right)$$

$$= -\,\text{grad}\;p + \text{div}\;\underline{\underline{\tau}}$$

and, further, the spray phase momentum equation may be written as

$$m_j^n\left(\frac{\partial}{\partial t}\left(\vec{u}_j^n\right) + \vec{u}_j^n\,\text{grad}\;\vec{u}_j^n \right) = \vec{F}_j^n$$

This was obtained by subtracting equation (2) from the expanded form of (4)
and the substitution:

$$\varrho_j^n = m_j^n\,N_j^n\;.$$

In one-dimensional constant area, non-viscous steady-state flow the simplicity
of the gas phase form for computing discontinuities is evident, e.g., for gas
phase momentum.

$$\frac{d}{dx}\left(\varrho\,u^2 + \varrho_j^n\left(u_j^n\right)^2 + p \right) = 0$$

Therefore,

$$\varrho\,u^2 + \varrho_j^n\left(u_j^n\right)^2 + p$$

is conserved across all discontinuities. Similarly, for the spray phase momentum,

$$m_j^n \, u_j^n \, \frac{d u_j^n}{dx} = F_j^n$$

and no loss of computational accuracy is incurred by writing the equation in this form. The drop velocity does not exhibit a discontinuity.

Even when viscous effects are retained the divergence free form for the gas phase equations is advantageous for numerical solutions by finite difference methods. Consequently, all of the programmed gas phase equations were initially written in this form and the spray phase equations were reduced to their simplest form.

The following sections detail the development of the one-dimensional models from the generalized formulation, and methods to evaluate the specified coupling terms. One-dimensional models are far more convenient to use (and program) than their multi-dimensional counterparts. Their use was made possible only because the experimental device is designed to produce a corresponding flow field.

Nonetheless, results obtainable from them pertaining to the coupling terms can be subsequently applied to more complex multi-dimensional situations. There are, of course, practical requirements also. The program outlined here would be impossible in other than a one-dimensional framework. Sufficient experimental data could not be obtained to specify all of the unkonwns in a

multi-dimensional model and little information in a multi-dimensional system could be directly deduced regarding variations of drop diameter, velocity, etc., with operating conditions. Subsequent evaluation of coupling term expressions would not be possible.

Based on this philosophy, the one-dimensional programs are presented below. The numerical techniques used in digital computation of the programs appear in Appendix III and IV.

<div align="center">Steady-State Model</div>

Development of the Steady-State Formulation

The steady-state equations were reduced directly from the general formulation. The area term, A, must be included. The one-dimensional reduction also allowed direct integration of the gas phase, and certain spray phase, equations which simplified the numerical analysis. Although in practice the equations are normally used with only one initial drop group size $(n = 1)$ and one spray species, oxygen $(j = 1)$ the equations as presented here (and were so programmed for) incorporate a range of initial droplet group sizes, $n = 1...N$, and various spray propellant species, $j = 1...J$.

Spray Phase Equations - Parent Droplets

a) Droplet Number Concentration

$$Au_j^n \, N_j^n = \text{constant} = \frac{\dot{W}_j^n}{\frac{\pi}{6}\left(D_j^n\right)_o^3 \left(\rho_{\ell_j}^n\right)_o}$$

$j = 1...J$
$n = 1...N$

where $\dot{W}_{j_0}^n$ = weight flowrate of jth species, n^{th} initial droplet

group size injected at x = o

$\left(D_j^n\right)_o$ = diameter of oxidizer droplets injected, x = o, j, n^{th} group.

$\left(\rho_{\ell_j}^n\right)_o$ = liquid density of oxidizer droplets injected, x = o,

j, n^{th} group

A = chamber cross-sectional area

b) Droplet Mass Continuity

$$j = 1...J \quad u_j^n \frac{d}{dx}\left(m_j^n\right) = -\dot{m}_{j_{VAP}}^n - \dot{m}_{j_{B.U.}}^n + \quad . \quad . \quad . \quad . \quad .$$
$$n = 1...N$$

where m_j^n is the individual droplet mass and may be related to the

diameter, in the presence of temperature gradients within the drop,

or as simply as

$$m_j^n = \frac{\pi}{6}\left(D_j^n\right)^3 \rho_{\ell_j}^n = \frac{\rho_j^n}{N_j^n}$$

if the drop temperature is uniform.

c) Droplet Momentum

$$j = 1...J \quad m_j^n u_j^n \frac{d}{dx}\left(u_j^n\right) = g F_j^n$$
$$n = 1...N$$

where

$$F_j^n = \frac{\pi}{8g}\left[\rho\left(D_j^n\right)^2\left(u-u_j^n\right)\left(|u-u_j^n|\right)C_{d_j}^n\right]$$

$$- 24 \pi \left(D_j^n\right)^3 \frac{dP}{dx}$$

d) Droplet Energy

$$j = 1\ldots J \qquad n = 1\ldots N \qquad u_j^n \frac{d}{dx}\left(T_j^n\, m_j^n\right) = \frac{Q_j^n}{C_{P_j}^n} - \left(\dot{m}_{j_{VAP}}^n + \dot{m}_{j_{B.U.}}^{n\,T\ldots}\right) T_{j\,s}^n$$

when $T_j^n m_j^n$ cannot be separated due to the presence of temperature
gradients within the drop. The relationship between T_j^n and m_j^n
may be complex, depending on the heating rate model used; or
completely decoupled as

$$m_j^n\, u_j^n \frac{d}{dx}\left(T_j^n\right) = \frac{Q_j^n}{C_{P_j}^n}$$

if the model considers the drop temperature to be uniform. It is
still necessary to calculate the entire drop enthalpy, H_j^n from the
temperature T_j^n (which may vary within the drop) because the entire
drop energy is used in the particular form of the gas phase equations
utilized. This may involve an integration of $m_j^n C_{P_j}^n\, dT$ throughout the
drop, or if the temperature is uniform, be as simple as

$$H_j^n = H_{j\,i}^n + \int_{T_{j\,i}^n}^{T_j^n} C_{P_j}^n\, dT$$

where $H_{j\,i}^n$ is a reference enthalpy at temperature $T_{j\,i}^n$. It is given
as a function of pressure for that temperature so that, at whatever
pressure the integration is performed (i.e., effect on $C_{P_j}^n$), the
proper H_j^n for T_j^n and p is calculated.

e) Droplet Wave Build-up

$$U_j^n \frac{d}{dx}\left(\psi_j^n\right) = \frac{1}{\tau_{j\ B.U.}^n}$$

As explained in the general formulation section, $\tau_{j\ B.U.}^n$ is an induction time to the onset of breakup, it allows ψ_j^n to reach a value of 1 which corresponds to breakup. Both $\tau_{j\ B.U.}^n$ and the rate of breakup $\dot{m}_{j\ B.U.}^n$ depend on the particular breakup model being used and the critical $\frac{W_e}{\sqrt{R_e}}$ number. Breakup stops when this number falls below the critical value. It is further supposed that if breakup occurs, the droplet has no memory of its history. This is perhaps an over-simplification; however, in most situations when breakup begins in a steady-state flow field the critical value of $\frac{W_e}{\sqrt{R_e}}$ is usually continuously exceeded up to a point where droplet drag and mass loss combine to produce a "critical" droplet diameter and relative velocity at which breakup abruptly ceases. It almost never reoccurs within the combustion chamber.

f) Droplet Residence Time

$$U_j^n \frac{d}{dx}\left(\tau_{j\ T}^n\right) = 1$$

$\tau_{j\ T}^n$ is the flight time of the droplet from injector face to location x.

Gas Phase Equations

a) Local Mixture Ratio Equation

In the absence of strong concentration gradients, gas phase diffusion is neglected. Further, in line with the previous discussion on coupling terms and chemical kinetics, the latter phenomena is contained only in the coupling terms. Bulk gas phase chemical kinetics are ignored compared to droplet processes; in practice they are found to have rates 2 to 3 orders of magnitude greater than those involved in the droplet dynamics. This is particularly true for the propellants considered here, LOX and GH_2, Ref. 112.

Thus with $\tilde{D}$ set equal to zero in Eq. (9) and under one-dimensional considerations, that equation may be formally integrated to the following.

$$C(x) = \frac{\sum\limits_{o=1}^{o} \dot{W}_o \Big|_o + \sum\limits_{j=1}^{ox}\left(\sum\limits_{n=1}^{N} \dot{W}_{j_o}^n\right)\Big|_o - \sum\limits_{j=1}^{ox}\left\{\sum\limits_{n=1}^{N} A\, u_j^n\, N_j^n\, m_j^n\right\}_x}{\sum\limits_{f=1}^{F} \dot{W}_f \Big|_c + \sum\limits_{j=1}^{Fuel}\left(\sum\limits_{n=1}^{N} \dot{W}_{j_o}^n\right)\Big|_c - \sum\limits_{j=1}^{Fuel}\left\{\sum\limits_{r=1}^{N} A\, u_j^n\, N_j^r\, m_j^c\right\}_x}$$

where

$\dot{W}_o$ = weight flow of gaseous oxidizer injected, note, it may be part of hot gas, as from a staged combustion system that injects fuel-rich preburner products into the main chamber. From the mixture ratio of these gases the amount of oxidizer that was utilized can be determined.

$\dot{W}_f$ = Weight flow of gaseous fuel injected, note it may also be part of injected, hot, combusted fuel-rich gas.

$\displaystyle\sum_{o=1}^{0}$ = Summation over all injected oxidizer gas species.

$\displaystyle\sum_{j=1}^{ox}$ = Summation over all oxidizer spray species.

$\displaystyle\sum_{f=1}^{F}$ = Summation over all injected gaseous fuel species.

$\displaystyle\sum_{j=1}^{Fuel}$ = Summation over all fuel spray species.

$\dot{W}_{jo}^{n}$ = Weight flowrate of injected spray - j, n^{th} group.

Note for both species, $Au_j^{2} N_j^{n}$ is a constant. Further, as an example, if only liquid oxidizer and gaseous fuel is injected, then all terms with $\displaystyle\sum_{o=1}^{0}$ and $\displaystyle\sum^{Fuel}$ are zero. If gaseous fuel and gaseous oxidizer along with sprays of one species are injected it is assumed that the gaseous injection is

uniform and gaseous combustion is instantaneous, i.e., neglect of gas phase

kinetics. Although the injection of one of the propellants in its natural

gaseous state is common, it is rare that same propellant is also injected

as a liquid. It is common, however, that an engine may operate on a staged

combustion cycle in which, say, all of the fuel and a small portion of the

oxidizer are combusted in preburners (used to supply hot gas to the turbine-

pumps) and the remainder of the oxidizer is injected in the liquid state

and burned with this fuel-rich, hot, combustion gas in the main chamber. In

such a case the $\dot{W}_o$ and $\dot{W}_f$ are the initial species of this hot gas, that is

all the $\dot{W}_o$ and a portion of the $\dot{W}_f$ may form the burned products, H_2O for

example. In such a case it is necessary to consider the initial species to

perform proper calculation of the mixture ratio. Should it occur that an

appreciable portion of both oxidizer and fuel species are injected in the

gaseous state, then this model is not sufficiently accurate to handle this

case (i.e., a gas-gas rocket). Such cases are rarely injected uniformly and

mixing considerations (hence a multi-dimensional model) are important.

In the case of hot combustion gas injection (staged cycle) the model is

adequate as long as it refers to the initial amount of oxidizer and fuel and

performs proper calculation of the proportion of mass, momentum and energy

assigned to each.

b) Global Continuity

$$A \rho u + \sum_{j=1}^{ox} \left(\sum_{n=1}^{N} A u_j^n N_j^n r_j^n \right) + \sum_{j=1}^{Fuel} \left(\sum_{n=1}^{N} A u_j^n N_j^n r_j^n \right)$$

$$= \text{constant} = \sum_{o=1}^{o} \dot{W}_o \Big|_o + \sum_{f=1}^{F} \dot{W}_f \Big|_o$$

$$+ \sum_{j=1}^{ox} \left(\sum_{n=1}^{N} \dot{W}_{j_o}^{n} \right) \Big|_o + \sum_{j=1}^{Fuel} \left(\sum_{n=1}^{N} \dot{W}_{j_o}^{n} \right) \Big|_o$$

= total propellants injected

c) Global Momentum

$$A \rho u^2 + \sum_{j=1}^{ox} \left(\sum_{n=1}^{N} A u_j^n N_j^n m_j^n u_j^n \right)$$

$$+ \sum_{j=1}^{Fuel} \left(\sum_{n=1}^{N} A u_j^n N_j^n m_j^n u_j^n \right) + g(144) A P$$

$$- g(144) \int_0^X P \left(\frac{dA}{dx} \right) dx - g A \tau_{xy}$$

$$+ g \int_0^X \tau_{xy} \left(\frac{dA}{dx} \right) dx = \text{constant}$$

$$= g (144) P A \Big|_o + \sum_{o=1}^{o} \dot{W}_o u_o \Big|_o$$

$$+ \sum_{f=1}^{F} \dot{W}_f u_f \Big|_o + \sum_{j=1}^{ox} \left\{ \sum_{n=1}^{N} \dot{W}_{j_o}^{n} u_{j_o}^{n} \right\} \Big|_o$$

216

R-8377

$$+ \sum_{j=1}^{Fuel} \left\{ \sum_{n=1}^{N} \dot{W}_{j_0}^{n} u_{j_0}^{n} \right\} \Big|_0$$

$\simeq$ total momentum of propellants injected

where

$$\tau_{xx} = \frac{4}{3} \mu \frac{du}{dx}$$ and involves invocation of the Stokes criteria in the absence of better data for reacting gases.

u_f - velocity of injected gaseous fuel

u_o - velocity of injected gaseous oxidizer

$u_{j_o}^{n}$ - velocity of injected droplets j, n^{th} group.

Viscosity is retained to add a smoothing effect to the digital computation; although for this case, steady-state analysis, its presence is negligible. Again, if the injected gaseous species result from staged cycle combustion, $u_f = u_o$.

d) Global Energy

$$\rho A u \left(H + \frac{u^2}{2gJ}\right) + \sum_{j=1}^{ox}\left\{\sum_{n=1}^{N} A u_j^n N_j^n m_j^n \left(H_j^n + \frac{(u_j^n)^2}{2gJ}\right)\right\} + \sum_{j=1}^{fuel}\left\{\sum_{n=1}^{N} A u_j^n N_j^n m_j^n \left(H_j^n + \frac{(u_j^n)^2}{2gJ}\right)\right\} - \frac{A U \tau_{xy}}{J} + \int_0^x \frac{u \tau_{xx}}{J}\left(\frac{dA}{dx}\right) dx$$

$$+ A q - \int q \left(\frac{dA}{dx}\right) dx = constant$$

$$= \sum_{o=1}^{o} \dot{W}_o \left(H_o + \frac{u_o^2}{2gJ}\right)\bigg|_o + \sum_{f=1}^{F} \dot{W}_f \left(H_f + \frac{u_f^2}{2gJ}\right)\bigg|_o$$

$$+ \sum_{j=1}^{ox}\left\{\sum_{n=1}^{N} \dot{W}_{j_o}^n \left(H_{j_o}^n + \frac{(u_j^n)^2}{2gJ}\right)\right\}\bigg|_o$$

$$+ \sum_{j=1}^{Fuel}\left\{\sum_{n=1}^{N} \dot{W}_{j_o}^n \left(H_{j_o}^n + \frac{(u_j^n)^2}{2gJ}\right)\right\}\bigg|_o$$

$\sim$ Total Injected Energy

where

H = enthalpy of the reacted gas, sensible + chemical,

$$= \sum_i \omega_i H_i = \int_{T^0}^{T} \sum_i \omega_i C_{P_i} dT + \sum_i \omega_i H_{f_i}^{\circ}$$

and is provided from tables discussed later.

and

T = gas temperature

ω_i = mass fraction of species i

$$= \frac{\rho_i}{\rho} \quad , \text{ provided from tables.}$$

H_i = enthalpy of species i

$H_{f\,i}^{\circ}$ = heat of formation of species i at the standard of temperature T_o, and pressure, 1 atm

C_{p_i} = Specific heat of species i

H_o = Enthalpy of injected gaseous oxidizer

H_f = Enthalpy of injected gaseous fuel

$H_j{}^n$ = sensible + chemical (if any) enthalpy of spray, j, n^{th} group. It may involve integration of the temperature gradient throughout the drop if one exists.

$H_{j\,o}{}^n$ = enthalpy of injected spray, j, n^{th} group. It is a function of the injected temperature, $T_{j\,o}^n$, and pressure only, since the initially formed spray is assumed to have no internal droplet temperature gradient.

$$q_o : \quad - k \frac{dT}{dx} - \sum_i e \, \mathcal{D}_i \, H_i \frac{d\omega_i}{dx}$$

and

k = thermal conductivity of reacted gas

$\mathcal{D}_i$ = gas diffusion rate of species i into all other species.

For consistency $\mathcal{D}_i \approx \bar{\mathcal{D}} = 0$ so that

$$q_o \approx - k \frac{dT}{dx}$$

only. This is in agreement with the mixture ratio equation.

The enthalpy of the injected propellants mus$^+$ be related to the standard reference conditions. In this program the JANNAF standard is utilized; the enthalpy of the "dead state elements" at $537°R$, 1 atm pressure is identically zero. For this case gaseous O_2 and H_2 at this point have zero enthalpy. All liquid spray reference enthalpies must reflect this fact and have negative values. Further, the heats of formation of all products and constituents other

than the dead state elements (for which $H_{f\ i}^{o}$ is zero) are evaluated on the basis that heat release (exothermic reaction) is considered to be negative in value.

The injected gas enthalpies can be related to their incoming temperature if they are injected separately. If they are injected as part of staged cycle combustion gas at some mixture ratio, temperature and pressure, then the enthalpy for that gas can be determined from the tables discussed later and H_f and H_o are assigned that value.

e) Equation of State

$$\frac{P(144)}{\rho} = RT \left[\sum_i \frac{\omega_i}{M_i} \right]^{-1}$$

where R is the universal gas constant

M_i = molecular weight of species i

Subroutines Utilized in the Steady State Program.

a) Combustion properties table

Throughout the gas phase equations the variables H, ρ, T, M_i, etc., have been used. Obviously, these and other variables depend on the actual constituents of the multi-component, reacting gas. As for example, the density of the gas as calculated from the equation of

state depends on the total gas molecular weight. Now under the assumption, which has been used, of bulk gas phase equilibrium, all gas phase parameters may be expressed in terms of any three independent variables. The most logical of these are the following. Specification of C, p and H, or C, p and T provide all other variables. Since both H and T are required in the calculations (T is often the parameter most useful in the coupling term expressions) and the temperature is a monotonic function of H, the most convenient form of property tables to provide gas phase data was determined to be a set using various combinations of C and p as the entrance parameters.

C, p
↓

H_i — Enthalpy of species i

ω_i — Mass weight fraction of species i

H — Total enthalpy $= \sum_i \omega_i H_i$

T — Temperature

M_i — Molecular weight of species i

M — Total molecular weight $= \sum_i \dfrac{\omega_i}{M_i}$

S — Entropy

C_{p_i} — Constant pressure specific heat - species i

C_p — Total specific heat $= \sum_i \omega_i C_{p_i}$

μ — Viscosity

k — Thermal conductivity

a — Shifting speed of sound

γ_f — Frozen gamma $= \dfrac{C_p}{C_v}$

γ — Shifting gamma $= \dfrac{\partial \ln p}{\partial \ln \rho}\bigg|_\rho$ constant entropy

Thus the tables for a given C and p may be searched for either a given H or T and when found, double interpolation within the tables provides all the required gas phase data. Obviously since C, p and H are determined from equations which are inter-related with the other gas phase variables, the processes of solution involving the tables and the equations are iterative.

The tables are based on equilibrium propellant composition of ideal gases. The mixture ratio provides the ratio of fuel to oxidizer present, pressure and enthalpy complete the requirements needed to specify a state point. For the most part at the temperatures considered, usually greater than $1000°R$, the assumption of ideal gases is valid. Below this, for the very fuel-rich, low temperature gases near the injector face, adjustments for real gas effects have been made. Viscosity for the gas mixture is based on Wilke's method, Ref.113, and the thermal conductivity is found by the modified Eucken's method, also Ref. 113.

Computation of the tables is based on a Rocketdyne standardized n-propellant equilibrium composition program, which in turn is an outgrowth of the original work of Huff,Ref. 30. Because the tables are used in the solution method, extreme accuracy in interpolation is required. For this reason the tables are extensive in nature, requiring interpolation only over a very small range of values; over 55,000 data points are contained in the tables for $O_2 - H_2$ combustion products.

By setting the mixture ratio C = to zero and infinity, the tables can also provide the properties of the pure gaseous fuel and pure gaseous oxidizer injected. The same is also true of injected staged cycle fuel-rich combustion gas.

b) Stagnation properties computation

The computation of equilibrium stagnation properties can be rigorously done only through use of the tables. It is assumed that the stagnation pressure, etc., one would measure with a probe would result from an isentropic, fully shifting flow process. Hence $S_s(x) = S(x)$ and, of course, the mixture ratio between static and stagnation is the same.

If C, H, p, T, S, u, etc. are known at the static flow point, then

$$H_s \text{ at stagnation} = H + \frac{u^2}{2gJ}$$

and $S_s = S$

Calculation of the stagnation point properties utilizes the same tables but with a different interpolation technique. Hence, for the known C and various assumed pressures a search of the tables under the constraint of known H_s is commenced until $S_s = S$ is determined. This determines the stagnation pressure and other properties.

In practice the maximum static temperature deviation of the combustor flow field from stagnation is normally about 5%, reaching a maximum of less than 20% at the engine throat. Hence the composition of the static gases is often little different from the stagnation gases. Hence $\omega_{i_s} \approx \omega_i$ and $C_{p_s} \approx C_p$. Then to a first approximation

$$C_p T_s \approx C_p T + \frac{u^2}{2gJ}$$

and T_s can be approximated directly. P_s then follows from

$$\frac{P_s}{P} = \left(\frac{T_s}{T} \right)^{\frac{\gamma_f}{\gamma_f \cdot 1}}$$

In actuality this latter equation is also correct for reacting gas isentropic processes if shifting gamma, γ, is used. However, since T_s in this equation was determined from frozen gas considerations, consistency requires the use of γ_f in determining P_s. Values found from this equation differ little from the more rigorous table calculation. The error is proportional to the order of the mach number squared.

c) Spray properties

A set of properties relating to the spray must also be provided. In addition, properties of the film around the droplets are also required. This latter set may be dependent on the particular

droplet burning, etc., model being utilized. Hence the spray
properties can be subdivided into two categories. Drop properties
and film properties.

Drop Properties

$\rho_{\ell_j}{}^n$ - Density of liquid droplet as function of temperature
and pressure, Table.

$C_{p_j}{}^n$ - Constant pressure specific heat of the liquid,
again a function of temperature and pressure,
Table.

M_j - Drop molecular weight

$P_{v_j}{}^n$ or $X_{v_j}{}^n{}_s$ - Vapor pressure of drop vapor, or the mole
fraction of drop vapor at its surface. This
is a function of drop temperature and total
pressure, Table or Eq.

$\Delta H_{v_j}{}^n$ - The difference between the liquid enthalpy and
vapor enthalpy at a given droplet temperature and
total pressure, Table or Eq.

These properties are for real substances and must be input as
such. In particular, the effects of total pressure, i.e., the

presence of other gases, must be considered in the computation of $X_{v_{js}}^n$ or $\Delta H_{v_j}^n$. These parameters will not have the same values as if the spray were vaporizing only into its own vapors. Normally to calculate the effects of total pressure on such variables, an equation of state must be assumed and fugacity relations used. For LOX-hydrogen the Redlich-Kwong Equation of State was used and the methods of Ref. 113 and 115 determined the variation of vapor pressure and "heat of vaporization" with total pressure in the presence of other gases. The effect was found to be small at pressures low compared to the critical pressure of LOX, 737 psia.

Film Properties

Most droplet burning models, etc., utilize equations which require specifications of mean film properties around the droplet. The actual specification process depends on the model being used but in general the following parameters are important.

$T_{f_j}^n$ - Mean film temperature between drop surface and bulk combusting gas, R.

$X_{v_j}^n$ - Film mole fraction of drop vapor, Eq.

$M_{f_j}^n$ - Film molecular weight, Eq.

$\rho_{f_j}^n$ - Film density, Eq.

$k_{v_{f_j}}^n$ - Vapor thermal conductivity at film conditions, Table

$\mu_{v_{f_j}}^n$ - Vapor viscosity at film conditions, Table

$C_{p_{v_{f_j}}}^n$ - Vapor specific heat at film conditions, Table

$C_{p_{f_j}}^n$ - Film specific heat - includes effect of external gas at film conditions, Eq.

$\mu_{f_j}^n$ - Viscosity of film, Eq.

$k_{f_j}^n$ - Thermal conductivity of film, Eq.

$\mathcal{D}_{f_j}^n$ - Film diffusion coefficient, Eq.

The actual equation for most of these variables depends on the model used. Hence they will be discussed more fully in the Results Section where a specific model was used for analytical calculation. In addition there are other nondimensional groupings that usually occur such as the Nusselt mass and heat transfer correlations. These utilize the film properties. The specific correlation used depends on the model, most often, as has been mentioned, it is Ranz and Marshall's.

d) Coupling Terms

The coupling term expressions involve models for droplet evaporization, heating, breakup and drag. Various expressions may be used and as a consequence the portion of the program that calculates the coupling terms when they are specified a priori is subroutinized to allow efficient interchange of a number of models. Equations and results of predictions using a specified set of models for the coupling terms are presented in the Results Section.

Boundary Conditions for the Steady-State Program.

a) Chamber geometry

The model utilizes, as an input, the cross-sectional area of the combustor from the injector to the throat. The chamber geometry most often used was that corresponding to the experimental hardware.

b) Spray input parameters

$\dot{W}_{j\,o}^{n}$ — Injection mass flowrate of j, n^{th} group, may be fuel and/or oxidizer

$T_{j\,o}^{n}$ — Injection drop temperature

$u_{j\,o}^{n}$ — Injection drop velocity calculated from

$$= \frac{\dot{W}_{j\,o}^{n}}{e_{\lambda\,j\,o}^{n}\,A_{inj}}$$

where

$$\rho_{\ell_{jo}}^{n}$$ - Initial liquid density

$$A_{inj}$$ - Area of spray injection orifices

$$D_{jo}^{n}$$ - Initial drop diameter

All of these parameters may be arbitrarily specified for computer runs or may be obtained directly from measurements made during the operation of the experimental device.

c) Gas phase input parameters

$$\dot{W}_{ox}$$ - Gaseous oxidizer injected flowrate

$$\dot{W}_{f}$$ - Gaseous fuel injected flowrate

$$T_{o}$$ - Temperature gaseous oxidizer injected

$$T_{f}$$ - Temperature gaseous fuel injected

$$H_{o}, H_{f}$$ - Enthalpies of injected gaseous propellants obtain from Tables for C, p and T

p - In absence of experimental data the pressure at the injector face can be closely estimated from shifting characteristic velocity data.

$$\text{i.e., } P \approx \frac{\dot{W}_{Total} \times C^{*}}{A_{throat} \times g}$$

where c* provided from Tables, is the shifting characteristic velocity dependent on propellant type, mixture ratio and pressure.

and $\dot{W}_{total} = \sum_{j} \sum_{n} \dot{W}_{j_o}^{n} + \sum_{o} \dot{W}_o + \sum_{f} \dot{W}_f$

This assumes 100% efficiency and no stagnation pressure loss from the injector to the throat. This is usually sufficient for the first guess: the actual pressure is found by iterative procedure. Various injection pressures are assumed until the velocity of the burned gas is sonic at the nozzle throat. Experimental data alleviates this problem.

u_f - Injected gaseous fuel velocity found from

$$= \frac{\dot{W}_f}{\rho_f A}$$

u_o - Injected gaseous oxidizer velocity found from

$$= \frac{\dot{W}_o}{\rho_o A}$$

and the densities, ρ_f, ρ_o, are found from the equation of state. Note that for both the velocity and temperatures if the injected gas is from staged cycle combustion products, $T_o = T_f$ and $u_f = u_o$, $\dot{W}_f + \dot{W}_o$ = flowrate of injected gas and the enthalpy is found from the tables at the proper mixture ratio. The velocity is determined from continuity of the entire injected hot gas.

Utilization of the Steady-State Program and Experimental
Data to Evaluate the Coupling Terms

It is evident from the description of the model presented thus far that it may be utilized as a separate entity. Specification of proper boundary conditions and use of presently existing expressions for the coupling terms allows analytical predictions regarding the performance of proposed engine design, etc. However, the validity of those predictions will depend greatly on the accuracy of the terms used to describe the coupling processes. It is with the evaluation of these terms that this contract is most concerned. In this respect the model is most efficiently used, not with a priori specification of coupling terms, but with direct spray data supplied from the experimental program.

Specification of Gas Phase Flow Field. Reference to the steady state spray/ gas conservation equations reveals that the coupling terms are $\dot{m}_{j_{vap}}^n$, $\dot{m}_j^n{}_{B.U.}$, $C_{d_j}^n$ and Q_j^n. No coupling terms appear in the gas phase equations, in fact only the droplet mass, m_j^n, velocity, u_j^n, and enthalpy H_j^n, appear as variables; recall that $(A u_j^n N_j^n)$ is a constant everywhere. It would be desirable to be able to provide $\dot{m}_j^n$, u_j^n, and H_j^n directly to the gas phase equations without having to specify equations for $\dot{m}_{j_{vap}}^n$, $\dot{m}_j^n{}_{B.U.}$, $C_{d_j}^n$. If this were possible then the gas flow field p, ρ, u, H(T) could be very accurately calculated without worry as to the validity of expressions used to supply mass, momentum and energy to the gas. It is necessary to have accurate description of the gas flow field because the gas flow field parameters cannot be provided by the experiment. The coupling terms expressions and hence evaluation of them

depend not only on the droplet spray parameters, such as diameter, velocity, etc., which the experiment can provide, but also on the gas phase compositions and conditions as well. Both flow fields must be adequately specified to allow evaluations.

Now m_j^n depends only on the diameter of the drop and the temperature gradient within it, which in turn specifies the density variation. If the drop temperature is uniform, for example,

$$m_j^n = \frac{\pi}{6} \left(D_j^n \right)^3 \rho \ell_j^n$$

and $\rho_{\ell_j}^n$ depends only on chamber pressure and the drop temperature. The drop velocity, u_j^n, is even simpler. All parts of the drop, regardless of density gradient, move at the same velocity. The drop enthalpy (or its equivalent, temperature) may be uniform throughout the droplet or it may also be a function of the gradient existing within the drop.

In actuality the gas flow field is really only sensitive to m_j^n. This is the only drop variable in the mixture ratio equation, which determines C, and also the only drop variable in the global continuity equation, which is used to determine the gas velocity, u (refer to the computer flow charts in Appendix III). The momentum equation contains both m_j^n and u_j^n but is nearly insensitive to both parameters as very large variations in either m_j^n or u_j^n (hence ρ and u) are required to alter the pressure in the constant area section of the chamber. Hence, p, determined from this equation, remains nearly constant in the chamber prior to nozzle convergence. In the global energy equation, the effect of the chemical heat of formation of the combustion products reflected in H, completely

masks the effects of H_j^n regardless of the mass flowrate of the drops. This reflects the fact that less than 3 - 5% of the gas energy is used in heating the droplets to a wet bulb temperature. Consequently H (and the gas temperature) depend almost solely on the mixture ratio, equation, and to some extent, the gas velocity. Density of the gas follows directly from the equation of state, which again is influenced primarily by the mixture ratio and continuity equations, since they exert the controlling influence on H (or T) and p is nearly constant.

As a consequence, since the momentum equation is relatively unimportant compared to the other equations ($p \approx$ constant), the mixture ratio and continuity equations primarily determine the gas flow field. And these equations are entirely dependent, in turn, on m_j^n. Thus if this parameter is adequately specified, slight errors in u_j^n or H_j^n only negligible propagate into the prediction of the gas flow field.

It is of course, important to also accurately determine u_j^n and H_j^n, since these spray parameters are directly involved in evaluating the coupling terms. However the discussion above was presented in order to show that slight measurement errors in u_j^n and H_j^n would not directly compound problems in preventing prediction of the gas flow field.

The equations presented thus far appear somewhat burdensome in that they are written in general form to handle multi-species and drop sizes. When used with the experimental data, which provides monodisperse liquid oxygen spray burning in co-currently injected GH_2, the parameters j and n in the model are set equal

to one, eliminating all summation terms. Furthermore $\dot{W}_o$ is zero and

$$\sum_f^F \dot{W}_f = \dot{W}_{GH_2} \text{ only.}$$

Because the experiment does provide monodisperse spray, photographic techniques provide the axial variation of droplet diameter and velocity which is representative of the flow field as a whole. Breakup, should it occur will be photographically visible as will the plane of droplet burnout. The primary input to the analytical model, however, is D_{LOX} and u_{LOX} as a function of the axial length, x.

Thus the spray velocity, one of the desired inputs to the gas phase equations is directly provided. This completely eliminates the need to use the droplet momentum equation. A prior specification of C_d is neither necessary nor required.

Computation of m_j^n and H_j^n is not nearly so simple, but is still straightforward. m_j^n is dependent, as discussed previously, only on the droplet diameter and droplet density (density gradient if it exists). The droplet diameter is directly supplied from the experimental data, but unfortunately the droplet temperature (hence density and enthalpy) cannot be determined experimentally. Although the spray data allows elimination of the droplet momentum and droplet continuity equations, it does not allow elimination of the spray energy equation. This latter equation is necessary to calculate the droplet temperature and density variation needed to compute m_j^n and H_j^n.

As a consequence the only coupling term that is required a priori is a model for Q_j^n. The important point to be considered is how greatly does the computation

of m_j^n differ with various coupling term models for Q_j^n. As discussed, m_j^n must be accurately determined to provide the gas phase flow field. The droplet heating and vaporization rate for liquid oxygen in gaseous hydrogen is rapid compared to most other propellants. This is primarily due to the physical properties of each constituent, such as C_p and k, etc. Liquid oxygen may be imagined to heat by either of two extremes: (1) the droplet has a finite thermal conductivity and hence heats by internal temperature gradients, (2) the droplet has a large internal circulation caused by convective flow and hence the thermal conductivity is large and the droplet temperature is uniform.

In the first case typical models for such phenomena, such as Grossman's or Agosta's, Ref. 65, predict that the internal droplet temperature remains nearly uniform (at the injection condition) with rapid vaporization, i.e., surface wet bulb conditions, carrying off the bulk of heat penetrating the surface layers of the drop. In the second case, as Fig. 44 of the Results show, LOX droplets very rapidly reach a wet bulb condition and thence remain at near constant temperature and density for the remainder of their lifetimes.

Hence if LOX were injected at $\sim 150°R$ its density would be about 73 lbs/cu ft, but if heated to wet bulb conditions, (215°R for the example shown) its density would decrease to ~ 63 lb/cu ft, a difference of some 15%. This would be the maximum difference in density and hence the maximum difference between the methods in predicting m_j^n. This is clearly not acceptable accuracy.

It is fortunately relatively easy to determine which of these heating models is applicable to LCX. In the former case the droplet diameter would continuously decrease. However, in the latter case of uniform heating, the droplet diameter initially grows, then decreases, as in Fig. 42 in the Results Section. This is due to expansion, heating initially being greater than vaporization. Observation of the drop diameter during the experimental operation will determine the proper type of model to use.

Since the various models representing each extreme predict very nearly the same result (relative to their extreme) determination of the proper extreme is sufficient. It is unlikely that there is a regime between the two because only small amounts of internal circulation are required to produce uniform heating. Further, in a strong convective flow field, such as the combustion process with a rocket, it is difficult to imagine a droplet in which strong circulating currents are not induced. Surface shear requires such a phenomena to occur. There is also considerable experimental evidence for such an event as discussed in the coupling terms review.

In the presence of uniform drop heating, considered the most likely model to apply, the amount of mass remaining by the time the density has reached its final constant value is nearly 70%, Fig. 43. This is a fortunate result (and one of the reasons for choosing the propellant combination); if slight errors are made in predicting the heat-up rate of the droplet to the wet bulb condition using such a model, it will have only a minor effect on predicting the gas phase flow in the mass of the drop. This is so because the heat up rate occurs during the portion of the droplets lifetime that its total mass and mass rate loss is low.

R-8377

237

For this reason the droplet heating rate is of lesser importance than the other coupling terms. And if the initial term used for that expression is at first not entirely accurate, it has only a minimal effect in determining either the gas phase flow or in allowing evaluations of the other, more important coupling expressions.

Evaluation of the Important Coupling Term Expressions. Having established that with experimental data and somewhat insensitive analytical modeling (the spray energy equation) it is possible to accurately establish the gas phase flow field, it is now necessary to deduce from this information the methods to evaluate the coupling terms.

a) Drag Coefficient

With the gas flow field now determined, the spray momentum equation (which has not been utilized) and the experimental data allow direct calculation of the drag force and consequently the drag coefficient. The spray momentum equation is

$$m_{ox} \ U_{ox} \frac{d U_{ox}}{d x} = g \ F_{ox}$$

Now both u_{ox} and m_{ox} are known as a function of length, u_{ox} directly from the experimental data and m_{ox} from D_{ox} and the spray energy equation (yielding density). Hence F_{ox} is directly calculated, from this equation, and prescribed as a function of chamber length (i.e., flow conditions).

In turn

$$F_{ox} = \frac{\pi}{g} \left[\ell \left(D_{ox} \right)^{2} \left| u - u_{ox} \right| \cdot \left(u - U_{ox} \right) \right. $$
$$\left. \times C_{d} \right] - 24 \ \pi \left(D_{ox} \right)^{3} \frac{d P}{d x}$$

In this equation ρ, u and p are known as functions of length from the gas phase flow calculation, D_{ox}, of course, is determined directly from the experiment. The only unknown is C_d and it can be directly calculated.

The drag coefficient is usually thought to be a function of relative R_e and perhaps density loading (sheltering effects). The calculation of

$$\bar{R}_e = \frac{D_{ox} \, |u - u_{ox}|}{g \, \mu}$$

as a function of chamber length is straightforward, all values are known. Similarly, the density loading (D.L.) at any point

$$D.L. = \frac{A \, u_{ox} \, N_{ox} \, M_{ox}}{\rho \, A u}$$

is easily determined since $A \, u_{ox} \, N_{ox}$ = constant, and all other variables have been determined.

C_d may then be plotted as a function of R_e or D.L. or various combinations of both and the best dependence of C_d on these and other parameters (Mach No., etc.) determined. A number of steady state firings with different contraction ratios, D.L., etc., will allow a sufficient variation of parameters to determine the functional dependence of C_d over a wide range of operating conditions.

b) Vaporization (Burning) Rate Models

Evaluation of this coupling term, $\dot{m}_{ox_{vap}}$, is determined in a similar manner to the evaluation of C_d. The spray continuity equation (again

not used until this point is

$$U_{ox} \frac{d}{dx} (m_{ox}) = - \dot{m}_{ox_{vap}}$$

Both u_{ox} and m_{ox} as functions of x are known, hence $\dot{m}_{ox_{vap}}$ is

determined as a function of chamber length and conditions. It

is important to use this data only upstream of breakup so that

$\dot{m}_{ox_{vap}}$ can be delineated from $\dot{m}_{ox_{B.U.}}$ etc. Breakup considerations

can also be eliminated by using data obtained at larger contraction

ratios (lower gas velocities).

Obtaining $\dot{m}_{ox_{vap}}$ as a function of length does not immediately

yield functional relationship as is the case with C_d. The vaporiza-

tion rate is complexly dependent on many variables, as was shown for

the different models presented in the coupling term review. However,

the only variables on which the vaporization rate can be dependent are

the drop liquid and vapor properties, the spray parameters, and the

gas flow field parameters. These variables are all known and all

parameters, which may enter into the vaporization rate calculation,

such as Nusselt numbers and film properties are all dependent on, and

functions of these known variables. Consequently various existing

models for $\dot{m}_{ox_{vap}}$ are computed and the results directly compared to the

experimentally determined $\dot{m}_{ox_{vap}}$. In this manner the most appropriate

vaporization rate model is delineated. Should none of the existing

models yield sufficiently accurate comparisons to the experimental

burning rate, the information obtained by making the comparison will

allow new and better formulations to be derived.

R-8377

c) Droplet Breakup Rate Models

Evaluation of this coupling term is also possible. If such a phenomena occurs it can be observed photographically by noting the occurrence of shearing of the drop surface layers. Under such conditions the remaining droplet diameter (or volume) axial variations can be experimentally determined. This droplet mass variation now depends upon both parent droplet breakup and vaporization. The sheared off droplets are normally so small (in the micron or submicron range) that they cannot be singularly observed and vaporize almost immediately upon formation. Having determined the vaporization rate from previous correlations, this predicted mass loss can be subtracted from the measured mass loss occurring under breakup conditions. The remaining mass loss is then due solely to the break-up rate, that is

$$U_{ox} \frac{d}{dx}\left(m_{ox}\right) + \dot{m}_{ox_{vap}} = -\dot{m}_{ox_{B.U.}}$$

and $\dot{m}_{ox_{B.U.}}$ can be computed. Further correlation is then the same method as used for $\dot{m}_{ox_{vap}}$. This method does assume that the mass loss mechanisms can be superimposed; however the breakup rate is usually fast compared to the vaporization rate and under such conditions $\dot{m}_{ox_{B.U.}} >> \dot{m}_{ox_{vap}}$, and

$$U_{ox} \frac{d}{dx}\left(m_{ox}\right) \approx -\dot{m}_{ox_{B.U.}}$$

only.

d) Droplet Heating Rate Models

Unlike all the other coupling models it is necessary to specify a priori a model for this phenomena. Specification of such models and the results of comparing extremes of proposed models have been discussed as they concern the calculation of the m_j^n and hence the gas flow field. Having once selected the proper extreme (non-uniform or uniform heating) through experimental observation, the droplet heating rate at least for subcritical pressure conditions, was shown to be of lesser importance than the other coupling mechanisms. However, it is desirable to have an accurate model for this phenomena. In almost all expressions describing the heat up rate, most of the parameters used in calculating the other coupling terms are present. Thus having once obtained the first estimate of the other coupling terms an iteration of these terms into the chosen heating rate expression can be performed. Should this significantly change the heating rate then further iterations involving all the coupling terms and experimental data will be performed to determine the best expressions for all coupling mechanisms.

This process may also be accomplished for various droplet heating rate expressions; iterative analysis with the experimental data will allow determination of the most consistent total set of coupling term expressions. It is not, however, expected that the resulting expressions for C_d and $\dot{m}_j^n$ will differ significantly from their initial determination.

242

Numerical Analysis of the Steady-State Programs

Numerical analysis of the steady-state program for digital computer computation was relatively straightforward. Primarily the trapezoidal integration formula was used for the set of ordinary differential equations.

In practice it was found that the viscous term, τ_{xx}, for the steady-state case was of negligible importance. It was subsequently dropped from the gas phase computations. The heat conduction term also proved to be of somewhat minor importance, but of considerably greater magnitude than the effects of τ_{xx}. Consequently, terms pertaining to q in the energy equation were retained.

A complete description of the numerical methods used for the steady-state program appears in Appendix III Block diagrams for both versions of the programs are presented. A description of Rocketdyne's computing facilities is presented in Appendix V.

Transient Model

Development of the Non-steady Formulation

As with the steady-state model the transient equations were reduced directly from the general formulation. Again, recall that the area term A must be included. Because of the non-steady inclusion of the formulation the one-dimensional reductions do not allow direct integration of any of the equations; the complete partial differential formulation was retained. Also, the equations as presented below incorporate a range of droplet initial group sizes, n, and

various spray propellant species, j, and though they were programmed with this form they are primarily used in practice with n and $j = 1$. Many of the variables are defined the same as those for the steady-state case, hence where this is so the definition will not be repeated.

Spray Phase Equations - Parent Droplets

a) Droplet Number Concentration

$$j=1...N \qquad \frac{\partial (AN_j^n)}{\partial t} + \frac{\partial (AU_j^n N_j^n)}{\partial x} = 0$$
$$n=1...N$$

b) Droplet Mass Continuity

$$n=1...N \qquad \frac{\partial (m_j^n)}{\partial t} + U_j^n \frac{\partial (m_j^n)}{\partial x} = -\dot{m}_{j_{vap}}^n - \dot{m}_{j_{B.U.}}^n + \cdots$$
$$j=1...J$$

where m_j^n, the droplet mass may again be a complex relation with the droplet diameter, or given as simply as

$$m_j^n = \frac{\pi}{6} (D_j^n)^3 \ell \ell_j^n = \frac{\ell_j^n}{N_j^n}$$

if the drop temperature is uniform.

c) Droplet Momentum

$$m_j^n \frac{\partial U_j^n}{\partial t} + m_j^n U_j^n \frac{\partial U_j^n}{\partial x} = g F_j^{''}$$
$$n=1...N$$
$$j=1...J \qquad \text{and } F_j^n \text{ is still given as}$$

$$F_j^n = \frac{\pi}{g} \left[C (D_j^n)^2 (U - U_j^n)(|U - U_j^n|) Cd_j^n \right]$$
$$- 24 \pi (D_j^n)^3 \frac{\partial P}{\partial x}$$

R-8377

d) Droplet Energy

$$\frac{\partial (m_j^n T_j^n)}{\partial t} + u_j^n \frac{\partial (m_j^n T_j^n)}{\partial x}$$

$$j=1\ldots J$$
$$n=1\ldots N$$

$$= \frac{Q_j^n}{Cp_j^n} - \left(\dot{m}_{j\,vap}^n + \dot{m}_{j\,B.u.}^n + \cdots \right) T_{j\,s}^n$$

when T_j^n m_j^n cannot be separated due to the presence of temperature gradients within the drop. On the other hand if the droplet heats uniformly, then the equation becomes

$$m_j^n \frac{\partial T_j^n}{\partial t} + m_j^n u_j^n \frac{\partial T_j^n}{\partial x} = \frac{Q_j^n}{Cp_{\ell_j}^n}$$

Again it is still necessary to calculate the entire drop enthalpy, H_j^n, because that term is used in the gas phase transient equation. The relation between H_j^n and T_j^n is as in the steady-state case.

e) Droplet Wave Build-up

$$\frac{\partial \psi_j^n}{\partial t} + u_j^n \frac{\partial (\psi_j^n)}{\partial x} = \frac{1}{\tau_{j\,B.u.}^n}$$

$$n=1\ldots N$$
$$j=1\ldots J$$

The same assumptions regarding $\dfrac{W_e}{\sqrt{R_e}}$ critical values are used here as in the steady-state case.

f) Droplet Residence Time

$$\frac{\partial \tau_{j\,\tau}^n}{\partial t} + u_j^n \frac{\partial (\tau_{j\,t}^n)}{\partial x} = 1$$

For the transient case $\tau_{j\,T}^n$ calculates residence time as a function of conditions existing at a specified time. Only in steady-state does it actually "track" the drop.

Gas Phase Equations

a) Local Mixture Ratio Equation

Although stronger concentration gradients can develop in the transient case than in steady-state operation, the corresponding gas phase convective velocity gradients are also larger and still tend to mask the effects of gas phase diffusion. Hence $\bar{D}$ is set equal to zero in the mixture ratio equation. In line with previous discussion, chemical kinetic effects are relegated to the coupling terms and are considered of negligible effect once mixed into the bulk gas. Thus the one-dimensional mixture equation is obtained by summing over all species equations, and is

$$\frac{\partial (A \rho C)}{\partial t} + \frac{\partial}{\partial x}\left(A V C \right)$$

$$= -\left(2C + 1 \right) \sum_{j=1}^{OX} \sum_{n=1}^{N} \left(\frac{\partial A N_j^n m_j^n}{\partial t} + \frac{\partial (A U_j^n N_j^n m_j^n)}{\partial x} \right)$$

$$+ \left(C^2 \right) \sum_{j=1}^{Fuel} \sum_{n=1}^{N} \left(\frac{\partial A N_j^n m_j^n}{\partial t} + \frac{\partial (A U_j^n N_j^n m_j^n)}{\partial x} \right)$$

where of course C is the mixture ratio and initial conditions for the gas and spray phases are discussed later, and $V = \rho u$ The reason for substituting a single parameter for ρu was for computational purposes. As is discussed in Appendix IV, the continuity and momentum equations were solved simultaneously.

b) Global Continuity

$$\frac{\partial\left(A\rho + \sum_{j=1}^{J}\sum_{n=1}^{N}A N_j^n m_j^n\right)}{\partial t} + \frac{\partial\left(AV + \sum_{j=1}^{J}\sum_{n=1}^{N}\left(A u_j^n N_j^n m_j^n\right)\right)}{\partial x} = 0$$

c) Global Momentum

$$\frac{\partial\left(AV + \sum_{j=1}^{J}\sum_{n=1}^{N}\left(A u_j^n N_j^n m_j^n\right)\right)}{\partial t} + \frac{\partial\left(A\frac{V^2}{\ell} + \sum_{j=1}^{J}\sum_{n=1}^{N}\left(A(u_j^n)^2 N_j^n m_j^n\right)\right)}{\partial x} = -gA(144)\frac{\partial P}{\partial x} + \frac{4}{3}\mu gA\frac{\partial}{\partial x}\left(\mu\frac{\partial u}{\partial x}\right)$$

Here the viscous term is more important than in the steady-state case. It does little to alter the final answer, but it adds a smoothing effect to the digital computation in the presence of steep waves.

d) Global Energy

$$\frac{\partial\left[A_3 + \sum_{j=1}^{J}\sum_{n=1}^{N}\left(A N_j^n m_j^n\left(H_j^n + \frac{(u_j^n)^2}{2gJ}\right)\right)\right]}{\partial t}$$

$$+ \frac{\partial\left[A u\left(_3 + .185 P\right) + \sum_{j=1}^{J}\sum_{n=1}^{N}\left(A u_j^n N_j^n m_j^n\left(H_j^n + \frac{(u_j^n)^2}{2gJ}\right)\right)\right]}{\partial x} = -A\frac{\partial q}{\partial x} +$$

$$+ \frac{4}{3J} A \frac{\partial \left(\mu U \frac{\partial U}{\partial x} \right)}{\partial x}$$

where

$$3 = e \left(H + \frac{(U)^2}{2gJ} \right) - .185 P$$

and this artifice was used to enable the term $\frac{\partial PA}{\partial t}$ to be put
into the derivatives on the left hand side to simplify numerical
analysis of the equations. Definitions of the terms are the same
as for the steady-state case. All enthalpies are referenced to
JANNAF data as previously discussed; boundary conditions, discussed
later, specify the amounts and form of the injected gas, i.e., fuel,
oxidizer or staged cycle combustion products.

e) Equation of State

$$\frac{P(144)}{e} = RT \left[\sum_i \frac{W_i}{M_i} \right]^{-1}$$

Subroutines Utilized in the Transient Program.

a) Combustion properties tables

Identical to the tables of the steady-state program.

b) Stagnation properties computation

Identical to the method used in the steady-state program.

c) Spray properties

The drop properties are identical to the steady-state case; the film
properties are only if other than quasi-steady models are used. The
latter is discussed in the context of a specific model.

d) Coupling terms

   As in the steady-state formulation when coupling terms are
   specified a priori, that portion of the program which utilizes
   expressions for them is subroutinized to allow efficient inter-
   change of models. Although the droplet dynamic physical processes
   during instability are in essence the same type of phenomena as in
   the steady-state case, i.e., droplet vaporization, heating, breakup
   and drag, etc., the quasi-steady assumptions may not be valid and
   more general and complex coupling term expressions may be necessary
   for describing unstable combustion. Effects such as flashing,
   micro-mixing of vapors, etc., are included in what is called droplet
   vaporization. Very simplified models were used for checkout of the
   transient program and these will be discussed in the Results Section.

Boundary and Initial Conditions for the Transient Program.

Unlike the steady-state program the transient model computation requires both
initial and boundary conditions.

Initial conditions must be specified at $t = o$, for all x from $x = o$ (injector
face) to $x = L$ (nozzle throat). Boundary conditions are required at the injector
face, $x = o$, (mass influx) and nozzle throat for all t (no downstream boundary
condition is required for the spray as it burns out at random locations and its
movement is controlled by the gas flow field).

All initial conditions are supplied by the steady-state program data (which may
in turn have resulted directly from experimental data). In all aspects, the

steady-state model is as rigorous in formulation as is the transient program and utilizes the same spray and gas property tables. The steady-state program is also designed to provide direct card punched input to the transient model.

Following input of the initial conditions the transient computer program is run for several time steps with no initial perturbation. This insures that the steady-state input is compatible with that finally predicted by the transient program as it settles to a steady-state solution. To insure compatibility the steady-state limit of the coupling terms in the transient program must be the same as in the steady-state model. Further, although some differences in numerical technique are inevitable, to avoid long computational times for the transient model to "settle out" to its own steady-state solution, and to avoid significant discrepancies from its final predicted steady-state solution and the input condition from the steady-state model, it is imperative that the two models be as identical and compatible as possible. It was primarily for this reason that the new steady-state model was developed. Subsequent tests reported in the Results Section have shown that, using the same coupling terms, virtually no difference exists between the input condition and the final steady-state flow field predicted by letting the transient model run under a no-perturbed condition.

&) Chamber geometry

When comparisons are made to the experimental data, the actual hardware geometry is used. However, for model checkout purposes, a shortened arbitrary chamber geometry was used. Cross-sectional area of the combustor as a function of length was supplied.

b) Spray input parameters

Initial Conditions - spray

D_j^n - Droplet diameter as a function of length, j, n^{th} group.

u_j^n - Droplet velocity as a function of length

N_j^n - Drop number concentration as a function of length. Note the steady-state program has no problem in computing this variable, since in steady operation

$$A u_j^n N_j^n = \text{known constant}$$

and the equation can be used to solve for N_j^n

T_j^n The droplet temperature (or temperature gradient) from the spray energy equation used in the steady-state program, as a function of axial length.

m_j^n The droplet mass, function of length and obtained from steady-state program depending on the relationship used between D_j^n and T_j^n.

H_j^n The droplet enthalpy, function of length and again dependent on droplet heating model.

$\psi_j^n, \tau_{j\,B.U.}^n$ The droplet wave build-up parameters - values given for droplets throughout the chamber.

τ_j^n Droplet residence times from injection, specified for all droplets in chamber.

Boundary Conditions - spray

Boundary conditions for a transient program can be quite complex depending on the degree of interaction allowed with the manifolding supply system. Feed system effects can be of overwhelming importance. Alternatively the system may be designed with close coupled high pressure drop devices (sonic or cavitating venturis, etc.) which essentially eliminates feed system fluctuations. Since the experimental hardware was designed in this manner and because the frequencies of interest are high (>1500 cps), the mass flowrate injection of spray will be considered constant. Boundary conditions for the spray then are, at $x = 0$, all t.

$\dot{W}_{j\,o}^{n}$ = Injection mass flowrate of j, n^{th} group, considered to be constant for all t.

$u_{j\,o}^{n}$ = Initial injection velocity of drops

$$= \frac{\dot{W}_{j\,o}^{n}}{\ell\ell_{j\,o}^{n} A_{inj}}$$

where

$\ell\ell_{j\,o}^{n}$ = Injection density of spray, which can vary with the oscillating chamber pressure

A_{inj} = Area of spray injector orifices

Note that even though $\dot{W}_{j}^{n}\big|_{o}$ is constant $u_{j}^{n}\big|_{o}$ may vary slightly.

$T_{j\,o}^{\,n}$ = Initial droplet temperature. The initial droplet temperature is always uniform because the supplied liquid that forms the spray has a uniform temperature.

$D_{j\,o}^{\,n}$ = Initial droplet diameter formed. It may well depend on the actions of the wave and the injected jets. However, first assumptions, until experimental data is available is that the distribution and size of droplets follows that determined for the steady-state program.

$N_{j\,o}^{\,n}$ = The initial number concentration of n, j drops injected

$$= \frac{\dot{W}_{j\,o}^{\,n}}{A\,u_{j\,r}^{\,n}\,\frac{\pi}{6}\left(D_{j\,o}^{\,n}\right)^3 e\,\ell_{j\,o}^{\,n}}$$

and this parameter depends on the specification of $D_{j\,o}^{\,n}$ and the effect of pressure on $u_{j\,o}^{\,n}$.

$m_j^{\,n}$ = The initial droplet mass. It is equal to

$$= \frac{\pi}{6}\left(D_{j\,o}^{\,n}\right)^3 e\,\ell_{j\,o}^{\,n}$$

since the initial droplet temperature is uniform. Hence it depends on the variation of $\left(D_j^{\,n}\right)_o$ with time.

$H_{j\,o}^{\,n}$ = The droplet initial enthalpy. Since the drop temperature is uniform, so is its enthalpy and it is simply related to the drop temperature.

$\psi_j^{\,n}; \tau_{j\,B.U.}^{\,n}$ = No boundary conditions

$\tau_{j\,\tau}^{\,n}$ = Always equal to zero at x = o.

c) Gas phase input parameters

As for the spray parameters, the transient model computation also
requires both initial and boundary conditions for the gas variables.
Because the formulation is for a finite domain both upstream and down-
stream boundary conditions on the gas phase are required.

Initial Conditions - Gas

The entire gas phase flow field must be specified as an initial
condition. This involves

    C - Mixture ratio

    H - Gas enthalpy

    ρ - Gas density

    u - Gas velocity

    T - Gas temperature

    p - Gas pressure

   ω_i - Gas composition

μ, k, etc. Gas physical properties

These are all provided by the steady-state program in combination with
the gas phase combustion properties tables.

Boundary conditions - gas

Again as for the spray case, boundary conditions in the gas in transient
operation, can be quite complex, involving wave motion within the feed
system. However, if very close-coupled sonic venturis supply the
gas flow then feed system effects are minimal. As this is the case
for the experimental hardware of this program, the assumption is made

that the injected mass and energy flux of gas remains
constant. Boundary conditions for the gas then are

1) Injector Face

   a') No Gas Injection

   If all propellants injected are in the liquid phase, the
   only boundary condition on the gas phase at the injector
   face is that the axial velocity

   $$u = 0$$

   b') Gas Injection

   The injected gas may be fuel, oxidizer (or both) or staged
   cycle combustion gases. Because the injected inflow of any
   of these alternatives is normally subsonic, the upstream
   boundary condition becomes somewhat complicated as the
   incoming density (hence velocity) is strongly coupled with
   the combustor conditions. This is so even if the mass injection
   rates are constant. Boundary conditions for these cases then
   are,

   $\dot{w}_{ox}$ = gaseous oxidizer injected flow rate = constant

   $\dot{w}_f$ = gaseous fuel injected flow rate = constant

   and assuming as before, if both gaseous oxidizer and fuel are
   uniformly injected in their natural states, combustion is
   instantaneous.

   $$A\rho u = AV = \dot{w}_{ox} + \dot{w}_f = \dot{w}_T$$

   The $\dot{w}_T$ could also be staged cycle combustion gas. In the usual
   case $\dot{w}_{ox} = 0$ and $\dot{w}_T = \dot{w}_f$.

Also the assumption is made that the entering total energy/
unit mass does not fluctuate, i.e.

$$H + \frac{u^2}{2gJ} = H + \frac{V^2}{2gJe^2} = \frac{\dot{W}_{ox} H_{ox_s} + \dot{W}_f H_{f_s}}{\dot{W}_T} = H_s$$

where

H_{ox_s} = Stagnation enthalpy of gaseous oxygen source

H_{f_s} = Stagnation enthalpy of gaseous fuel source

H_s = Unit mass stagnation enthalpy (form to use if gases are injected as staged cycle combustion products).

The enthalpies are determined from measured gas temperatures T_{ox_s}, T_{f_s} or T_s, the appropriate source stagnation pressures and the combustion tables where $C = 0$ for fuel, ∞ for oxidizer and a finite value for the staged cycle combustion products. Normally, these stagnation enthalpies are the same as those computed for the steady-state program boundary conditions.

The boundary condition for the gas mixture ratio is given simply as

$$C = \frac{\dot{w}_{ox}}{\dot{w}_f}$$

However, although the stagnation enthalpies, initial mixture
ratio and mass flow rates are specified these do not allow
separate determination of ρ, u and H. The inlet mass and energy
relations with the tables are not sufficient to allow compu-
tation of all the variables. The density is strongly dependent
on p and T(H) and C(from the tables). Specification of the
density would then determine u and hence H. Clearly an iterative
solution at the injector face is required. In reality this is
resolved by simultaneously solving the continuity and momentum
equations throughout the chamber at each time step. These
equations are solved iteratively with the other equations,
using the upstream and downstream boundary conditions on V and
C. H at the injector face is then determinable as part of the
iterative scheme. The exact method is presented in Appendix IV.

2) Downstream Boundary Condition

The downstream gas-phase boundary condition has been and still is
a source of some confusion among various authors. Many have placed
the downstream boundary condition at the beginning of nozzle con-
vergence and applied the short nozzle approximation (Mach number at
this point remains constant). This is somewhat oversimplified.

The actual effect on movement and warpage of the mach plane at or
near the throat due to nonlinear wave motion, oscillatory droplet
flow and heat release, is uncertain. To avoid such problems
Burstein, Ref. 64, utilized a downstream boundary condition that is
located in the supersonic portion of the nozzle. At sufficiently
large expansion ratios $\frac{A_N}{A_t}$ like 3 (Mach No. $\sim$ 2) he sets all
gas parameter first derivatives with respect to x equal to zero

for all t. This is not entirely accurate but is felt to be
sufficiently far removed from the chamber that the boundary condition
is fairly insensitive in nature and gives information about throat
mach plane movement. On the other hand in the absence of burning
near the nozzle throat, throat plane movement may not be great
even with fairly high amplitude waves and one may imagine that the
throat flow would always be at or very near local sonic conditions.

Both boundary conditions can be utilized in the formulation. At
present the latter has been programmed and the downstream boundary
condition is taken to be

$$\dot{w} = \rho_t \, A_t \, u_t$$

where

ρ_t = density at throat

A_t = throat cross-sectional area

u_t = local shifting speed of sound, depending
on C, H and p at time t at throat.

1) Perturbation Condition

Perturbations are applied at the throat, simulating the experimental
method. The perturbation is produced by physically stopping the flow
or a prescribed portion of it at the throat plane. Thus either
specifying

$$u_t = 0$$

or

$$\dot{w}_t = \rho_t \, A_p \, U_t$$

where

A_p = net resultant area for gas expulsion

for a specified number of time steps is sufficient to allow the computer
formulation to calculate the ram pressure wave produced.

Utilization of the Transient Program and Experimental Data to Evaluate the Coupling Terms

The transient model, similar to the steady-state formulation, may be utilized as a separate entity. Specification of presently existing expressions for the coupling terms allows analytical prediction regarding the stability of proposed engine designs, etc. Naturally, those predictions will depend greatly on the accuracy of the terms used to describe the coupling processes. The coupling processes during unstable combustion need not be and in fact probably are not exactly the same as those during steady-state operation. The processes, still are mass vaporization, etc., breakup, heating, drag, but the rates and controlling parameters may be different in the two modes of operation; in particular, the quasi-steady assumptions of current coupling term expressions may be invalid for instability analysis. It is with the evaluation of these terms under instability conditions that this portion of the program is primarily concerned.

Specification of the Gas Phase Flow Field. It would be advantageous if, as with the steady-state formulation, the transient model could be used, not with a priori specifications of the coupling terms, but with direct spray data supplied from the experimental program.

The spray variables that appear in the gas phase transient equations are N_j^n, u_j^n, m_j^n, and H_j^n. Note that N_j^n appears as a variable since $A u_j^n N_j^n$ is no longer a constant. No coupling terms appear, of course, in the form of the gas phase equations utilized. For the same reasons as in the steady-state case it would be desirable to be able to provide these spray variables to the gas phase equations without providing equations for $\dot{m}_{j_{vap}}^n$, $\dot{m}_{j_{B. U.}}^n$, $C_{d_j}^n$ and Q_j^n.

Transient combustion through observation of the equational formulation and physical reasoning appears to be primarily controlled by the fluctuating rate of mass release. Under such conditions large fluctuations in local gas density and energy release can occur. This in turn produces localized overpressures which further alter the local temperatures and generate large velocity gradients. These large velocity gradients and other effects, pressure, temperature, etc., may in turn interact with the coupling processes and organize and sustain the pressure oscillations. During such events the gas flow field is sensitive to the specifications of both m_j^n and u_j^n. This is so because the mass release is dependent on both N_j^n and m_j^n and the parameter N_j^n is also dependent on the local value of u_j^n.

Hence in both the time-varying gas mixture ratio and continuity equations, N_j^n, u_j^n and m_j^n are important spray parameters. This is also now true, at least indirectly, for the momentum equations, in that the large fluctuations of m_j^n, N_j^n and u_j^n cause the density fluctuation that can produce large pressure gradients at any point in the chamber.

The global energy equation enthalpy, H, is still fairly directly insensitive to H_j^n for the same reasons as in the steady-state case. H is primarily dependent on the mixture ratio equation. the gas velocity and in addition the pressure-time variation because of the $\dfrac{\partial PA}{\partial t}$ term in the equation. Thus, although H_j^n may still not be directly important in specifying the gas phase flow rate, it is now necessary to very accurately specify at least both u_j^n and m_j^n and preferably N_j^n.

In principle, it is possible to approach the problem in the same manner as specified for the calculation of the gas phase flow rate during steady state that is, eliminate the transient spray mass continuity and momentum equations.

These equations are replaced by experimental data yielding D_j^n and u_j^n. Naturally, when used directly with experimental data or even when comparisons to the experimental data are performed, n and j are set equal to 1. and only GH_2 enters as the gaseous component. This greatly simplifies the form and computation of the equations. These reductions are of course possible because the experimental data are produced by the monodisperse spray engine where $D_j^n = D_{LOX}$ and $u_j^n = u_{LOX}$ only. This remains true so long as the wave does not disturb the injection process. Similar to the previous method m_j^n must be calculated through D_j^n and the drop energy equation. This, as before, requires a priori specification of at least one of the coupling terms, Q_j^n.

There are a number of very serious problems with this technique. First, and the least of the problems, the accuracy of the gas phase flow field calculation now depends on the accurate specification of two variables, u_j^n and m_j^n rather than just one. Hence, not only small errors in specification of D_j^n (hence m_j^n) but also in u_j^n could propagate into calculation of the gas conditions, compounding problems. u_j^n is needed for evaluation of N_j^n; it would be desirable to specify N_j^n experimental, but this is an impossible task. The number of drops/unit volume is sufficiently large that even with holographic techniques accurate determination of N_j^n would be both unfeasible and uneconomical. Thus it is necessary to use an additional spray equation; the drop number concentration equation to determine N_j^n.

Secondly, and of more importance, u_j^n depends on both D_j^n and the energy equation utilized. In the steady-state situation, there is a wealth of information from many models and experimental data comparisons that indicate the quasi-steady assumptions do not appear to be grossly in error. Under such conditions u_j^n was shown to be not terribly sensitive to the energy equations

R-8377

utilized and the experimental/analytical methods proposed appear quite
feasible. This may not be the case during transient combustion. As yet,
fully non-steady drop heating and vaporization models which do not invoke
some very simplifying assumptions have not been derived. As a consequence
m_j^n may, under transient conditions, be highly dependent on the particular
model for ω_j^n utilized.

Thirdly, and the most serious problem, the equations to be replaced and
those to be determined are time, space dependent; that is, they are partial
differential equations. Hence u_j^n and D_j^n must be specified as both functions
of time and axial length. This is experimentally prohibitive; continuous
photography in time for the entire chamber length would have to be utilized.
The data reduction from such photography to obtain u_j^n and m_j^n as function of
x and t, for a sufficient time span to allow calculation of the effects of the
pressure wave throughout the chamber, is enormous. Possible errors involved
preclude the use of such a method.

It thus appears that, during transient operations, the gas phase flow field
cannot be directly determined from experimental data. Rather it must be
calculated by a prior specification of all the coupling terms and retention
of all the spray equations.

Evaluation of the Coupling Terms. Undeniably, the fact that the gas phase
flow field cannot be specified independent of the coupling terms complicates
the evaluation of the terms. However it does not make the task impossible.

Although transient combustion is certainly much more complex than its steady-
state counterpart there is experimentally one advantage as far as measurement
of one of the varying gas phase parameters. The pressure, which is nearly

constant during stable operation, is just the opposite during unstable burning. It is fluctuating widely or growing or decaying in magnitude. This can be accurately measured by the transducers along the length of the engine. The characteristics of the pressure fluctuations will also be a function of engine operating conditions and initial disturbance levels. It is possible experimentally to map out the entire regime of operation in which growth or decay of pressure waves occur. Since the perturbation is always produced at the throat, the pressure wave propagates into monodisperse spray. Further, even if the injection process is disturbed on the first pass the resultant wave reflection off of the injector face propagates back into the remainder (if any) of the initial monodisperse spray. Reflection from the throat results in at least a portion of the third pass which still could be interacting with the initial spray. Thus there is sufficient data in which monodisperse spray assumptions are valid to determine the growth or decay of the pressure wave. Further, additional passes may be valid if the wave does not greatly interrupt the spray production process.

It is to be expected that the directly measured parameter, pressure, which is easily characterized as a function of time and space, is a very strong function of the coupling term expressions. It appears then that the most appropriate method to evaluate the coupling terms is to first input the best expressions determined directly from the steady-state computations and parametrically evaluate these terms by comparing program predictions to the observed experimental values of pressure growth or decay.

Pressure is not the only experimental parameter which may be used in the comparisons. At selected times during the experimental observations, droplet

diameters, velocities and the location of the onset of breakup can be
determined, again because of the monodisperse spray produced. The
coupling terms must allow predictions for these selected times which agree
with the drop data as well as with pressure. All of this information is
sufficient to evaluate the validity of any set of specified coupling terms.

It is true that this method does not allow direct computation of individual
coupling terms. But it can determine the validity of those expressions in
current use; this is particularly true with regard to evaluating the quasi-
steady assumptions. This in itself is a major objective of the program.
It is also true that if the coupling processes differ during transient
combustion, expressions describing such processes must reduce to those
determined from the steady-state work as the waves decay and die out.
Hence a combination of steady-state coupling term knowledge and direct
experimental data of p, D_{LOX} and u_{LOX} during transient conditions can
produce information needed to expand the description of the coupling pro-
cesses to render them valid during unstable combustion.

Numerical Analysis of the Transient Formulation

The numerical analysis of the transient formulation was exceedingly complex.
The final set of finite difference equations (the technique utilized) evolved
over more than a year's work of trial and error effort. The complexity was
primarily due to lack of prior experience upon which to base the analyses.
This is not to say that there have not been other longitudinal or even
transverse instability programs developed in the past. Rather this is the
first transient program to utilize a complete set of conservation equations

including a time varying: droplet concentration number equation, gas phase mixture ratio equation, and a dissociated energy equation. Coupled with this set of equations was a table of equilibrium gas-phase combustion properties containing over 55,000 separate data points. The solution of the equations involved iterative predictor - correction cycles coupled with various interpolations of the tables. Several important criteria were considered, convergence of the scheme, order of accuracy, and numerical stability and feasibility of computation. In a transient computation it is imperative to know that predicted instabilities are "physically real" and not due to numerical problems. Computations involving particularly the mixture ratio equations (and properties tables) effect on the continuity and momentum equations was found to be extremely sensitive. Further the feasibility of the computations depended on the rapidity with which the tables could be searched during iterations.

Following consideration (and often considerable trial and error effort) of various techniques: method of characteristics (when the viscosity was set equal to zero, evolving first-order, nonlinear hyperbolic equations) and finite difference techniques (useful for the more complete solution, when viscosity is retained and the equations are parabolic), the latter method was selected. In particular, a semi-first order, backward difference implicit scheme, which utilizes a system of equations, centered in space, and in which the momentum and continuity equations are simultaneously solved throughout the chamber, was used. This scheme was selected because of its inherent numerically stable characteristics. It was possible to show that the selected technique, in the absence of the mixture ratio equation and combustion tables, unconditionally satisfied the Van Newman necessary conditions for stability. Other higher order, hence supposedly more accurate, techniques,

such as the two-step Lax-Wendroff (Ref. 111), have more stringent stability requirements for the same set of equations. Thus, since it was not possible to directly determine the stability of any of the methods when the mixture ratio and combustion properties tables were utilized, it was decided to use the scheme which resulted in the most stable solution for the simplified set of equations. This is not to say that the other higher order schemes may not also be as appropriate (or even better) than the scheme selected, but economy and reason dictated that the more simple scheme be selected first. Perhaps, once more information is gathered with this technique it may be desirable and possible to advance to other techniques. Thus, some small accuracy was perhaps disregarded (though since momentum and continuity are solved simultaneously, this may not be true) in favor of stability considerations. The justification of such an approach will be discussed in the Results Section in which it was computationally possible, by application of the chosen technique, to show numerical stability of a sample case of the entire set of conservation equations.

Details of the numerical method are presented in Appendix IV. This appendix also includes a short discussion of finite numerical techniques and definition of the terms used in this section, i.e., order, accuracy, stability, etc. Along with representative finite difference equations, a flow chart of the computer program, derivations of the stability criteria and order of accuracy are presented.

RESULTS

PRELIMINARY RESULTS

The primary effort during this investigation has been directed toward the development of the experimental and analytical techniques to obtain and evaluate the required data. Consequently the majority of this report has been concerned with: 1) the design, initial experiments, development, fabrication, and cold flows of the monodisperse spray spray apparatus, and 2) a review of past analytical models, then formulation and computational development of new, overall combustion models. Although a great deal of discussion, argument, formulation, hardware and even initial experiments have been presented, the success of the primary effort of this program to date can only be judged if the experimental device and the analytical programs work. Thus a small portion of the effort was relegated to the task of obtaining actual preliminary experimental and analytical results. These preliminary checkouts were to be accomplished under realistic conditions, closely approximating actual use in future measurements and correlations.

The experimental preliminary results have suffered from coincidental problems which have not, as yet, allowed successful droplet data measurements under hot firing conditions. On the other hand the analytical programs have been checked out quite thoroughly and judged satisfactory in all respects. Despite the coincidental problems of the hot firings both the experimental and analytical programs are considered operational. Preliminary results and problems encountered, where applicable, are described in detail below for each program.

EXPERIMENTAL RESULTS

It is not surprising that problems were encountered during initial hot firing checkouts of the combustion device. Although a great deal of effort went into the initial design to eliminate potential problems, the checkouts first subjected the combustion system to actual high temperatures and pressures. Probelms encountered during such events, particularly with transparent hardware, are often not foreseen. Experience indicates that a considerable number of actual hot firings are required to eliminate initial difficulties. Consequently on the funds available for the experimental systems checkouts, two sets of hot firing tests were accomplished.

The first set of hot firings employed ambient temperature hydrogen as the fuel. Although photography of the first test of the set indicated that the combustion flow field appeared uniform, no droplets were evident, even near the injector face. Additional tests, at somewhat different operating conditions but still using ambient temperatures, revealed much the same results. Occasionally in some of the latter tests jets and droplets were present but their appearance was random and quite ragged. Closer observance of those jets that were present revealed that they were very bushy, appearing two-phase in nature. Further investigation of this set of runs indicated that the liquid nitrogen cooling to the engine system, particularly the engine bath, was inadequate to prevent heat transfer from the warm hydrogen to the liquid oxygen. This heat transfer was sufficient to cause vaporization of most of the liquid oxygen in the injection site region. The resulting two-phase, nearly vapor, injected flow destroyed the monodisperse spray production and in fact produced nearly gas-gas combustion within the chamber.

The second set of firings incorporated appropriate changes to provide adequate liquid nitrogen cooling. As added insurance the hydrogen fuel temperature was reduced to approximately 160°R. Photography revealed excellent drop production until just after the hydrogen mainvalve opened and hydrogen flow began. At this point, with the occurrence of ignition, the resulting photography revealed only a bright white opaqueness on the window. The reason for this was not readily apparent. During this set of firings, one test failed to ignite even though the ignition source was operable. This test, however, proved to be fortuitous in analyzing the test data. Photography from this run revealed that as the hydrogen flow was increasing with the main valve opening, transverse flow currents were set up across the injector face. The result of this flow was to cause propagation of the spray field towards one side of the engine and finally around and onto the windows. Subsequent photographs revealed that the windows were covered with a dense, dark, opaque liquid film. Had ignition occurred, this dense liquid film burning during combustion would appear, as it did, bright and opaque, primarily due to the effect of window glazing and light scattering.

Production of the transverse flow was not due to normal introduction of the fuel. In previous cold flow tests the addition of a high velocity gas simulating the hydrogen had no disrupting effect on the spray formation. In fact, the gas flow improved the spray production in previous tests. Analysis of the gas flow from the photographs and inspection of the hardware following the tests revealed that the injector face seals had failed. This allowed hydrogen to flow directly from the open manifolds evident in Figures 29 and 30. These manifold openings resulted from the machining process and are normally isolated from the combustion chamber by the injector face seals. When these seals

failed, hydrogen rather than flowing into the passages behind the Rigimesh, entered the chamber transversely across the injector face, producing the disrupted flow.

Although additional firings were not possible during this contract, a minor redesign is presently being incorporated that will seal these manifolds permanently from the chamber. There is no evidence from all the results to date that indicates that monodisperse spray production and photography cannot be achieved during combustion firings. Lack of achievement to date is felt to be a result of the described coincidental problems and does not reflect problems of a fundamental nature. Additionally, a new contract is to follow in which the experimental effort is to be the prime concern. During that contract full use will be made of the combustion system. Although minor problems may occasionally occur and have to be solved in the future effort, the combustion system device is presently considered operational.

ANALYTICAL RESULTS

The stability, accuracy, convergence and feasibility of the numerical methods employed to program the steady-state and transient formulations are formally discussed in Appendices III and IV. As presented there it is possible to show that a finite mesh size (Δx or Δx, Δt) exists which results in numerically stable and accurate solutions for the chosen finite difference technique and the equations analyzed. These conclusions require of course that the solution to the finite difference equations be feasible; i.e., that a solution is possible, has the required insensitivity to perturbations, and is economical, at least to some reasonable extent, in computation time. Moreover as also discussed in the Appendices the fin ... arence techniques for the spray

equations (particularly the mass continuity and heating equations), which contain the coupling terms, may have to be altered, to retain reasonable computation time and accuracy as the complexity of the coupling terms is increased. A general guide for satisfactory computational techniques is presented in the Appendices. It is of interest therefore to show that the analytical computer programs are numerically stable, accurate and feasible in practical application. Moreover, utilizing existing coupling terms that appear to have some validity, at least for stable combustion, yields results that give an indication of the feasibility of the proposed program to evaluate the coupling term expressions.

Unlike the experimental program, the nature of the analytical program was such that development and checkout of the computer formulation proceeded simultaneously. That is, the finite difference technique is selected by its degree of feasibility. Hence at the point of completion of development of the computer programs, they were also operational. The following sections present some preliminary results of computation with the analytical models.

Steady-State Program

For the example selected, three coupling terms are considered, droplet evaporation (burning) rate, droplet heating and droplet drag. Since no experimental data exists, the droplet dynamic models had to be selected a priori and the first version of the model was utilized, however, a monodisperse spray case was selected with the initial drop size taken to be the same as that determined from experimental cold flows. A number of droplet dynamic processes were envisioned during the review of the existing coupling term expressions which describe those processes. The El Wakil equations for droplet heating and vaporization were selected for the sample computation. This coupling model considers the droplet to be

evaporating into a convective flow of bulk chamber gases and to have sufficient internal circulation so that droplet heating is uniform. By inference, since no flame sheet or reaction in the boundary layer is included in the formulation, burning of the drop vapors occur in or near the droplet wake. As discussed in the coupling terms review there is some justificati n for this model and it represents the lower bound of all existing droplet burning models. Note that the El Wakil equations are obtained by setting the term A = 0 in Schuman's Model (Ref. 114). As discussed, at low pressures, A ⟶ 0, thus making Schuman's and El Wakil's equations identical.

The droplet drag expression selected was that developed at Rocketdyne for accelerating burning single droplets.

Selected Coupling Term Equations. Specifically, the coupling term expressions selected are

$$\dot{m}_{VAP_{Lox}} = \frac{Nu_{m_{j_{Lox}}} \pi D_{Lox} M_{Lox} \mathscr{D}_{j_{Lox}} P}{R T_{j_{Lox}}} \left[LN \left(\frac{1 - X_{v_e}}{1 - X_{v_{Lox_s}}} \right) \right]$$

$$Q_{Lox} = \frac{\pi D_{Lox} k_{j_{Lox}} Nu_{H_{j_{Lox}}} (T - T_{Lox_s}) Z_{Lox}}{e^{Z_{Lox}} - 1}$$

$$- \dot{m}_{VAP_{Lox}} \Delta H_{v_{Lox}}$$

where

$$Z_{Lox} = \frac{\dot{m}_{VAP_{Lox}} C_{Pv_{j_{Lox}}}}{\pi D_{Lox} k_{j_{Lox}} Nu_{H_{j_{Lox}}}}$$

and

$$F_{Lox} = \frac{\pi}{8g}\left[\rho \left(D_{Lox}\right)^2 \left| u - u_{Lox} \right| \left(u - u_{Lox}\right) C_{d_{Lox}} \right]$$

$$- 24\pi \left(D_{Lox}\right)^3 \frac{dP}{dX}$$

where

$$C_{d_{Lox}} = 24 \, Re_{Lox}^{-0.84} \qquad Re_{Lox} \leq 80$$

$$= .271 \, Re_{Lox}^{0.217} \qquad 80 < Re_{Lox} \leq 10^4$$

$$= 2 \qquad Re_{Lox} > 10^4$$

$$Re_{Lox} = \frac{\rho \, D_{Lox} |u - u_{Lox}|}{g \mu}$$

Since the droplet temperature is uniform the droplet spray mass is related to the diameter as follows,

$$\rho_{Lox} = N_{Lox} \, m_{Lox} = N_{Lox} \frac{\pi}{6} \left(D_{Lox}\right)^3 \rho_{\ell_{Lox}}$$

Note that because of the low temperatures of the droplet the $X_{V_{LOX_s}}$

and $\Delta H_{V_{LOX}}$ are computed from an equation of state (Redlech-Kwong) and fugacity relationships. This corrects for the presence of other gases (Ref. 113,115). The other vapor properties that will be utilized are at the much higher film temperature and hence such corrections are not required.

Specification of Terms and Film Property Equations. All of the models one may consider for burning, heating, etc. have to include convective effects. For this reason Nusselt number corrections appear and integrations through the convective boundary layer are usually averaged and called "film properties," hence the subscript f that appears in many of the terms in the equations just presented. When comparing models it is necessary that the same method of calculating film properties be used. This was discussed in the Coupling Term Review Section and is particularly important with LOX-GH$_2$ propellants. Thus it is necessary to define the methods used to obtain the film properties as the method will determine the coefficients of the Nusselt number correction. Most of the terms used in the equations presented have been previously defined in the Analytical Program Section, Subroutine (c). Only those terms which were not defined there will be defined here. In the use of the terms, the subscript V refers to drop vapor, f, the film, j has been set equal to LOX (one species), and n is equal to one and thus deleted from the equations. Thus $X_{V_{f_j}}^n$ becomes $X_{V_{f_{LOX}}}$.

A linear film averaging technique has been selected here as it is consistent with the method used in obtaining the Ranz-Marshall Nusselt number corrections which are employed. These corrections for convective conditions are

$$\frac{Nu_{m_{f_{LOX}}}}{2} = \text{Nusselt number for Mass Transfer (Often called the Sherwood Number).}$$

$$= 1 + 0.3 \left(Re_{f_{LOX}} \right)^{1/2} \left(Sc_{f_{LOX}} \right)^{1/3}$$

where

$$Re_{f_{LOX}} = \frac{\rho_{f_{LOX}} \, D_{LOX} \, |u - u_{LOX}|}{g \, \mu_{f_{LOX}}}$$

$$Sc_{f_{LOX}} = \frac{g \, \mu_{f_{LOX}}}{\rho_{f_{LOX}} \, \mathcal{D}_{f_{LOX}}}$$

and

$$\frac{Nu_{H_{f_{LOX}}}}{2} = \text{Nusselt number for Heat Transfer}$$

$$= 1 + 0.3 \left(Re_{f_{LOX}} \right)^{1/2} \left(Pr_{f_{LOX}} \right)^{1/3}$$

where

$$Pr_{f_{LOX}} = \frac{C_{p_{f_{LOX}}} \, \mu_{f_{LOX}} \, g}{k_{f_{LOX}}}$$

Note when
$$Le_{f_{LOX}} = \frac{Pr_{f_{LOX}}}{Sc_{f_{LOX}}} = \frac{\rho_{f_{LOX}} \, \mathcal{D}_{f_{LOX}} \, C_{p_{f_{LOX}}}}{k_{f_{LOX}}}$$

$$= 1 \text{, an assumption often made in combustion analysis, then}$$

$$Nu_m = Nu_H$$

This assumption (Le = 1) is known to be poor for O_2 - H_2 combustion. Hence it has not been used for any calculations in this report.

Then the necessary equations for computing all film properties are:

$$T_{f_{LOX}} = \frac{T + T_{LOX_s}}{2}$$

$$X_{V_{f_{LOX}}} = \frac{X_{V_{LOX_s}} + X_{V_e}}{2}$$

where

$$X_{V_e} = \text{mole fraction of the LOX vapor of the external gas.}$$

Note: for burning conditions $X_{v_e} \approx 0$ and at "wet bulb" conditions $X_{v_{LOX_s}} \approx 1$ and hence $X_{v_{f_{LOX}}} \approx 1/2$. The saturation temperature for the pure droplet in the presence of other gases is defined as that temperature for which $X_{v_{LOX_s}}$ is identically one. It differs little from the pure substance saturation temperatures at low pressures.

Returning to the film property equations

$$X_{f_{comb.gas}} = 1 - X_{v_{f_{LOX}}}$$

$$M_{f_{LOX}} = X_{v_{f_{LOX}}} M_{LOX} + X_{f_{comb.gas}} M_{f_{comb.gas}}$$

where
$$M_{LOX} = 32.0$$

$M_{f_{comb.gas}}$ = molecular weight of combustion gas at $T_{f_{LOX}}$, assumed to shift equilibrium from T to $T_{f_{LOX}}$, obtained from combustion tables at C, p, $T_{f_{LOX}}$

$$\mathcal{P}_{f_{LOX}} = \frac{.0933 \times p \times M_{f_{LOX}}}{T_{f_{LOX}}}$$

Vapor Properties at Film Conditions are:

$C_{p_{v_{f_{LOX}}}}$ — supplied from tables for GOX specific heat at p and $T_{f_{LOX}}$

$\mu_{v_{f_{LOX}}}$ — supplied from tables for GOX viscosity at p and $T_{f_{LOX}}$

$k_{v_{f_{LOX}}}$ — may be supplied from tables for GOX thermal conductivity at p and $T_{f_{LOX}}$. However it is most often calculated from Euckens Equation

$$= \left(3.6 \times 10^{3}\right)\left(2.480 + M_{LOX}\, C_{p_{v_{f_{LOX}}}}\right) \frac{\mu_{v_{f_{LOX}}}}{M_{LOX}}$$

At the normal film temperatures this is compatible with the same method as used in the combustion property tables.

The vapor properties at the film are, except for $C_{p_{v_{f_{LOX}}}}$, unimportant except for their use in calculating the actual mixed film conditions.

Actual Film Conditions

$$C_{p_{f_{LOX}}} = \left(\frac{M_{LOX}\; X_{v_{f_{LOX}}}}{M_{f_{LOX}}}\right) C_{p_{v_{f_{LOX}}}}$$

278   R-8377

$$+ \left(\frac{M_{f \text{ comb. gas}} \; X_{f \text{ comb. gas}}}{M_{f \text{ LOX}}} \right) C_{P_{f \text{ comb. gas}}}$$

Here the specific heat of the film around the droplet is taken as the simple low pressure rule, although $C_{p_{v_{f_{LOX}}}}$ and $C_{p_{f_{comb\ gas}}}$ are each evaluated at the system total pressure. Errors introduced are negligible because $T_{f_{LOX}}$ is normally high enough to eliminate pressure considerations. This is also true of the properties for the following film equations. Lack of knowledge of actual film composition precludes the use of more complex "mixing" rules.

$\mu_{f_{LOX}}$ = fcn of ($\mu_{v_{f_{LOX}}}$ and $\mu_{f_{comb\ gas}}$) computed from Wilkes Equation (Ref. 113).

$k_{f_{LOX}}$ = $(3.6 \times 10^3)\, (2.480 + M_{f_{LOX}}\, C_{p_{f_{LOX}}})\, \dfrac{\mu_{f_{LOX}}}{M_{f_{LOX}}}$

$\mathcal{D}_{f_{LOX}}$ = Multicomponent Diffusion Coefficient for one species diffusing through the film gases and follows the method of Ref. 113. An example for mixture ratio less than stoichiometric is given below:

For $C < 8.00$ (LOX-GH$_2$) and at $T_{f_{LOX}}$ the majority of the species present at the mean film condition are either O_2, H_2 or H_2O. Hence

$$\mathcal{D}_{f_{LOX}} = \cfrac{1}{\cfrac{Y_{H_2}}{\mathcal{D}_{O_2, H_2}} + \cfrac{Y_{H_2O}}{\mathcal{D}_{O_2, H_2O}}}$$

$$Y_{H_2} = \frac{M_{H_2O} - M_{f \, comb. \, gas}}{16.00} \geq C$$

$$Y_{H_2O} = 1 - Y_{H_2}$$

$$\mathcal{D}_{O_2, H_2} = \frac{8.89 \times 10^{-7} \left(T_{f \, Lox}\right)^{3/2}}{P \; \Omega_{(O_2, H_2)}}$$

$$\mathcal{D}_{O_2, H_2O} = \frac{4.22 \times 10^{-7} \left(T_{f \, Lox}\right)^{3/2}}{P \; \Omega_{(O_2, H_2O)}}$$

R-8377

and Ω is a molecular property of the type of molecules colliding, and includes polar-bipolar effects, etc. (see Ref.113). It is also a function of $T_{f_{LOX}}$

For other mixture ratios, appropriate forms of $\mathcal{O}_{f_{LOX}}$ are used.

Results of Steady-State Computations. Following specification of the coupling terms and film properties subroutines steady-state computations were performed. The following conditions were input to the model:

Initial Drop Diameter	-	720 μ
Initial Drop Temperature	-	140°R
Initial Fuel Temperature	-	200°R
Mixture Ratio , C	-	5.0:1
Initial Droplet Velocity	-	Calculated internally but = 4.53 ft/sec
Chamber Pressure	-	Reiterated until throat velocity sonic $\approx$ 157 psia.
Initial Gas Velocity	-	Calculated internally but = 8.9 ft/sec
Chamber Geometry	-	Identical to Combustion Device, 19" Straight Section, convergence to Nozzle from 19" to 20".
Contraction Ratio	-	12.33 to 1
Mach Number Start of Convergence	-	.05

These input conditions correspond to actual conditions encountered during the hot firings and represent a LOX jet injection R_e = 2300. The numerical technique

as presented in Appendix III was retained for all equations except for the spray mass and heating equations. A more sophisticated bi-section routine was employed so that heating of the drop would not allow temperature overshoot of the "wet bulb" condition. The vaporization model is very sensitive to the correct "wet bulb" temperature andthe bi-section technique between the drop temperature as the lower limit and the saturation temperature as the upper limit permitted accurate and smooth solution to the finite difference equation. Utilizing such a technique the model was run with step sizes down to .05"; below this point no discernible difference could be detected in any of the predicted values of spray or gas parameters. Hence the practical error involved in any of the predicted values from a given equation is nearly zero.

The results are presented in Fig. 42 through 46. The first three graphs are primarily concerned with the spray parameters. Note that the drop diameter first increases, due to heating, for nearly the first four inches (Fig. 42). During this same period the droplet essentially reaches the "wet bulb" temperature of 215°R and remains at this level for the remainder of its lifetime (Fig. 44). Further, very little of the mass of the drop has burned, 70% is still remaining when "wet bulb" conditions are attained (Fig. 43). Drop velocity is presented in Fig. 46. For the first four inches the droplet velocity changes little, then increases nearly linearly to 175 ft/sec at the start of convergence. At the point of burnout the droplet velocity reaches a maximum of 260 ft/sec.

Pertinent gas parameters as a function of length are shown in Fig. 45 and 46. As is expected, both gas velocity and gas temperature follow the curve of percent burned. Within approximately 7" the gas velocity and temperature reach 90% of their final values. Pressure was not plotted as except for the convergent region it remains constant to within 1/2 psi throughout the chamber.
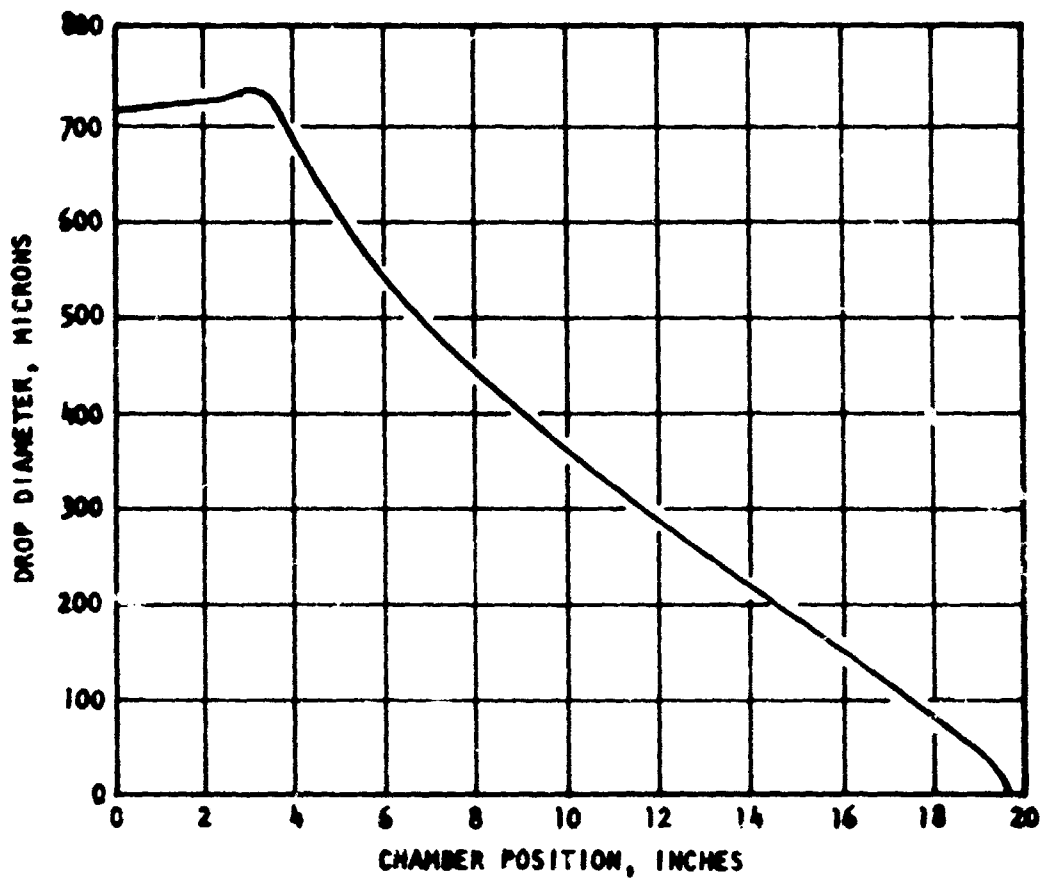
Figure 42. Axial Steady-State Distribution of LOX Drop Diameters
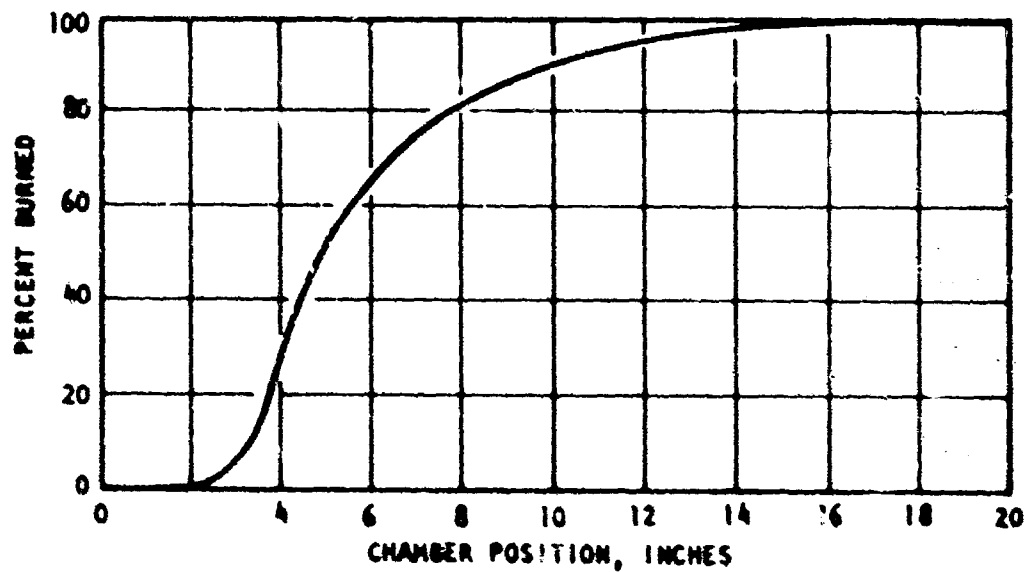
Figure 43. Steady-State LOX Spray Burning Profile
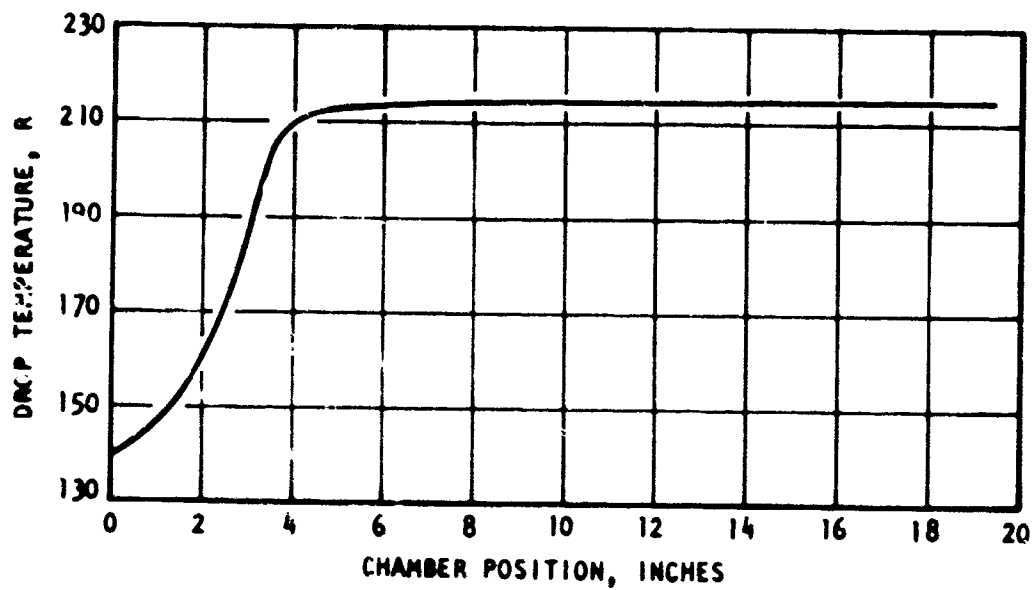
Figure 44. Axial Steady-State Distribution of LOX Drop Temperatures
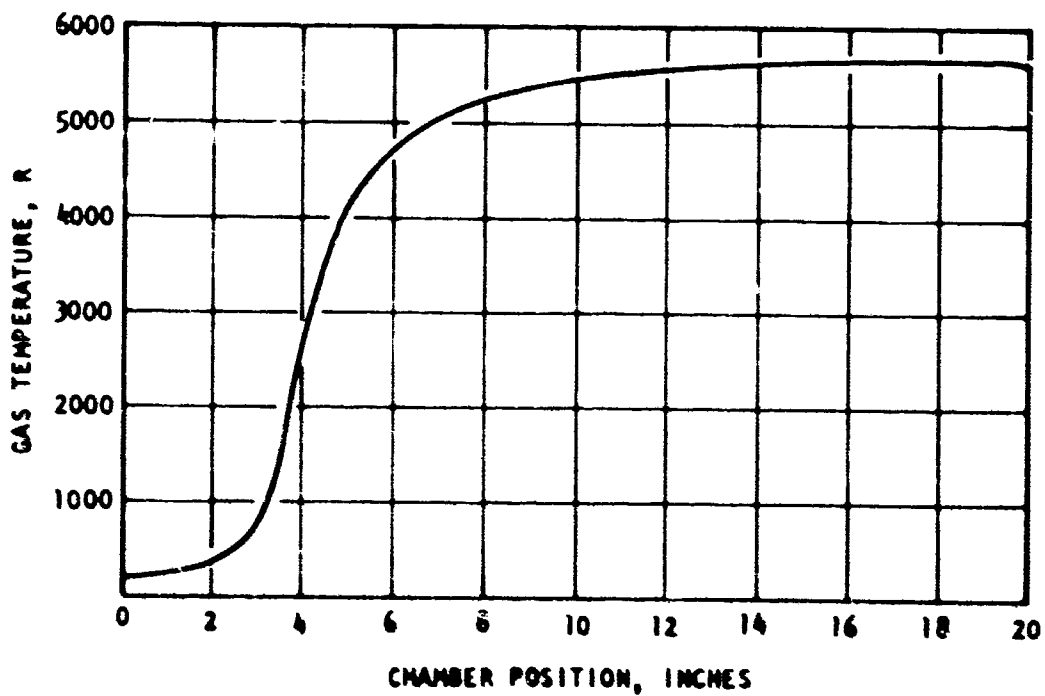
Figure 45. Steady-State Axial Distribution of Combustion Gas Temperature
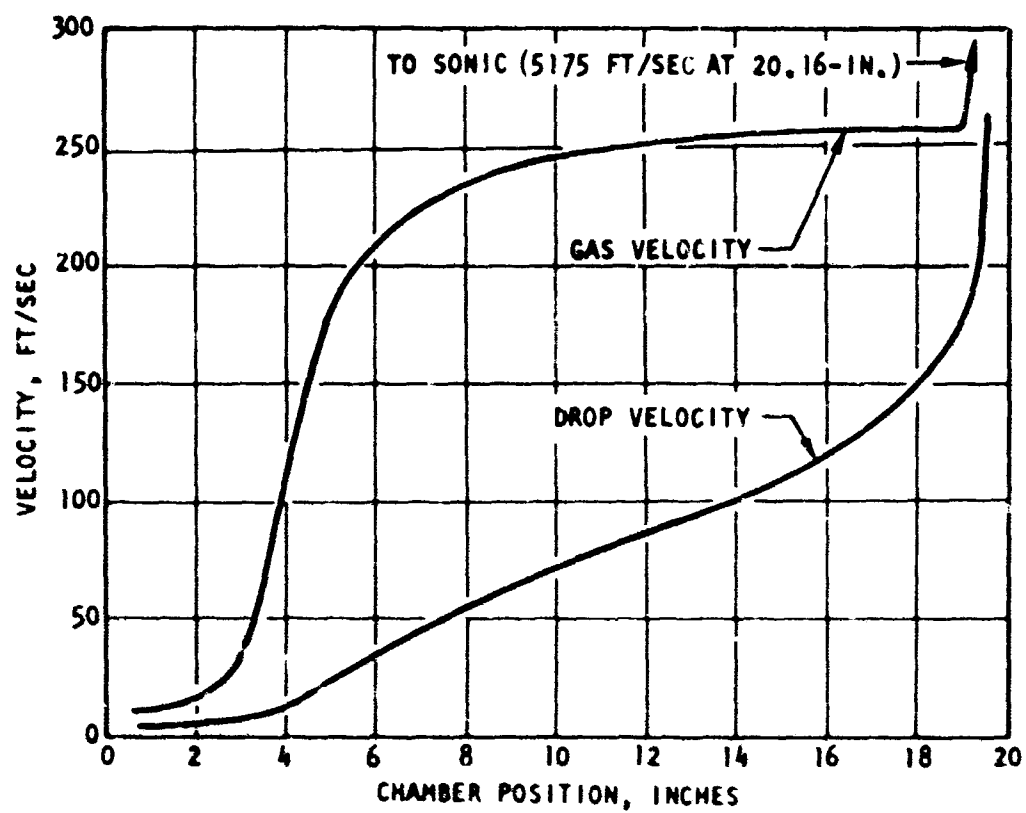
Figure 46. Axial Steady-State Distribution of LOX Drop
and Combustion Gas Velocities

Relation of Results to the Program Effort. The importance of these analytical results, as they relate to the entire program effort, cannot be underestimated. Some mention of them, as they pertained to a pertinent portion of the program being described, has previously occurred in the report. At this point it is proper to summarize the more salient features of these results as they pertain to successful culmination of the entire program.

Photographically it is necessary that the relation between drop diameter and velocity be such that the droplets can be photographed down to at least $100\,\mu$ with rather simple equipment.

Analytically it must be possible to distinguish, from photographic data, which extreme of droplet heating model to use. Further it must be possible to distinguish which droplet burning model is proper, convective evaporation or flame sheet descriptions. Of necessity, events must not occur so fast, regardless of the processes envisioned that photographic results would not be possible to obtain.

The droplet models used for the computations presented yield the slowest burning and surface heating rate of any available. The remaining burning rate models do yield rates of change of droplet diameters, etc., which are more noticeably rapid.   Snould one of the other models happen to represent the real combustion process, the more rapid results would also affect the experimental observations. The questions to be answered are: first, are the analytical results shown here compatible with the goals of the overall program, and second, since the results represent the lower boundary of droplet burning, can one extrapolate these results to show that, within present knowledge of the extremes of the coupling processes, any of the envisioned coupling processes would yield adequate experimental data?

First then, for the results shown, over 95% of the droplet mass lifetime can be observed with simple Fastax-Strobe photography. The droplet processes are spread out over 19 in. in length, at least 15 in. of which can be observed by the simple equipment mentioned above. Though not plotted, the computer results also indicate that the mass weighted average $Re_{f_{LOX}}$ for the droplet through this process is above 750. Thus the $Nu_f \approx 16 - 20$. Recalling that

$$\bar{D}_f \approx \frac{D_{LOX}}{1 - \frac{2}{Nu_f}}$$

this supports the previous contention that D_{LOX} is nearly 90% of the average film diameter. This figure alone would eliminate the photographic problem of distinguishing the drop from its film. However, this represents the average film thickness including portions of the wake, thus the actual zone around the girth of the droplet viewed by the camera is considerably less than $\bar{D}_f$; this even further eliminates the potential problem of droplet distinguishment.

To answer the second question, the model used does have the slowest surface heating rate of all present expressions. Since droplet surface temperature controls the rate of evaporation, the mass loss (diameter change) with this model is slower than the others. Hence if a finite thermal conductivity heating rate model were used in place of uniform heating, the droplet surface temperature would rise more rapid and mass evaporation would be faster than with uniform heating. The droplet diameter would continuously decrease rather than grow initially as shown in Fig. 42. Distinguishment of heating models would be evident and the mass of the drop could be calculated in either case. Of more importance, the surface temperature can never rise above the local wet bulb condition and hence the evaporation rate can never be greater than that of the uniform droplet heating

model presented here once the entire droplet has reached wet bulb conditions. Utilizing a finite thermal conductivity model would be like starting the maximum evaporation rate at x = o, i.e., moving the average slope of $\frac{dD_{LOX}}{dx}$ in Fig. 42 to x = o and it can be easily inferred that the evaporation process would still be spread out over 14 or more inches. Although the velocity would increase with length somewhat faster than Fig. 46, the change would not be great enough to cause large effects in the spatial relationship between D_{LOX}, u_{LOX} and photographic capability. These are advantages of the propellant combination, flowrates and drop sizes selected. Liquid oxygen, even if a uniform heating model is assumed, heats rapidly to wet bulb, and when wet bulb conditions are reached most of the droplets lifetime is spent at that condition.

The most rapid droplet burning rate model presently envisioned would be one having finite thermal conductivity heating within the droplet and the exterior surrounded by a flame sheet even during convective flow. This model of a rather "unreal" process would have the effect of increasing the initial burning rate rapidly to that near the final wet bulb condition of Fig. 44 and 45, since the droplet would be receiving heat from a near stoichiometric flame rather than from the bulk gas. Initial effects would be noticeable, even over the same model with no flame sheet, but the overall effect would not be as great as first imagined. This is evident in Fig. 45 ; clearly the bulk gas temperature, even for a uniform heating and hence slower vaporizing droplet reaches 90% of its final temperature by 7 in. Hence from that point on the droplet burns similar to a flame sheet model. Even if such a flame sheet type process occurred in the engine, comparisons to the results presented in Figs. 42 , 45, and 46

indicate that resultant burning would not be so fast that it could not be adequately observed. Note that the final gas temperature of the example presented, Fig. 45, for M.R. = 5.0 is little less than that for stoichiometric conditions, and most of the droplets lifetime as mentioned, is spent during the wet bulb condition when the gas temperature is at or near its final and highest value.

Transient Program

Preliminary checkouts of the transient programs were primarily directed toward determining numerical stability of the finite difference technique and compatibility of the formulation with the steady-state program which supplies the initial inputs. The reader is referred at this point to the Evaluation of Solution Method section in Appendix IV and the discussion of the Boundary and Initial Conditions for the Transient Program in the Analytical Program section of the main report.

As presented in Appendix IV, it was possible to show that a simplified form of the conservation equations (eliminating the mixture ratio equation and combustion property tables) unconditionally satisfied Von Newmans necessary criteria for numerical stability. The derivation of numerical stability further revealed that the satisfaction of this necessary criteria was independent of the ratio $\frac{\Delta t}{\Delta x}$ of finite mesh size. This is true so long as a Δt is selected that is sufficiently small that a vector term containing the coupling expressions may be neglected. Thus the stability criteria could be considered independent of the coupling term expression. The derivation did utilize, along with the simplified conservation equations, a set of nearly non-responsive (i.e., insensitive to

pressure or velocity waves) coupling term expressions for drop heating and burning rates, that is, $\dot{m}_{LOX}$ was taken to be a function of $f(x)$ D_{LOX}, where T_{LOX} and H_{LOX} were considered to be constant. The drag force had C_d equal to a constant (although this was only for convenience). The results of the derivation, however, as discussed above, revealed the form of the coupling terms to be inconsequential so long as the proper Δt was selected. Hence the form of the coupling terms used for simplicity in the derivation did not alter the final results concerning numerical stability predictions. For a discussion of the "feasibility" of finding the correct Δt for more complex coupling terms, the reader is referred to Appendix IV.

It was deemed necessary to establish the relation of the stability of the simplified set of conservation equations to the complete conservation equations (including use of the combustion properties tables). Further it was necessary to evaluate the actual compatibility of the transient and steady-state models, both with regards to accuracy and stability on the part of the transient model. To establish these relations actual computer computations were performed.

Selected Coupling Term Expressions and Inputs to the Transient Formulations.
The running time of the transient model is quite lengthy. In the absence of actual experimental data with which to compare results it was decided to retain the use of simplified nonresponsive coupling terms, as in the stability derivation, and to utilize inputs as if combustion were occurring in a 7 in. long rocket. Use of these nonresponsive coupling terms is actually quite important as will be seen later.

Initial steady-state calculations were performed using nearly the same input conditions given earlier in discussion of the results of that program. The GH_2 temperature was increased to 300°C and the initial droplet diameter was readjusted, down to 250μ from 750μ so that droplet combustion would be completed in the length of the 7 in. rocket to be modeled. Cross-sectional area of this imaginary engine was similar to the real 20 in. rocket as regards contraction ratio, however the convergent section of the 7 in. rocket was longer, starting at 4 in. from the injector face. The El Wakil equations and film properties technique presented earlier were utilized. Complete steady-state results were obtained. Refer now to the El Wakil burning rate equation during heating (the general equation). At wet bulb conditions, this equation for burning rate becomes,

$$\dot{m}_{LOX \atop @ wet \atop bulb} = -\frac{\pi' \, D_{LOX} \, k_{f\,LOX} \, Nu_{H\,f\,LOX}}{C_{P_{V_{f_{LOX}}}}} \left[Ln\left(1 + \frac{(T-T_{LOX}) \, C_{P_{V_{f\,LOX}}}}{\Delta H_{V_{LOX}}}\right)\right]$$

This equation was obtained by setting Q_{LOX} equal to zero and substituting the resulting equation into the general expression for $\dot{m}_{LOX}$. Both of these equations for the burning rate (general and at wet bulb) reveal the burning rate to be proportional to the first power of the droplet diameter and other parameters. In fact, at the wet bulb

$$\frac{\dot{m}_{LOX \, @ \, wet \, bulb}}{Nu_{H\,f\,LOX}} \approx Constant \, (D_{LOX})$$

It was not difficult then to fit the entire burning rate curve for the steady-state selection to

$$\dot{m}_{LOX} = f(x) \, D_{LOX}$$

with very little error.

This equation for $\dot{m}_{LOX}$ was then substituted back into the spray mass continuity equation in the steady-state model; the LOX droplet temperature was set equal to a constant (chosen as the final wet bulb temperature, still $\sim 215°R$ and eliminating the spray energy equation) and the gas phase flow field was recalculated. There were of course minor differences between the two sets of gas flow field calculations because of the assumption of constant temperature in the latter. In each case the complete drag force was retained, allowing $C_{d_{LOX}}$ to be the normal variable of R_e.

Results of Transient Computations. The latter coupling terms specified above (including variable C_d in the drag force) and the results of their use in the steady-state program were input to the complete transient model. Selecting reasonable values of Δt and Δx the model was then allowed to run under a "no perturbed condition" for a considerable number of time steps. It is during this time that if numerical instability is present, errors particularly in $\frac{\partial P}{\partial t}$, will begin to propagate and grow. However, the transient model predictions after the several time steps "settled out" to a non-time varying solution nearly identical with the steady-state input. This was true for all spray and gas phase parameters. Also the compatibility of the two models was established since the "settling out" period required only 15 time steps. Further, numerical stability during this "no perturbed" condition was demonstrated. The "steady-state" pressure profile is shown in Fig.47 as the solid line.
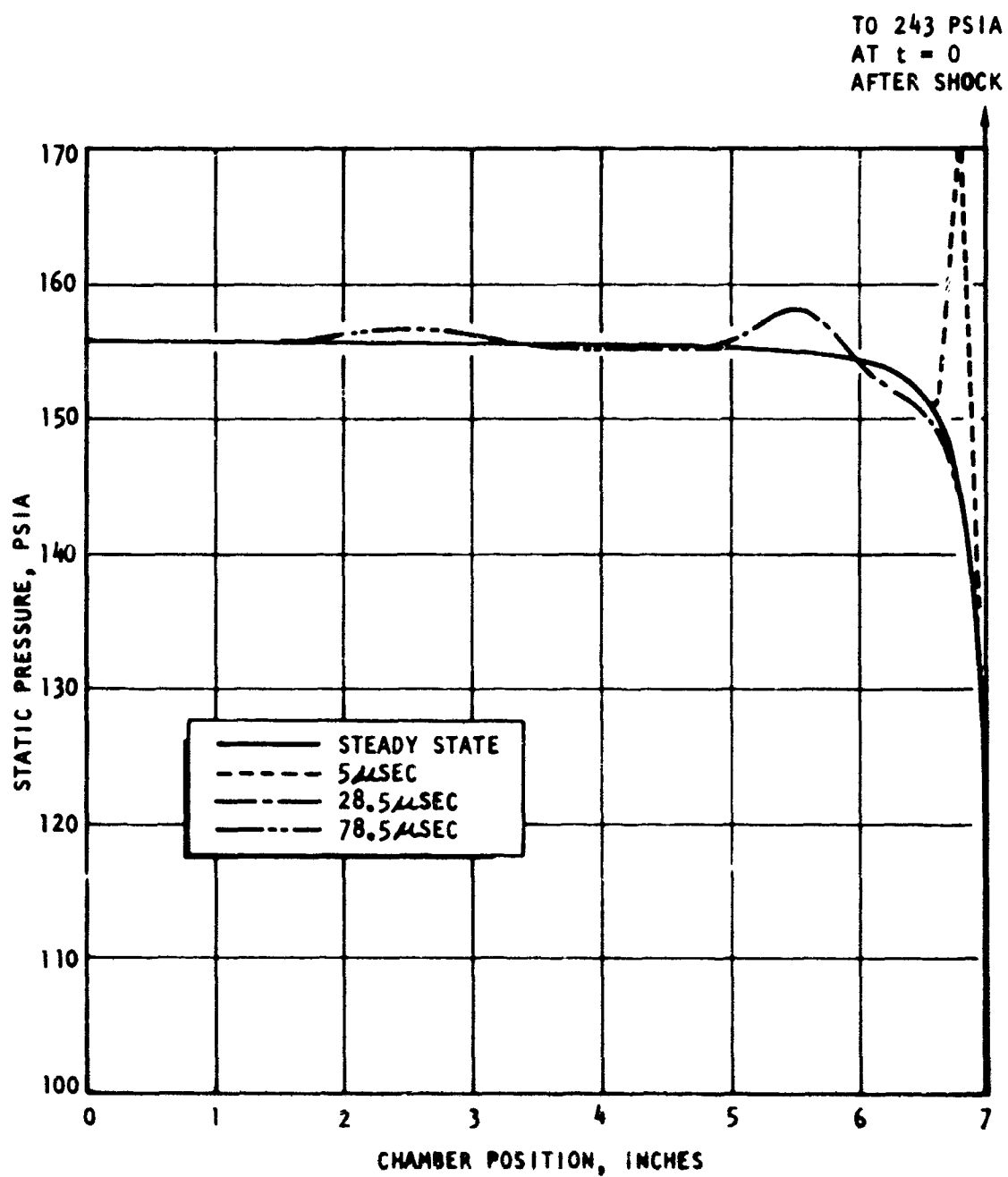
Figure 47 Transient Decay of a Pressure Pulse Resulting From a Momentary Closure of the Nozzle Throat

Of more importance, however, is the establishment of the numerical stability of the complete program when subjected to large perturbations. At this point use of the nonresponsive coupling terms assumes overwhelming importance. It is often difficult in practice to distinguish physical instabilities from numerical problems. However, with nonresponsive coupling mechanisms for the droplet heating and burning rates any induced wave in a combustion flow field must physically die due to gas viscosity, droplet drag and expansion processes. Hence a more severe test of the model was performed. A large perturbation was introduced at the throat by setting the throat velocity equal to zero for two time steps (as a ram closure of the throat akin to the perturbation device of the experimental system). The results are shown in Figs. 47, 48, and 49. Resultant pressures following the perturbation are shown for 5, 28.5 and 78.5 μ sec. following reopening of the throat. The initial closure produced a 152 Δ P overpressure (total of 243 psia) at the throat; by 78.5 μ sec. this pressure front had moved up the chamber at nearly the speed of sound and decayed to less than 1.5 psi over the steady-state conditions. The wave decay is clearly evident in Fig. 48 which is a plot of $(P - P_{S.S.})$ versus chamber length, for various times following shock production.

Perhaps more revealing is the physical decay of $\dfrac{\partial P}{\partial t}$ as a function of both length and time shown in Fig. 49. By 78.5 μ sec the rate of pressure rise is rapidly falling and smoothing behind the wave. In summary, the transient model, using nonresponsive droplet burning and heating properly predicted wave damping and a return to steady-state conditions. This is as predicted by the numerical stability analysis for the simplified conservation equations and such coupling
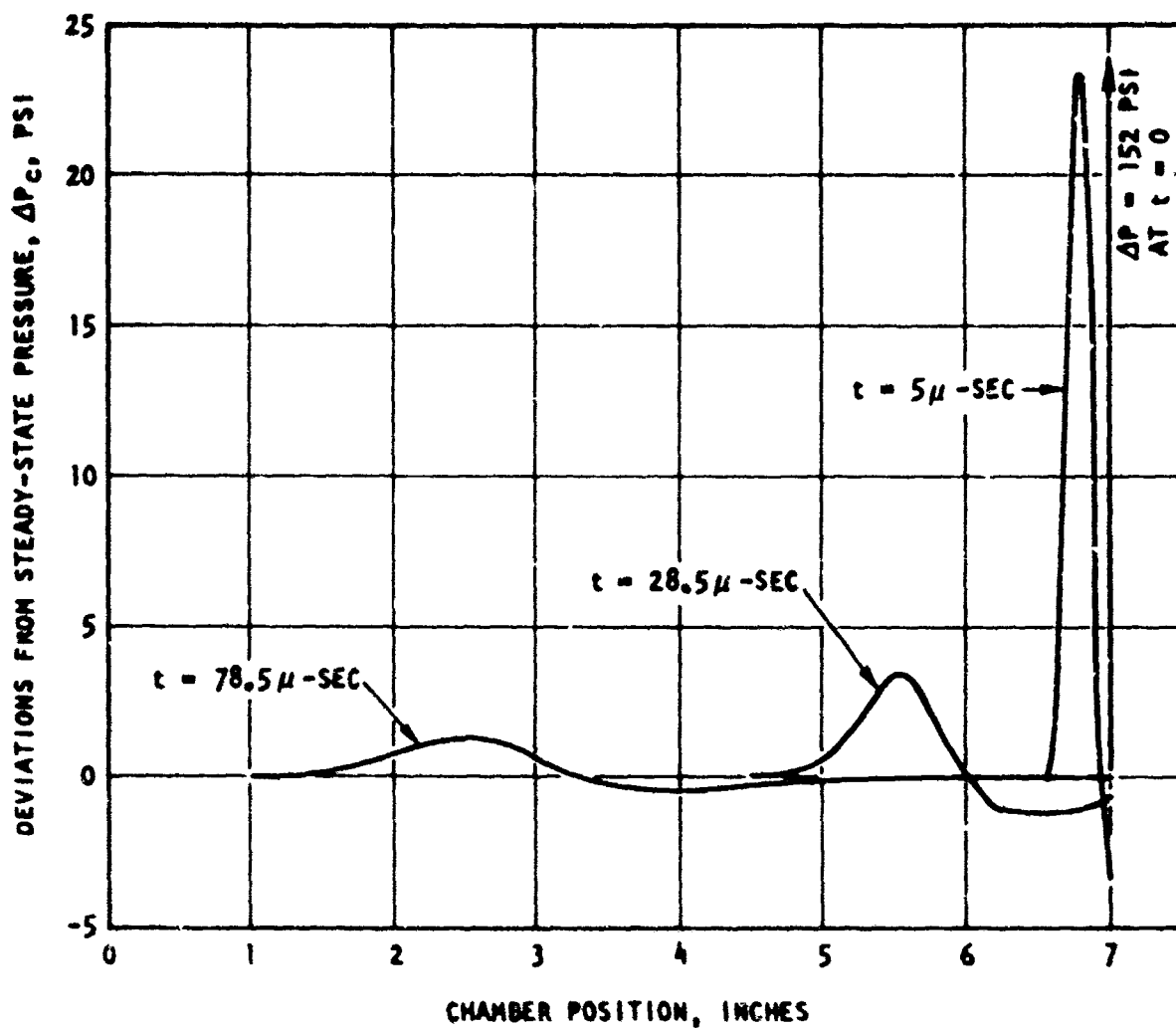
Figure 48. Instantaneous Deviations from Steady-State
Pressure During Transient Decay of a
Nozzle Closure Pulse
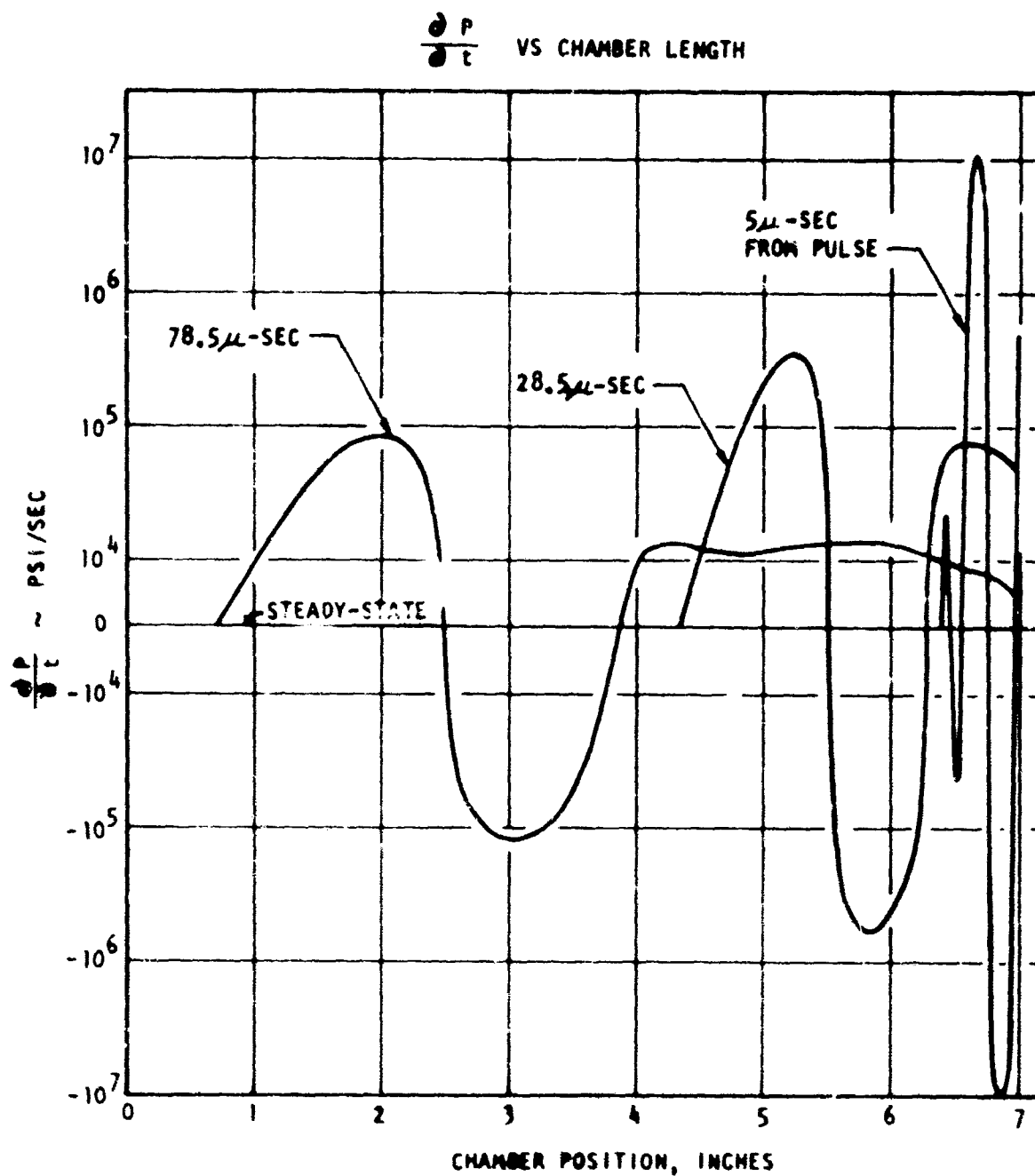
Figure 49. Instantaneous Deviations of Chamber Pressure with Respect to Time During Transient Decay of a Nozzle-Closure Pulse

term expressions. For further numerical stability considerations in the presence of complex coupling terms, refer to Appendix IV.

GENERAL NOMENCLATURE

Other Specific Nomenclature Defined in Text

A = area, parameter in Schuman diffusion model

B = parameter in Schuman diffusion model

C_D = drag coefficient

c = mixture ratio

c_p = specific heat at constant pressure

D = droplet diameter

$\mathcal{D}$ = molecular diffusivity

$\vec{F}$ = drag force vector

F = component of drag force

g_c = gravitational coefficient

H = enthalpy

ΔH_V = heat of vaporization (effective)

k = thermal conductivity

M = molecular weight

m = droplet mass

$\dot{m}$ = rate of change of mass

N = droplet concentration (no/volume), molar diffusion flux

$\dot{N}$ = number flowrate of droplets

Nu = Nusselt number

p = pressure

Q = spray heating rate

$\vec{q}$ = heat flux vector

R_e = Reynolds number

$\mathcal{R}$ = universal gas constant

r = volumetric gas phase reaction rate, drop radius

T	=	temperature
t	=	time
$\vec{U}^i$	=	i^{th} species diffusion velocity
$\vec{u}$	=	flow velocity vector
u	=	component of flow velocity
x, y, z	=	rectangular coordinates; x also equals mole fraction
z_o	=	axial plane separating injection/atomization and rapid combustion zones
γ	=	ratio of specific heats
ρ	=	density
$\underline{\underline{\tau}}$	=	stress tensor
$\Omega_{i,j}$	=	proportional mass fraction of species i generated per unit weight of propellant j burned
ω_i	=	mass fraction of ith species in a gas mixture
σ	=	surface tension

Superscripts

n	=	concerned with the nth initial droplet size group

Subscripts

BU	=	breakup or disintegration of droplets
d	=	droplet
i	=	concerned with i^{th} chemical species
j	=	concerned with j^{th} propellant
ℓ	=	liquid
cg	=	combustion gas
f	=	film
h	=	heat
m	=	mixture of gases, mass
v	=	drop vapor

Vector Operators

grad ( ) = ∇( ) = gradient of a scalor quantity

div ($\rightarrow$) = $\nabla\cdot$($\rightarrow$) = divergence of a vector quantity

$\vec{u})\vec{u}$ = dyadic product

REFERENCES

1. Lewis, J. D.: "Studies of Atomization and Injection Processes in the Liquid Propellant Rocket Engine," Combustion and Propulsion, Fifth AGARD Colloquim: High Temperature Phenomena, MacMillan Co., New York, 141-169 (1963).

2. Lawhead, R. B.: "Photographic Studies of Combustion Processes in Liquid Propellant Rockets, Eighth Symposium (International) on Combustion, Williams and Wilkins, Baltimore, 1140-1150 (1962).

3. Elverum, G. W., Jr. and Staudhammer, P.: "The Effect of Rapid Liquid-Phase Reaction on Injector Design and Combustion in Rocket Motors," Progress Report 30-4, Jet Propulsion Laboratory, Pasadena, California (August 1959).

4. Bittker, D. A. and Brokaw, R. S.: Journal of the American Rocket Society, Vol. 30, No. 2, 179-185 (1960).

5. Mitchell, R. C.: "The Effect of Nozzle Combustion on Engine Performance," R-7103, Rocketdyne, a Division of North American Rockwell Corporation, Canoga Park, California (January 1968).

6. Sutton, R. D.: "Gas Phase Mixing Under F-1 Combustion Conditions, "Research Memo 1278, Rocketdyne, a Division of North American Rockwell, Canoga Park, California, 21 December 1966.

7. Fenwick, J. R. and Bugler, G. J.: "Oscillatory Flame Front Flowrate Amplification Through Propellant Injection Ballistics (The Klystron Effect)," 3rd ICRPG Combustion Conference, CPIA Publ. No. 138, Vol. 1 (February 1967).

8. Harrje, D. T. and Reardon, F. H., editors: ICRPG Reference Book on Combustion Instability in Liquid Rockets, Princeton University (to be published, 1971).

9. Probert, R. P.: Phil Magazine, Vol. 37, 94 (1946).

10. Tanasawa, Y.: Tech Report, Tohuher University, Vol. 18, 195 (1954).

11. Tanasawa, Y. and Teisma, T.: Bulletin JSME, Vol. 1, 36 (1958).

12. Williams, F. A.: Phys. Fluids, Vol. 1, 541 (1958).

13. Williams, F. A.: Eighth Symposium (Int.) on Combustion, Williams and Wilkins Co., Baltimore, 50-69 (1962).

14. Williams, F. A.: Combustion Theory, Addison Wesley, Chapter 11 (1965).

15. Miesse, C. C.: _Industrial and Engineering Chemistry_, Vol. 50, No. 9, 1303-4 (1958).

16. Adler, J.: "A One-Dimensional Theory of Liquid Fuel Rocket Combustion, Part II, The Influence of Chemical Reaction," _ARC Tech Report No. 20-189_, Current Paper No. 446 (1959).

17. Mayer, E.: _Journal of the American Rocket Society_, Vol. 29, No. 7, pp 505, (1959).

18. Spalding, D. B.: _Aero Quart._, Vol. 10, No. 1 (1959).

19. Godsave, G. A. E.: _Fourth Symposium (International) on Combustion_, Baltimore, Maryland, Williams and Wilkens, Co., 818-830 (1953).

20. Spalding, D. B.: "A One-Dimensional Theory of Liquid Fuel Rocket Combustion," A.R.C. Tech Report No. 20-175 Current Paper No. 445 (1959).

21. Priem, R. J. and Heidmann, M. F.: "Propellant Vaporization as a Design Criteria for Rocket Engine Combustion Chambers," NASA TR R-67 (1960).

22. El Wakil, M. M.: "Experimental and Calculated Temperature and Mass Histories of Vaporizing Fuel Droplets," NACA TN 3480 (January 1956).

23. Kors, D. L., Bassham, L. B. and Walker, R. E.: "A Liquid Rocket Performance Model Based on Vaporization Interactions," AIAA Paper No. 69-470 (June 1969).

24. Burstein, S. F., Hammer, S. S. and Agosta, V. D.: "A Spray Combustion Model With Droplet Breakup, Analytical and Experimental Results," _Progress in Astronautics and Rocketry_, Vol. 6, Academic Press, New York (1962).

25. Lambiris, S., Combs, L. P., and Levine, R. S.: "Stable Combustion Processes in Liquid Propellant Rocket Engines," _Combustion and Propulsion, Fifth AGARD Colloquium on High Temperature Phenomena_, McMillan Co., Baltimore (1962).

26. Rabin, E. A., Schallenmuller, A. R. and Lawhead, R. B.: "Displacement and Shattering of Propellant Droplets," Final Summary Report, AFOSR-TR-60-75, Rocketdyne, a Division of North American Rockwell Corporation, Canoga Park, California (March 1960).

27. Breen, B. P., Zung, L. B., Lawver, B. R., Kosvic, T. C. and Coates, D. E.: "Injection and Combustion of Hypergolic Propellants," AFRPL-TR-69-48, Dynamic Science, Monrovia, California (April 1969).

28. Campbell, D. T. and Chadwick, W. D.: "Combustion Instability Analysis at High Chamber Pressures," AFRPL-TR-67-222, Rocketdyne, a Division of North American Rockwell Corporation, Canoga Park, California (August 1967).

29. Sutton, R. D., and Combs, L. P.: "Research on Pressure Wave Growth in a Homogeneous Spray/Gas Mixture," AFOSR Contract AF49(632)-1705, 1966-1970. Final report to be published October 1970.

30. "ICRPG One-Dimensional Equilibrium Reference Program-Preliminary Description of ODE, a Computer Program for the Calculation of Chemical Equilibrium Compositions With Applications," ICRPG Performance Standardization Working Group (July 1968).

31. Hammer, S. S., Agosta, V. D., and Peschke, W. T.: "Combustion Instability in Liquid Propellant Rocket Engines: Bipropellant Spray Combustion," AFOSR 66-0858, Polytechnic Institute of Brooklyn (PIBAL) Report No. 891 (Jan 1966)

32. Dickerson, R., Tate, K., and Barsic, N.: "Correlation of Spray Injector Parameters With Rocket Engine Performance," AFRPL-TR-68-147, Rocketdyne, a Division of North American Rockwell, Canoga Park, California (June 1968).

33. Combs, L. P. and Schuman, M. D.: "Steady-State Rocket Combustion of Gaseous Hydrogen and Liquid Oxygen, Part II: Analysis for Coaxial Injection,: RR64-29, Rocketdyne, a Division of North American Rockwell, Canoga Park, California (March 1965).

34. Sutton, R. D. and Schuman, M. D.: "Liquid Rocket Combustion Analysis for Coaxial Jet Injection of Gas/Liquid Propellants," 7th JANNAF Combustion Conference, Oct, 1970. Proceedings to be published, CPIA Publication in 1971.

35. Wrubel, J. R.: "Some Effects of Gas Stratification on Choked Nozzle Flows," AIAA Paper 64-266 (1964).

36. Pieper, J. L., Dean, L. E., and Valentine, R. S.: "Mixture Ratio Distribution -- Its Impact on Rocket Thrust Chamber Performance," J. Spacecraft Rockets, Vol. 4, No. 6, pg 786-789 (June 1967).

37. Sutton, R. D., Hines, W. S., and Combs, L. P.: "Comprehensive Analysis of Liquid Rocket Combustion," AIAA Paper No. 70-622 (June 1970). Also see Hines, W. S., et al, "Development of Injector Chamber Compatibility Analysis," AFRPL-TR-70-12, Rocketdyne (March 1970).

38. "Dynamic Properties of a Pair of Impinging Streams and the Uniformity of Mixture Ratio Distribution in the Resulting Spray," Progress Report No. 20-209, Jet Propulsion Laboratory, Pasadena, California (28 March 1956).

39. Falk, A. Y., Clapp, S. D., and Nagai, C. K.: "Space Storable Propellant Study - Final Report," R-7677, NASA Contract NAS11199, Rocketdyne, a Division of North American Rockwell, Canoga Park, California (1968). See also current Monthly Reports of Follow-On Contract.

40. "Chamber Technology for Space Storable Propellants," Fourth Interim Report, for Period 29 June 1967 - 26 August 1969, R-7985, Rocketdyne, a Division of North American Rockwell Corporation, Canoga Park, California (September 1969).

41. Combs, L. P., Chadwick, W. D., and Campbell, D. T.: "Liquid Rocket Performance Computer Program With Distributed Energy Release," R-8298, Rocketdyne, a Division of North American Rockwell Corporation, Canoga Park, California (September 1970).

42. Pieper, J. L., "ICRPG Liquid Propellant Thrust Chamber Performance Manual," CPIA Publ. No. 178, Chemical Propulsion Information Agency, Silver Spring, Md. (September 1968).

43. Crocco, L. and Cheng, S. I.: Theory of Combustion Instability in Liquid Propellant Rocket Motors, AGARD Monograph No. 8, Butterworth Pub., Ltd. London, 1956.

44. Summerfield, M.,:Journal of American Rocket Society, 21, 108-114 (1951).

45. Tsien, H. S.,:Journal of American Rocket Society, 22, 256-262, 268 (1952).

46. Crocco, L.: Journal of American Rocket Society, 21, 163 (1951) and 22 7 (1952).

47. Scala, S. M.: "Transverse Wave and Entropy Wave Combustion Instability in Liquid Propellant Rockets," Princeton University, Aeronautical Engrg. Report H380 (April 1957).

48. Reardon, F. H.: "An Investigation of Transverse Mode Combustion Instability in Liquid Propellant Rocket Motors," Princeton University, Aero Engrg. Report 550 (June 1961).

49. Crocco, L. and Sirignano, W. A.: "Behavior of Supercritical Nozzles Under Three-Dimensional Oscillatory Conditions," AGARD-ograph 117, North Atlantic Treaty Organization, Paris, 1967.

50. Sirignano, W. A.: "Theoretical Study of Nonlinear Combustion Instability Longitudinal Mode," Tech. Report H677, Dept. of Aerospace and Mech. Sciences, Princeton University (March, 1964).

51. Zinn, B. T.: "A Theoretical Study of Nonlinear Transverse Combustion Instability in Liquid Propellant Rocket Motors," Princeton University, Dept. of Aerospace and Mech. Sciences, Tech. Report #732 (May, 1966).

52. Mitchell, C. E.: Axial Mode Shockwave Combustion Instability in Liquid Propellant Rocket Engines, NASA CR72259, Tech. Report, Dept. of Aerospace and Mech. Sciences, Princeton University (July, 1967).

53. Zinn, B. T. and Powell, E. A.: "Application of the Galerkin Method in the Solution of Combustion-Instability Problems," Paper No. P69, 19th Congress of the International Astronautical Federation, New York, 1968.

54. "An Experimental Investigation of Combustion Stability Characteristics at High Chamber Pressure," Final Report, Vol. I, 11741/SA6-F, Aerojet-General Corp., Sacramento, Calif. (August, 1966).

55. Smith, A. J., Jr. and Reardon, F. H.: "The Sensitive Time Lag Theory and Its Application to Liquid Rocket Combustion Instability Problems," in two volumes, AFRPL-TR-67-314 and 317, Aerojet General Corp., Sacramento, Calif. (1967).

56. Culick, F. E. C.: "Stability of High Frequency Pressure Oscillations in Gas and Liquid Rocket Combustion Chambers," M.I.T. Aerophysics Lab Report 480 (June 1961).

57. Torda, T. P., and Burstein, S. Z.: "Nonlinear Theory of Combustion Instability - Liquid Propellant Rocket Motor," AFOSR Doc No. TR.59-60, Polytechnic Institute of Brooklyn (Dec 1, 1958).

58. Torda, T. P. and Schmidt, L. A.: "One-Dimensional Unsteady Aerothermo-chemical Analysis of Combustion Instability in Liquid Rocket Engines," Pyrodynamics, 1, 89-111 (1964).

59. Burstein, S. Z. and Agosta, V. D.: "Combustion Instability Non-Linear Analysis of Wave Propagation in a Liquid Propellant Rocket Motors," AFOSR 2614, Polytechnic Institute of Brooklyn (March 1962).

60. Summerfield, M. and Krier, H.: "Errors in Nonsteady Combustion Theory in the Past Decade (A Review)," AIAA Paper 69-178 (January 1969).

61. Priem, R. J. and Guentert, D. C.: "Combustion Instability Limits Determined by a Nonlinear Theory and a One-Dimensional Model," NASA TND-1409 (October 1962).

62. Coultas, T. A. and Kesselring, R. C.: "Extension of the Priem Theory and Its Use in Simulation of Instability on the Computer," 2nd ICRPG Combustion Conference, CPIA Publ. No. 105 (May 1966).

63. Hoffman, R. J., Beltran, M. R., Breen, B. P. and Wright, R. D.: "Extension of the Priem-Guentert Annular Combustion Instability Model to a Bipropel-lant System," 3rd ICRPG Combustion Conference, CPIA Publ. No. 138 (Feb 1967).

64. Burstein, S. Z. and Schechter, H.: "A Two-Dimensional Time-Dependent Annular Combustion Model," 6th ICRPG Combustion Conference, CPIA Publ. No. 192 (December 1969).

65. Agosta, V. D.: "Nonlinear Combustion Instability: Longitudinal Mode," 6th ICRPG Combustion Conference, CPIA Publ. No. 192 (December 1969).

66. Migdal, D. and Agosta, V. D.: "A Source Flow Model for Continuum Gas-Particle Flow," Trans. of the ASME, Paper No. 67-APM-Y, 1967.

67. Seamans, T. F., Vampie, M. and Agosta, V. D.: "A Fundamental Model of Hypergolic Ignition in Space Ambient Engines," AIAA Journal, 5, p 1216 (September 1967).

68. Nicholls, J. A., et al: "Detonation in Two-Phase Media and Drop Shattering Studies," NASA CR-72421, University of Michigan, Ann Arbor, Mich (May 1968).

69. Strahle, W. C.: 11th Symposium (International) on Combustion, The Combustion Institute, Pittsburgh, Penna, 747-754 (1965).

70. Manrique, J. A.: "Theory of Droplet Vaporization in the Region of the Thermodynamic Critical Point," NASA CR-72558, Department of Mechanical Engineering, University of Wisconsin, Madison, Wicsonsin (June 1969).

71. Ledwell, T. A.: "The Burning of Hydrocarbon Fuel Droplets at High Pressures," Ph.D. Thesis, Department of Mechanical Engineering, University of Waterloo, Waterloo, Ontario (1968).

72. Ledwell, T. A. and Brzustowski, T. A.: "A Simple Quasisteady Model of the Combustion of a Fuel Droplet with Convection, Including the Effect of Pressure," AIAA Paper No. 69-147, AIAA 7th Aerospace Sciences Meeting, New York, New York (Jan 1969).

73. Ranz, W. E., and Marshall, W. R., Jr.: Chem. Eng. Progress, 48, 141-146, and 173-180 (1952).

74. Savery, C. W.: "Experimental Studies of the Vaporization of Droplets In Heated Air at High Pressures," NASA CR-72574, Department of Mechanical Engineering, University of Wisconsin, Madison, Wisconsin (August 1969).

75. Penner, S. S.: Chemistry Problems in Jet Propulsion, Pergamon Press, New York (1960).

76. Spalding, D. B.: "Combustion of Liquid Fuels," Fourth Symposium (International) on Combustion, William and Wilkins, Baltimore, 1953.

77. Dickerson, R. A.: "Comprehensive Single Droplet Combustion Model," EE-70-12-7, Rocketdyne Internal Memo, Rocketdyne, a Division of North American Rockwells Corp., Canoga Park, Calif. (March 1970).

78. Parks, J. M., et al,: "Temperature Distribution Within a Particle During Evaporation," AIAA Journal, Vol. 4, No. 6, pg 1032-1035, 1966.

79. Sotter, J. G.: "Non-Steady Evaporation of Liquid Propellant Drops: The Grossman Model," Tech. Report 32-1061, Jet Prop. Laboratory, Pasadena, Calif. (Jan 1968).

80. El Wakil, M. M., Uyehara, O. A. and Myers, P. S.:"A Theoretical Investigation of the Heating-up Period of Injected Fuel Droplets Vaporizing in Air," NACA TN-3179 (1954).

81. Fendell, F. E.: "Flame Structure in Initially Unmixed Reactants Under One-Step Kinetics," Chem. Eng. Sci., 22, 1829 (1967).

82. Fendell, F. E., Coats, D. C. and Smith, E. B.: "Compressible Slow Viscous Flow Past a Vaporizing Droplet," AIAA J. 6, 1953 (1968).

83. Spalding, D. B.: Some Fundamentals of Combustion, Gas Turbine Series C, Academic Press Inc., New York (1955).

83a. Agoston, G. A., Wise, H. and Rosser, W.: "Dynamic Factors Affecting the Combustion of Liquid Spheres," Sixth Symposium (International) on Combustion (Reinhold, New York, 1957) pp. 708-717.

84. Schlichting, H.: _Boundary Layer Theory_, Chapter 5, 6th Edition, McGraw-Hill Book Co., New York (1968).

85. Rosenhead, L., Editor: _Laminar Boundary Layers_, Oxford Univ. Press, London (1963).

86. Soo, S. L.: _Fluid Dynamics of Multi-phase Systems_, Blaisdell Publishing Co., Waltham, Mass. (1967).

87. Happel, J. and Brenner, H.: _Low Reynolds Number Hydrodynamics (with Special Applications to Particulate Media)_, Prentice-Hall, Inc., Englewood Cliffs, N. J. (1965).

88. Rowe, P. N.: "Drag Forces in a Hydraulic Model of a Fluidized Bed - Part II," _Trans. Instn. Chem. Engrs._, Vol. 39, 175-180 (1961).

89. Rudinger, G.: "Effective Drag Coefficients for Gas-Particle Flow in Shock Tubes," Proj. Squid Tech. Rpt. No. CAL-97-PU, Cornell Aeronautical Laboratory, Inc., Buffalo, N. Y. (February 1969).

90. Carlson, D. J. and Hoglund, R. F.: "Particle Drag and Heat Transfer in Rocket Nozzles," _AIAA Journal_, Vol. 2, 1980-1984 (1964).

91. Crowe, C. T.: "Drag Coefficients of Particles in a Rocket Nozzle," _AIAA Journal_, Vol. 5, 1021-2 (1967).

92. Ingebo, R. D.: "Drag Coefficients for Droplets and Solid Spheres in Clouds Accelerating in Airstreams," NACA TN3762 (September 1956).

93. Crowe, C. T., Nicholls, J. A. and Morrison, R. B.: "Drag Coefficients of Inert and Burning Particles Accelerating in Gas Streams," _Ninth Symposium (International) on Combustion_, (1963).

94. Rabin, E., Schallenmuller, A. R., and Lawhead, R. B.: "Displacement and Shattering of Propellant Droplets," AFOSR TR60-75, Rocketdyne, a Division of North American Aviation, Inc., Canoga Park, Calif. (1960).

95. Clamen, A. and Gauvin, W. H.: "Effects of Turbulence on the Drag Coefficients of Spheres in a Supercritical Flow Regime," _AIChE J._, Vol. 15, No. 2, 184-189 (1969).

96. Dabora, E. K., Ragland, K. W., Ranger, A. A. and Nicholls, J. A., "Two-Phase Detonations and Drop Shattering Studies," Rept. No. 06324-2-T, Aircraft Propulsion Laboratory, University of Michigan, Ann Arbor, Michigan (April 1966).

97. Lane, W. R.: "Shatter of Drops in Streams of Air," _J. of Ind. and Eng. Chemistry_, Vol. 43, No. 6, 1312-1317 (June 1951).

98. Hanson, A. R., Domich, E. G. and Adams, H. S.: "An Experimental Investigation of Impact and Shock Wave Break-up of Liquid Drops," Res. Rept. 125, Rosemount Aero Lab, Minneapolis, Minn (January 1956). Hanson, A. R., Domich, E. G.: "The Effect of Liquid Viscosity on the Break-up of Droplets by Air Blasts - A Shock Tube Study," Eng. Res. Rept. 130, Univ. of Minnesota Institute of Technology (June 1956).

99. Hinze, J. O.: "Fundamentals of the Hydrodynamic Mechanism of Splitting in Dispersion Processes," *AIChE Journal*, Vol. 1, No. 3, 289-295 (September 1955).

100. Rabin, E., Schallenmuller, A. R. and Lawhead, R. B.: "Displacement and Shattering of Propellant Droplets," Final Summary Rept. AFOSR, TR 60-75, Rocketdyne, a Division of North American Aviation, Inc., Canoga Park, California (March 1960).

101. Wolfe, H. and Anderson, W.: "Aerodynamic Breakup of Liquid Drops," American Physical Society Paper SP70 (April 1965).

102. Engel, O. G.: "Fragmentation of Waterdrops in the Zone Behind an Air Shock," *J. of Res. Nat'l. Bur. Standards*, Vol. 60, No. 3 (March 1958).

103. Ranger, A. A. and Nicholls, J. A.: "Aerodynamic Shattering of Liquid Drops," *AIAA Journal*, Vol. 7, No. 2, 285-290 (February 1969).

104. Ranger, A. A. and Nicholls, J. A.: "Shape and Surrounding Flowfield of a Drop in a High-Speed Air Stream," *AIAA Journal*, Vol. 8, No. 9, 1720-1722 (September 1970).

105. Rayleigh, J. W. S.: "Instability of Jets," *Proc. London Math. Soc.*, 1878, Vol. 10, pp. 4-13.

106. Nicholls, J. A., et al,: "A Study of Two-Phase Detonation As It Relates To Rocket Motor Combustion Instability," NASA CR-272, University of Michigan, Ann Arbor, Mich. (August 1965).

107. Wiekemeyer, R. H.: "Breakdown of a Liquid Filament Into Drops Under the Action of Acoustic Disturbances," Report No. AS-67-6, College of Engineering, Univ. of California, Berkeley, Calif. (June 1967).

108. Rudinger, G.: *Wave Diagrams for Non-Steady Flow In Ducts*, Dr. Van Nostrand Company, Inc., New York, New York, 1955.

109. Wruker, R. F. and Mathews, R. B.: "Holography of Injection and Combustion Phenomena - A Progress Report," 6th ICRPG Combustion Conference, CPIA Publication, No. 192, Vol. 1 (December 1969).

110. Burstein, S. Z.: "Nonlinear Combustion Instability in Liquid-Propellant Rocket Engines: The Transverse Mode, 7. The Hydrodynamic Differential and Difference Equations and Computer Algorithm, NASA TR-32-1111 (September 15, 1967).

111. Richtmyer, R. D. and Morton, K. W.: *Difference Methods for Initial-Value Problems*, 2nd Edition, Interscience Publishers, New York, New York, 1967.

112. Skinner, G. B. and Ringrose, G. H.: "Ignition Delays of a Hydrogen-Oxygen-Argon Mixture at Relatively Low Temperatures," *J. Chem. Phys.*, 42, 6, 2190-2192 (1965).

113. Reid, R. C. and Sherwood, T. K.: *The Properties of Gases and Liquids*, 2nd Edition, McGraw and Hill, New York, New York (1966).

114. Schuman, M. D. and Sutton, R. D.: "Development of a Comprehensive Continuous Sub and Supercritical Pressure, Convective, Droplet Vaporization Model," Rocketdyne Combustion Stability Memo, Rocketdyne, a Division of N.A.R., Canoga Park, Calif. (In preparation.)

115. Chueh, P. L. and Prausnitz, J. M.: "Calculation of High Pressure Vapor-Liquid Equilibria," Industrial and Engineering Chemistry, Vol. 60, 1968, pp. 34-52.

APPENDIX I

FACILITIES

The experimental portion of the program was conducted at the Facilities of the Research Division, chiefly those located at the Propulsion Field Laboratory. Here, the Research Division maintains fully equipped laboratories and test stands for research in all phases of rocket propulsion. Included are facilities for research in combustion, heat transfer, fluid transport, ignition, and instrumentation. The laboratories are supported by extensive machine shop, data processing, photographic and other service units.

COMBUSTION AND HEAT TRANSFER LABORATORY

The experimental portion of the program was conducted at this laboratory, which consists of a number of high-instrumented test bays, grouped around a control and data-recording center. Two large, reinforced concrete test bays are used for motor firings and five smaller test bays are used fo. shock tube testing, heat transfer studies, bomb tests, and other hazardous operations. Two large, covered areas are used for conducting lower-hazard tests.

Facilities are available for model motor testing from 100 to 30,000-pounds thrust and chamber pressures up to 2000 psia. A number of shock tubes and specialized combustor devices are available as well. In support of these installations are supplies of high-pressure gaseous nitrogen, hydrogen, and helium and high-pressure liquid oxygen, nitrogen, and hydrogen. These facilities are extensively instrumented with high-response pressure measuring capabilities and high-speed photographic coverage. Both framing and streak

camera coverage are available with Fastax cameras to 14,000 frames per second, while an ultra-speed Beckman-Whitley framing camera, Model 189, takes 25 exposures on 35 mm film at a maximum rate of 1.2 million pictures per second.

In addition to this equipment, the laboratory contains a small shop for fabrication, instrumentation, and repair of test equipment. An instrumentation service center is connected to the laboratory for precision calibration of instruments and transducers.

Data Management

Rocketdyne has provisions for a variety of types of data gathering. For very long-term testing (i.e., on the order of hours or days), conventional multi-point and strip chart recorders are utilized for analog recording of temperatures, pressures, etc. They are capable of 1/10-percent full-scale accuracy, calibrated to within 1/4 percent of full scale with lines and transducers in place. Charts from these recorders are hand reduced to either finished data or raw numbers suitable for computer manipulations.

For short-term tests, on the order of minutes, a nonlinear digital data system is used. This instrument is capable of near-simultaneous recording of up to 200 measurements at 40 samples per second, It uses X-1 type digital voltmeters having 0.003 percent precision in the typical 100-millivolt range. Automatic range selection of d-c voltage is available for ranges up to 100 vdc. Another similar system has 40-channel capacity and two samples per second total sampling rate. Output of both of these digital systems is on printed paper tape. Again, these numbers may be hand or computer manipulated.

For even shorter duration testing, on the order of seconds, data are gathered by a Beckman 210 system. This analog-to-digital converter enables consideration of a multitude of analytical techniques requiring several accurately measured test parameters. The system is available by transmission cable to all test areas within the Research Division, and is capable of a sampling rate of 85-bits per second, and 50-channel capability with one part in 4000 precision for full-scale ranges of 20, 50, and 100 millivolts. An additional 15 channels are available for pressure transducers with 0-to 5-volt signal range. The digital output can be directly utilized by computers to obtain reduced parameters directly from the measured data. This type of data acquisition system will be utilized on the program. Steady-state rocket operational data then can be reduced quickly to final data.

For higher-frequency combustion instability data, a variety of tape recorders are available to record the output from high-frequency pressure transducers such as the Kisler or Photocon. In particular, the Ampex FR1400 presently in use at Rocketdyne is a seven-channel, direct-recording machine. This tape recorder has a frequency response from 400 Hz to 1.5 megaHz at 120 in./sec tape speed. Data can be reduced by playing the type back into a Tektronix No. 551 dual-beam oscilloscope and photographing the trace on the CRT, or it may be played at 30 in./sec into one of several Ampex FR100 machines. The Ampex FR100 machines and a Hewlett-Packard Model 3955E machine can also be used to record the original data with frequency response up to 20 kiloHz. Further data analysis may be accomplished by use of existing sonic analyzers or power spectral density apparatus. **Misseleizers** and a **Diane** system for digitization of high-frequency data for subsequent analysis may be used in either a spectral analysis or frequency response program.

APPENDIX II

SUMMARY OF TECHNIQUES FOR PHOTOGRAPHING DROPLETS
WITH A FASTAX CAMERA AND STROBE FLASH

The object of this appendix is to present a concise summary of formulas which
will aid those using the Fastax-Strobe technique of droplet photography. Most
of the information contained was generated while working on projects to photo-
graph droplets in a monodisperse spray engine under cold and hot firing of
H_2/LOX, and in a 2-D engine firing NTO/50-50 propellants. In this technique
the droplets are photographed in silhouette by using a prismless Fastax camera
and backlighting the droplets with a sychronized strobe flash lamp. The photo-
graphic data can yield information on droplet size, velocity, and time-dependent
behavior.

The droplet diameter, d, can be measured from the film image diameter, d',
according to the expression

$$d = \frac{d'}{m}$$

m, the optical magnification is determined by calibrating the camera magnifi-
cation using a test target of known size.

Velocity, v, can be determined by measuring y', the frame-to-frame image dis-
placement of a given droplet, and then inserting it in the expression

$$v = \frac{S \, y'}{m}$$

where S is the camera framing rate. Time dependent behavior is observed from frame-to-frame views of a given droplet.

Table I is a number of additional equations which effectively aid droplet photography projects.

A descriptive title, term definitions, and in some cases additional information accompanies each formula.

Table II is a summary of all term definitions in alphabetical order.

APPLICATION OF EQUATIONS

All the given equations can be solved with simple arithmetic using relatively few parameters. These parameters are droplet velocity, v, and diameter, d; magnification, m; lens f/no., Γ ; the ratio of tolerable blur spot diameter or length to droplet diameter, k; and flash lamp pulse width, γ .

The values of v, d, are fixed by the droplet spray under study.

Table A below gives γ and the relative light output for the EG&G strobe system

γ (microseconds)	Relative Energy per Flash
1.2	1
1.6	2
2.1	4

Table A

m is set as small as is consistent with m_{min} given by Eq. IX. This will pro-
duce a droplet with somewhat blurred edges. If a sharp edge is desired, in-
crease m by two or three times. Γ is made as large as possible and is generally
limited by the flash lamp illumination level required for good film exposure.
k is a measure of the image sharpness and is made as large as possible consis-
tent with the resolution desired. Ideally, k, for a given droplet study pro-
ject should be determined experimentally. However, for a working rule of
thumb one may use the following criteria for k: If a sharp edged droplet is
required, set k from 0.1 to 0.2. If a blurred droplet image is tolerable,
let k = 0.5 to 1.0 or even greater. A generally satisfactory value should range
from 0.2 to 0.5 for most cases.

Other considerations which are outside the scope of this appendix, but which
nevertheless can be important in obtaining satisfactory photographic records
are 1) quality of lenses and windows, 2) illumination optics, and 3) filters
to block flame light.

TABLE I

SUMMARY OF PHOTO-OPTICAL FORMULAS FOR FASTAX-

STROBE PHOTOGRAPHY

I   Dept of Field,   Z

$$\Delta z = 2k \Gamma d \frac{m+1}{m}$$

where $K = \frac{c}{d}$

   c = tolerable blur circle diameter

   Γ = f/no

   d = minimum droplet diameter

   m = magnification = $\frac{d'}{d}$

   d' = image diameter on film

Note: if $k = 0.1$, worst-focus droplet appears with fairly sharp
         edge

      if $k = 1.0$, worst-focus droplet appears with highly bluured

            edges.

II   Film-to-object distance, L

$$L = \frac{f (m + 1)^2}{m}$$

III Velocity of moving droplet image, V'

$v' = vm$

where v = droplet velocity

IV   Minimum and Maximum Tolerable

Film Speeds, S_{min} and S_{max}

A. Film moving parallel to droplet direction, S(P)

$$S(P)_{min} = m \left(v - \frac{dk}{y}\right); \quad S(P)_{max} = m\left(v + \frac{dk}{y}\right)$$

TABLE I (cont.)

IV   B. Film moving transverse to droplet direction, S(T)

$$S(T)_{min} = 0 \qquad S_{max}(T) = \frac{md\ k_1}{\gamma}$$

where γ = flash lamp pulse width

$$k_1 = \frac{1}{d} \quad \text{where } 1 = \text{tolerable blur length}$$

V   Number of Frames per Droplet, N

A. Film moving parallel to droplet direction, N(P)

$$N(P) = \frac{S}{mv}$$

B. Film moving transverse to droplet direction, N_T

$$N(T) = \frac{1.33S}{mv}$$

        S = film velocity in feet per second

        v = droplet velocity in feet per second

VI   Maximum tolerable number of frames per droplet, N_{max}

A. Film moving parallel to droplet direction, $N(P)_{Max}$

$$N_{Max.}(P) = 1 + \frac{k_1 d}{v}$$

B. Film moving transverse to droplet direction, $N_{Max}(T)$

Note: If $N_{Max}(P)$ is less than 4 frames/second, then $N_{Max}(P)$

       is greater than $N_{Max.}(T)$

VII   Maximum tolerable Droplet Velocity to Record Same Drop on Two Frames

V_{max}

A. Film moving parallel to droplet direction, $V_{max}(P)$

$$V_{max}(P) = \frac{k_1 d}{\gamma}$$

B. Film moving transverse to droplet direction, $V_{Max}(T)$

$$V_{max}(T) = (\ \ \ \ \ )$$

TABLE I (cont.)

VIII   Linear filed of view in object space

$P = \dfrac{0.3}{m}$ inches; $T = \dfrac{0.4}{m}$ inches

where

P = field of view parallel to film length

T = field of view transverse to film length

IX   Minimum Magnification Required to Resolve a Droplet on 5498RAR Film, m_{Min}

$$m_{Min} \approx \frac{75}{d}$$

X   Curvature of Field, $\triangle S$, in Object Space, Resulting from Film Curvature

$$\triangle S - 0.011 \left(\frac{2X}{P}\right)^2 \quad \frac{1}{m} \text{ inches}$$

where $\triangle S$ = deviation of the best focus surface in object space from a plane surface

     X = fraction of distance from center to edge of field in direction of film length

Displacement From Plane in Object Space $\triangle S$ (inches)

m = 0.1

m = 0.5

$\dfrac{2X}{P}$

Normalized Distance from Center of Field in Object Space Along Film Length
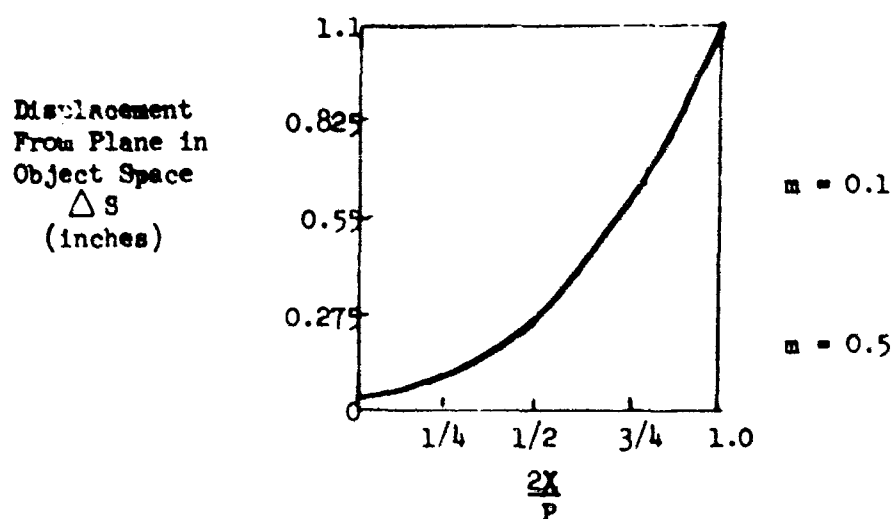
Curvature of Best-Focus Object Space Surface

TABLE I (cont.)

XI Thin Lens Formulas

A. $\dfrac{1}{t} + \dfrac{1}{t'} = \dfrac{1}{f}$ or $t' = \dfrac{t\,f}{t-f}$

where t = distance between lens and object

t' = distance between lens and image
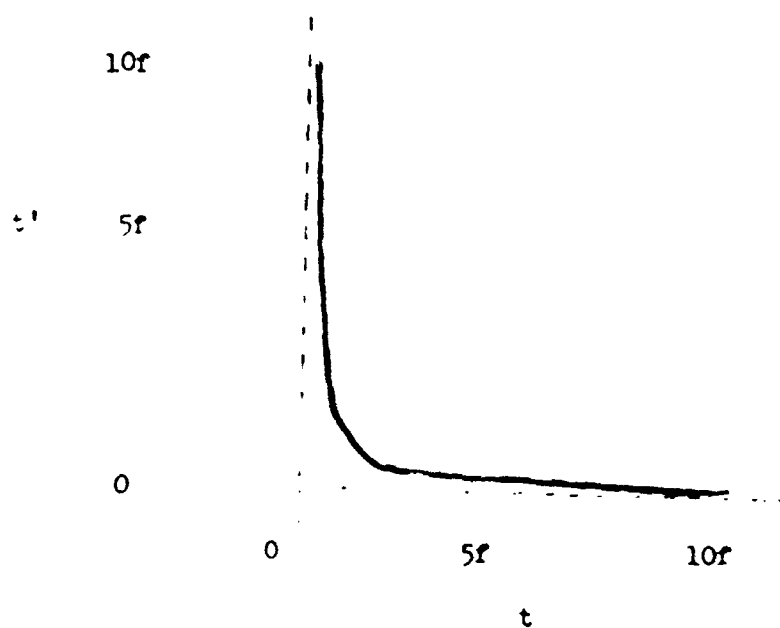
Figure 2. Graph of $\dfrac{1}{t} + \dfrac{1}{t'} = \dfrac{1}{f}$

B. $t = f\ \dfrac{m+1}{m}$

C. $t' = f\,(m + 1)$

D. $m = \dfrac{t'}{t}$

TABLE II

DEFINITIONS OF SYMBOLS USED

c = tolerable blur circle diameter

d = droplet diameter

d' = diameter of droplet image

f = focal length of camera lens

k = $\frac{c}{d}$ = ratio of tolerable blurspot diameter to droplet diameter

k_1 = $1/d$ = ratio of tolerable blurspot length to droplet diameter

L = distance between film and object

l = maximum tolerable blur length

m = magnification

m_{Min} = Minimum magnification to resolve a droplet on 5498 RAR film

N = Number of frames per droplet

N_{Max} = maximum tolerable number of frames per droplet

P = linear field of view in object space parallel to film length

S = film speed

S_{Min}, S_{Max} = minimum and maximum tolerable film speeds

$\triangle s$ = deviation of best-focus object surface from a plane surface resulting
from film curvature

t = distance between lens and object

t' = distance between lens and image

T = linear field of view in object space transverse to film length

v = velocity of droplet

v_{Max} = maximum velocity of droplet for 2-frame imaging

v' = velocity of drop image

R-8377

TABLE II (cont.)

y' = displacement of droplet image between film frames

Δz = depth of field

Γ = f/no. of lens

γ = width of flash lamp pulse

322

NUMERICAL ANALYSIS OF THE STEADY-STATE FORMULATION

This appendix describes the procedure currently being used to solve the system of equations which describe one-dimensional steady-state combustion inside rocket engines. The equations are identical to those presented in the Analytical Program Section of this report and will not be repeated here. The only exception is that the viscous stress term τ_{xx} was dropped from the gas phase momentum and energy equations. It was found to be of negligible influence.

METHOD OF SOLUTION

Finite difference methods are used to solve the differential equations. In particular, the trapezoidal integration formula is used. That is,

$$y_1 = y_{1-1} + \frac{\Delta X}{2}(y_1' + y_{1-1}')$$

where i refers to the X position.

For example, the droplet mass continuity equation becomes

$$m_{j\,i}^{n} = m_{j\,i-1}^{n} - \frac{\Delta X}{2}\left(+\frac{\dot{m}_{j\,i}^{n}}{u_{j\,i}^{n}} + \frac{\dot{m}_{j\,i-1}^{n}}{u_{j\,i-1}^{n}}\right)$$

The system of equations produced is solved iteratively for the unknown at the new space level. In each equation, only one of the dependent variables

$$u_{j\,i}^{n}\,,\; N_{j\,i}^{n},\; m_{j\,i}^{n},\; T_{j\,i}^{n},\; C_i,\; e_i,\; u_i,\; P_i,\; \rho_i,\; T_i,\; H_i$$

is assumed unknown. All the others are set equal to the best current value, either an old level value or a predicted value. The following table lists the correspondence made between variables and equations.

TABLE I

N_j^n concentration number continuity

m_j^n drop continuity or experimental data and relationship between

         m_j^n and D_j^n

u_j^n drop momentum or experimental data

T_j^n drop energy

C mixture ratio

u gas continuity

P gas momentum

H gas energy

q gas heat transfer

ρ equation of state

$\left.\begin{array}{l} T \\ M \\ \mu \\ k \\ c_p \end{array}\right\}$ Tables

$\left.\begin{array}{l} Q_j^n \\ F_j^n \\ \dot{m}_j^n \end{array}\right\}$ Subroutines or experimental data replacing F_j^n and $\dot{m}_j^n$

$\left.\begin{array}{l} \text{film} \\ \text{and} \\ \text{drop} \\ \text{properties} \end{array}\right\}$ Tables

                          R-8377

One clarification required is the procedure employed to calculate the integrals in the gas phase equations. The parabolic rule is used where possible; otherwise the trapezoidal rule is used. There was found to be no discernable difference in the computed results.

The parabolic rule takes the form

$$\int_0^{x_i} P_i \frac{dA}{dx} dx = \int_0^{x_{i-1}} P \frac{dA}{dx} dx + \int_{x_{i-1}}^{x_i} P \frac{dA}{dx} dx$$

$$= \int_0^{x_{i-1}} P \frac{dA}{dx} dx + \left[-\frac{1}{12} P_{i-2}(A_{i-1} - A_{i-2}) + \frac{2}{3} P_{i-1}(A_i - A_{i-1}) + \frac{5}{12} P_i(A_i - A_{i-1}) \right]$$

This is used for corrector cycles and only then if $A_{i-1} \neq A_{i-2}$ and $i \geq 3$. Otherwise, the trapezoidal rule is used. This takes the form:

$$\int_0^{x_i} P_i \frac{dA}{dx} dx = \int_0^{x_{i-1}} P \frac{dA}{dx} dx + \int_{x_{i-1}}^{x_i} P \frac{dA}{dx} dx = \int_0^{x_{i-1}} P \frac{dA}{dx} dx$$

$$+ \left[P_{i-1}(A_i - A_{i-1}) + P_i(A_i - A_{i-1}) \right] / 2$$

The integrals are broken into two parts to avoid recomputing known results. Furthermore, the P_i appearing in the expressions are treated as unknowns and solved for explicitly.

The same method is currently being employed to compute $\int_0^{x_i} q \frac{dA}{dx} dx$

Program Flowcharts

The following section presents flowcharts of the basic iterative procedures used for computation of the steady-state formulation. Two flowcharts are presented, the first represents the procedure used when the model employs a prior specification of the coupling terms. The second flowchart represents the procedure used when the model employs direct utilization of experimental data for D_j^n, u_j^n (i.e. D_{iox}, u_{iox})
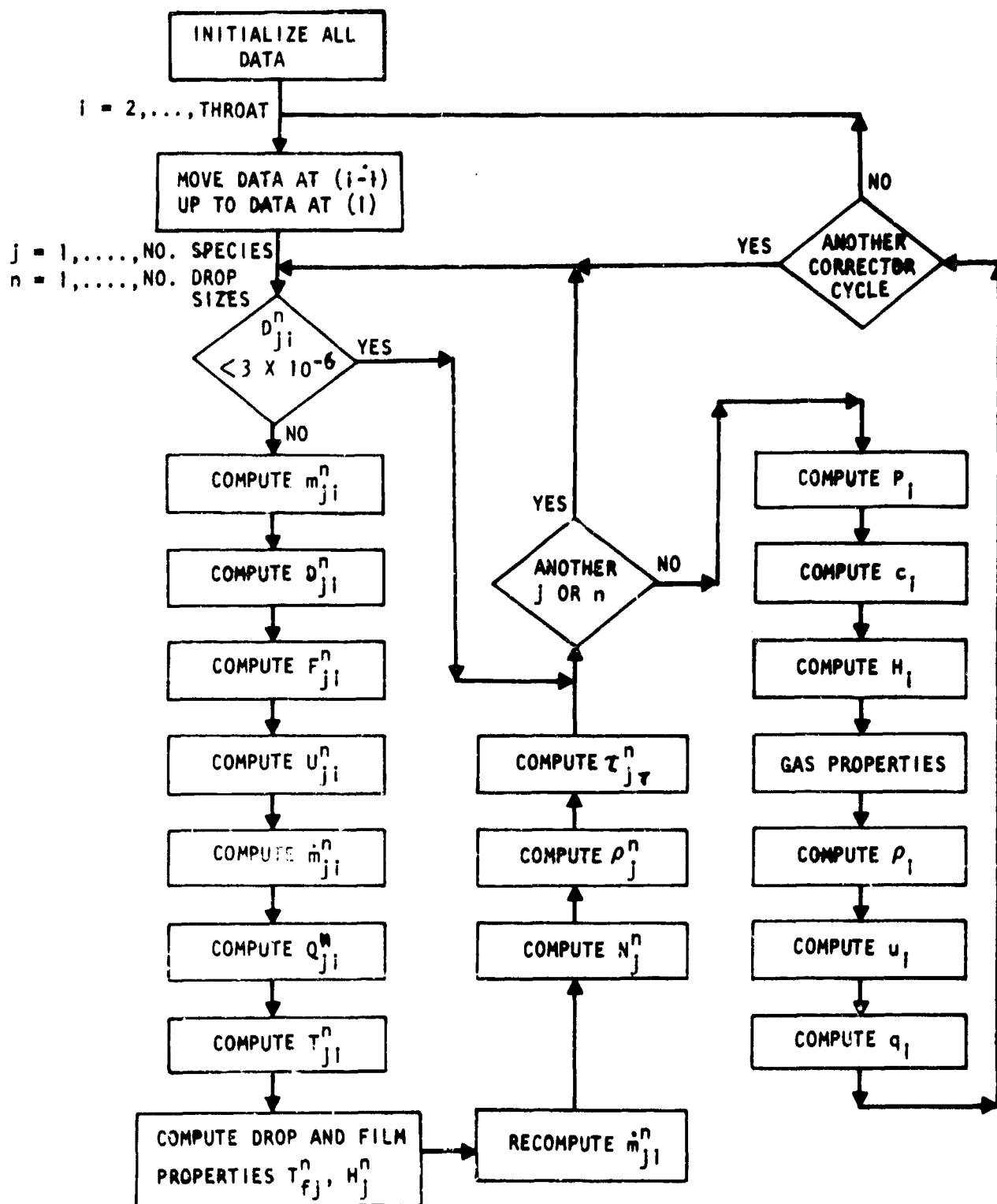
Figure 50. Block Diagram for Steady-State Computer Program
with Initial-Plane Initialization .
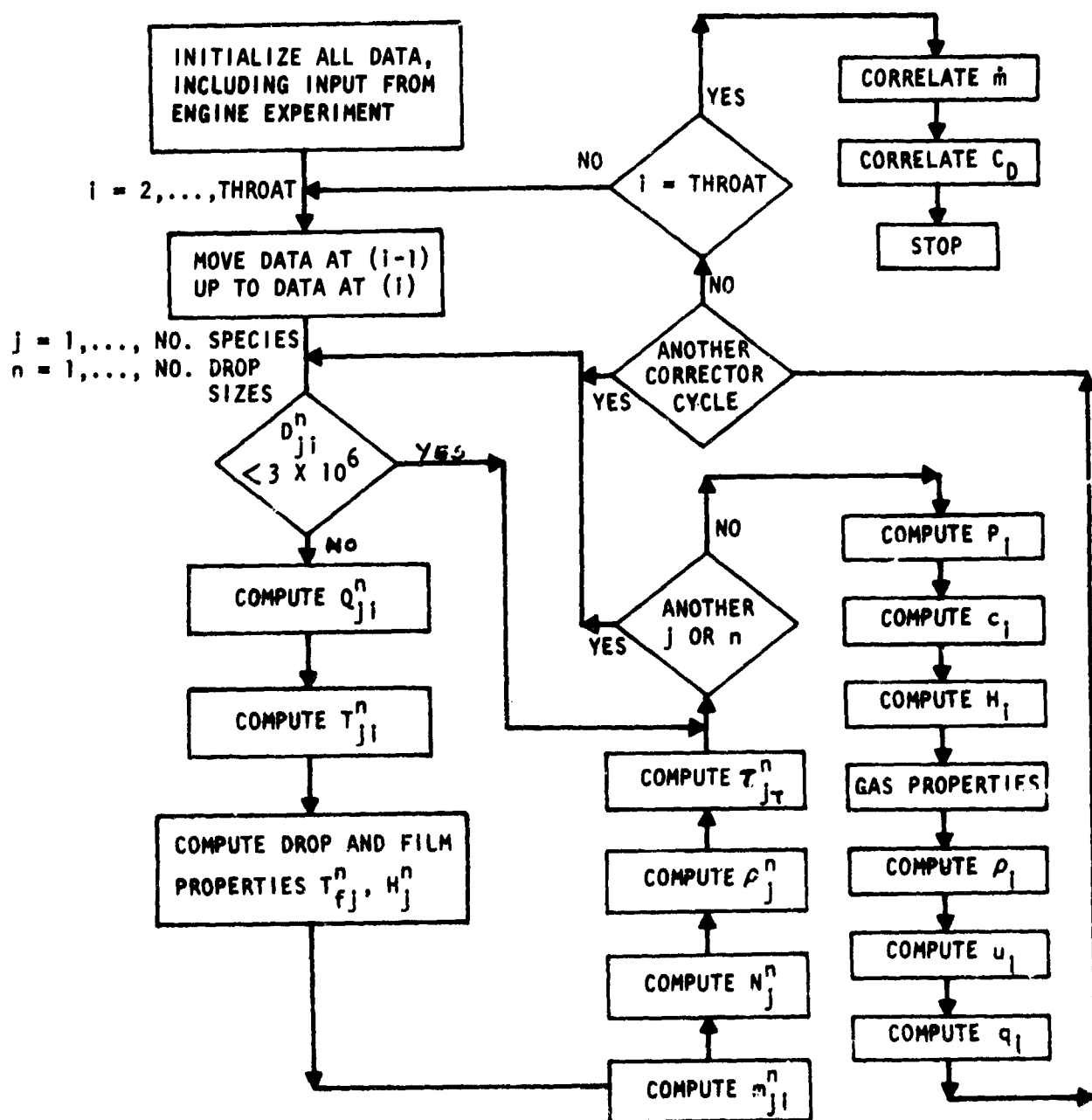
Figure 51. Block Diagram for Steady-State Computer Program with Spatial Experimental Spray Parameter Initialization

EVALUATION OF THE SOLUTION METHOD

There are a number of important criteria to consider concerning the evaluation
of a numerical scheme. Among these are convergence, order of accuracy, stability
and feasibility of the technique. Most of these terms are self-explanatory,
but they are defined in detail in the next appendix pertaining to the transient
formulation.

All of the criteria are dependent, for the steady-state formulation, on the
spray phase equations. This is so because the gas phase equations are entire-
ly algebraic and can be solved in closed form. The spray phase equations are
differential, highly interrelated and considerably more complex to solve.

The methods used to solve the given steady-state formulation are standard tech-
niques. The difference operators are centered in space and hence the error of
the program is to $(\triangle X)^3$. The "order of accuracy" is said to be, thus of second
order. The derivation of the order of accuracy is not presented here, because it
is well known for this technique. The method of derivation would follow similarly
to that presented later for the transient solution.

Likewise the solution procedure is stable for small enough values of ΔX. Obviously the
form of the coupling terms, number of iterations, etc. location in chamber, etc.,
affect this required value. A proof for the stability of the model is not
included.

R-8377

In practice by running the program at different Δ X values, a fairly accurate error bound on each equation at particular locations can be determined. By reducing the step size r Δ X can be determined which results in virtually no difference in resultant predictions. This, at least physically, confirms convergence of the finite difference scheme to the solution of the ordinary differential equations.

The last criteria to consider is the feasibility of the solution. The finite difference equations, themselves, must be solvable and yield "physically real values." Now although the general method given to solve the ordinary differential equations is the standard trapezoidal rule (Δ X^3 errors and stable for small Δ X), this may not always be entirely sufficient in the practical sense. Program computation time at very small Δ X levels may become unreasonable. Obviously the coupling term expressions control the gradients (derivatives) of some of the parameters. This is particularly true of the droplet mass continuity equation,(m_j^n and $\dot{m}_j^n$), and the droplet heating equation, (T_j^n and Q_j^n). The coupling terms are obtained from separate subroutines; when $\dot{m}_j^n$ and Q_j^n are closed form expressions their effect on the finite difference technique used in their respective spray equations is usually (though not always) minimal. Often, however, the expressions for the coupling terms are either very complex, involving a number of iterative equations themselves, or are sensitive to certain gas phase parameters, etc. Then of course these expressions may require more sophisticated solution techniques for the finite difference equations in which they appear in order to reduce running time and still retain accuracy. Hence the previous statement that the coupling terms affect stability, etc.

It would be inappropriate to place in this appendix all of the possible expressions used for computing or evaluating the coupling terms. The expressions are all lengthy and the subroutines for each are unique for the particular coupling term expression specified. As a consequence it is also inappropriate to specify exactly how the spray mass continuity or heating rate finite difference equations are effected or altered.

In practice, for both the steady-state and non-steady analysis it is necessary to subject the procedures for calculating both the chosen coupling term expression subroutine and the finite difference equation (of whatever form) in which it appears to stringent analysis separate from their use in the total program. If two of the coupling terms and their respective equations in which they appear are highly interrelated then both sets must be subjected together to this separate analysis. This usually involves calculating the subroutines and equations used under arbitrary specified extremes of engine operating conditions. In this separate "mini-model" the feasibility, accuracy and stability of the set of equations can be determined. Not until this criteria is achieved is the set then utilized in the full program.

It is most often extremely difficult to determine the resultant stability of the entire combined program when a variance of finite difference techniques are used for the equations. However, the method described above for determining separate stability of sensitive equations is at present the most reasonable method for producing overall stability. In practice the program can be employed, as previously mentioned, at different Δ X values to obtain approximate error bounds on various equations and at reduced Δ X values to check convergence.

An example of the techniques described above were used for the droplet burning and heating model employed in the Results Section. The finite difference equations containing the burning and heating rate terms utilized a bisection technique that resulted in quite accurate solutions.

APPENDIX IV

NUMERICAL ANALYSIS OF THE TRANSIENT FORMULATION

This appendix is intended to describe the technique currently employed in the transient program which solves the system of non-linear partial differential equations that describe the spray-gas field for a one-dimensional transient flow inside a rocket engine thrust chamber. The equations are identical to those presented in the Analytical Program Section of this report and will not be repeated here. Is is also the intention of this appendix to briefly introduce some of the techniques utilized in finite differencing methods and to define pertinent terms related to the analysis.

PRELIMINARY DISCUSSION

The general mode of attack leading to the current algorithm being employed has been based on finite differencing schemes. Although there are other numerical techniques available for solving systems of non-linear partial differential equations, the finite difference technique offers a straightforward, easy to implement approach. In a finite difference scheme the continuous independent variables x and t are replaced by discrete variables i and k. This corresponds to defining a net on x, t space say $\left\{ x_1 \cdots x_L \right\} \times \left\{ t_1 \cdots t_m \right\} = \left\{ (x_i, t_k) \right\}$ and making the natural 1-1 correspondence between $\left\{ (x_i, t_k) \right\}$ and (i, k). For a given system of partial differential equations, say

$$\frac{\partial W}{\partial t} + \frac{\partial F(W)}{\partial x} = B(W) \tag{1}$$

The solution function $W(x, t)$ is approximated by the function w_i^k, where w_i^k satisfies the same initial conditions as W on $(x_i, 0)$, similar boundary conditions, together with the following system of difference equations:

$$D_{T_k} W_i^k \;+\; D_{x_i} F\left(W_i^k\right) = \bar{B}_i^k$$

Here, D_T represents a finite difference operator approximating $\dfrac{\partial}{\partial t}$ at (x_i, t_k) and D_{x_i} does the same for $\dfrac{\partial}{\partial x}$. For the case under discussion, the mesh is assumed uniform (i.e., $\Delta t, \Delta x$ constant) and that $D_{T_{k'}} = D_{T_k}$ and $D_{x'} = D_x$ except possibly at the boundaries. We therefore have the following system of difference equations:

$$D_T W_i^k \;+\; D_x F\left(w_i^k\right) = \bar{B}\left(w_i^k\right) \tag{2}$$

$$i = 1 \cdots L$$
$$k = 1, 2 \cdots$$

Various Difference Operators

Some examples of difference operators for the space dimension are:

(a) Forward difference operator

$$\frac{\partial f}{\partial x} \;\approx\; \frac{1}{\Delta x}\, \Delta^+ f_i^k = \frac{f_{i+1}^k - f_i^k}{\Delta x}$$

(b) Backward difference operator

$$\frac{\partial f}{\partial x} \;\approx\; \frac{1}{\Delta x}\, \Delta^- f_i^k = \frac{f_i^k - f_{i-1}^k}{\Delta x}$$

(c) Central difference operator

$$\frac{\partial f}{\partial x} \;\approx\; \frac{1}{2\Delta x}\, \Delta^\circ f_i^k = \frac{1}{2\Delta x}\left(\Delta^+ + \Delta^-\right) f_i^k$$

$$= \frac{f_{i+1}^k - f_{i-1}^k}{2\Delta x}$$

Consider the difference equations approximating system (1) given by:

$$\frac{W_i^{k+1} - W_i^k}{\Delta t} + \frac{F\left(W_i^k\right) - F\left(W_{i-1}^k\right)}{\Delta x} = B\left(W_i^k\right) \quad (3)$$

$$\frac{W_i^k - W_i^{k-1}}{\Delta t} + \frac{F\left(W_i^k - F\left(W_{i-1}^k\right)\right)}{\Delta x} = B\left(W_i^k\right) \quad (4)$$

$$\frac{W_i^k - W_i^{k-1}}{\Delta t} + \Theta\left[\frac{F\left(W_i^k\right) - F\left(W_{i-1}^k\right)}{\Delta x}\right] + (1-\Theta) \quad (5)$$

$$\left[\frac{F\left(W_i^{k-1}\right) - F\left(W_{i-1}^{k-1}\right)}{\Delta x}\right] = \Theta\, B\left(W_i^k\right) + (1-\Theta)\, B\left(W_i^{k-1}\right)$$

One says (3) and (4) utilize forward and backward time differences respectively (meaning relative to the time t at which the space differences are expressed). Equation (5) reduces to (3) for $\Theta = 0$ and to (4) for $\Theta = 1$. If $\Theta = 0$, the w_i^k can be defined explicitly in terms of w_i^{k-1} and w_{i-1}^{k-1}; such a system is termed explicit. If $\Theta \neq 0$, then in general w_i^k is defined implicitly in terms of the old time-level values and new time-level values for other i; such a system is called implicit.

Important Criteria

There are several important criteria that come into play when chosing a finite difference scheme. Among them are convergence, order of accuracy, stability

and feasibility of the scheme.

<u>Convergence.</u> Let $W(i\Delta x, \quad k\Delta t)$ be the true solution to (1). Let w_i^k be a finite difference approximation. A convergent scheme is simply one in which the approximation w_i^k converges to $W(i\Delta x, k\Delta t)$ as $\Delta t, \Delta x \longrightarrow 0$ i, $k \longrightarrow \infty$ (for all x, t in the range of interest) such that $i\Delta x = x$, $k\Delta t = t$ remain fixed.

<u>Order of Accuracy.</u> In general, $W_i^k = W(i\Delta x, \quad k\Delta t)$ will satisfy the difference equations used to define w_i^k to within some power of Δx and Δt (or alternatively to within some power of Δt if we let $x = g(\Delta t)$). Thus if one writes

$$w_i^k = \varnothing(w_i^{k-1}, \Delta t, \Delta x)$$

where $\varnothing$ represents the process of solving the difference equations, then if

$$\| W_i^k - \varnothing(W_i^k, \Delta t, g(\Delta t)) \| = O(\Delta t^{k+1})$$

The scheme is said to be of kth order accuracy.

<u>Stability.</u> Stability on the other hand has to do with the nature in which the errors are propagated in the difference equations. Emperically, if the error grows exponentially with the number of time steps, the scheme is said to be unstable. Specifically, the behavior of $\| W^k \|$ as $\Delta t \longrightarrow 0$ ($k \longrightarrow \infty$ such that $k\Delta t = t$ fixed) is considered. This answer depends upon the relative rates at which Δt and Δx go to zero. In general, however, one can see it will take an increasing number of cycles to approximate $W(x,t)$ with w_i^k. A method is stable if

$\| W^k \|$ remains bounded as $k \longrightarrow \infty$, $\Delta t \longrightarrow 0$ $k\Delta t = t$ fixed
and $\Delta X = g(\Delta t)$ prescribed.

More precisely, if $w^k = C(\Delta t) w^{k-1}$, where $C(\Delta t)$ is an operator, then $w^k = \left[C(\Delta t)\right]^k w^0$. (By setting $\Delta x = g(\Delta t)$, c is considered as a function of Δt only). The method is stable if for some $\gamma > 0$, the infinite set of operators

$$\left[C(\Delta t)\right]^k \quad \begin{cases} 0 < \Delta t < \gamma \\ 0 \le k \Delta t \le T \end{cases}$$

remains uniformly bounded.

Feasibility. Also to be considered in a difference scheme is its feasibility of operation. Of foremost concern here is whether or not the nonlinear system of algebraic equations defined by the difference scheme are computationally solvable. When the scheme is implicit, this can often be a very significant problem. Stability and accuracy are defined in terms of the exact solution to the difference equations. These become irrelevant if the difference equations cannot be solved or take too long to solve or if the solution process is too sensitive to perturbations.

DEVELOPMENT OF THE CURRENT ALGORITHM

It was felt that, due to the extremely complex nature of the specific system of transient equations, the following scheme would be fruitful:

$$\frac{w_i^k - w_i^{k-1}}{\Delta t} + \frac{F\left(w_i^k\right) - F\left(w_{i-1}^k\right)}{\Delta x} = B\left(w_i^k\right) \quad (6)$$

Here, both the derivatives are replaced by backward difference operators and the right-hand side is totally implicit. The arrows above the variable indicate that these are the unknowns in the equation. With system (6) one marches forward in time and space; i.e., in computing w_i^k, one has available the values at w_{i-1}^k and w_i^{k-1}. From the initial and boundary

conditions, one can determine w_0^k and w_1^o for all i, k. (This statement is modified later.)
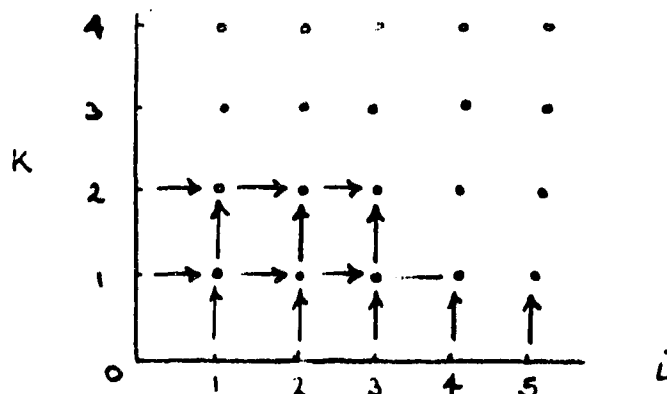
In the above picture, the arrows indicate the procedure employed. From w_0^1 and w_1^o, w_1^1 can be determined from system (6). Then from w_1^o and w_2^o, w_2^1 can be likewise determined, etc. This differencing procedure is well known to be unconditionally stable, for functions without exponential growth, when applied to a hyperbolic partial-differential equation with constant coefficients. This fact, along with its simplicity, was one of the primary motives in chosing it. Actually, in attempting to implement (6), the boundary condition at the throat is employed for one component of w. At first this was done iteratively. That is, the velocity is predicted at the injector face based on old time level data for which the velocity at the throat was sonic. Then the new time level data was computed keeping the throat velocity at sonic. However, due to the sensitive nature of the algebraic system of difference equations, this method proved to be relatively unsatisfactory. Alternatively, it was decided to solve the momentum and continuity equations simultaneously with the boundary conditions $(\rho u)_1 = \dot{w}_0$ and u_{throat} = sonic. Moreover, due to the natural evolution of practical numerical analysis, the following difference scheme was substituted for (6):

$$\frac{w_i^k - w_i^{k-1}}{2\Delta t} + \frac{w_{i-1}^k - w_{i-1}^{k-1}}{} + \frac{F(w_i^k) - F(w_{i-1}^k)}{\Delta x} =$$

338

$$\frac{1}{2} \left\{ B(W_i^k) + B(W_{i-1}^k) \right\} \tag{7}$$

This system of equations is now centered in space (about $i - 1/2$), hence its accuracy should be better than (6), although not by an order of magnitude).

Stability of Scheme

Also, it is possible to demonstrate that this scheme unconditionally satisfies Von Newman's necessary condition for stability. In other words, if a solution is expressed in its fourier series, the coefficients of the lth component of this series V_l^k at time $k \Delta t$, satisfy

$$V_l^{k+1} = G \ V_l^k = G^k \ V_l^0$$

where G is the (amplification) matrix determined by the difference scheme. Von Newman requires that the eigenvalues of G (a measure of the amplifying effect of G) be less than one in absolute value. (See the derivation given later for details). As a comparison, the Von Newman stability condition for the Lax-Wendroff two-step scheme is $(|u| + a) \frac{\Delta t}{\Delta x} < 1$. However, it should be remembered that the result that (7) is unconditionally stable holds only if it is solved exactly (and if one assumes constant coefficients). Thus, in practice, the number of iterations performed in trying to solve the nonlinear algebraic system of difference equations will have a definite effect on the stability.

METHOD OF SOLUTION

The equations to be solved are identically those presented earlier in this report. The chamber is partitioned from x_1 (injector face) to x_L (throat) by Δx,

$(x_i = (i-1)/\triangle x)$. For brevity, the entire system of algebraic equations resulting from differencing scheme (7) will not be written down here. Typically however, they take the following form as exemplified by the drop momentum equations. Note that in this section both time, k, and space, i, denoters now appear as subscripts to avoid confusion with the drop group size.

$$\frac{u^n_{j\,i,\kappa} - u^n_{j\,i,\kappa-1} + u^n_{j\,i-1,\kappa} - u^n_{j\,i-1,\kappa-1}}{\lambda\,\triangle t} + \frac{\left(u^n_{j\,i,\kappa} + u^n_{j\,i-1,\kappa}\right)}{2} \tag{8}$$

$$\left(\frac{u^n_{j\,i,\kappa} - u^n_{j\,i-1,\kappa}}{\triangle x}\right) = \frac{1}{2}\left[\frac{g\,F^n_{j\,i,\kappa}}{m^n_{j\,i,\kappa}} + \frac{g\,F^n_{j\,i-1,\kappa}}{m^n_{j\,i-1,\kappa}}\right]$$

for $i = 2, \ldots, L$

Ideally, one would want to solve the system of algebraic equations simultaneously for all unknowns. This process, however, is impractical due to the non-linearity of the system. Instead, we identify particular unknowns with particular equations and solve the system iteratively. For example, in (8) we assume $m_j{}^n_{i,k}$ and $F_j{}^n_{i,k}$ are known (either from previous iterations or from the old time level). Further, we have that $u_j{}^n_{i-1,k}$ and $u_j{}^n_{i,k-1}$ are known from previous space and time calculations. The equation can then be written explicity for $u_j{}^n_{i,k}$ and is thus used to get a better estimate of $u_j{}^n_{i,k}$. The following is a table of each unknown versus its defining equation:

TABLE I

Name	Symbol	Computed From

Drop Data

Name	Symbol	Computed From
Concentration number	N_j^n	Concentration number equation
Spray density	$\rho_j^n = N_j^n m_j^n$	Spray continuity equation
Drop temperature	T_j^n	Drop energy equation
Drop velocity	u_j^n	drop momentum equation.
Surface enthalpy	H_{js}^n	Tables: function T_{js}^n, P
Drop enthalpy	H_j^n	same as H_{js}^n
Drop diameter	D_j^n	From N_j^n, ρ_j^n, $\rho_{\ell j}^n$
Film temperature	$T_{f_j}^n$	From T_{js}^n, T
Evaporization, breakup rate	$\dot{m}_j^n$	Subroutine
Drag force	F_j^n	Subroutine
Drop heating	Q_j^n	Subroutine
Various drop, film and vapor properties		Tables and subroutines as a function of T_{js}^n, $T_{f_j}^n$, T, p, C

Gas Data

Name	Symbol	Computed From
Pressure	p	Equation of state
Mixture Ratio	C	Mixture ratio equation
Flow vector	v	Simultaneously from
Density	ρ	continuity and momentum
Velocity	u	Function of v and ρ
z-vector	z	Gas energy equation
Enthalpy	H	Function of z, ρ, u, M, T
Various gas properties	T, M, μ, K	Tables as function of C, H, p

Essentially, the program steps through each equation and gets an updated esti-
mate of the variable associated with that equation. A complete cycle consists
of passing through all difference equations, functional relations (i.e., state,
vaporization rate, etc.), and the property tables. Since the differencing
procedure employs only two time levels, the program requires only two arrays
for each variable that appears in a time derivative. Since the procedure is
totally implicit, that is all variables not in a time derivative are taken at
the new time level, only one array is needed for those variables that never
appear in a time derivative, (vaporization rate, gas temperature, all pro-
perties, etc.).

The program has been arranged as follows. At the end of each time step,
say $t = t_0$, the arrays of the new-time variables at t_0 are written over the
arrays of the old time variable at $t_0 - \triangle t$. Then for the next time step at
$t_0 + \triangle t$ the program initially has the variables at t_0 in the new-level array
as well as the old level array. This is tantamount to saying the first guess
for the variable at $t_0 + \Delta t$ is its value at t_0. Not only does this procedure
save a vast amount of core storage, but it also saves writing a separate set
of equations for the predictor cycle as distinguished from the corrector
cycle.

Program Flowchart

The following section presents a flowchart of the basic iterative procedures
used for computation of the transient formulation. Several clarifying state-
ments can be made relative to the flowchart at this point. First, "gas
coupling terms" refers to the finite difference approximations using (7) of
the following equations:

INITIALIZE ALL DATA

MOVE ALL DATA AT NEW TIME BACK TO OLD

SPRAY BOUNDARY CONDITIONS

CONCENTRATION NUMBER SPRAY DENSITY

$\rho^n_{j1,2} < 10^{-20}$

DROP DIAMETER

$D^n_{ji} < 3 \times 10^{-16}$

DRAG FORCE

DROP VELOCITY

EVAPORAZATION RATE

DROP HEATING

DROP TEMPERATURE

FILM TEMPERATURE

DROP ENTHALPY

DROP FILM VAPOR PROPERTIES

END DROP

GHOST

REPEAT FOR $i = 2,...,L$

ANOTHER CORRECTOR CYCLE

OUTPUT (OPTIONAL)

$q_i \quad i = 1,...,L$

GAS PROPERTIES AND PRESSURE $i = 2,...,L$

MIXTURE RATIO

ENTHALPY

z VECTOR

REPEAT $L = 2,...,L$

GAS BOUNDARY CONDITIONS FOR H,z,q,c,P AND PROPERTIES

GAS VELOCITY $i = 1,...,L$

FLOW VECTOR AND DENSITY $i = 1,...,L$

GAS COUPLING TERMS $i = 2,...,L$

P-0377

Figure 52. Block Diagram for Transient Computer Program

$$-\left[\frac{\partial(A\rho_j^n)}{\partial t} + \frac{\partial(A\rho_j^n u_j^n)}{\partial x}\right]$$

$$e_j^n = N_j^n m_j^n$$

$$-\left[\frac{\partial(A\rho_j^n u_j^n)}{\partial t} + \frac{\partial(A\rho_j^n u_j^{n2})}{\partial x}\right]$$

$$-\left[\frac{\partial\left(A\rho_j^n\left(H_j^n + \frac{u_j^{n2}}{2gJ}\right)\right)}{\partial t} + \frac{\partial\left(A\rho_j^n u_j^n\left(H_j^n + \frac{u_j^{n2}}{2gJ}\right)\right)}{\partial x}\right]$$

The gas pressure, which used to be a very troublesome term, is calculated from the equation of state using the most current ρ, M, T.

Further Notes on the Solution of the Gas Phase Continuity and Momentum Equations

The most involved portion of the program is the calculation of ρ and v. All other parameters are either computed directly from known functions or tables, or "marched off" from the finite difference equations. The density and flow vector on the other hand are solved for simultaneously from the $2L-1$ finite difference equations and the boundary conditions on v at the injector face and nozzle throat. In the finite difference equation for the gas momentum the pressure term is replaced by the equation of state so that the density appears explicity. This system of 2L linear equations in the 2L unknowns ρ_1, ρ_2, . . ., ρ_L; v_1, v_2, . . ., v_L can be advantageously organized. Define a new vector P with 2L components such that

$$F_\ell = \begin{cases} v_{\frac{\ell+1}{2}} & \ell \text{ odd} \quad\quad \ell = 1, \ldots, 2L \\ \rho_{\ell/2} & \ell \text{ even} \end{cases}$$

and identify equation 1 as $v_1 = \dot{v}_{\not{L}}$, equation 2 as continuity for i = 2, equation 3 as momentum for i ≥ 2, equation 4 as continuity for i ≤ 3, etc., and the last equation at 2L or $v_L = a\rho_L$; then, this system, written in the matrix representation $M_p = f$ has the following form

$$p = \begin{bmatrix} p1 \\ p2 \\ \cdot \\ \cdot \\ \cdot \\ \cdot \\ p_{2L} \end{bmatrix} = \begin{bmatrix} v_1 \\ \rho_1 \\ v_2 \\ \rho_2 \\ \cdot \\ \cdot \\ \rho_n \end{bmatrix}$$

$$M = \begin{bmatrix} x & & & & \\ xxxx & & & & \\ xxxx & & & & \\ & xxxx & & & \\ & xxxx & & \bigcirc & \\ & & xxxx & & \\ & \bigcirc & xxxx & & \\ & & xxxx & & \\ & & xxxx & & \\ & & xx & & \end{bmatrix}$$

That is, there are at most four unknowns to each equation and they are centered about the diagonal as indicated. Since M is banded, Mp = f is relatively easy to solve. The program does this using a modified version of Gaussian elimination which takes advantage of the particular pattern of zero entries in M.

Physical Structure of Program - Running Time

To conclude, a word may also be appropriate concerning the physical structure of the program and its running time. The structure of the program is quite modular. This allows for ready modification. There is a specific subroutine

to calculate each of the drop properties. There is one routine that handles the film property equations, one to handle the gas properties, one for the vaporization rate, one for drag force, etc. The heart of the program is subroutine ALL. All the finite difference equations appear in this routine. For each corrector cycle, ALL is called once. During each pass, ALL calls the various other subroutines as required.

As to running time, with "physically real" coupling terms, unfortunately it is rather lengthy. If the chamber is broken up into approximately 150 mesh points, the program will take approximately ten minutes to step 200 timesteps with four iterations per time step. This rather lengthy running time is due to the fact that the program considers actual gas composition and must search combustion properties tables during the iterations.

EVALUATION OF SOLUTION METHOD

Again the important criteria to consider are convergence, order of accuracy, stability and feasbility of the technique. These terms have now all been defined and in some cases related to the chosen method.

All of the criteria are dependent on the entire set of equations because each is partial differential in form, no closed form equations are present. The methods used to solve the transient formulation, as discussed, are far from "standard". The difference operators are centered in space while backward in time. Hence the accuracy of the model is firstorder in time as derived in a subsequent section.

A highly complex stability analysis was performed for a simplified set of the conservation equations (primarily removal of the mixture ratio equation and combustion properties tables) and non-responsive (to pressure or velocity waves) coupling terms. Complete details regarding the simplifications and their consequences are given in the derivation presented later. What is significant however is the results of the stability analysis. For the set of equations used the results indicate that the method unconditionally satisfies Von Newman's necessary criteria for stability. Further the stability results is shown to be independent of the value of $\frac{\Delta t}{\Delta x}$ step size ratio as long as $\frac{\Delta t}{\Delta x}$ is sufficiently small that a vector term containing the coupling expressions may be neglected. The actual size of Δt depends of course on the form of the coupling terms, number of iterations, location in the chamber, time, etc., and though possible in principle to compute, would entail a horrendous task. The point is that, as for the Δx in the steady state model, a Δt can be found, regardless of the form of physically real coupling terms, that allow the finite difference method for the simplified set of equations to satisfy the

necessary conditions for stability. This is not to say that the stability condition is as strong as that for the steady state case; it may not be possible to determine both necessary and sufficient stability conditions for any formulation as complex as this transient model.

To relate the simplified set of conservation equations to the complete conservation equations and combustion property tables, actual computer model (still, however, retaining the non-responsive coupling terms) computations were performed and are reported in the Results Section. Selecting reasonable values of ΔT and Δx the model received initial inputs from the steady-state program; these inputs were calculated

using the same coupling terms as in the transient model. The transient model was then allowed to run for a considerable number of time steps under a "no perturbed" condition. It is during this time that if numerical instability is present, errors will begin to propagate. However, after the specified time level, the transient model predictions were identical to those of the steady-state input. At this point a more severe test was performed. A large perturbation was introduced at the throat. Now with non-responsive coupling terms (except for the velocity effects which were retained in the drag force) the wave must physically die due to expansion from the throat, gas viscosity and drag; this is precisely what occurred. The transient model predicted wave damping and a return to steady-state conditions.

In practice, combined with the stability analysis for the simplified conservation equations, these results were sufficient to allow the predicition that a Δt could be found, regardless of the coupling term expressions, that would result in numerical stability. Additionally by running the program at different Δt and Δx values a fairly accurate error bound on each equation at particular locations and time can be determined. By reducing the step sizes a Δt, Δx can be determined which results in virtually no difference in resulted predictions. This, at least physically, confirms convergence.

However, just as in the steady-state model, feasibility of the solution must be considered. The same problems exist; "real" coupling terms may require Δt values that result in unreasonable running time. To alleviate this probelm more sophisticated solution techniques for the spray finite difference equations in which the coupling terms appear may be necessary. In such cases the same tech-

nique is used for the required transient spray equations as was outlined in Appendix III for the steady-state spray equations. The method applies to both subroutines, for coupling terms, and their respective spray equations. Accuracy and stability are determined under arbritrary conditions; this is often quite complex as the spray equations are variable in x and t.

The same limitation on determining the resultart stability of the combined set of varying finite difference technique exists here as in the steady-state case. However, the method utilized is the best found to date and can be checked by computer computations, as described previously, at various Δt, Δx values.

Derivation of Stability

As mentioned earlier it was possible to show that the selected numerical method as applied to the transient formulations satisfied Von Newman's necessary criteria for stability. This section presents the derivation of this result.

It must be pointed out that the results pertain to a simplified set of the conservation equations. That is, it was not analytically possible to apply the stability criteria to the full set of equations including the combustion property tables. Thus the following simplifications were made: 1) the mixture ratio equation was eliminated, thus also eliminating the combustion properties tables, 2) the gas composition was assumed to be frozen, 3) gas viscosity and heat conduction were neglected, and, 4) simplified forms of the coupling terms were used.

Assumptions 1) and 2) imply that the enthalpy $H \approx C_p T$ (assuming a reference of zero temperature) and that the chemical energy is carried in the spray. Since C_p is constant it is equal to $\frac{\gamma_\ell R}{\gamma_\ell - 1}$ and hence $H = \frac{\gamma_\ell}{\gamma_\ell - 1} P/\rho$ (through the equation of state). Although useful here for this analysis, these are physically poor approximations for combustion under conditions of changing mixtures ratio.

Assumption 3) is inconsequential to the analysis.

Assumption 4) utilized simplified coupling term expressions. In particular, the burning rate model was specified as a function of x and diameter only, i.e., $\dot{m} = \int (x) D$. In this sense it is similar to any of the quasi-steady models upon reaching wet bulb. The drop temperature was kept constant for the analysis thus eliminating the spray energy equation. The drag coefficient was also assumed to be a constant, but velocity variation was retained in the drag force equation.

In essence two of these coupling terms are non-responsive in that the gas phase flow field fluctuations cannot effect $\dot{m}$ or the drop temperature, (Q_j^n assumed zero). Though C_d is assumed constant, the drag force can fluctuate because the velocity terms were retained.

The results of assuming $\dot{m}$ and Q_j^n to be non-responsive are shown to be inconsequential to the analysis as the stability results were achieved by assuming a Δt sufficiently small that the term, $(\Delta t\ B^{-1}\ Q)$, in which B is of order 1 and Q contains all of the coupling terms can be neglected.

The realism of this assumption on Δt, the meaning of the final stability results, and the relation of the simplified set of equations to the complete model has been discussed in the previous section.

It is interesting to note, however, that the very simplified conservation equations remaining are still somewhat more complex (except for the coupling terms) than those used by most authors in past transient formulations.

In any event considering the system of equations given by assuming

1. T_d = const, H_d = const

2. $\dot{m}$ = $b(x)D$ = $b_1 D$

3. P = $\dfrac{\gamma_j - 1}{\gamma_j} e H$ = $ae H$

4. F = $edm_d^{2/3}|u-u_d|(u-u_d)$

Then the equations to solve are nearly:

$$\frac{\partial A N_d}{\partial t} + \frac{\partial A u_d N_d}{\partial x} = 0$$

$$\frac{\partial m_d}{\partial t} + u_d \frac{\partial m_d}{\partial x} = -b'_i m_d^{1/3}$$

$$\frac{\partial u_d}{\partial t} + u_d \frac{\partial u_d}{\partial x} = \frac{e d}{m^{1/3}}|u-u_d|(u-u_d)$$

$$\frac{\partial A e}{\partial t} + \frac{\partial A e_s}{\partial t} + \frac{\partial A v}{\partial x} + \frac{\partial A e_s u_d}{\partial x} = 0$$

$$\frac{\partial A v}{\partial t} + \frac{\partial A e_s u_d}{\partial t} + \partial A \frac{\partial a e H}{\partial y} + \frac{\partial A e_s u_d^2}{\partial y} + \frac{\partial A \frac{v^2}{e}}{\partial x} = 0$$

$$\frac{\partial A_3}{\partial t} + \frac{\partial A[u_3 + .185 a_e u H]}{\partial x} + \frac{\partial A e_s \left(u_d + \frac{u_d^2}{2g J}\right)}{\partial t} + \frac{\partial \left(A e_s u_d \left[H_d + \frac{u_d^2}{2g J}\right]\right)}{\partial x} = 0$$

where here $C_s = N_d m_d$

consider this system in the form:

$$B(w) \frac{\partial w}{\partial t} + D'(w) \frac{\partial F(w)}{\partial x} = Q(w)$$

where

$$w = (A N_d, \ m_d, \ u_d, \ A e, \ A v, \ A_3)$$

Let

$$\bar{B}_i^k = \frac{1}{2}\left[B(w_i^k) + B(w_{i-1}^k) \right]$$ with similar expressions

for

$$\bar{D}'^k_i, \quad \bar{Q}^k_i$$

Then, using differencing scheme (7), we have

$$\bar{B}_i^k \frac{w_i^k - w_i^{k-1} + w_{i-1}^k - w_{i-1}^{k-1}}{2 \Delta t} + \bar{D}_i'^k \frac{F(w_i^k) - F(w_{i-1}^k)}{\Delta x} = \bar{Q}_i^k$$

If we assume $\frac{\partial F}{\partial v} = F_v$ is locally constant, and if we let $D = D' F_v$ and $h = \frac{2\Delta t}{\Delta x}$, then we have:

$$\bar{B}_i^k \left[w_i^k - w_i^{k-1} + w_{i-1}^k - w_{i-1}^{k-1} \right] + h \bar{D}_i^k \left[w_i^k - w_{i-1}^k \right] \qquad (9)$$
$$= 2 \Delta t \ \bar{Q}_i^k$$

This of course is the finite difference approximation to

$$B(w) \frac{\partial w}{\partial t} + D(w) \frac{\partial w}{\partial x} = Q(w)$$

The vector Q and the matrices B and D are given below.

$$B = \begin{bmatrix} 1 & 0 & 0 & 0 & 0 & 0 \\ 0 & 1 & 0 & 0 & 0 & 0 \\ 0 & 0 & 1 & 0 & 0 & 0 \\ w_2 & w_1 & 0 & 1 & 0 & 0 \\ w_2 w_3 & w_1 w_3 & w_1 w_2 & 0 & 1 & 0 \\ w_2\left(H_d + \frac{w_3^2}{2g J}\right) & w_1\left(H_d + \frac{w_3^2}{2g J}\right) & \frac{w_1 w_2 w_3}{g J} & 0 & 0 & 1 \end{bmatrix}$$

$$D = \begin{bmatrix}
W_3 & 0 & 0 & 0 & 0 & 0 \\
0 & W_3 & 0 & 0 & 0 & 0 \\
0 & 0 & W_3 & 0 & 0 & 0 \\
W_2 W_3 & W_1 W_3 & W_1 W_3 & 0 & 1 & 0 \\
W_2 W_3^2 & W_1 W_3^2 & 2 W_1 W_2 W_3^2 & \dfrac{W_6^2}{W_4^2}\left[\dfrac{1}{eJ}-1\right] & \dfrac{2W_5}{W_4}\left(1-\dfrac{1}{eJ}\right) & \dfrac{g}{eJ} \\
W_2 W_3\left(1+\dfrac{W_3^2}{2gJ}\right) & W_1 W_3(\quad) & \begin{array}{c} W_1 W_2(\quad)+ \\ \dfrac{W_1 W_2 W_3^2}{3J} \end{array} & f_1 & f_2 & f_3
\end{bmatrix}$$

where

$$e = \frac{\gamma}{\gamma-1} \cdot .185$$

$$f_1 = \frac{.185\, W_5^2}{A e\, gJ\, W_4^3} - \left(1+\frac{.185}{Ae}\right)\left(\frac{W_5 W_6}{W_4^2}\right)$$

$$f_2 = -\frac{3(.185)\, W_5^2}{2 gJ\, W_4^2\, Ae} + \left(1+\frac{.185}{Ae}\right)\left(\frac{W_6}{W_4}\right)$$

$$f_3 = \left(1+\frac{.185}{Ae}\right)\frac{W_5}{W_4}$$

$$Q = \begin{bmatrix} 0 \\ 0 \\ \dfrac{d\,w_4}{A\,w_2^{1/3}}\left(\dfrac{w_5}{w_4}-w_3\right)\left|\dfrac{w_5}{w_4}-w_3\right| \\ 0 \\ \dfrac{g}{A\rho^2}\left[w_6-\dfrac{w_5^2}{2g J\,w_4}\right]\dfrac{\partial A\rho}{\partial x} \\ \dfrac{.165}{A^2\rho^2 w_4}\left[w_6-\dfrac{w_5^2}{2g J\,w_4}\right]\dfrac{\partial A\rho}{\partial x} \end{bmatrix}$$

If we assume that in (9) $\bar{B}_i^k$ and $\bar{D}_i^k$ are nearly constant and that $\bar{Q}_i^k = \tfrac{1}{2}Q\left[w_i^k + w_{i-1}^k\right]$ where Q is a constant matrix, then (9) can be rewritten as:

$$\left[B + hD - \Delta t\,Q\right]w_i^k + \left[B - hD - \Delta t\,Q\right]w_{i-1}^k - Bw_i^{k-1} \quad (10)$$

$$- Bw_{i-1}^{k-1} = 0$$

Let the fourier series for $w\,(i\triangle x,\ k\triangle t)$ be given by

$$W(x,t) = \sum_\ell u(\ell,t)\,e^{j\ell x} \qquad j = \sqrt{-1}$$

or

$$W_i^k = \sum_\ell u^k(\ell)\,e^{j\ell i \Delta x} \qquad \text{Note } u - \text{not velocity here}$$

Substituting this expression into (10) and equating like terms in $e^{j\ell x}$, we

get
$$\left[B + hD - \Delta t\,Q\right]u_\ell^k + \left[B - hD - \Delta t\,Q\right]u_\ell^k e^{-j\ell \Delta x} + (-B)u_\ell^{k-1}$$

$$+ (-B)\,u_\ell^{k-1}e^{-j\ell \Delta x} = 0$$

or

$$\left[(B + hD - \Delta t\,Q) + e^{-j\ell \Delta x}(B - hD - \Delta t\,Q)\right]u_\ell^k$$

$$= B\left(1 + e^{-j\ell \Delta x}\right)u_\ell^{k-1}$$

The amplification matrix $G(\Delta t, \ell)$ is defined as that matrix such that

$$u_\ell^k = G(\Delta t, \ell)\, u_\ell^{k-1}$$

Clearly,

$$G = \left[(B + hD - \Delta t Q) + e^{-j\ell \Delta x}(B - hD - \Delta t Q)\right]^{-1} B\left(1 + e^{-j\ell \Delta x}\right)$$

or

$$G^{-1} = \left(1 - e^{-j\ell \Delta x}\right)^{-1} B^{-1}\left[(B + hD - \Delta t Q) + e^{-j\ell \Delta x}(B - hD - \Delta t Q)\right]$$

let $\quad \alpha = \ell \Delta x$

Then

$$G^{-1} = \left[B(1 + e^{-j\alpha})\right]^{-1}\left[B(1 + e^{-j\alpha}) + hD(1 - e^{-j\alpha}) - \Delta t Q(1 - e^{-j\alpha})\right]$$

$$= \left[I + \frac{j\sin\alpha}{1 + \cos\alpha}\, h\, B^{-1} D - \Delta t\, B^{-1} Q\right]$$

The Von Newman necessary condition for stability is that the eigenvalues of G be less than or equal to one in absolute value. The eigenvalues of G are the reciprocals of the eigenvalues of G^{-1}. Further, since the eigenvalues of B are all one, then the eigenvalues of $B^{-1} D$ and $B^{-1} Q$ are the same as the eigenvalues of D and Q respectively. That this is so follows from:

Let λ be eigenvalue of D corresponding to eigenvector v. Let $w_1 \cdots w_6$ be six independent eigenvector of B^{-1}. Then $v = \sum_i \alpha_i w_i$

$$B^{-1} D v = B^{-1} \lambda v = \lambda B^{-1} v = \lambda \sum B^{-1} \alpha_i w_i$$

$$= \lambda \sum \alpha_i B^{-1} w_i = \lambda \sum \alpha_i (1) w_i = \lambda \sum \alpha_i w_i = \lambda v$$

Hence λ is eigenvalue of $B^{-1} D$.

Note: i here is the summation index, not space index

Let us assume that Δt is so small so that $\Delta t\, B^{-1} Q v \approx 0$.

Then if λ is an eigenvalue of D, an eigenvalue of G is given by

$$ g = \cfrac{1}{1 + \cfrac{j \sin \alpha}{1 + j \cos \alpha}\, h\lambda} $$

Since λ is real by hyperbolicty of the system, $|g| \le 1$ for all h.

Therefore, the method unconditionally satisfies Von Newman necessary criteria

for numerical stability.

Derivation of the Order of Accuracy

We consider the finite difference scheme

$$ \frac{W_i^k - W_i^{k-1} + W_{i-1}^k - W_{i-1}^{k-1}}{2\,\Delta t} + \frac{F(W_i^k) - F(W_{i-1}^k)}{\Delta x} = \frac{B(W_i^k) + B(W_{i-1}^k)}{2} $$

which approximates:

$$ \frac{\partial W}{\partial t} + \frac{\partial\, F(W)}{\partial x} = B(W) $$

If V_i^k is the true solution at $x = i\Delta x$, $t = k\Delta t$. Then

$$ \frac{\partial V_{i-1}^k}{\partial t} + \frac{\partial F(V_i^k)}{\partial x} = B(V_i^k) $$

$$ \frac{\partial V_{i-1}^k}{\partial t} + \frac{\partial F(V_{i-1}^k)}{\partial x} = B(V_{i-1}^k) $$

$$ \Rightarrow \frac{\partial V_i^k}{\partial t} + \frac{\partial V_{i-1}^k}{\partial t} + \frac{\partial F(V_i^k)}{\partial x} + \frac{\partial F(V_{i-1}^k)}{\partial x} = B(V_i^k) + B(V_{i-1}^k) $$

$$ V_{i-1}^k = V_{i-1}^{k-1} + \Delta t\, \frac{\partial V_{i-1}^k}{\partial t} + 0\,(\Delta t^2) $$

$$ V_i^k = V_i^{k-1} + \Delta t\, \frac{\partial V_i^k}{\partial t} + 0\,(\Delta t^2) $$

$$\Rightarrow \quad \frac{V_i^k - V_i^{k-1} + V_{i-1}^k - V_{i-1}^{k-1}}{2\Delta t} = \frac{1}{2}\left[\frac{\partial V_i^k}{\partial t} + \frac{\partial V_{i-1}^k}{\partial t}\right] + \, \, O\,(\Delta t)$$

Also

$$F\left(V_i^k\right) = F\left(V_{i-1}^k\right) + \Delta x \, \frac{\partial F\left(V_{i-1}^k\right)}{\partial x} + A \, \frac{\Delta x^2}{2} + O\,(\Delta x)^3$$

$$F\left(V_{i-1}^k\right) = F\left(V_i^k\right) + (-\Delta x) \, \frac{\partial F\left(V_i^k\right)}{\partial x} + A\,\frac{(-\Delta x)^2}{2} + O\,(\Delta x)^3$$

Substracting, we get

$$2F\left(V_i^k\right) - 2F\left(V_{i-1}^k\right) = \Delta x \, \frac{\partial F\left(V_{i-1}^k\right)}{\partial x} + \frac{\partial F\left(V_i^k\right)}{\partial x} + O\,(\Delta x)^3$$

or

$$\frac{F\left(V_i^k\right) - F\left(V_{i-1}^k\right)}{\Delta x} = \frac{1}{2}\left(\frac{\partial F\left(V_i^k\right)}{\partial x} + \frac{\partial F\left(V_{i-1}^k\right)}{\partial x}\right) + O\,(\Delta x)^2$$

$\therefore$ V satisfies (7) to within $O(\Delta t) + O(\Delta x^2)$ i.e.,

$$\frac{V_i^k - V_i^{k-1} + V_{i-1}^k - V_{i-1}^{k-1}}{2\Delta t} + \frac{F\left(V_i^k\right) - F\left(V_{i-1}^k\right)}{\Delta x} - \frac{1}{2}B\left(V_i^k\right)$$

$$+ \, B\left(V_{i-1}^k\right) = O\,(\Delta t) + O\,(\Delta x^2)$$

this can be interpreted as

$$\| R_1 V^k - R_2 V^{k-1} \| = O\,(\Delta t) + O\,(\Delta x)^2$$

Since

$$R_1 = O\left(\frac{1}{\Delta t}\right) \,; \quad R_1^{-1} = O\,(\Delta t) \quad \text{for} \quad \Delta x = g\,\Delta t$$

$$\Rightarrow \| V^k - R_1^{-1} R_2 V^{k-1} \| = O\,(\Delta t)^2 + O\,(\Delta x)^3$$

$$\| V^k - \phi \, V^{k-1} \| = O\,(\Delta t)^2 + O\,(\Delta x)^3$$

Therefore scheme is first order in time.

COMPUTER FACILITIES

The digital computer facilities located at Rocketdyne consist of several IBM System/360 computers coupled with considerable peripheral equipment. Scientific type programs are processed on a Model 40/65I computer in which a Model 40 computer is coupled with a Model 65 computer as an auxiliary support processor (ASP). The ASP system provides very efficient processing by utilizing the Model 40 for handling the input/output functions, i.e., from punched card to direct access storage and out from direct access storage to printer, and for scheduling the work for the Model 65 computer (which eliminates delay time between batch jobs). The Model 40/65 not only executes faster than its IBM 7094 predecessor, but its cost per hour at Rocketdyne is less than half that of the 7094. Rocketdyne's Model 65 computer has a large-size, 524, 288 bite-size core, which is equivalent to 131,072 (32-bit) words.

DOCUMENT CONTROL DATA - R & D

(Security classification of title, body of abstract and indexing annotation must be entered when the overall report is classified)

1. ORIGINATING ACTIVITY (Corporate author)	2a. REPORT SECURITY CLASSIFICATION
Rocketdyne, a Division of North American Rockwell Corporation, 6633 Canoga Avenue, Canoga Park, California 91304	Unclassified
	2b. GROUP

3. REPORT TITLE

PROPELLANT SPRAY COMBUSTION PROCESSES DURING STABLE AND UNSTABLE LIQUID ROCKET COMBUSTION

4. DESCRIPTIVE NOTES (Type of report and inclusive dates)

Scientific   Final

5. AUTHOR(S) (First name, middle initial, last name)

R D SUTTON

6. REPORT DATE	7a. TOTAL NO. OF PAGES	7b. NO. OF REFS
October 1970	367	115

8a. CONTRACT OR GRANT NO.	9a. ORIGINATOR'S REPORT NUMBER(S)
AF 49(638)-1705	
b. PROJECT NO. 9711-01	
c. 61102F	9b. OTHER REPORT NO(S) (Any other numbers that may be assigned this report)
d. 681308	AFOSR- 70-2714TR

10. DISTRIBUTION STATEMENT

1. This document has been approved for public release and sale; its distribution is unlimited.

11. SUPPLEMENTARY NOTES	12. SPONSORING MILITARY ACTIVITY
TECH, OTHER	AF Office of Scientific Research (NAE) 1400 Wilson Boulevard Arlington, Virginia 22209

13. ABSTRACT

The purpose of this program is the acquisition of detailed analytical and experimental information concerning the mechanisms of energy addition from propellant spray combustion to steady flow fields and propagating pressure disturbances. Data are to be obtained and used to evaluate present or formulate new expressions describing the dynamics that contribute to the coupling processes between the spray and gas flow fields. These expressions appear in steady-state and transient propellant combustion models and bear directly on the prediction of performance and onset of high frequency combustion instability in liquid propellant rocket engines. To overcome past difficulties in comparing analytical and experimental results, an experimental apparatus which produces a monodisperse propellant spray uniformly distributed throughout the combustor has been built. The motor, to be operated as a rocket engine combustor under either stable or transient conditions, provides for optical observation and is extensively instrumented to record pressure wave amplification or decay as a function of parameter variation. Test data (drop diameters, velocity and pressure wave growth or decay as functions of chamber length and initial conditions) can be input to the newly-developed combustion models and the validity of the coupling term expressions evaluated by directly comparing the resulting predictions to experimental data. These newly-developed combustion models are described in detail.

DD FORM 1473
(1 NOV 65)

KEY WORDS	LINK A		LINK B		LINK C	
	ROLE	WT	ROLE	WT	ROLE	WT
Chemical Propulsion						
Liquid Rocket Propellants						
Combustion,						
Combustion Efficiency						
Combustion Stability						
Atomizing						
Two-Phase Flow						
Equations of Motion						
Drops (liquid)						
Drops, Drag						
Drops, Heating						
Drops, Evaporation						